frontiers | Research Topics

Regulation of pollen tube growth, volume II

Edited by
Stefano Del Duca, Delia Fernández-González and Giampiero Cai

Published in
Frontiers in Plant Science

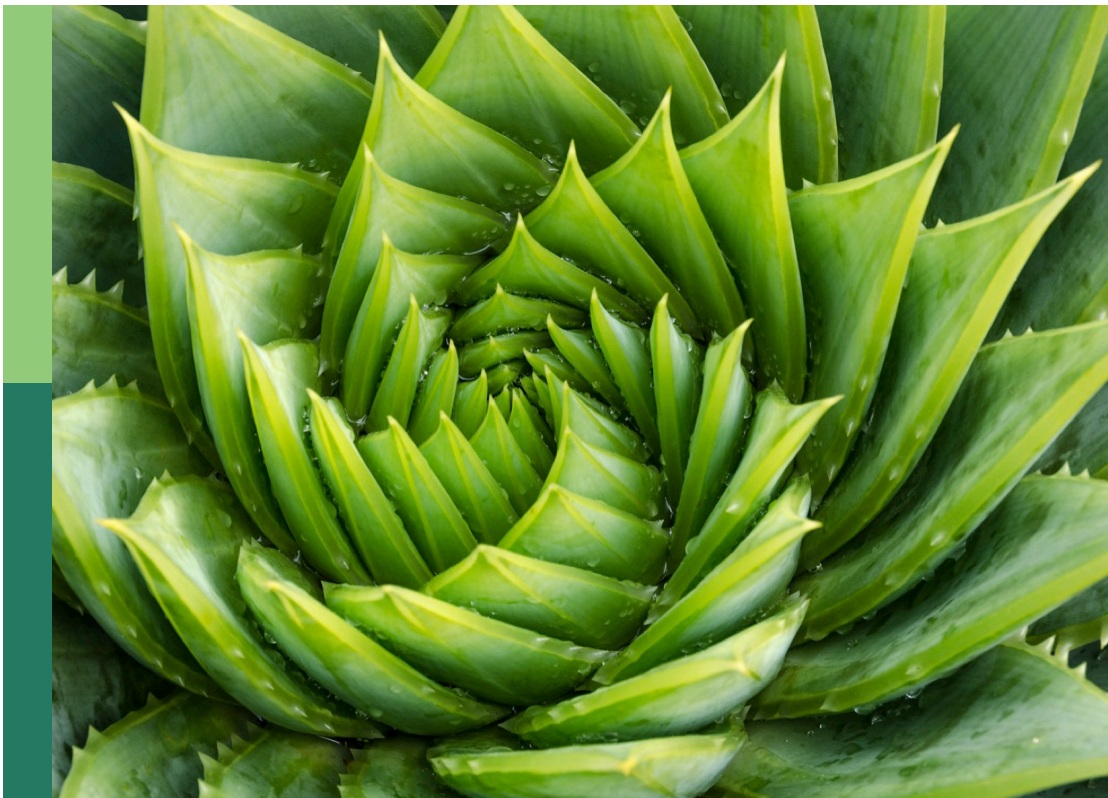

ISSN 1664-8714
ISBN 978-2-8325-3077-1
DOI 10.3389/978-2-8325-3077-1

About Frontiers

Frontiers is more than just an open access publisher of scholarly articles: it is a pioneering approach to the world of academia, radically improving the way scholarly research is managed. The grand vision of Frontiers is a world where all people have an equal opportunity to seek, share and generate knowledge. Frontiers provides immediate and permanent online open access to all its publications, but this alone is not enough to realize our grand goals.

Frontiers journal series

The Frontiers journal series is a multi-tier and interdisciplinary set of open-access, online journals, promising a paradigm shift from the current review, selection and dissemination processes in academic publishing. All Frontiers journals are driven by researchers for researchers; therefore, they constitute a service to the scholarly community. At the same time, the *Frontiers journal series* operates on a revolutionary invention, the tiered publishing system, initially addressing specific communities of scholars, and gradually climbing up to broader public understanding, thus serving the interests of the lay society, too.

Dedication to quality

Each Frontiers article is a landmark of the highest quality, thanks to genuinely collaborative interactions between authors and review editors, who include some of the world's best academicians. Research must be certified by peers before entering a stream of knowledge that may eventually reach the public - and shape society; therefore, Frontiers only applies the most rigorous and unbiased reviews. Frontiers revolutionizes research publishing by freely delivering the most outstanding research, evaluated with no bias from both the academic and social point of view. By applying the most advanced information technologies, Frontiers is catapulting scholarly publishing into a new generation.

What are Frontiers Research Topics?

Frontiers Research Topics are very popular trademarks of the *Frontiers journals series*: they are collections of at least ten articles, all centered on a particular subject. With their unique mix of varied contributions from Original Research to Review Articles, Frontiers Research Topics unify the most influential researchers, the latest key findings and historical advances in a hot research area.

Find out more on how to host your own Frontiers Research Topic or contribute to one as an author by contacting the Frontiers editorial office: frontiersin.org/about/contact

Regulation of pollen tube growth, volume II

Topic editors
Stefano Del Duca — University of Bologna, Italy
Delia Fernández-González — University of León, Spain
Giampiero Cai — University of Siena, Italy

Citation
Del Duca, S., Fernández-González, D., Cai, G., eds. (2023). *Regulation of pollen tube growth, volume II*. Lausanne: Frontiers Media SA. doi: 10.3389/978-2-8325-3077-1

The authors declare that the research was conducted in the absence of any commercial or financial relationships that could be construed as a potential conflict of interest

Table of contents

04 Editorial: Regulation of pollen tube growth, volume II
Stefano Del Duca, Delia Fernández-González and Giampiero Cai

06 An F-Actin Mega-Cable Is Associated With the Migration of the Sperm Nucleus During the Fertilization of the Polarity-Inverted Central Cell of *Agave inaequidens*
Alejandra G. González-Gutiérrez, Antonia Gutiérrez-Mora, Jorge Verdín and Benjamín Rodríguez-Garay

18 Effect of boron toxicity on pollen tube cell wall architecture and the relationship of cell wall components of *Castanea mollissima* Blume
Weiwei Zhang, Qing Zhang, Yu Xing, Qingqin Cao, Ling Qin and Kefeng Fang

31 Finding new *Arabidopsis* receptor kinases that regulate compatible pollen-pistil interactions
Stephen J. Bordeleau, Laura E. Canales Sanchez and Daphne R. Goring

37 Comprehensive analysis of glycerolipid dynamics during tobacco pollen germination and pollen tube growth
Natalia Serrano, Přemysl Pejchar, Hana Soukupová, Martin Hubálek and Martin Potocký

51 Possible molecular mechanisms of persistent pollen tube growth without *de novo* transcription
Kazuki Motomura, Naoya Sugi, Atsushi Takeda, Shohei Yamaoka and Daisuke Maruyama

59 Peptides/receptors signaling during plant fertilization
Tian-Ying Yu, Chun-Xia Xu, Wen-Jia Li and Bo Wang

74 Small extracellular vesicles released from germinated kiwi pollen (pollensomes) present characteristics similar to mammalian exosomes and carry a plant homolog of ALIX
Chiara Suanno, Elisa Tonoli, Enzo Fornari, Maria P. Savoca, Iris Aloisi, Luigi Parrotta, Claudia Faleri, Giampiero Cai, Clare Coveney, David J. Boocock, Elisabetta A. M. Verderio and Stefano Del Duca

90 Removal of the endoplasma membrane upon sperm cell activation after pollen tube discharge
Naoya Sugi, Rie Izumi, Shun Tomomi, Daichi Susaki, Tetsu Kinoshita and Daisuke Maruyama

97 Discovery of a *cis*-regulatory element *SaeM* involved in dynamic regulation of synergid-specific *MYB98*
Prakash Babu Adhikari, Shaowei Zhu, Xiaoyan Liu, Chen Huang, Liyang Xie, Xiaoyan Wu, Jiale He, Nobutaka Mitsuda, Benjamin Peters, Lynette Brownfield, Shingo Nagawa and Ryushiro Dora Kasahara

113 How pollen tubes fight for food: the impact of sucrose carriers and invertases of *Arabidopsis thaliana* on pollen development and pollen tube growth
Jessica Seitz, Theresa Maria Reimann, Carolin Fritz, Carola Schröder, Johanna Knab, Walter Weber and Ruth Stadler

frontiers | Frontiers in Plant Science

TYPE Editorial
PUBLISHED 11 July 2023
DOI 10.3389/fpls.2023.1242416

OPEN ACCESS

EDITED AND REVIEWED BY
Benedikt Kost,
University of Erlangen Nuremberg,
Germany

*CORRESPONDENCE
Giampiero Cai
giampiero.cai@unisi.it

RECEIVED 19 June 2023
ACCEPTED 29 June 2023
PUBLISHED 11 July 2023

CITATION
Del Duca S, Fernández-González D and Cai G (2023) Editorial: Regulation of pollen tube growth, volume II. *Front. Plant Sci.* 14:1242416. doi: 10.3389/fpls.2023.1242416

Editorial: Regulation of pollen tube growth, volume II

Stefano Del Duca[1], Delia Fernández-González[2] and Giampiero Cai[3]*

[1]Department of Biological, Geological and Environmental Sciences, University of Bologna, Bologna, Italy, [2]Department of Biodiversity and Environmental Management, University of León, León, Spain, [3]Department of Life Sciences, University of Siena, Siena, Italy

KEYWORDS

fertilization, plant reproduction, pollen, cell-to-cell communication, environmental stress

Editorial on the Research Topic
Regulation of pollen tube growth, volume II

The pollen tube is an extension produced by the pollen grain when conditions are favorable; thus, the pollen tube is important in seed plant reproduction because it transports male gametes. However, it is also an excellent system for studying various plant cell processes that are common to sink organs or tissues (Kroeger and Geitmann, 2012). The pollen tube has been used to study a variety of processes, including vesicular transport, cytoskeletal organization, cell wall deposition, ion gradients, intracellular signaling. Since the pollen tube grows by contacting and signaling to pistil cells, it is also a model for studying cell-cell communication (Broz and Bedinger, 2021). Moreover, the pollen tube is involved in self-incompatibility (SI) processes that regulate reproduction and thus promote hybridization and genetic variability (Mandrone et al., 2019). SI is regulated by several factors, and in some cases, such as citrus, it is an important tool for producing seedless mandarins (Gentile et al., 2012). Pollen tube and pollen can also be targets of environmental stresses (Ledesma and Sugiyama, 2019), which can impair plant reproductive success, resulting in lower productivity of agronomically important plants and increasing allergenicity (pollinosis) (Armentia et al., 2019; Singh and Mathur, 2021).

New information about the pollen tube is being published on a regular basis allowing us to better understand how the pollen tube promotes plant reproduction; the data also provides insight into how plant cells can change shape in response to specific external signals; and the data help us select plant genotypes that are more resistant to environmental stresses (Liu et al., 2006). For these reasons, we have agreed to serve as guest editors for this Research Topic on pollen tube growth regulation, which is a continuation of a previous one and covers a wide range of subjects.

A frequently asked question is whether the pollen tube nucleus is necessary for pollen tube growth. Motomura et al. used enucleated cells to show that the pollen tube can grow in the absence of its nucleus. This raises several concerns about the presence of persistent transcripts and thus the relative stability of previously produced mRNAs. Furthermore, this article emphasizes the independence of the pollen tube from the vegetative nucleus, at least with respect to growth.

Several colleagues discussed cell-to-cell communication. In their review, Bordeleau et al. summarized the known aspects of pollen-pistil communication in the terminal tract, but also highlighted the lack of knowledge about early pollen-pistil communication. Another review by Yu et al. focused on the role of peptides and receptors in pollen-pistil communication, a relatively unknown system of plant cell communication. The authors discussed the role of peptides in pollen tube growth and interaction with pistils, as well as communication between sperm cells and egg/central cells of the embryo sac. Serrano et al. also addressed the topic of cell-to-cell communication in their article. They focused on the lipidomic aspect of pollen and pollen tubes, examining changes in the levels of specific lipids during pollen tube growth. They found increasing levels of phosphatidic acid during cell growth, suggesting that proper cell-to-cell communication may require extensive use of these specific lipid components. Suanno et al. published another article on cell-cell communication, this time looking at a different and lesser-known pathway. The authors studied the production of small extracellular vesicles known as pollensomes and their possible role in the pollen-pistil communication mechanism. They found that extracellular vesicles can only be produced by germinated pollen and that they contain the ALIX protein, which is a known marker of extracellular vesicles in other cell systems. The manuscript helps us understand a new, unexplored mode of communication.

In their article, Seitz et al. studied the energy aspect of the pollen tube. They looked at the expression of sucrose transporters in pollen and found a gene (AtSUC1) that is critical for the pollen tube to accumulate the disaccharide. At the same time, they looked at genes for cell wall invertases that hydrolyze extracellular sucrose and allow the pollen tube to accumulate glucose *via* monosaccharide transporters. This is an important study because it advances our understanding of the energy dependence of the pollen tube on the pistil.

The attraction of the pollen tube by the synergid cells is clearly a priority before the fusion of the nuclei. Adhikari et al. examined the expression of MYB98 in synergid cells and found that this gene is important for guiding the pollen tube to contact the egg cell. The authors investigated the gene structure by identifying a cis-regulatory sequence and other genes that may target the above sequence. After the pollen tube is attracted, the next step is the fusion of sperm cells with egg cell and central cell, which is a fascinating topic that is unfortunately only partially understood; Sugi et al. investigated the removal of the inner vegetative plasma membrane (IVPM) of sperm cells prior to fusion and found that membrane disruption is required, emphasizing the importance of proper lipid composition. The mechanisms that control cell fusion are also unknown; González-Gutiérrez et al. described the presence of actin bundles that connect the central cell nucleus to the micropyle and may play a role in guiding male sperm cells to fuse. This aspect is only sporadically addressed in plant reproductive biology due to technical difficulties, but it sheds important light on the final step of the fertilization process. Indeed, the final stage of fertilization (e.g., the contact between pollen, egg cell, and synergids, as well as the fusion of the sperm nuclei with those of the female gametophyte) is undoubtedly less well understood.

Finally, Zhang et al. investigated the effects of environmental stress, focusing on the toxic effects of excess boron, by analyzing the composition of pollen tube cell walls. The cell wall is often the first target of contaminants because it is the outermost component. The authors have shown how excess boron alters the distribution of cell wall components, resulting in abnormal deposition of polysaccharides at the pollen tube tip; as a result, pollen tube growth is inhibited, leading to reduced reproductive success.

Author contributions

SDD, DF-G, and GC contributed equally to the preparation and revision of the manuscript and approved the submitted version.

Conflict of interest

The authors declare that the research was conducted in the absence of any commercial or financial relationships that could be construed as a potential conflict of interest.

Publisher's note

References

Armentia, A., Martín-Armentia, S., Álvarez-Nogal, R., Armentia, B. M., Gayoso, M. J., and Fernández-González, D. (2019). Germination of pollen grains in the oesophagus of individuals with eosinophilic oesophagitis. *Clin. Exp. Allergy* 49, 471–473. doi: 10.1111/cea.13312

Broz, A. K., and Bedinger, P. A. (2021). Pollen-pistil interactions as reproductive barriers. *Annu. Rev. Plant Biol.* 72, 615–639. doi: 10.1146/annurev-arplant-080620-102159

Gentile, A., Antognoni, F., Iorio, R. A., Distefano, G., Las Casas, G., La Malfa, S., et al. (2012). Polyamines and transglutaminase activity are involved in compatible and self-incompatible pollination of citrus grandis. *Amino Acids* 42, 1025–1035. doi: 10.1007/s00726-011-1017-9

Kroeger, J. H., and Geitmann, A. (2012). Pollen tube growth: getting a grip on cell biology through modeling. *Mechanics Res. Commun.* 42, 32–39. doi: 10.1016/j.mechrescom.2011.11.005

Ledesma, N., and Sugiyama, N. (2019). Pollen quality and performance in strawberry plants exposed to high-temperature stress. *J. Am. Soc. Hortic. Sci.* 130, 341–347. doi: 10.21273/JASHS.130.3.341

Liu, Z., Yuan, Y., Liu, S., Yu, X., and Rao, L. (2006). Screening for high-temperature tolerant cotton cultivars by testing *in vitro* pollen germination, pollen tube growth and boll retention. *J. Integr. Plant Biol.* 48, 706–714. doi: 10.1111/j.1744-7909.2006.00276.x

Mandrone, M., Antognoni, F., Aloisi, I., Potente, G., Poli, F., Cai, G., et al. (2019). Compatible and incompatible pollen-styles interaction in *Pyrus communis* L. show different transglutaminase features, polyamine pattern and metabolomics profiles. *Front. Plant Sci.* 10, 741. doi: 10.3389/fpls.2019.00741

Singh, A. B., and Mathur, C. (2021). Climate change and pollen allergy in India and south Asia. *Immunol. Allergy Clinics* 41, 33–52. doi: 10.1016/j.iac.2020.09.007

frontiers in Plant Science

ORIGINAL RESEARCH
published: 24 November 2021
doi: 10.3389/fpls.2021.774098

An F-Actin Mega-Cable Is Associated With the Migration of the Sperm Nucleus During the Fertilization of the Polarity-Inverted Central Cell of *Agave inaequidens*

Alejandra G. González-Gutiérrez[1], Antonia Gutiérrez-Mora[1], Jorge Verdín[2] and Benjamín Rodríguez-Garay[1]**

[1] Unidad de Biotecnología Vegetal, CIATEJ, Centro de Investigación y Asistencia en Tecnología y Diseño del Estado de Jalisco, A.C., Zapopan, Mexico, [2] Unidad de Biotecnología Industrial, CIATEJ, Centro de Investigación y Asistencia en Tecnología y Diseño del Estado de Jalisco, A.C., Zapopan, Mexico

OPEN ACCESS

Edited by:
Ramin Yadegari, University of Arizona, United States

Reviewed by:
Tomokazu Kawashima, University of Kentucky, United States
Takashi Okamoto, Tokyo Metropolitan University, Japan
Daisuke Maruyama, Yokohama City University, Japan

***Correspondence:**
Jorge Verdín
jverdin@ciatej.mx
Benjamín Rodríguez-Garay
agavero01@hotmail.com

Specialty section:
This article was submitted to Plant Development and EvoDevo, a section of the journal Frontiers in Plant Science

Received: *10 September 2021*
Accepted: *01 November 2021*
Published: *24 November 2021*

Citation:
González-Gutiérrez AG, Gutiérrez-Mora A, Verdín J and Rodríguez-Garay B (2021) An F-Actin Mega-Cable Is Associated With the Migration of the Sperm Nucleus During the Fertilization of the Polarity-Inverted Central Cell of Agave inaequidens. Front. Plant Sci. 12:774098. doi: 10.3389/fpls.2021.774098

Asparagaceae's large embryo sacs display a central cell nucleus polarized toward the chalaza, which means the sperm nucleus that fuses with it during double fertilization migrates an atypical long distance before karyogamy. Because of the size and inverted polarity of the central cell in Asparagaceae, we hypothesize that the second fertilization process is supported by an F-actin machinery different from the short-range F-actin structures observed in *Arabidopsis* and other plant models. Here, we analyzed the F-actin dynamics of *Agave inaequidens,* a classical Asparagaceae, before, during, and after the central cell fertilization. Several parallel F-actin cables, spanning from the central cell nucleus to the micropylar pole, and enclosing the vacuole, were observed. As fertilization progressed, a thick F-actin mega-cable traversing the vacuole appeared, connecting the central cell nucleus with the micropylar pole near the egg cell. This mega-cable wrapped the sperm nucleus in transit to fuse with the central cell nucleus. Once karyogamy finished, and the endosperm started to develop, the mega-cable disassembled, but new F-actin structures formed. These observations suggest that Asparagaceae, and probably other plant species with similar embryo sacs, evolved an F-actin machinery specifically adapted to support the migration of the fertilizing sperm nucleus within a large-sized and polarity-inverted central cell.

Keywords: Polygonum-type embryo sac, chalazal central cell polarity, cytoplasmic strands, double fertilization, helobial endosperm, Asparagaceae

INTRODUCTION

Two sperm cells are released from the pollen tube at the egg apparatus boundary during Angiosperm's fertilization. One of the sperm fuses the egg cell leading to the first plasmogamy and, subsequently, the first karyogamy that generates the zygote (Hamamura et al., 2011). Almost simultaneously, the second sperm fuses with the central cell leading to the second plasmogamy and karyogamy and further endosperm development (Berger et al., 2008). In *Arabidopsis*, whose

central cell nucleus is polarized toward the micropylar end (Sprunck and Gross-Hardt, 2011), the distance the second sperm nucleus travels from the plasmogamy site to the central cell nucleus is around 1 μm (Kawashima and Berger, 2015). However, species in the Asparagaceae family, along with other 13 monocotyledonous families, harbor embryo sacs with a polarity-inverted central cell nucleus, i.e., it localizes near the chalazal pole (Davis, 1966; Bhojwani and Bhatnagar, 1983). In *Agave tequilana,* the distance between the egg cell and the central cell nucleus is about 200-times longer than in *Arabidopsis* (González-Gutiérrez et al., 2014). The latter implies that the second sperm nucleus needs to undertake a longer journey in Asparagaceae. Thus, it is plausible that these plant species evolved a specialized long-range transport machinery to support the migration of the sperm nucleus.

An established model to explain the sperm nuclei migration during fertilization proposes they are carried to the fusion sites by a cytoskeleton-supported mechanism (Huang and Russell, 1994; Zhang and Russell, 1999; Wallwork and Sedgley, 2000; Ye et al., 2002). Kawashima et al. (2014) demonstrated that F-actin, but not microtubules, transports the immotile sperm nuclei during *Arabidopsis* fertilization. Once inside the central cell, the second sperm nucleus is surrounded by an aster-shaped F-actin structure (Kawashima et al., 2014) that migrates in synchrony with inward moving (plasma membrane to central cell nucleus) F-actin cables attached to the plasma membrane by formins and ROP8 (Ali et al., 2020; Ali and Kawashima, 2021). These F-actin cables form a mesh-like structure whose movement and stability depend on class XI myosin XI-G (Ali et al., 2020). A similar F-actin arrangement and meshwork movement have been observed in rice zygotes (Ohnishi and Okamoto, 2017), which suggested the migration mechanism of this sperm nucleus might be general among angiosperms (Ali et al., 2020). Nevertheless, a physical connection between the aster-shaped structure and the inward moving F-actin cables has not been established yet.

The F-actin arrangement for cargo transport has been demonstrated to largely rely on the distance the cargo has to travel. Precise short-distance cargo exocytosis is usually mediated by fanned thin actin cables arrays (Geitmann and Emons, 2000). On the other hand, thick actin cables are primarily associated with sizeable long-distance movements, such as those that allow the movement of organelles in root hairs and pollen tubes (Chebli et al., 2013). Nevertheless, the precise mechanisms that determine the different conformations that actin can adopt remain unknown (Geitmann and Emons, 2000).

Because of the exceptional configuration of the embryo sac of Asparagaceae species and the F-actin arrangement dependence on the distance the cargo needs to travel, we hypothesize F-actin-supported migration of the second sperm nucleus in Asparagaceae central cell fertilization may be different from that observed in *Arabidopsis* and other classical plant models. As this megagametophyte configuration is found beyond Asparagales, a similar mechanism for long-distance migration of the sperm nucleus may be more widespread. Here, we addressed such hypotheses by characterizing F-actin structures of the *Agave inaequidens* megagametophyte, from the mature embryo sac and sperm nuclear migration during double fertilization to the early endosperm development.

MATERIALS AND METHODS

Plant Material

Inflorescences with mature flowers from *A. inaequidens* plants were collected in the State of Jalisco, Mexico, during the flowering seasons (May-June) of 2017–2020.

Pollination and Collection of Specimens

Inflorescences were maintained at the laboratory in freshwater. Flowers were emasculated at anthesis and covered with glassine paper bags to avoid free pollination. Extracted anthers were kept in Petri dishes at 4°C until dehiscence. At this time, mature pollen grains were recovered from the anthers and tested for viability using the *in vitro* method for pollen germination of the *Agave* genus, described by López-Díaz and Rodríguez-Garay (2008).

Once the stigmas of emasculated flowers were receptive (presence of a pollination drop), ten flowers per inflorescence were selected and processed as described below. Unpollinated flowers collected at this stage were considered "time 0." The remaining flowers at this developmental stage were hand-pollinated (cross-pollination) and collected at different times between 1 and 48 h after pollination (HAP). Thus, it was possible to record actin cytoskeleton dynamics in mature *A. inaequidens* embryo sacs during double fertilization and the first endosperm divisions (**Table 1**). Ovules of the same flower were dissected with fine-point tweezers and an insulin needle under the stereoscope and evenly divided into two centrifuge tubes to be processed using the histological techniques described below.

Only "normal" megagametophytes were considered, i.e., piriform embryo sacs with a pronounced haustorial tube and the four cellular types contained in seven cells. Collapsed embryo sacs and embryo sacs lacking any cellular type due to abnormal growth of the nucellar tissue were discarded. At least 500 ovules encompassing the different developmental stages were analyzed with each staining technique.

Feulgen Staining

Although Feulgen staining (Barrell and Grossniklaus, 2005) primarily binds to DNA (Kalinowska et al., 2020), some other structures, such as cell walls (Barrell and Grossniklaus, 2005) and cytoplasm can be weakly stained (Chieco and Derenzini, 1999). Feulgen staining adapted with minor modifications for agave ovules was used as the primary method for analyzing the general development stage of embryo sacs. In short, after fixation in FAA (10:5:50:35 formaldehyde: acetic acid: ethanol: distilled water) for 24 h and kept overnight in 70% ethanol, 4°C, ovules were treated with 1 M HCl for 1.5 h, 5.8 M HCl for 2 h, and 1 M HCl for 1 h at room temperature. Subsequently, ovules were rinsed three times with distilled water and stained with Schiff

TABLE 1 | Fertilization timing and F-actin dynamics in *Agave inaequidens*.

Hours after pollination (HAP)	F-actin structural change before, during and after fertilization	Sample number with reported F-actin structures
Time 0–18*	Mature embryo sac-actin filaments are restricted to perinuclear and cortical areas of each cell of the four cellular types.	*n* = 40
24–30	Actin filaments at the central cell micropylar and chalazal ends started to project from the cortical area to the center of the cell. An arch-shaped F-actin accumulation is formed in the vicinity of the egg apparatus.	*n* = 43
3–36	Parallel F-actin cables extending from the central cell nucleus and aligned to the chalazal-micropylar axis, formed the actin-tunnel.	*n* = 50
38–42	F-actin mega-cable connected the nucleus with the micropylar end of the central cell, close to the egg cell. The sperm nucleus was observed at different stages of its journey (half-, 3/4 and close to the central cell nucleus, just before karyogamy).	*n* = 81
44–48	Early stages of endosperm development, from first division of the primary endosperm nucleus to the eight nucleate stage. F-actin is located around each endosperm nuclei and connects them to each other.	*n* = 50

**These patterns were observed in embryo sacs from non-pollinated (time 0) and pollinated flowers up to 18 HAP.*

reagent (Sigma cat. no. S5133) for 3 h at room temperature. Dehydration was carried out by an increasing concentration series of 30, 50, 70, 90, 95, 100% ethanol for 30 min, and an additional 100% ethanol incubation for 30 min. Finally, ovules were clarified by a series of methyl salicylate: ethanol solutions of 3:1, 1:1, 1:3 for 1 h each. For observation, samples were mounted in 100% methyl salicylate and examined on a Leica TCS SPE confocal microscope at Ex = 532 nm and Em = 555–700 nm. Images were acquired and processed with the LAS X® software (Leica Microsystems).

F-Actin Whole-Mount Staining

F-actin whole-mount staining was performed as reported by González-Gutiérrez et al., 2020. Ovules previously dissected were pre-incubated in ASB (Actin Stabilizing Buffer) (50 mM PIPES, 10 mM EGTA, and 1 mM MgCl2, pH 6.8 adjusted with 10 M KOH) at 55°C for 5 min. Then, ovules were fixed with 4% formaldehyde in ASB for 10 min at room temperature (25°C). Afterward, ovules were washed twice with ASB. Two quick rinses with acetone (−20°C), followed by a 5 min incubation in acetone (−20°C), were performed for cuticle solubilization and membrane permeabilization. After this time elapsed, acetone was removed from the microtubes, and ovules were washed 3 times with ASB until the solution remained crystalline. Ovules were then incubated in blocking solution (1% BSA in ASB) for 20 min at room temperature and stained with 0.33 μM rhodamine-phalloidin and 3 μg/ml Hoechst 33258 (diluted in blocking solution), overnight at 4°C. Before clarification, ovules were dehydrated in an increasing concentration series of isopropanol (diluted in ASB) at 4°C, for 7 min each: 75, 85, 95, 100%, and an additional 100% isopropanol step for 12 min. Tissue clarification was carried out by adding 1:1 methyl salicylate-isopropanol solution until all ovules precipitated at the microtube bottom. Finally, ovules were incubated in 100% methyl salicylate for at least 30 min before observation. Samples were analyzed under a Leica TCS SPE confocal microscope using a 532 nm laser for rhodamine-phalloidin (ex/em = 540/556 nm) and a 405 nm laser for Hoechst 33258 observation (ex/em = 352/461 nm). Images were taken and managed with the LAS X® software (Leica Microsystems).

RESULTS

Agave inaequidens Harbors a Central Cell With Inverted Polarity

To elucidate the mechanism that supports the transport of sperm nuclei during the central cell fertilization in Asparagaceae species, we studied the mature embryo sac of non-pollinated flowers of a so far uncharacterized family member: *A. inaequidens*. *A. inaequidens* mature embryo sac (238.58 ± 16.28 μm, long; and 128.51 ± 12.20 μm, wide; *n* = 40) was piriform with an hypostase at the chalazal end, below which three antipodal cells were located (**Figures 1A,B**). Moreover, the embryo sac harbored a large central cell (144.03 ± 13.96 μm, long; 124.79 ± 8.89 μm, wide; *n* = 40). Its vacuole occupied most of the central part of the cell, while its nucleus was polarized toward the chalazal pole, just below the antipodal cells (**Figures 1A,B**). The egg apparatus was located at the opposite side of the embryo sac (central cell nucleus-egg cell nucleus distance: 156.28 ± 22.62 μm, *n* = 40), composed of an egg (**Figures 1A,C**) and two synergid cells (**Figures 1A,D**).

F-Actin in the Mature Embryo Sac Is Restricted to Perinuclear and Cortical Areas

To observe F-actin structures, mature ovules from *A. inaequidens* non-pollinated flowers were stained with rhodamine-phalloidin. Actin filaments were observed layering the cytosolic side of the membrane of each cell of the mature embryo sac of *A. inaequidens* flowers (**Figure 2A**). The nuclei of these cells were also enveloped by actin filaments that extended until reaching the cell periphery (**Figures 2A–D**). Compared to profuse actin filaments in the egg apparatus (**Figures 2A,C,D**), perinuclear actin filaments were less abundant around nuclei of antipodal cells (**Figure 2B**).

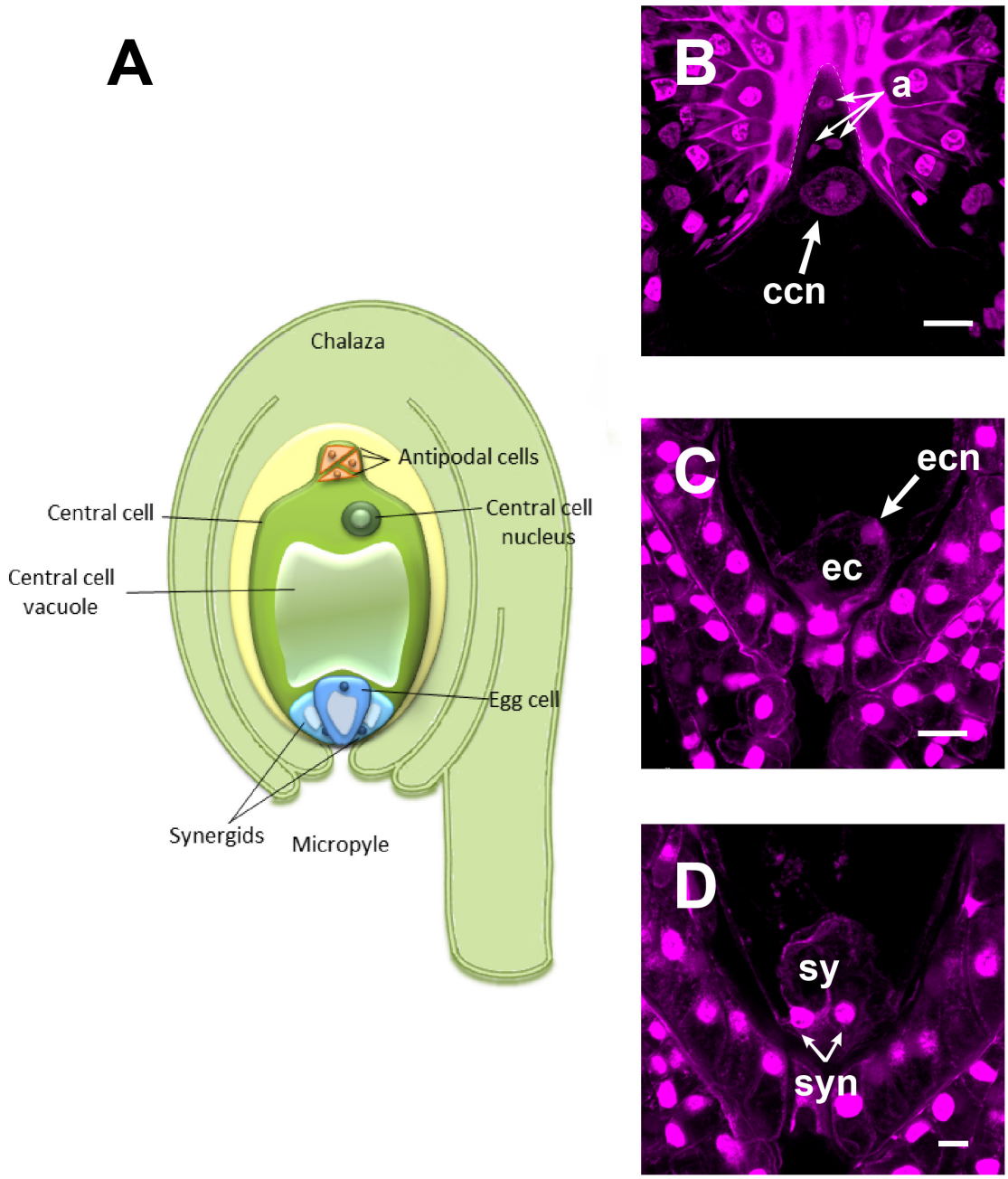

FIGURE 1 | The mature female gametophyte of *Agave inaequidens* (time "0"). **(A)** Scheme of a seven-celled embryo sac arranged in four cell types: three antipodal cells, placed just below the hypostase, and a large central cell with its nucleus polarized toward the chalaza **(B)**. At the micropylar end, the egg apparatus is composed of an egg cell **(C)** and two synergids **(D)**. **(B–D)** Are Feulgen-stained z-stack images. a, antipodal cells; ccn, central cell nucleus; ec, egg cell; ecn, egg cell nucleus; sy, synergids; syn, synergids nuclei. Bar in **(B,C)** = 20 μm and **(D)** = 10 μm.

In addition to perinuclear actin, synergids displayed a pronounced aggregation of actin filaments at the micropylar end, around the space occupied by their nuclei (**Figure 2C**). A similarly biased F-actin accumulation, but oriented to the chalazal pole, was observed around the egg cell nucleus (**Figure 2D**).

In the central cell nucleus, perinuclear F-actin was observed as a dense coat from which several actin filaments extended toward the cell periphery, attaching it to the chalazal area of the cell (**Figure 2A**). Most of the space in the central cell was occupied by a large vacuole (**Figure 2A**), and actin filaments were restricted to the cell periphery (**Figure 2A**).

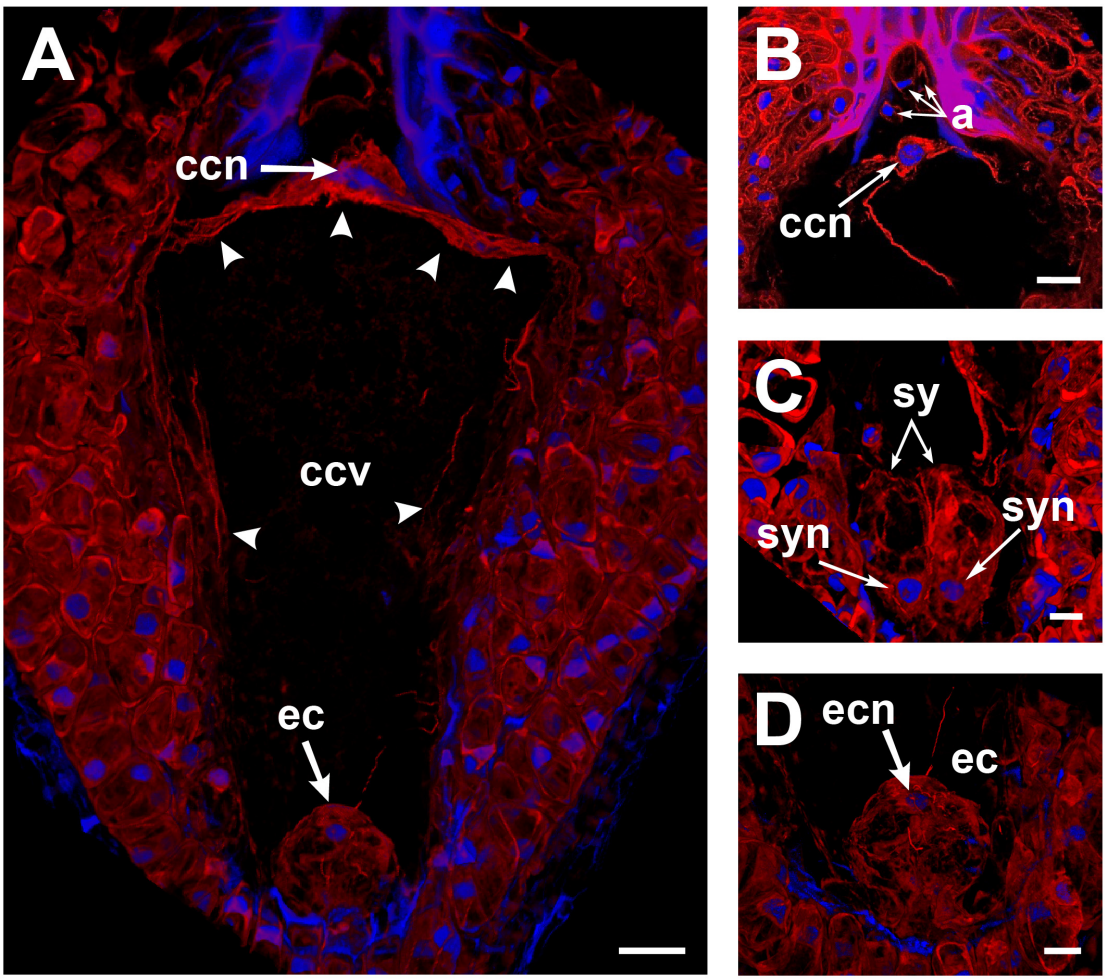

FIGURE 2 | Perinuclear and cortical F-actin in the *Agave inaequidens* mature embryo sac from time "0" up to 18 HAP. **(A)** Rhodamine-phalloidin-stained actin filaments were located at the periphery of the central cell. **(B)** The central cell nucleus displayed a dense perinuclear F-actin coat, while it was less abundant in the antipodal cells. **(C)** F-actin was denser at the synergids' micropylar end, where their nuclei were located. **(D)** Egg cell cortical and perinuclear actin filaments. ccn, central cell nucleus; ccv, central cell vacuole; a, antipodal cells; sy, synergids; syn, synergid nucleus; ec, egg cell; ecn, egg cell nucleus. Arrow heads, cortical actin filaments of the central cell. All micrographs are z-stack projections oriented with the chalazal pole at the top. Bar in **(A–C)** = 20 μm and **(D)** = 10 μm.

F-Actin Cables Projected From the Central Cell Nucleus Form a Tunnel-Like Structure Before Fertilization

To observe changes in the actin cytoskeleton during double fertilization, *A. inaequidens* flowers were hand-pollinated and collected at different hours after pollination (HAP, **Table 1**). In female gametophytes processed between 24 and 30 HAP, actin filaments at the central cell micropylar end started to project from the cortical area to the cell center (**Figure 3A**); in addition, an arch-shaped accumulation of filaments could be seen close to the egg apparatus (**Figure 3A**). Simultaneously, the F-actin coat of the central cell nucleus began to extend toward the middle part of the cell, forming thick F-actin cables parallel to the chalazal-micropylar axis (**Figure 3B**). Finally, around 32–36 HAP, those F-actin cables reached the micropylar end, in the vicinity of the egg apparatus, building a structure we named "actin tunnel," which generated a lobular chamber (**Figure 3C** and **Supplementary Video 1**).

An F-Actin Mega-Cable Interacts With the Migrating Sperm Nucleus During the Central Cell Fertilization

As stated in section "F-Actin in the Mature Embryo Sac Is Restricted to Perinuclear and Cortical Areas" for rhodamine-phalloidin staining, Feulgen-stained mature embryo sacs from non-pollinated flowers also showed a large vacuole occupying most of the space in the central cell. This developmental configuration was preserved even in ovules from pollinated flowers up to 18 HAP (**Figure 4A**); later, cytoplasmic accumulations in the form of thin longitudinal strands started to appear into the central cell (32–36 HAP) (**Figure 4B**). Subsequently, the pollen tube arrived at the receptive synergid in

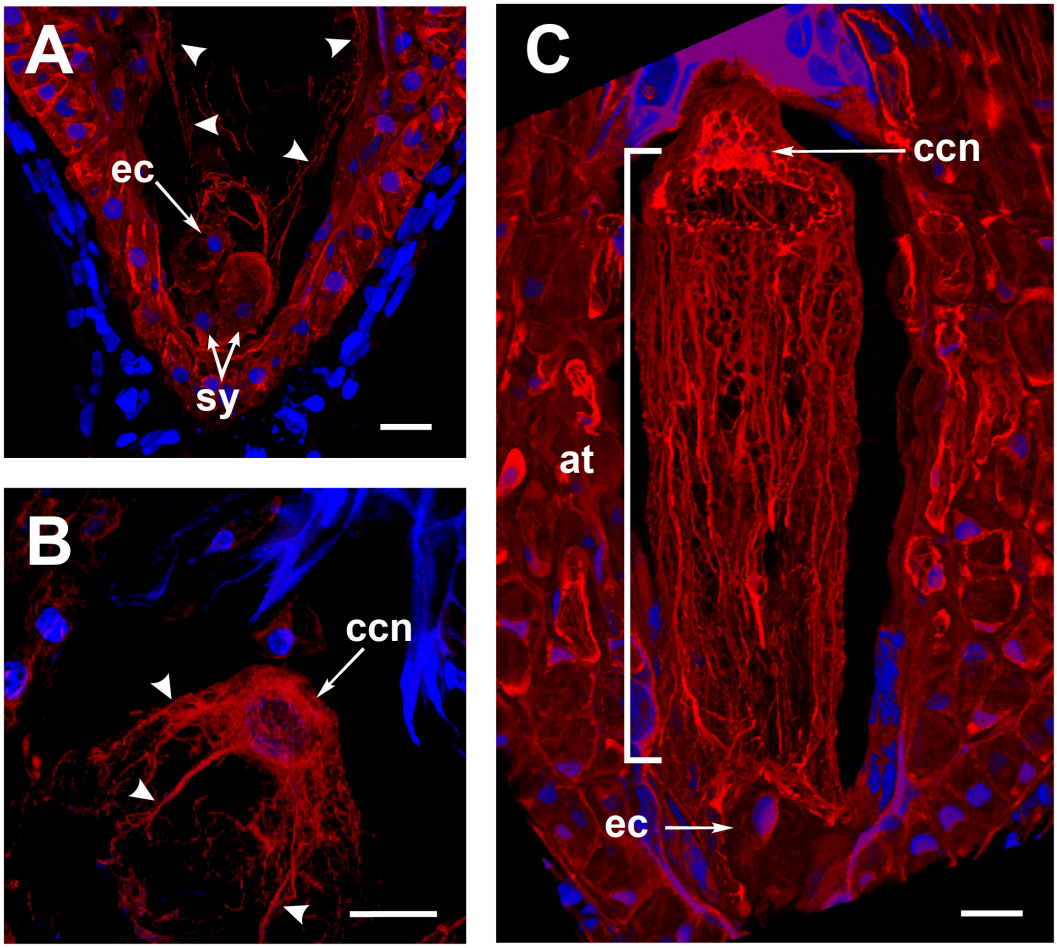

FIGURE 3 | The formation of the *Agave inaequidens* actin-tunnel. **(A)** Central cell F-actin starts accumulating at the cell body. **(B)** Actin filaments projected from the central cell nucleus toward the embryo sac micropylar pole (24–30 HAP). **(C)** Actin-tunnel formed by several parallel filaments extends from the central cell nucleus to the micropylar pole, next to the egg cell (32–36 HAP). ec, egg cell; sy, synergid; ccn, central cell nucleus; at, actin tunnel. Arrowheads in **(A,B)** = actin filaments. In all cases, F-actin was stained with rhodamine-phalloidin. Nuclei were stained with Hoechst 33258. All micrographs are z-stack projections oriented with the chalazal pole at the top. Bar in **(A–C)** = 20 μm.

the embryo sac (38–42 HAP) and released the two sperm cells that moved together toward the chalazal end of the synergid (**Figure 4C** and **Supplementary Video 2**). At this stage, a "central strand" traversing the putative central cell vacuole could be observed (**Figures 4C**, **5A**). This trans-vacuolar strand connected the central cell nucleus directly to the micropylar end at the egg cell boundary (**Figure 5A**). Afterward, plasmogamy and karyogamy of one of the sperm with the egg cell had occurred (**Figure 5A**). Meanwhile, the second sperm and the central cell fused their membranes, and the nucleus of the former started a journey through the large central cell vacuole moving along the trans-vacuolar strand (**Figure 5A**) to reach the central cell nucleus at the opposite side of the embryo sac (38–42 HAP) (**Figure 5B**).

Just before the second fertilization took place, a new thick F-actin cable that we name "mega-cable" began to extend from the actin coat of the central cell nucleus toward the micropylar pole of the cell, more precisely at the boundary of the central cell with the egg cell (**Figure 5C**). Since it was not possible to catch the early stages of the mega-cable development, it remains unclear whether the mega-cable formed from one or several of the pre-existing tunnel-forming cables or emerged *de novo* as a specialized structure. Moreover, the mega-cable encompassed the DAPI-stained sperm nucleus in transit to the central cell nucleus (**Figures 5C,D**). Imaging showed that the sperm nucleus moved "inside" the mega-cable rather on it, as may be expected if the nucleus migrates in a myosin-dependent way (**Figures 5C,D**).

The actin tunnel, the F-actin mega-cable, and the transvacuolar strand were present until karyogamy of the two sperm nuclei with the egg and central cells, respectively, was completed (**Figure 6A**). Those structures were disassembled just before the primary endosperm nuclei divided for the first time (**Figures 6B,C**). Subsequently, new F-actin structures around all endosperm nuclei were built, which connected them to each other (**Figure 6D**).

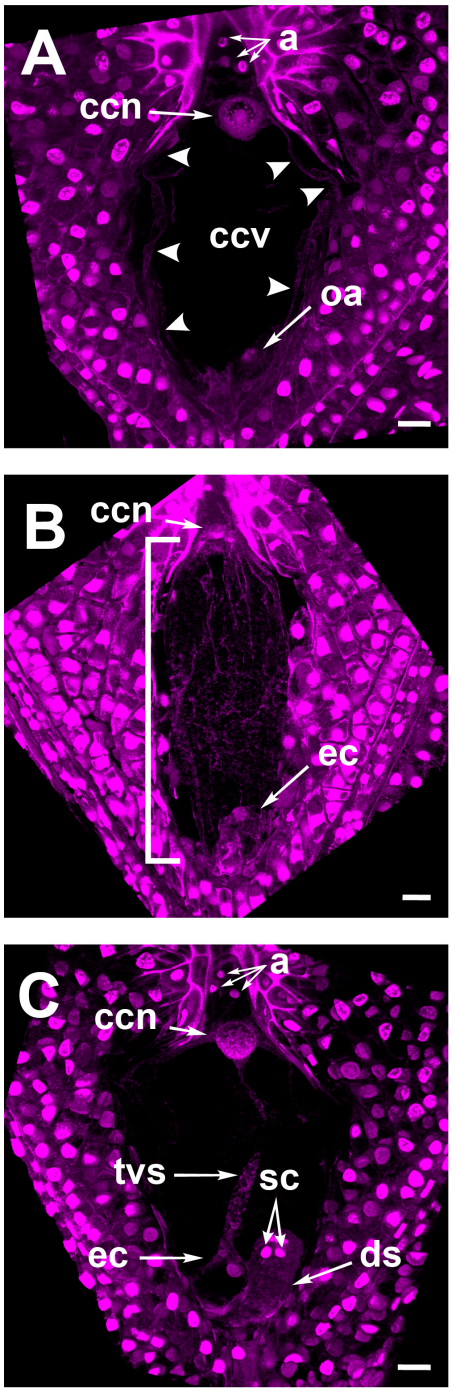

FIGURE 4 | Feulgen stained ovules of *Agave inaequidens* show the developmental specificity of the transvacuolar strand. **(A)** Mature embryo sac at 1–18 HAP. **(B)** Embryo sac at 32–36 HAP. **(C)** Detection of the transvacuolar strand at 38–42 HAP. The two sperm nuclei remain at the chalazal end of the receptive synergid after their discharge but before karyogamy with central and egg cells occurs. a, antipodal cells; ccn, central cell nucleus; ccv, central cell vacuole; oa, ovular apparatus; ec, egg cell; tvs, transvacuolar strand; sc, sperm cells; ds, degenerating synergid. The bracket indicates the accumulation of longitudinal cytoplasmic strands. All micrographs are z-stack projections oriented with the chalazal pole at the top. Bar in **(A–C)** = 20 μm.

DISCUSSION

Enormous progress has been gained in understanding the cellular mechanisms involved in sperm nuclear migration for karyogamy during double fertilization. It is generally accepted that the sperm nuclear migration is an actin-dependent process in both monocot and dicotyledonous species (Kawashima et al., 2014; Ohnishi et al., 2014; Peng et al., 2017). Recent analysis of central cell fertilization in *A. thaliana* shows that an F-actin mesh-like structure which moves from the periphery to the center of the cell, along with an F-actin star-shaped structure that encloses the sperm nucleus, mediates the transit of the latter to the central cell nucleus (Kawashima et al., 2014). Similar processes have been observed in other plant models (Ohnishi and Okamoto, 2017) and the mechanism has been proposed as a general one for Angiosperms (Ali et al., 2020). However, none of the plant species analyzed thus far have possessed a chalazal-polarized central cell nucleus. Members of the Asparagaceae family exhibit this feature, which, together with their large-sized embryo sacs, requires the sperm nucleus to travel an atypical long distance through the central cell in order to achieve karyogamy (González-Gutiérrez et al., 2020). Moreover, it has been observed that the conformation of the F-actin cables largely depends on the distance the cargo needs to travel (Geitmann and Emons, 2000). Because of the latter, we hypothesized that Asparagaceas could support the migration of the sperm nucleus during fertilization of the central cell in a different way to that described for *Arabidopsis*.

In order to test this hypothesis, we characterized the mature embryo sac of non-pollinated flowers from *A. inaequidens*, an agave mainly distributed in temperate areas of Mexico (1400–3000 MASL) (Torres-García et al., 2019). This monocarpic species belongs to the subfamily Agavoideae of the Asparagaceae family, formerly Agavaceae (Angiosperm Phylogeny Group [APG III], 2009). Typically, the flowering stalk is cut off when it starts to grow at 8–10 years and is used as food, or is allowed to accumulate carbohydrates in order to produce alcoholic beverages (Gentry, 1982; Figueredo et al., 2014). It is used in the traditional Mexican beverage industry, but less studied than classical *Agave* species, such as *Agave tequilana*. The mature embryo sac of *A. inaequidens* displays the Polygonum-type with the typical shape and polarization of the central cell nucleus also seen in *A. tequilana, A. colimana* (González-Gutiérrez et al., 2014; Barranco-Guzmán et al., 2019) and other Asparagales (**Figure 1**). It also shows the classical Asparagales final position of the secondary nucleus in the central cell relative to the micropylar-chalazal axis (**Figure 1**; Tilton and Lersten, 1981), as well as the presence of an hypostase at the proximal part of the nucellus, close to the antipodal cells (Rudall, 1997).

Polygonum-type megagametophyte is considered the Angiosperm's ancestral development pattern (Palser, 1975; Haig, 1990). It is present in more than 70% of the Angiosperms (Maheshwari, 1950). In Polygonum-type, the central cell nucleus is generally positioned at the central part of the cell or close to the egg apparatus at the micropylar pole, i.e., like in the classical gametophyte developmental models *A. thaliana* and *Zea mays* (Russell, 1978; Webb and Gunning, 1990). Variations to this developmental pattern have been reported

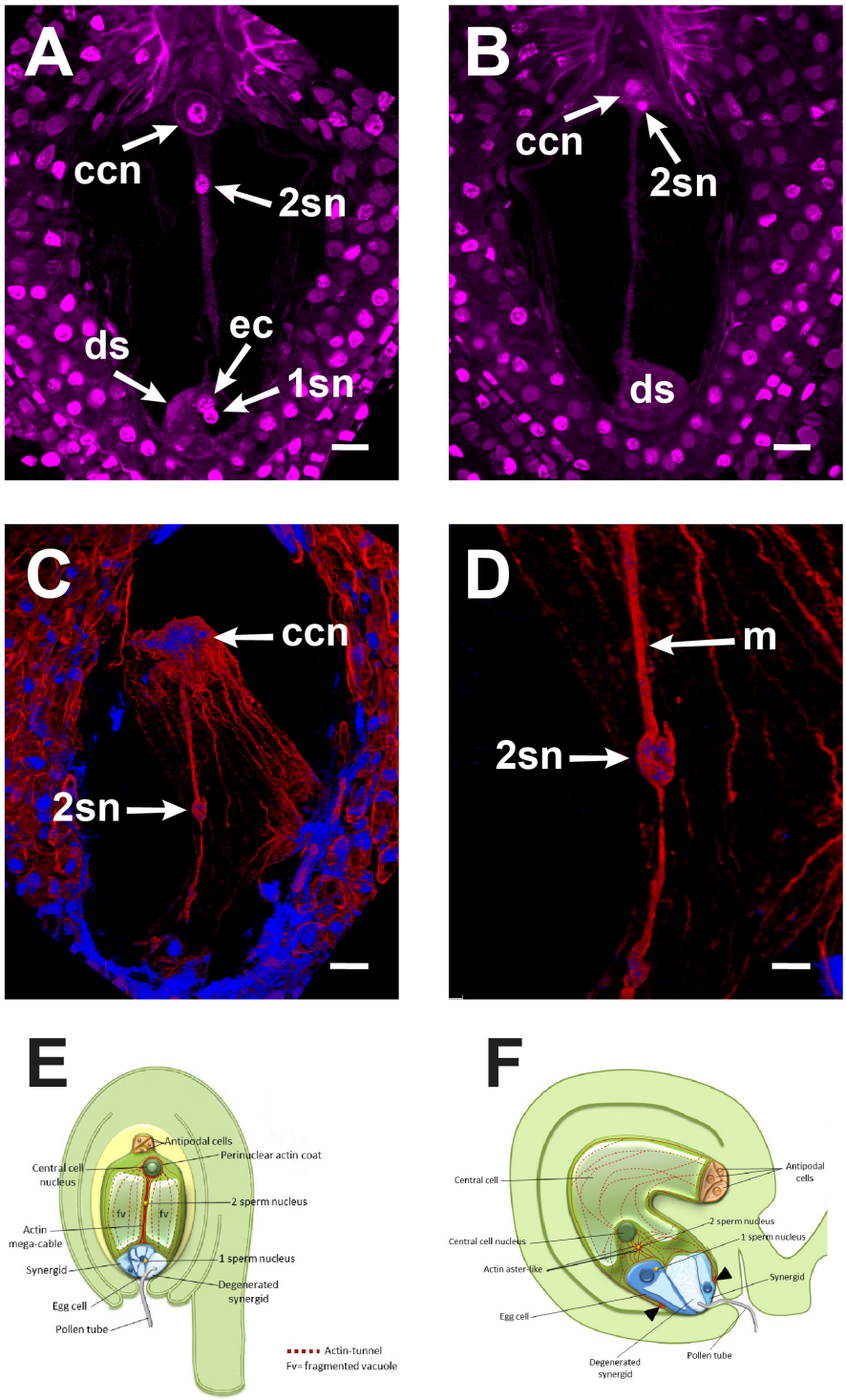

FIGURE 5 | The central cell fertilization of *Agave inaequidens* occurred from 38 to 42 HAP. **(A)** A cytoplasmic trans-vacuolar strand and the second sperm nucleus revealed by Feulgen staining were observed at the central cell. **(B)** Second sperm nucleus getting close to karyogamy. **(C)** The rhodamine-phalloidin stained actin mega-cable traversing the central cell vacuole wrapped the second sperm nucleus (stained with Hoechst 33258). **(D)** Close up of the sperm (in C) wrapped by actin. **(E)** Model of the central cell fertilization in *Agave* embryo sac where an actin-based mega-cable traverses the central vacuole, wraps the sperm nucleus and supports its migration for the second karyogamy event. **(F)** In *Arabidopsis*, during the second fertilization, the sperm nucleus is surrounded by an aster-shaped structure that moves it toward the central cell one (inspired in Dresselhaus et al., 2016). ccn, central cell nucleus, 2sn = second sperm nucleus, ec, egg cell; ds, degenerated synergid; m, actin mega-cable. All micrographs are z-stack projections oriented with the chalazal pole at the top. Bar in **(A–C)** = 20 μm and **(D)** = 10 μm.

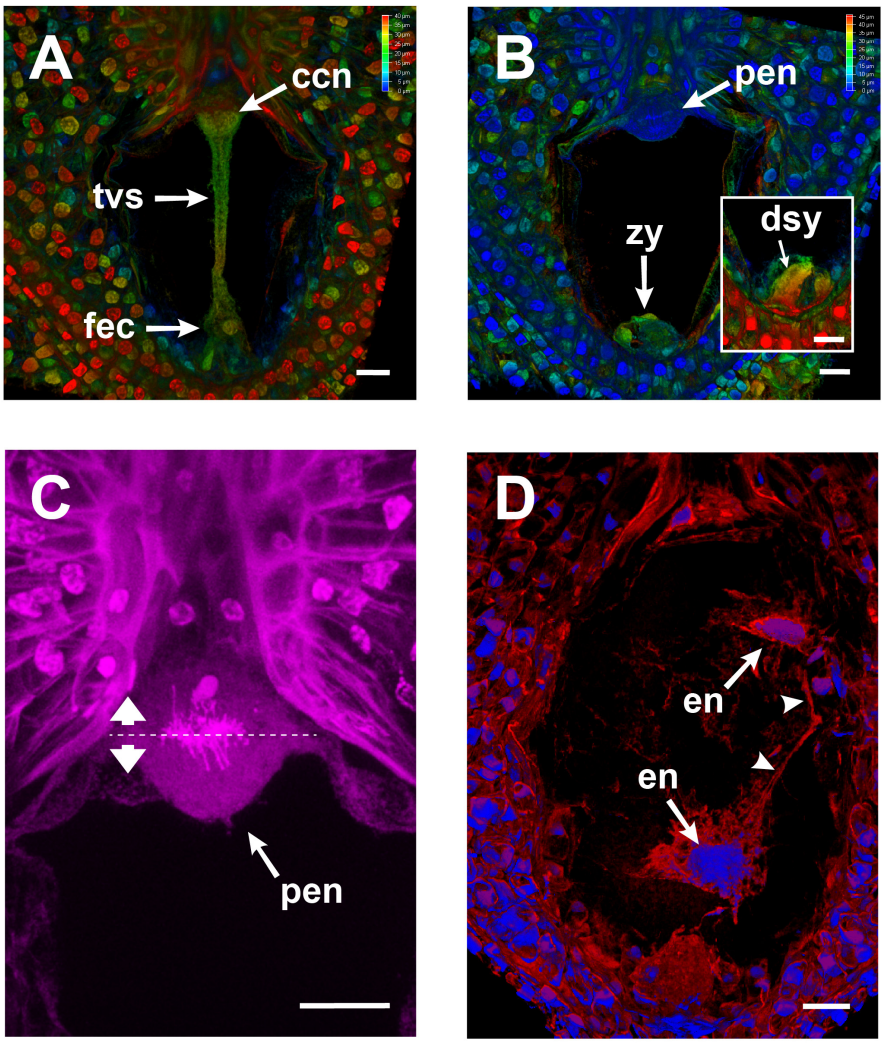

FIGURE 6 | Changes in the embryo sac of *Agave inaequidens* after karyogamy and early endosperm development (44–48 HAP). **(A,B)** Color-coded projection of z-stacked micrographs of similar thickness from Feulgen-stained fertilized ovules. **(A)** A transvacuolar strand connected the chalazal and micropylar poles right after karyogamy of the egg and central cells. **(B)** The transvacuolar strand was no longer detectable before the primary endosperm nucleus divided. **(C)** Close up of the primary endosperm nucleus at anaphase; the dashed line shows the division plane. **(D)** F-actin (red) surrounded and connected (arrowheads) each nucleus (blue) of the developing endosperm in the coenocyte. F-actin was stained with rhodamine-phalloidin; nuclei were stained with Hoechst 33258. ccn, central cell nucleus; tvs, transvacuolar strand; fec, fertilized egg cell; zy, zygote; dsy, degenerated synergid; pen, primary endosperm nucleus; en, endosperm nuclei. Micrographs are z-stack projections oriented with the chalazal pole at the top. Bar in **(A–D)** = 20 μm.

for different plant families and are conserved within them (Bhojwani and Bhatnagar, 1983; Herr, 1984; Tobe, 1989). Variations include the behavior of mature antipodal cells (which can be ephemeral, persist after fertilization, or proliferate) (Tilton, 1978; Williams and Friedman, 2004; Holloway and Friedman, 2008), the timing of the polar nuclei fusion (Jensen, 1973), and the final position of the secondary nucleus in the central cell relative to the micropylar-chalazal axis (Tilton and Lersten, 1981). Embryo sacs with the central cell nuclei polarized toward the chalazal end have been observed in several members of the Asparagaceae family, and in other 17 angiosperm families, 14 of them belonging to the monocotyledoneae class (Davis, 1966).

After confirming the Asparagales-like embryo sac configuration of *A. inaequidens*, the F-actin dynamics along the fertilization of its central cell was characterized. When staining non-pollinated mature embryo sacs with rhodamine-phalloidin, actin filaments were found at each cell's cortical and perinuclear areas (**Figure 2**). Actin filaments provide structural stability to the plasma membrane and contribute to the polarization and anchoring of nuclei within a cell (Davidson and Cadot, 2020), which, in turn, are developmentally programmed and associated with the cell function (Smith, 2003; Starr and Han, 2003; Gu et al., 2005). In the central cell of *A. inaequidens*, cortical actin filaments were restricted to the cell periphery, alongside the plasma membrane, while most of the space was occupied by

its large vacuole (**Figures 2A**, **4A**). The link between the actin cytoskeleton and vacuole structure has been previously studied in *Arabidopsis* root epidermal and egg cells, as well as in Tobacco somatic BY-2 cells, showing that the size and dynamics of vacuoles are F-actin-dependent (Higaki et al., 2006; Kimata et al., 2016; Scheuring et al., 2016).

A. inaequidens possesses a highly chalazal polarized central cell nucleus, whose position seems to depend on the actin filaments displayed between the nucleus and the central cell plasma membrane (**Figures 2A,B**). The positioning of the central cell nucleus by actin filaments was demonstrated by Kawashima and Berger (2015), who disrupted central cell F-actin in *A. thaliana* mature embryo sacs causing a shift of the central cell nucleus from its micropylar to a central position.

After pollination, cortical and perinuclear actin filaments at the central cell gradually changed their configuration, which finally formed an "actin tunnel" mainly composed of several parallel actin cables running from the central cell nucleus to the ovular apparatus at the opposite pole (**Figure 3C** and **Supplementary Video 1**). Considering the spatio-temporal establishment of the actin tunnel in *A. inaequidens,* it seems to represent the functional equivalent of the actin cables meshwork of *Arabidopsis* central cell, which show an inward (plasma membrane to nucleus) movement associated with the sperm nuclear migration (Kawashima et al., 2014). Nevertheless, the structure and organization of actin filaments in both systems are distinct. While in *Arabidopsis* central cell F-actin forms a mesh-like structure growing from and attached to the plasma membrane by formins and ROP8, *Agave* actin-tunnel is predominantly formed by parallel actin cables that run along the chalazal-micropylar axis from the central cell nucleus (**Figure 3C** and **Supplementary Video 1**). When Ali et al. (2020) inhibited the myosin activity with 50 mM BDM (2, 3-butanedione monoxime) in the *Arabidopsis* central cell, they observed the straightening of the F-actin meshwork, which adopted a similar configuration to those observed in *Agave*.

The exact physiological role of the actin tunnel is intriguing as it is associated with the fertilization process here. Because of the opposite polarity of the tunnel cables (central cell nucleus to the micropylar plasma membrane), it is unlikely they have a homologous function to the mesh-like structure of *Arabidopsis* that seems to escort the sperm nucleus in its transit to the central cell nucleus (Kawashima et al., 2014). Alternatively, *Agave* actin tunnel could have a role in remodeling the central cell vacuole as suggested by the positioning of the tunnel cables, the timing of their development, and the appearance of a trans-vacuolar strand necessary for the transit of the sperm nucleus that fertilizes the central cell (**Figures 4**, **5A,B**).

This trans-vacuolar strand, which traversed the central cell vacuole and was putatively composed of cytoplasm, was observed in Feulgen-stained ovules whose pollen tube had already arrived at one of the synergids (**Figures 4**, **5A,B** and **Supplementary Video 2**). After plasmogamy, *Agave* sperm nuclei were detected in different regions of the cytoplasmic strand from the egg cell boundary to the border of the central cell nucleus (**Figures 5A,B**). In *Torenia fournieri,* a similar thick cytoplasmic strand appeared above the ovular apparatus approximately 15 HAP and 5 h after karyogamy of the first sperm nucleus with the egg cell one (Higashiyama et al., 1997). In tobacco, after plasmogamy, some cytoplasmic strands appeared between the sperm nucleus and the central cell nucleus, allowing the former to migrate (Peng et al., 2017). In the presence of cytochalasin B, the cytoplasmic strands were disrupted, and the sperm nucleus migration was prevented (Peng et al., 2017).

Transvacuolar strands also aid in the mobility of polar nuclei, which fuse to form the central cell nucleus. In *Polianthes tuberosa,* another member of the Asparagaceae family, before the migration of the micropylar polar nucleus toward the chalazal end, where the other polar nucleus is located, a thin cytoplasmic strand appears traversing the central vacuole and connecting both polar nuclei (Gonzalez-Gutierrez and Rodriguez-Garay, 2016). Similarly, analysis of the developmental dynamics of *A. thaliana* female gametophyte demonstrated that the migration of polar nuclei occurs through the middle (Susaki et al., 2021) but not along the periphery of the cell (Higaki et al., 2006). Therefore, dynamic changes in the central vacuole could be involved (Susaki et al., 2021).

In agreement with the previous observation, the apparition of the trans-vacuolar strand in *Agave*, and the movement of the sperm nucleus through it was simultaneous with the emergence of a vigorous F-actin mega-cable that extended from the central cell nucleus to the micropylar end (**Figures 5C,D**). Because of the similar position of the cytoplasmic strand and the F-actin mega-cable within the embryo sac, it is reasonable to hypothesize that the latter fills the space created by the cytoplasmic strand to allow the transit of the sperm nucleus. It is well known that actin filaments are involved in cytoplasmic streaming and that cytoplasmic strands function as transport routes for proteins and organelles (Shimmen and Yokota, 2004). In *A. inaequidens*, the actin mega-cable seems to be the functional equivalent of *Arabidopsis* actin track and aster-like structure associated with the migration of the second sperm nucleus during central cell fertilization (Kawashima et al., 2014). Nevertheless, due to the differences between both structures, the mechanistic implications are also different. While the actin track and the aster-like structure are pleomorphic and do not connect the sites of plasmogamy and karyogamy, the mega-cable establishes a continuous connection between the central cell nucleus and its micropylar end, where most probably the second plasmogamy occurs (**Figure 5C**). There, the sperm nucleus may be taken and actively transported by the mega-cable until it gets in touch with the central cell nucleus (**Figure 5D**). In addition to *Agave*, F-actin mega-cables have been observed in other Asparagaceae members such as *Prochnyantes, Yucca, and Manfreda* (González-Gutiérrez et al., 2020).

Although our staining methodology did not allow either higher-resolution or live imaging, our observations suggest that the fertilizing sperm nucleus is wrapped by the F-actin mega-cable, implying that an actin-associated motor protein does not move the sperm nucleus. Instead, the sperm nucleus might be transported together with the mega-cable by a treadmilling mechanism. Although these observations demonstrate a direct association of the actin mega-cable with the second sperm nucleus migration, the sperm nucleus transporting mechanism should be further investigated. Comparative diagrams summarizing the principal differences and similarities

between the F-actin structures during the second fertilization of *Agave* and *Arabidopsis* are shown in **Figures 5E,F**.

Our observations suggest the actin tunnel, but especially the actin-mega cable might be an evolutionary solution in these plant species to the challenge of transporting an immotile sperm nucleus a long distance. Despite the actin tunnel and the mega cable seem to have functional analogs in *Arabidopsis* central cell fertilization (the track and the aster-like structure), their structure and functional scope are clearly different. Why is the fertilizing sperm nucleus in *A. inaequidens* not moved by an aster-like structure? We hypothesize that the differences in F-actin structures developed on each system depend on the distance the sperm nucleus needs to be transported. Actin structures adopt different configurations depending on the distance the cargo needs to be transported in plant cells. Individual or thin actin filaments are associated with short-range cargo targeting, while thicker actin cables are necessary for long-distance transport (Geitmann and Emons, 2000). Because of its thin-cable configuration, an aster-like structure might be more convenient for a short-range movement. Thus, as observed, a robust mega-cable seems a better solution for a long journey.

DATA AVAILABILITY STATEMENT

The original contributions presented in the study are included in the article/**Supplementary Material**, further inquiries can be directed to the corresponding author/s.

AUTHOR CONTRIBUTIONS

AGG-G performed the experimentation. AGG-G and BR-G designed the experiments. AGG-G, JV, and BR-G analyzed the data and drafted the manuscript. AG-M, JV, and BR-G wrote funding grants. All authors reviewed and approved the final version of the manuscript.

FUNDING

This study was supported by the Mexican National Council of Science and Technology (CONACyT-Mexico), project 544; Laboratorio Nacional PlanTECC CONACyT, project 315918; and COECyTJAL DyD, project 9296-2021.

ACKNOWLEDGMENTS

We thank Rosa Isela Martínez-Contreras for the technical support, José Aldana-Padilla for the drawings, and Hiram Rodríguez-Julián for the layout of the figures. We appreciate the efforts of three peer reviewers and editor for the improvement of this article. We also acknowledge the valuable work of CIATEJ administrative staff.

SUPPLEMENTARY MATERIAL

The Supplementary Material for this article can be found online at: https://www.frontiersin.org/articles/10.3389/fpls.2021.774098/full#supplementary-material

Supplementary Video 1 | The structure of the actin tunnel in an embryo of *Agave inaequidens* 32–36 HAP. The tunnel is formed by F-actin cables that run from the central cell nucleus at the chalazal end to the micropylar one, and generates a chamber where a vacuole might be contained.

Supplementary Video 2 | Feulgen stained *Agave inaequidens* embryo sac (38–42 HAP). After their release from the pollen tube, the two sperm cells stayed together at the chalazal pole of the degenerated receptive synergid cell. Video of a color-coded projection of z-stacked micrographs. Bar = 20 μm.

REFERENCES

Ali, M. F., Fatema, U., Peng, X., Hacker, S. W., Maruyama, D., Sun, M. X., et al. (2020). ARP2/3-independent WAVE/SCAR pathway and class XI myosin control sperm nuclear migration in flowering plants. *Proc. Natl. Acad. Sci. U.S.A.* 117, 32757–32763. doi: 10.1073/pnas.2015550117

Ali, M. F., and Kawashima, T. (2021). Formins control dynamics of F-actin in the central cell of *Arabidopsis thaliana*. *Plant Signal. Behav.* 16:1920192. doi: 10.1080/15592324.2021.1920192

Angiosperm Phylogeny Group [APG III] (2009). An update of the Angiosperm Phylogeny Group classification for the orders and families of flowering plants. *Bot. J. Linn. Soc.* 161, 105–121. doi: 10.1111/j.1095-8339.2009.00996.x

Barranco-Guzmán, A. M., González-Gutiérrez, A. G., and Rodríguez-Garay, B. (2019). The embryo sac development of *Manfreda elongata* (Asparagaceae). *Flora* 260:151480. doi: 10.1016/j.flora.2019.151480

Barrell, P. J., and Grossniklaus, U. (2005). Confocal microscopy of whole ovules for analysis of reproductive development: the *elongate1* mutant affects meiosis II. *Plant J.* 43, 309–320. doi: 10.1111/j.1365-313X.2005.02456.x

Berger, F., Hamamura, Y., Ingouff, M., and Higashiyama, T. (2008). Double fertilization caught in the act. *Trends Plant Sci.* 13, 437–443. doi: 10.1016/j.tplants.2008.05.011

Bhojwani, S. S., and Bhatnagar, S. P. (1983). *The Embryology of Angiosperms*. New Delhi: Vikas Publishing House Pvt. Ltd.

Chebli, Y., Kroeger, J., and Geitmann, A. (2013). Transport logistics in pollen tubes. *Mol. Plant* 6, 1037–1052. doi: 10.1093/mp/sst073

Chieco, P., and Derenzini, M. (1999). The Feulgen reaction 75 years on. *Histochem. Cell Biol.* 111, 345–358. doi: 10.1007/s004180050367

Davidson, P. M., and Cadot, B. (2020). Actin on and around the nucleus. *Trend. Cell Biol.* 31, 211–223. doi: 10.1016/j.tcb.2020.11.009

Davis, G. L. (1966). *Systematic Embryology of the Angiosperms*. New York, NY: Wiley.

Dresselhaus, T., Sprunck, S., and Wessel, G. M. (2016). Fertilization mechanisms in flowering plants. *Curr. Biol.* 26, R125–R139. doi: 10.1016/j.cub.2015.12.032

Figueredo, C. J., Casas, A., Colunga-GarcíaMarín, P., Nassar, J. M., and González-Rodríguez, A. (2014). Morphological variation, management and domestication of 'maguey alto' (*Agave inaequidens*) and 'maguey manso' (*A. hookeri*) in Michoacán, México. *J. Ethnobiol. Ethnomed.* 10:66. doi: 10.1186/1746-4269-10-66

Geitmann, A., and Emons, A. M. C. (2000). The cytoskeleton in plant and fungal cell tip growth. *J. Microsc.* 198, 218–245. doi: 10.1046/j.1365-2818.2000.00702.x

Gentry, H. S. (1982). *Agaves of Continental North America*. Tucson: The University of Arizona Press.

González-Gutiérrez, A. G., Gutiérrez-Mora, A., and Rodríguez-Garay, B. (2014). Embryo sac formation and early embryo development in *Agave tequilana* (Asparagaceae). *SpringerPlus* 3:575. doi: 10.1186/2193-1801-3-575

Gonzalez-Gutierrez, A. G., and Rodriguez-Garay, B. (2016). Embryogenesis in *Polianthes tuberosa* L var. Simple: from megasporogenesis to early embryo development. *SpringerPlus* 5, 1–13. doi: 10.1186/s40064-016-3528-z

González-Gutiérrez, A. G., Verdín, J., and Rodríguez-Garay, B. (2020). Simple whole-mount staining protocol of F-Actin for studies of the female gametophyte in Agavoideae and other crassinucellate ovules. *Front. Plant Sci.* 11:384. doi: 10.3389/fpls.2020.00384

Gu, Y., Fu, Y., Dowd, P., Li, S., Vernoud, V., Gilroy, S., et al. (2005). A Rho family GTPase controls actin dynamics and tip growth via two counteracting downstream pathways in pollen tubes. *J. Cell Biol.* 169, 127–138. doi: 10.1083/jcb.200409140

Haig, D. (1990). New perspectives on the angiosperm female gametophyte. *Bot. Rev.* 56, 236–274. doi: 10.1007/BF02858326

Hamamura, Y., Saito, C., Awai, C., Kurihara, D., Miyawak, I. A., Nakagawa, T., et al. (2011). Live-cell imaging reveals the dynamics of two sperm cells during double fertilization in *Arabidopsis thaliana*. *Curr. Biol.* 21, 497–502. doi: 10.1016/j.cub.2011.02.013

Herr, J. M. Jr. (1984). "Embryology and taxonomy," in *Embryology of Angiosperms*, ed. B. M. Johri (New York, NY: Springer-Verlag), 647–691. doi: 10.1007/978-3-642-69302-1_14

Higaki, T., Kutsuna, N., Okubo, E., Sano, T., and Hasezawa, S. (2006). Actin microfilaments regulate vacuolar structures and dynamics: dual observation of actin microfilaments and vacuolar membrane in living tobacco BY-2 cells. *Plant Cell Physiol.* 47, 839–852. doi: 10.1093/pcp/pcj056

Higashiyama, T., Kuroiwa, H., Kawano, S., and Kuroiwa, T. (1997). Kinetics of double fertilization in *Torenia fournieri* based on direct observations of the naked embryo sac. *Planta* 203, 101–110. doi: 10.1007/s00050170

Holloway, S. J., and Friedman, W. E. (2008). Embriological features of *Tofieldia glutinosa* and their bearing on the early diversification of monocotyledonous plants. *Ann. Bot.* 102, 167–182. doi: 10.1093/aob/mcn084

Huang, B. Q., and Russell, S. D. (1994). Fertilization in *Nicotiana tabacum*: cytoskeletal modifications in the embryo sac during synergid degeneration. A hypothesis for short-distance transport of sperm cells prior to gamete fusion. *Planta* 195, 200–214. doi: 10.1007/BF01101679

Jensen, W. A. (1973). Fertilization in flowering plants. *Bioscience* 23, 21–27. doi: 10.2307/1296363

Kalinowska, K., Chen, J., and Dresselhaus, T. (2020). "Imaging of embryo sac and early seed development in Maize after Feulgen staining," in *Plant Embryogenesis. Methods in Molecular Biology*, Vol. 2122, ed. M. Bayer (New York, NY: Humana). doi: 10.1007/978-1-0716-0342-0_14

Kawashima, T., and Berger, F. (2015). The central cell nuclear position at the micropyle is maintained by the balance of F-actin dynamics, but dispensable for karyogamy in *Arabidopsis*. *Plant Reprod.* 28, 103–110. doi: 10.1007/s00497-015-0259-1

Kawashima, T., Maruyama, D., Shagirov, M., Li, J., Hamamura, Y., Yelagandula, R., et al. (2014). Dynamic F-actin movement is essential for fertilization in *Arabidopsis thaliana*. *eLife* 3:e04501. doi: 10.7554/eLife.04501

Kimata, Y., Higaki, T., Kawashima, T., Kurihara, D., Sato, Y., Yamada, T., et al. (2016). Cytoskeleton dynamics control the first asymmetric cell division in *Arabidopsis* zygote. *Proc. Natl. Acad. Sci. U.S.A.* 113, 14157–14162. doi: 10.1073/pnas.1613979113

López-Díaz, S., and Rodríguez-Garay, B. (2008). Simple methods for *in vitro* pollen germination and pollen preservation of selected species of the genus *Agave*. *e-Gnosis* 6, 1–7. doi: 10.15625/2615-9023/15888

Maheshwari, P. (1950). *An Introduction to the Embryology of Angiosperms*. New York, NY: McGraw-Hill, 65–67.

Ohnishi, Y., Hoshino, R., and Okamoto, T. (2014). Dynamics of male and female chromatin during karyogamy in rice zygotes. *Plant Physiol.* 165, 1533–1543. doi: 10.1104/pp.114.236059

Ohnishi, Y., and Okamoto, T. (2017). Nuclear migration during karyogamy in rice zygotes is mediated by continuous convergence of actin meshwork toward the egg nucleus. *J. Plant Res.* 130, 339–348. doi: 10.1007/s10265-016-0892-2

Palser, B. F. (1975). The bases of angiosperm phylogeny: embryology. *Ann. Missouri Bot. Gard.* 62, 621–646. doi: 10.2307/2395269

Peng, X., Yan, T., and Sun, M. (2017). The WASP-Arp2/3 complex signal cascade is involved in actin-dependent sperm nuclei migration during double fertilization in tobacco and maize. *Sci. Rep.* 7:43161. doi: 10.1038/srep43161

Rudall, P. J. (1997). The nucellus and chalaza in monocotyledons: structure and systematics. *Bot. Rev.* 63, 140–181. doi: 10.1007/BF02935930

Russell, S. D. (1978). Fine structure of megagametophyte development in *Zea mays*. *Can. J. Bot.* 57, 1093–1110. doi: 10.2307/2440968

Scheuring, D., Löfke, C., Krüger, F., Kittelmann, M., Eisa, A., Hughes, L., et al. (2016). Actin-dependent vacuolar occupancy of the cell determines auxin-induced growth repression. *Proc. Natl. Acad. Sci. U.S.A.* 113, 452–457. doi: 10.1073/pnas.1517445113

Shimmen, T., and Yokota, E. (2004). Cytoplasmic streaming in plants. *Curr. Opin. Cell Biol.* 16, 68–72. doi: 10.1016/j.ceb.2003.11.009

Smith, L. G. (2003). Cytoskeletal control of plant cell shape: getting the fine points. *Curr. Opin. Plant Biol.* 6, 63–73. doi: 10.1016/s1369-5266(02)00012-2

Sprunck, S., and Gross-Hardt, R. (2011). Nuclear behavior, cell polarity, and cell specification in the female gametophyte. *Sex Plant Reprod.* 24, 123–136. doi: 10.1007/s00497-011-0161-4

Starr, D. A., and Han, M. (2003). ANChors away: an actin-based mechanism of nuclear positioning. *J. Cell Sci.* 116, 211–216. doi: 10.1242/jcs.00248

Susaki, D., Suzuki, T., Maruyama, D., Ueda, M., Higashiyama, T., and Kurihara, D. (2021). Dynamics of the cell fate specifications during female gametophyte development in *Arabidopsis*. *PLoS Biol.* 19:e3001123. doi: 10.1371/journal.pbio.3001123

Tilton, V. R. (1978). *A Developmental and Histochemical Study of the Female Reproductive System in Ornithogalum caudatum Ait. Using and Electron Microscopy*. Ph.D. thesis. Ames, IA: Iowa State University.

Tilton, V. R., and Lersten, N. R. (1981). Ovule development in *Ornithogalum caudatum* (Liliaceae) with a review of selected papers on angiosperm reproduction. III. Nucellus and megagametophyte. *New Phytol.* 88, 477–504. doi: 10.1111/j.1469-8137.1981.tb04094.x

Tobe, H. (1989). The embryology of Angiosperms: its broad application to systematic and evolutionary study. *Bot. Mag. (Tokyo)* 102, 351–367.

Torres-García, I., Casas, A., García-Mendoza, A. J., and González-Elizondo, M. (2019). *Agave Inaequidens. The IUCN Red List of Threatened Species 2019: e.T115630140A116353958*. Available online at: https://dx.doi.org/10.2305/IUCN.UK.2019-3.RLTS.T115630140A116353958.en. (accessed August 28, 2021).

Wallwork, M. A. B., and Sedgley, M. (2000). Early events in the penetration of the embryo sac in *Torenia fournieri* (Lind.). *Ann. Bot.* 85, 447–454. doi: 10.1006/anbo.1999.1093

Webb, M. C., and Gunning, B. E. S. (1990). Embryo sac development in *Arabidopsis thaliana:* megasporogenesis, including the microtubular cytoskeleton. *Sex. Plant Rep.* 3, 244–256. doi: 10.1007/BF00202882

Williams, J. H., and Friedman, W. E. (2004). The four-celled female gametophyte of *Illicium* (Illiciaceae; Austrobaileyales): implications for understanding the origin and early evolution of monocots, eumagnoliids, and eudicots. *Am. J. Bot.* 91, 332–351. doi: 10.3732/ajb.91.3.332

Ye, X.-L., Yeung, E. C., and Zee, S.-Y. (2002). Sperm movement during double fertilization of a flowering plant, *Phaius tankervilliae*. *Planta* 215, 60–66. doi: 10.1007/s00425-002-0736-2

Zhang, Z., and Russell, S. D. (1999). Sperm cell surface characteristics of *Plumbago zeylanica* L. in relation to transport in the embryo sac. *Planta* 208, 539–544. doi: 10.1007/s004250050591

Conflict of Interest: The authors declare that the research was conducted in the absence of any commercial or financial relationships that could be construed as a potential conflict of interest.

Publisher's Note: All claims expressed in this article are solely those of the authors and do not necessarily represent those of their affiliated organizations, or those of the publisher, the editors and the reviewers. Any product that may be evaluated in this article, or claim that may be made by its manufacturer, is not guaranteed or endorsed by the publisher.

frontiers | Frontiers in Plant Science

TYPE Original Research
PUBLISHED 26 July 2022
DOI 10.3389/fpls.2022.946781

OPEN ACCESS

EDITED BY
Giampiero Cai,
University of Siena, Italy

REVIEWED BY
Hannes Vogler,
University of Zurich, Switzerland
Jorge Lora,
Spanish National Research Council (CSIC), Spain

*CORRESPONDENCE
Kefeng Fang
fangkefeng@126.com
Ling Qin
qinlingbac@126.com

SPECIALTY SECTION
This article was submitted to Plant Cell Biology, a section of the journal Frontiers in Plant Science

RECEIVED 18 May 2022
ACCEPTED 04 July 2022
PUBLISHED 26 July 2022

CITATION
Zhang W, Zhang Q, Xing Y, Cao Q, Qin L and Fang K (2022) Effect of boron toxicity on pollen tube cell wall architecture and the relationship of cell wall components of *Castanea mollissima* Blume. *Front. Plant Sci.* 13:946781. doi: 10.3389/fpls.2022.946781

Effect of boron toxicity on pollen tube cell wall architecture and the relationship of cell wall components of *Castanea mollissima* Blume

Weiwei Zhang[1,2,3], Qing Zhang[2], Yu Xing[1,2], Qingqin Cao[1,2], Ling Qin[1,2]* and Kefeng Fang[1,4]*

[1]Beijing Advanced Innovation Center for Tree Breeding by Molecular Design, Beijing University of Agriculture, Beijing, China, [2]Key Laboratory for Agricultural Application and New Technique, College of Plant Science and Technology, Beijing University of Agriculture, Beijing, China, [3]Beijing Bei Nong Enterprise Management Co. Ltd, Beijing, China, [4]College of Landscape Architecture, Beijing University of Agriculture, Beijing, China

Boron (B) is essential to plant development. However, excessive B is toxic to plants. This research was performed to evaluate the effects of B toxicity on cell wall architecture of Chinese chestnut (*Castanea mollissima* Blume) pollen tubes with emphasis on the relationship among pectins, cellulose, and callose. Results showed that 0.8 mM H_3BO_3 inhibited pollen germination and led to abnormal morphology of the pollen tubes. B toxicity also affected the distribution of cell wall components of the pollen tube. In control pollen tube, esterified and acid pectins were distributed unevenly, with the former mainly at the tip and the latter on the distal region. Cellulose was distributed uniformly on the surface with less at the tip; callose reduced gradually from base to sub-tip of the pollen tubes and no callose at the tip of the tube was detected. B toxicity led to the deposition of esterified and acid pectins, cellulose, and callose at the tip of the pollen tube. Results from scanning electron microscopy and transmission electron microscopy showed that B toxicity also altered pollen tube wall ultrastructure. The results from enzymatic treatment illustrated that there existed a close relationship among pectins, cellulose, and callose. B toxicity also altered the relationship. In a word, B toxicity altered deposition and relationship of pectins, cellulose, and callose of pollen tube wall.

KEYWORDS

***Castanea mollissima* Blume, boron toxicity, pollen tube, pectin, callose, ultrastructure**

Introduction

Boron (B) is essential to the normal development of higher plants (Warington, 1923; Brdar-Jokanović, 2020). To date, B is defined as a crosslinking molecule in plant cell walls (Landi et al., 2019) and plays a structural role in the plasma membrane (Voxeur and Fry, 2014). The concentration range is narrow from deficiency to toxicity for B in higher plants (Matthes et al., 2020; Behera et al., 2022). B toxicity influences various

developmental processes such as hindering glutathione (Ruiz et al., 2003) and tocopherol formation (Keles et al., 2004), decreasing root cell division (Aquea et al., 2012), inducing reactive oxygen species (ROS) (Cervilla et al., 2007), changing the photosynthesis (Landi et al., 2013; Papadakis et al., 2018), expression of genes (Sakamoto et al., 2011; Aquea et al., 2012) altering signal transduction and biomacromolecule metabolism, thickening cell wall irregularly (Huang et al., 2014; Sang et al., 2017; Seth and Aery, 2017; Papadakis et al., 2018; Wu et al., 2018), and losing the balance of the C/N ratio (Sotiras et al., 2019). The research on leaf tissue of two citrus rootstocks showed that B toxicity resulted in damage to the pectin crosslinking structure, B deficiency induced more accumulation of cellulose (Wu et al., 2018), and miRNA397a regulated secondary cell-wall biosynthesis to tolerate the long-term B toxicity by targeting two laccase genes, *LAC17* and *LAC4* (Huang et al., 2016).

In angiosperm, the pollen tube carries a pair of sperm cells to fertilize the egg cell and the central cell, respectively, in the embryo sac to complete double fertilization. During this process, pollen tubes grow from their tips very fast and demand a great quantity of membrane and cell wall precursors to form the new cell wall (Zhang et al., 2010; Bou and Geitmann, 2011). Geitmann and Steer (2006) summarized that the pollen tube cell wall had several functions in growth including acting as physical control of cell shape, protecting the generative cell (sperm cells) from mechanical damage, resisting the turgor pressure, and adhering to the transmitting tissue. Thus, the pollen tube cell wall takes an active part in the process of fertilization. The pollen tube wall has been reported to be consisting of cellulose, callose pectins, and other components, such as hemicelluloses and proteins (Li et al., 1996, 2002; Ferguson et al., 1998). Esterified pectins are produced by the Golgi apparatus and transported to the pollen tube extreme tip (Hasegawa et al., 1998), where the esterified pectins are de-esterified to be acid pectins by the enzyme pectin methyl-esterase (PME) (Li et al., 2002). The crosslinks between the acidic residue of acid pectins and Ca^{2+} ions form a semi-rigid pectate gel (Braccini and Perez, 2001), which supports mechanically pollen tube elongation.

As a monoecious plant,the ratio of female and male flowers can reach 1:2400–4000 in Chinese chestnut (*Castanea mollissima* Blume). The male flowers consumed much nutrition, which influenced nutrition distribution and development of female flowers, and even causing empty bur phenomenon. And in field production, farmers sprayed boric acid to increase the fruit setting percentage. However, the amount of boric acid sprayed was difficult to measure, and the long-term spraying would induce boron accumulation in plants. Therefore, the study on the effects of B toxicity on Chinese chestnut pollen germination and pollen tube wall components is of great significance to improve yield.

As we know, B is essential for pollen germination and tube growth (Obermeyer et al., 1996; Fang et al., 2016), making the pollen a good system with which to study the effect of B toxicity. In our previous research, we found that B toxicity inhibited apple pollen tube growth by disrupting Ca^{2+} influx (Fang et al., 2016). However, the detailed effects of B toxicity on pollen tube wall components and ultrastructure remain to be clarified. In the present study, *Castanea mollissima* pollen was used as the material to study the influence of B toxicity on pollen tube growth, with focus on cell wall components, ultrastructure, and relationship among pectins, cellulose, and callose.

Materials and methods

Plant materials and culture procedure

Mature pollen grains were collected on 10 June 2018 from *C. mollissima* in the Chestnut Experiment Station in the Huairou District of Beijing, China. Then, they were placed on paper towels for 15 h at room temperature, and were stored in a refrigerator at -20°C.

The culture medium for *C. mollissima* pollen grain included 15% (w/v) sucrose and 3.6 mM $CaCl_2$. Different concentrations of H_3BO_3 (Sigma, St. Louis, MO, USA), 0, 0.08 mM, 0.4 mM, and 0.8 mM, were added to the culture medium at the beginning, pH 5.8. The pollen grains were cultured at 34°C in the darkness.

After 27 h of culture, the pollen germination rates were calculated as previously described (Fang et al., 2016) under a BX51 microscope (Olympus, Japan) with a CoolSNAP HQ CCD camera (Photometrics). Five hundred pollen grains were counted in each experiment to calculate germination rates, which was repeated three times. The length and diameter of 150 pollen tubes were measured with MetaMorph (Universal Imaging). Three independent experiments were performed. Based on the germination rate and morphology of the pollen tube (the swelling of the tube tip), the concentrations of boron at 0.08 mM and 0.8 mM were used as control and toxicity treatment for further tests, respectively.

Enzymatic treatment

After being cultured for 27 h, the pollen tubes were treated with 1% cellulase, pectinase, and β-1,3-glucanase (soluble in 100 mM Phosphate buffer, PBS) (Sigma, St. Louis, MO, USA), respectively, to detect the relationship among pectins, cellulose, and callose.

Fluorescent localization of cell wall components

The cultured pollen tubes were fixed with 3% paraformaldehyde (soluble in 100 mM PBS) before labeling

and staining. The esterified and acid pectins of pollen tubes were reacted first with the monoclonal antibodies JIM7 and JIM5 (provided by Dr Knox JP, diluted at 1:20), then with the secondary antibody FITC-labeled sheep anti-rat IgG (Sigma, St. Louis, MO, USA, diluted at 1:100 in PBS) according to Fang et al. (2016). The labeled pollen tubes were observed under the laser scanning confocal microscope (LSCM, Leica Co., Germany) with the excitation wavelength at 488 nm and emission wavelength at 515 nm, respectively. The above procedure without the monoclonal antibody was set as control.

For cellulose localization, the cultured pollen tubes were incubated with primary probe CBM3a (diluted at 1:100 in PBS) for 1 h, and second antibody:mouse anti-HIS (diluted at 1:100 in PBS), and finally incubated with tertiary antibody:anti-mouse:FITC (diluted at 1:50 in PBS). For callose localization, pollen tubes were first incubated with the monoclonal antibody to (1→ 3)-β-glucan (Cat. No. 400-2, Biosupplies Australia, diluted at 1:50 in PBS) and then incubated with the second antibody:anti-mouse:FITC (diluted at 1:50 in PBS). The labeled pollen tubes were observed under the LSCM (Leica Co., Germany) with the excitation wavelength at 488 nm and emission wavelength at 515 nm, respectively.

The relative intensity of the fluorescent signals from esterified and acid pectins, cellulose, and callose was measured with Image-Pro Plus 6.0 software (http://www.mediacy.com/) according to Fang et al. (2016). At least six pollen tubes of each treatment were measured. The fluorescent signals were measured along with the tube wall from the pole of the tube to the pollen grain, and the average fluorescence intensity was shown; the data of intensity were shown in Supplementary Table S1.

Fourier transform infrared analysis of tube wall components

The cultured pollen tubes were collected by centrifugation, then washed three times with deionized water, and dried in a layer on a barium fluoride wafer in 28°C incubators. The infrared (IR) spectra of the pollen tubes were recorded using a MAGNA 750 FTIR spectrometer (Nicolet Corp., Japan). At least nine pollen tubes were tested for each treatment, which was repeated three times.

Scanning electron microscopy (SEM)

For scanning electron microscopy, 2.5% glutaraldehyde in 100 mM PBS (pH 7.2) with 2% (w/v) sucrose was applied to fix pollen tubes for 2 h. Next, the pollen tubes were washed with 100 mM phosphate buffer. After that, the pollen tubes were post-fixed in 2% osmium tetroxide (soluble in deionized water) for 1 h, dehydrated in an ethyl-alcohol series, and then displaced with tret-butanol, and finally dried with a VFD-215 freeze-drying apparatus. Dried pollen tubes were placed on SEM stubs, coated with gold-palladium (Polaron SC7620; VG Microtech, Uckfield, UK), and examined with a TESCAN 5136 SEM (TESCAN Com., Czech).

Transmission electron microscope (TEM)

For transmission electron microscopy, 2.5% glutaraldehyde in 100 mM PBS (pH 7.2) with 2% (w/v) sucrose was applied to fix pollen tubes for 2 h. After that, the pollen tubes were washed with 100 mM phosphate buffer. Then, the pollen tubes were post-fixed in 2% osmium tetroxide (soluble in deionized water) for 1 h, dehydrated in an ethyl-alcohol series, and finally embedded in Spur resin. Ultrathin sections (50 nm) were cut on an ultramicrotome (EM UC6&FC6, Leica, Germany), examined with a TEM (JEOL Ltd., Tokyo, Japan), and imaged with a CCD camera (H7650, HITACHI, Japan).

Statistical analysis

Sigma Plot 10.0 was used to produce line charts of the data. IBM SPSS Statistics v20 was used for statistical analysis, and data were analyzed by ANOVA and Duncan's test. All statistical tests were performed at $P = 0.05$.

Results

Effects of B toxicity on pollen germination and tube growth

B affected pollen germination. Pollen germination rate was 21.89% without H_3BO_3, while it was 31.60% with 0.08 mM H_3BO_3. However, 0.8 mM H_3BO_3 made the germination rate decrease to 14.57%. In the following research, 0.08 mM H_3BO_3 was used as control, while 0.8 mM H_3BO_3 was used as a B toxicity treatment.

B also affected pollen tube growth. After 27 h of culture, the tube length was only 15.08 μm without H_3BO_3, while it was 38.22 μm and 39.82 μm with 0.08 mM and 0.8 mM H_3BO_3, respectively (Table 1). No obvious difference existed concerning the pollen tube length of control and B toxicity.

B toxicity led to abnormal morphology of pollen tube. Control pollen tubes were straight with a slender uniform diameter (Figures 1A,B); however, B toxicity-treated pollen tube tip was swollen with a larger diameter (Figures 1C,D). The tube width is shown in Table 1, and the tube width was 5.53 μm without H_3BO_3 and 5.71 μm with 0.08 mM H_3BO_3, while it reached 20.91 μm with 0.8 mM H_3BO_3.

10.3389/fpls.2022.946781

Effects of B toxicity on pectins of pollen tube

B toxicity induced more esterified pectins at the pollen tube wall (Figure 2). In the control pollen tube, esterified pectins distributed uniformly along the whole tube (Figure 2A), while B toxicity induced much more esterified pectins along the whole tube (Figure 2B). Fluorescent intensity data supported the above results (Figure 2C).

B toxicity affected the distribution of acid pectins on pollen tubes. In the control pollen tube, acid pectins are mainly distributed on the surface beyond the tip (Figure 2D). B toxicity strengthened acid pectins at the wall near grain and tip (Figure 2E). Fluorescent intensity supported the above results (Figure 2F).

TABLE 1 Germination rate and length of *C. mollissima* pollen tubes under different concentrations of H_3BO_3.

H_3BO_3 treatment/mM	Germination rate/%	Pollen tube length/μm	Pollen tube width/μm
0	21.89 ± 1.68 ab	25.80 ± 0.75 b	5.53 ± 0.26 c
0.08	31.60 ± 0.45 a	38.22 ± 0.36 a	5.71 ± 0.20 c
0.4	19.78 ± 1.55 b	39.10 ± 0.53 a	16.23 ± 3.34 b
0.8	14.57 ± 1.04 c	39.82 ± 2.84 a	20.91 ± 1.37 a

Different letters indicate statistically significant differences between pollen tubes grown in various condition ($P \leq 0.05$).

Effects of B toxicity on cellulose and callose of pollen tube

B toxicity stimulated accumulation of cellulose at the pollen tube tip. Fluorescent signals of cellulose appeared through the control pollen tube except for the tip (Figure 3A). However, B toxicity induced the accumulation of cellulose at the pollen tube tip (Figure 3B). Fluorescent intensity also supported the above results (Figure 3C).

Similar to cellulose distribution, B toxicity stimulated the accumulation of callose at the pollen tube tip. Stronger fluorescent signals appeared through the control pollen tube except for the tip (Figure 3D). However, callose accumulated at the pollen tube tip after B toxicity treatment (Figure 3E). Fluorescent intensity also supported the above results (Figure 3F).

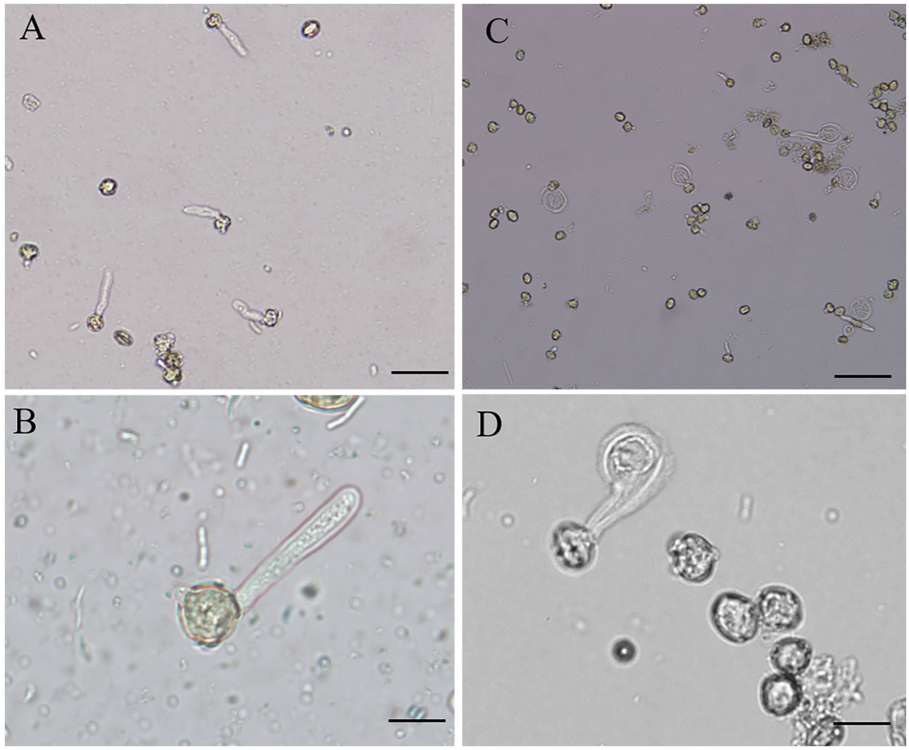

FIGURE 1
Morphology of *Castanea mollissima* pollen tubes under different culture conditions. Bar = 50 μm in A and C. Bar = 20 μm in B and D. **(A,B)** Pollen tubes in control medium. **(C,D)** Pollen tubes in B toxicity medium.

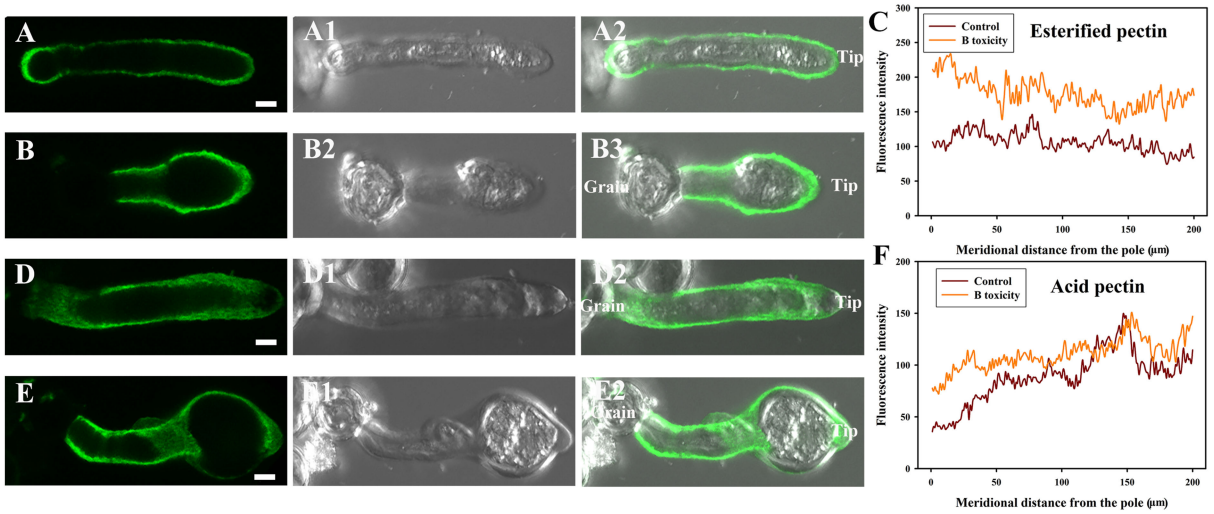

FIGURE 2
Influence of B toxicity on esterified and acid pectins distribution of *C. mollissima* pollen tube wall. **(A)** Esterified pectins in the control pollen tube indicated by JIM 7 labeling. **(B)** Esterified pectins in B toxicity-treated pollen tube. **(C)** Quantitative analysis of the fluorescent intensity of esterified pectins in the wall of control (Control) and B toxicity-treated pollen tubes (0.8 mM H_3BO_3). **(D)** Acid pectins in control pollen tube indicated by JIM 5 labeling. **(E)** Acid pectins in B toxicity-treated pollen tube. **(F)** Quantitative analysis of acid pectins fluorescent intensity in the wall of control (Control) and B toxicity-treated pollen tubes. Bar = 5 μm.

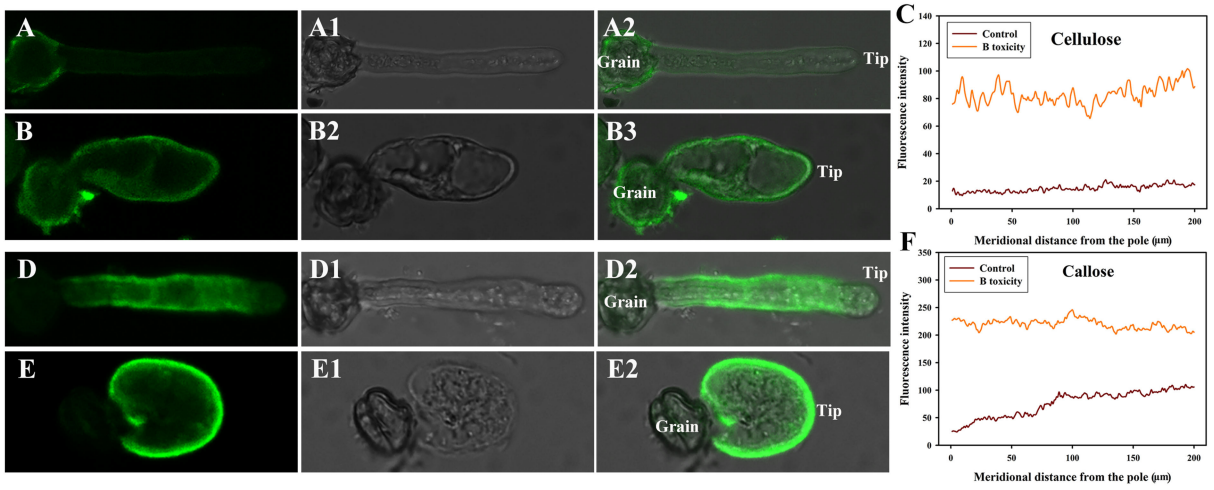

FIGURE 3
Effects of B on cellulose and callose distribution on *C. mollissima* pollen tube wall. **(A)** Cellulose in control pollen tube indicated by CBM3a labeling. **(B)** Cellulose in B toxicity-treated pollen tube. **(C)** Quantitative analysis of the fluorescent intensity of cellulose in the wall of control and B toxicity-treated pollen tubes. **(D)** Callose in control pollen tube indicated by monoclonal antibody to (1→ 3)-β-glucan labeling. **(E)** Callose in B toxicity-treated pollen tube. **(F)** Quantitative analysis of callose fluorescent intensity in the wall of control and B toxicity-treated pollen tubes. Bar = 10 μm.

Effects of B toxicity on pollen tube wall ultrastructure

The surface of the control pollen tube did not appear smooth but instead showed that cell wall material oriented slightly parallel to the direction of the tube elongation (Figure 4A). Control pollen tube was straight with many longitudinal furrows on the surface (Undulating outer layer). There were many longitudinal furrows on the swollen surface of B toxicity-treated pollen tubes (Figure 4B).

There were two layers of walls behind the tip of the control pollen tube namely the outer wall (OW, the fibrous pectic layer)

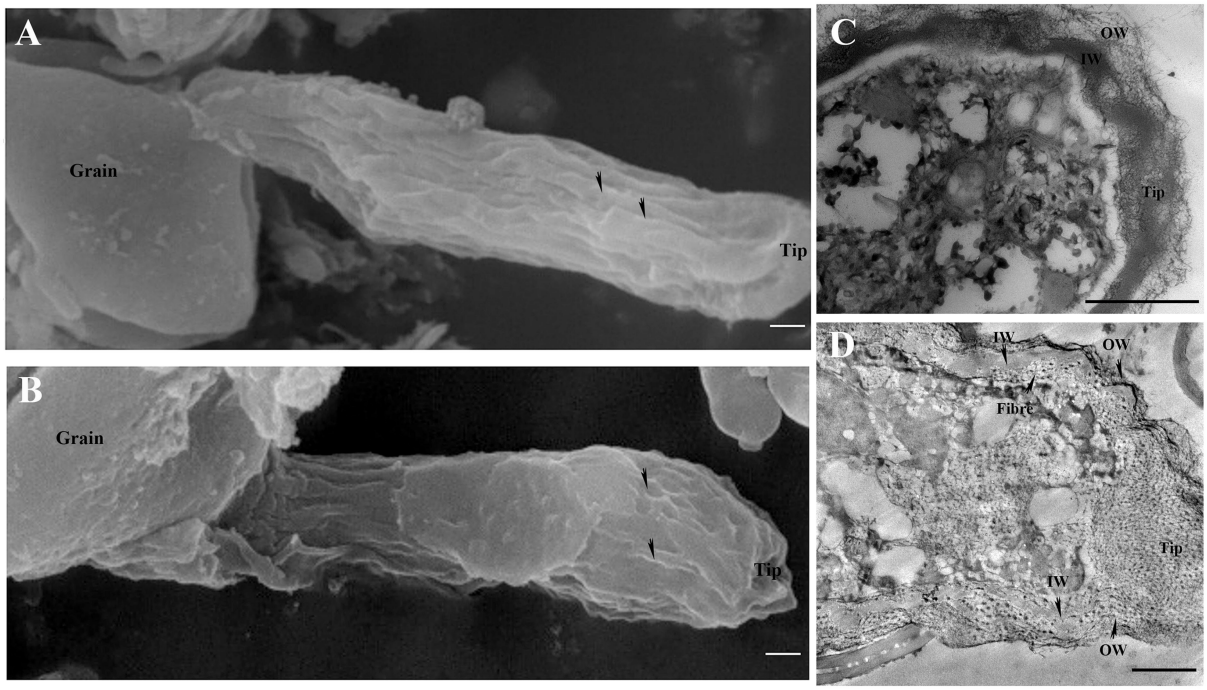

FIGURE 4
Effects of B toxicity on the ultrastructure of *C. mollissima* pollen tubes. **(A)** Scanning electron micrograph (SEM) of the control pollen tube. **(B)** SEM of B toxicity-treated pollen tube. **(C)** TEM transverse section of the control pollen tube. One layer (fibrous wall) exited in the tips, but two layers (fibrous pectic layer in the OW and callose layer in the IW) exited in the tubes. **(D)** TEM transverse section of B toxicity-treated pollen tube. The disorganized fibrous wall existed at the pollen tube tip. And the OW and IW were crosslinked and fiber exited inside of IW. OW, Outer wall; IW, inner wall. Bar = 3 μm in A and B; Bar = 1 μm in **(C,D)**. The arrows indicated longitudinal furrows in A and B.

and the inner wall (IW, callose layer) (Figure 4C). Only one layer of wall existed on the tip of the control pollen tube (Figure 4C). However, B toxicity induced two layers of the wall at the pollen tube tip with distorted microfibril at the tip (Figure 4D). And the wall was thicker than that of the control. B toxicity induced deposition of callose at the tip of the pollen tube, resulting in two layers of walls there. In the control pollen tube, the outer wall was thinner at the sub-tip, while it was thicker at the shank. B toxicity led to a very thick and disorganized fibrous outer wall at the tip.

FTIR spectroscopy analysis of pollen tube wall components

In the control pollen tube tip spectrum, the distinct peaks of saturated esters were at 1,734 cm^1, the peaks of protein were at 1,641 and 1,540 cm^{-1}, peaks of lignin and carboxylic acid were at 1,641, 1,399, and 1,233 cm^{-1}, the peaks of cellulose and hemicellulose were around 1,331 and 1,156 cm^{-1}, and the peaks of other polysaccharides were at 1,200 to 900 cm^{-1}. However, the peaks of lignin and carboxylic acid, cellulose, pectins, and polysaccharides increased in spectra of pollen tubes treated with B toxicity (Figure 5), indicating that B toxicity influenced the deposition of cell wall components, such as carboxylic acid, pectins, and cellulose on pollen tube cell walls of *C. mollissima*.

To study the role of B toxicity on the relationship between pollen tube wall components, cellulase, pectinase, and β-1,3-glucanase were used to treat the pollen tube, respectively. Results are shown below.

Effects of B toxicity on cell wall architecture with cellulase treatment

In treatment with cellulase, the pectins decreased to some extent, obviously esterified pectins in control pollen tubes (Figures 6A–F), and B toxicity reduced signals strongly at the tip. However, the acid pectin signals were still strong after cellulase treatment, and the signals of pollen tubes with B toxicity treatment were stronger than that of control pollen. What's more, the esterified and acid pectins were discontinuously distributed in the tube wall with cellulase treatment.

After cellulase treatment, the cellulose signals of control pollen tubes were detected difficultly, and the cellulose signals of pollen tubes with B toxicity treatment were stronger. But

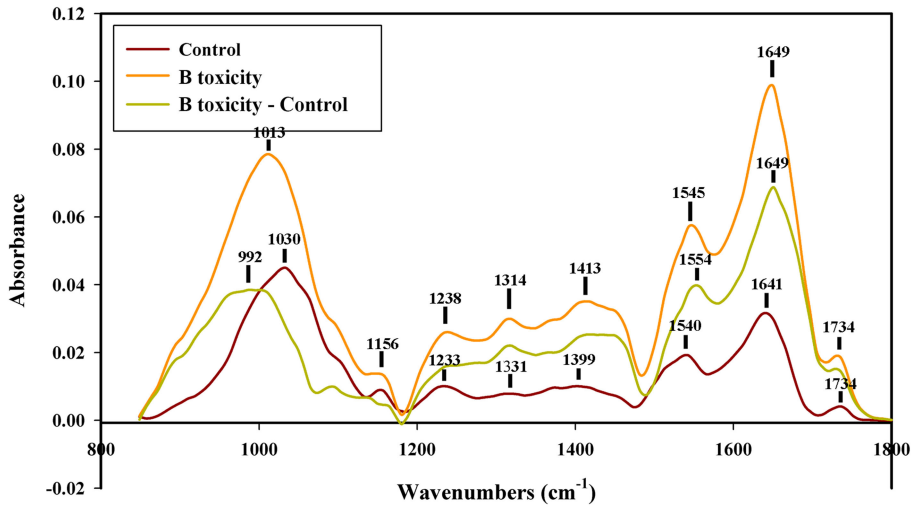

FIGURE 5
FTIR spectra from the tip regions of *C. mollissima* pollen tubes (control pollen tube: Control), B toxicity-treated pollen tubes and the FTIR differential spectrum (B toxicity−control) generated by digital subtraction of the control spectra from B toxicity-treated pollen tube spectra.

after cellulase treatment, the callose signals intensity had a little decrease in the tube wall, and the signals of pollen tubes with B toxicity treatment were stronger than that of control pollen tubes (Figures 6G–L).

Treatment with cellulase induced more obvious wave morphology at the control pollen tube surface (Figure 6M). There were many wave protuberances on the tip and swollen place of the pollen tube treated by B toxicity. Striped collaterals were distributed on the place except for the tip (Figure 6N).

Treatment with cellulase led to a very thin and loosened outer wall and inner wall of control pollen tubes (Figure 6O). However, it was difficult to distinguish the two layers of the wall under B toxicity treatment; a small number of fibers were present in OW, but much more fibers were crosslinked with the IW (Figures 6P,Q).

Effect of B toxicity on chemical components of pollen tube wall treated with cellulase was carried out with FTIR (Figure 6R). The results showed that the distinct peaks assigned to saturated esters (the peak at 1,734 cm^{-1}), proteins (the peaks at 1,639 and 1,540 cm^{-1}), lignin and carboxylic acid (the peaks at 1,399, and 1,233 cm^{-1}), cellulose and hemicellulose (the peaks around 1,331 and 1,156 cm^{-1}), and other polysaccharides (the peaks at 1,200–900 cm^{-1}) decreased in the control pollen tube spectrum and B toxicity increased the peaks assigned to lignin and carboxylic acid, cellulose, pectins, and polysaccharides, indicating that B toxicity influenced the deposition of cell wall components, such as carboxylic acid, pectins, and cellulose, in pollen tube cell walls of *C. mollissima*.

In a word, treatment with cellulase led to a discontinuous distribution of esterified pectins and acid pectins and decreased cellulose and callose content. There existed an intimate relationship among pectins, cellulose, and callose, which was supported by the ultrastructure.

Effects of B toxicity on cell wall architecture with pectinase treatment

No fluorescent signals of esterified pectins and acid pectins were detected on control and B toxicity treated pollen tube wall digested with pectinase treatment.

Weaker fluorescent signals of cellulose were detected on the whole control and B toxicity treated pollen tubes, the cellulose signals of B toxicity treated pollen tubes were stronger than in control pollen tubes (Figures 7A–C). Fluorescent signals of callose decreased after pectinase treatment (Figure 7D), but the callose signals at the tips of B toxicity-treated pollen tubes were stronger than that in control pollen tubes (Figures 7E,F).

Treatment with pectinase induced strip protuberances on the control pollen tube surface (Figure 7G). There were many wave protuberances on swollen pollen tubes treated with B toxicity (Figure 7H).

The microfibril of the control pollen tube treated with pectinase reduced substantially, only a small amount of fibers exited in OW and IW was difficult to be observed (Figure 7I). However, a small number of fibers were observed in OW, but the IW of B toxicity-treated pollen tubes was thick and much more fibers were crosslinked with the callose layer (Figures 7J,K).

Effect of B toxicity on chemical components of pollen tube wall treated with pectinase were carried out with FTIR

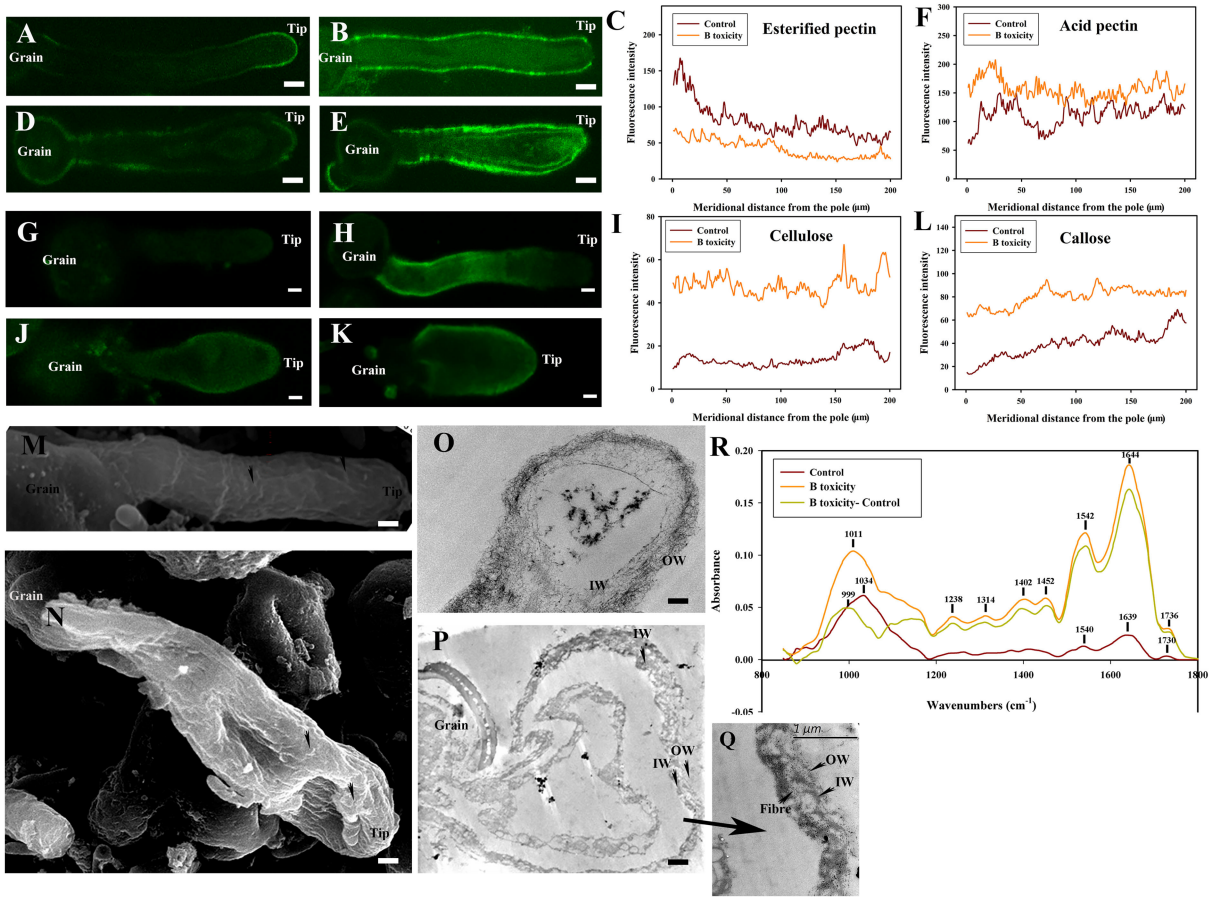

FIGURE 6
Effects of B toxicity on cell wall architecture with cellulase treatment. **(A)** Esterified pectins labeled with JIM7 in control pollen tube treated with cellulase. **(B)** Esterified pectins in B toxicity-treated pollen tube treated with cellulase. **(C)** Quantitative analysis of the fluorescent intensity of esterified pectins in the wall of control (Control) and B toxicity treated pollen tubes which were digested with cellulase. **(D)** Acid pectins indicated by JIM 5 labeling in control pollen tube treated with cellulase. **(E)** Acid pectins in B toxicity-treated pollen tube treated with cellulase. **(F)** Quantitative analysis of acid pectins fluorescent intensity in the wall of control pollen tubes (Control) and B toxicity-treated pollen tubes which were digested with cellulase. **(G)** Cellulose in control pollen tube digested with cellulase indicated by CBM3a labeling. **(H)** Cellulose in B toxicity-treated pollen tube and then digested with cellulase. **(I)** Quantitative analysis of the fluorescent intensity of cellulose in the wall of control (Control) and B toxicity-treated pollen tubes that were digested with cellulase. **(J)** Callose in control pollen tube indicated by monoclonal antibody to (1→ 3)-β-glucan labeling digested with cellulase. **(K)** Callose in B toxicity-treated pollen tube digested with cellulase. **(L)** Quantitative analysis of callose fluorescent intensity in the wall of control (Control) and B toxicity-treated pollen tubes that were digested with cellulase. **(M)** SEM of control pollen tube digested with cellulase. **(N)** SEM of B toxicity-treated pollen tube digested with cellulase. **(O)** TEM transverse section of control pollen tube digested with cellulase. The fibrous pectic layer in OW became loosened. **(P,Q)** TEM transverse section of B toxicity-treated pollen tube digested with cellulase. A small number of fibers were present in OW, but much more fibers were crosslinked with the callose layer. **(R)** FTIR spectra from the tip regions of *C. mollissima* pollen tubes digested with cellulase (control pollen tube: Control), B toxicity-treated pollen tubes digested with cellulase and the FTIR differential spectrum (B toxicity−control) generated by digital subtraction of the control spectra from B toxicity-treated spectra digested with cellulase (B toxicity). Bar = 10 μm in **(A,B,D,E,G,H,J,K)**. Bar = 3 μm in M and N; Bar = 2 μm in **(O,P)**. OW, Outer wall; IW, inner wall. The arrows showed the wave morphology **(M)** and wave protuberances **(N)**.

(Figure 7L). The results showed that the distinct peaks of saturated esters (the peak at 1,729 cm^{-1}), proteins (the peaks at 1,641 and 1,537 cm^{-1}), lignin and carboxylic acid (the peaks at 1,385 and 1,233 cm^{-1}), cellulose and hemicellulose (the peaks around 1,331 and 1,157 cm^{-1}), and other polysaccharides (the peaks at 1,200–900 cm^{-1}) decreased in the control pollen tube spectrum. B toxicity increased the peaks of lignin and carboxylic acid, cellulose, pectins, and polysaccharides and decreased other polysaccharides, indicating that B toxicity influenced the deposition of cell wall components, such as carboxylic acid, pectins, and cellulose, into pollen tube cell walls of *C. mollissima*.

In a word, treatment with pectinase resulted in the disappearance of esterified and acid pectins and decreased cellulose and callose. B toxicity caused disordered ultrastructure.

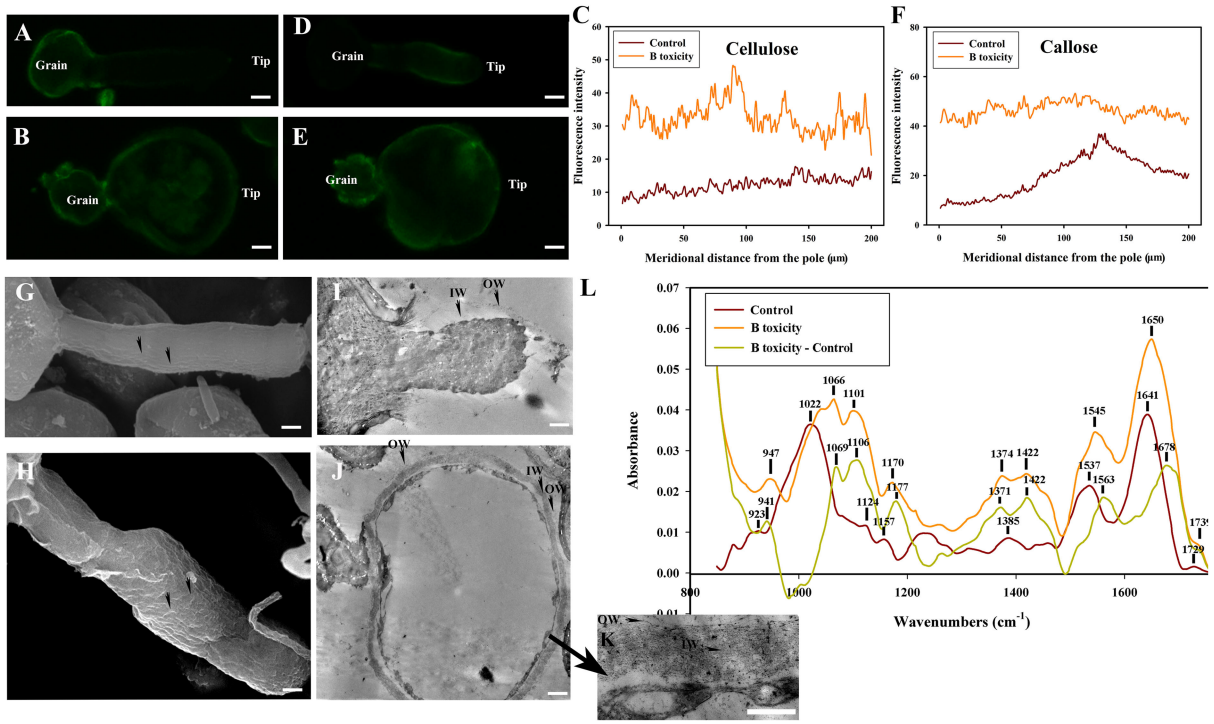

FIGURE 7
Effects of B toxicity on cell wall architecture with pectinase treatment. **(A)** Cellulose in control pollen tube digested with pectinase indicated by CBM3a labeling. **(B)** Cellulose in B toxicity-treated pollen tube digested with pectinase. **(C)** Quantitative analysis of the fluorescent intensity of cellulose in the wall of control (Control) and B toxicity-treated pollen tubes which were digested with pectinase. **(D)** Callose in control pollen tube indicated by monoclonal antibody to (1→ 3)-β-glucan labeling digested with pectinase. **(E)** Callose in B toxicity-treated pollen tube treated with pectinase. **(F)** Quantitative analysis of callose fluorescent intensity in the wall of control (Control) and B toxicity-treated pollen tubes which were digested with pectinase. **(G)** SEM of control pollen tube digested with pectinase. **(H)** SEM of B toxicity-treated pollen tube digested with pectinase. **(I)** TEM transverse section of control pollen tube digested with pectinase. After pectinase treatment, the fibrous pectic layer reduced substantially, only a small number of fibres exited in OW, and the callose layer was difficult to be observed. **(J,K)** TEM transverse section of B toxicity-treated pollen tube digested with pectinase. A small number of fibers were observed in OW, but the IW of B toxicity-treated pollen tubes was thick, and much more fibers were crosslinked with the callose layer. **(L)** FTIR spectra from the tip regions of *C. mollissima* pollen tubes digested with pectinase (control pollen tube: Control), B toxicity-treated pollen tubes digested with pectinase and the FTIR differential spectrum (B toxicity−control) generated by digital subtraction of the control spectra from B toxicity-treated spectra digested with pectinase. Bar = 10 μm in **(A,B,D,E)**. Bar = 3 μm in **(G,H)**; Bar = 2 μm in **(I,J)**. Bar = 1 μm in **(K)**. OW, Outer wall; IW, inner wall. The arrows indicated the strip protuberances **(G)** and wave protuberances **(H)**.

Effects of B Toxicity on cell wall architecture with β-1,3-glucanase treatment

No fluorescent signals of esterified pectins and acid pectins were detected on control and B toxicity-treated pollen tube wall digested with β-1,3-glucanase indicating that degradation of callose-induced disappearance of pectins.

Weaker fluorescent signals of cellulose were detected on the whole control pollen tube digested with β-1,3-glucanase (Figure 8A), but fluorescent signals of cellulose were stronger on B toxicity-treated pollen tubes digested with β-1,3-glucanase, especially at the tips (Figures 8B,C). After β-1,3-glucanase treatment, fluorescent signals of callose decreased, and appeared through the control pollen tube except for the tip (Figure 8D). However, B toxicity induced accumulation of callose at the pollen tube shank and tip (Figures 8E,F).

The surface was very smooth in control pollen tubes treated with β-1,3-glucanase (Figure 8G), while B toxicity led to an uneven surface of pollen tubs with swollen tips (Figure 8H).

Very thin outer wall were observed in the control pollen tubes, and the IW was difficult to be observed with β-1,3-glucanase (Figure 8I). The fibrous pectic layer reduced substantially and only a thin layer exited in OW of B toxicity-treated pollen tubes after β-1,3-glucanase treatment, but the IW of B toxicity-treated pollen tubes was still thick, and there were still some fibers crosslinked with the callose in IW to form an irregular crosslinking layer (Figures 8J,K).

Effect of B toxicity on chemical components of pollen tube wall treated with β-1,3-glucanase were carried out with FTIR (Figure 8L). The results showed that the peaks assigned to

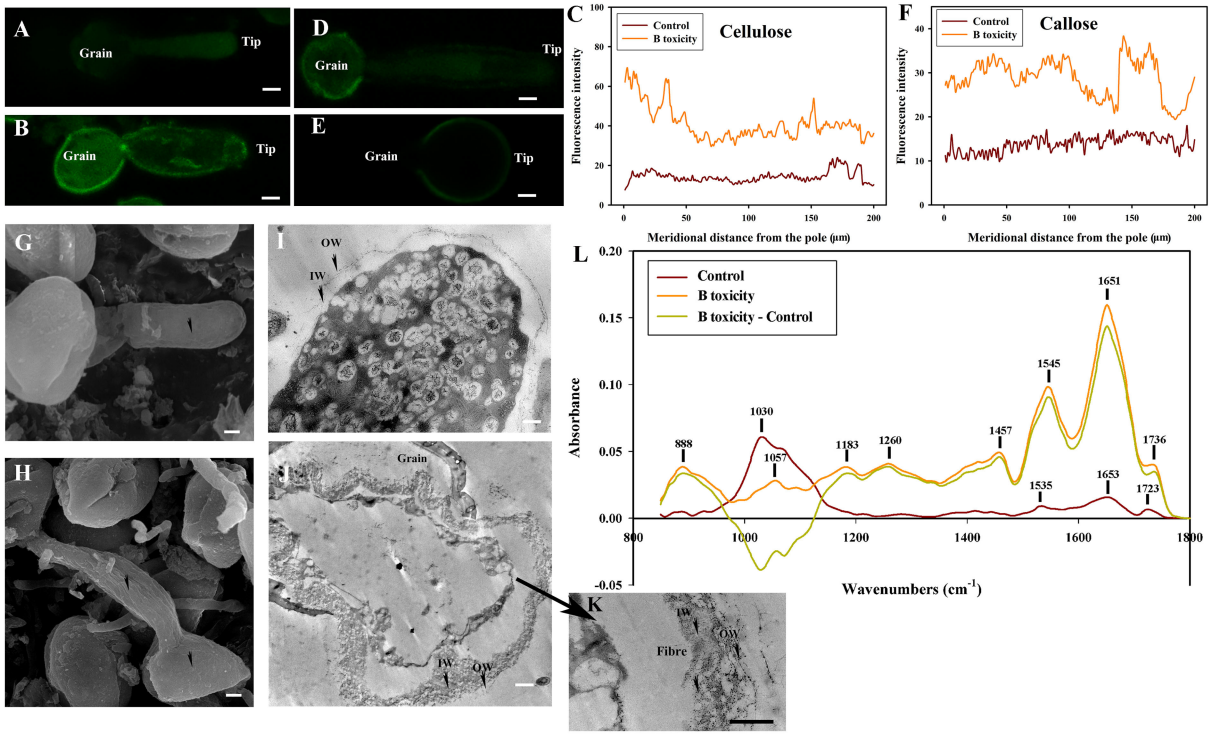

FIGURE 8
Effects of B toxicity on cell wall architecture treated with β-1,3-glucanase treatment.**(A)** Cellulose in control pollen tube digested with β-1,3-glucanase indicated by CBM3a labeling. **(B)** Cellulose in B toxicity-treated pollen tube digested with β-1,3-glucanase. **(C)** Quantitative analysis of the fluorescent intensity of cellulose in the wall of control (Control) and B toxicity-treated pollen tubes, which were digested with β-1,3-glucanase. **(D)** Callose in control pollen tube indicated by monoclonal antibody to (1→ 3)-β-glucan labeling digested with β-1,3-glucanase. **(E)** Callose in B toxicity-treated pollen tube digested with β-1,3-glucanase. **(F)** Quantitative analysis of callose fluorescent intensity in the wall of control (Control) and B toxicity-treated pollen tubes which were digested with β-1,3-glucanase. **(G)** SEM of control pollen tube digested with β-1,3-glucanase. **(H)** SEM of B toxicity-treated pollen tube digested with β-1,3-glucanase. **(I)** TEM transverse section of control pollen tube digested with β-1,3-glucanase. A thin fiber pectin layer in OW of control pollen tubes was observed and the IW was difficult to be observed with β-1,3-glucanase. **(J,K)** TEM transverse section of pollen tube treated with β-1,3-glucanase. After β-1,3-glucanase treatment, the fiber pectin layer in OW was observed with a thin layer, but the IW of B toxicity-treated pollen tubes was still thick, and there were still some fibers crosslinked with the callose layer to form an irregular crosslinking layer. **(L)** FTIR spectra from the tip regions of *C. mollissima* pollen tubes digested with β-1,3-glucanase (control pollen tube: Control), B toxicity-treated pollen tubes treated with β-1,3-glucanase and the FTIR differential spectrum (B toxicity−control) generated by digital subtraction of the control spectra from B toxicity-treated spectra digested with β-1,3-glucanase. Bar = 10 μm in **(A,B,D,E)**. Bar = 3 μm in G and H; Bar = 2 μm in **(I,J)**. Bar=1 μm in K. OW, Outer wall; IW, inner wall. The arrows showed the smooth surface **(G)** and the uneven surface **(H)**.

saturated esters (the peak at 1,723 cm^{-1}), proteins (the peaks at 1,653 and 1.535 cm^{-1}), carboxylic acid (1,457 cm^{-1}), and carbohydrates (the peaks at 1,200–900 cm^{-1}) decreased in the control pollen tube spectrum treated with β-1,3-glucanase. However, B toxicity increased the peaks assigned to esters and carboxylic acid and decreased carbohydrates, indicating that B toxicity influenced the deposition of cell wall components, such as carboxylic acid, pectins, and cellulose, into pollen tube cell walls of *C. mollissima*.

In a word, treatment with β-1,3-glucanase induced the disappearance of esterified and acid pectins and decreased cellulose and callose of control pollen tubes. B toxicity increased cellulose and callose on the pollen tubes. The degradation of callose decreased cellulose and pectins. The result illustrated that there existed an intimate relationship among cellulose, callose, and pectins, which was supported by the ultrastructure.

Discussion

Although B is an essential micronutrient for plant growth, an excessive concentration of B due to arid and saline soils, as well as low rainfall and poor irrigation, usually produces toxicity in plants (Matthes et al., 2020). Many research illustrated that B toxicity affected mechanical properties of the plant cell wall and thus affected various developmental processes in plants (Landi et al., 2019). In one model of tip growth–root hair, the inhibition of root elongation has been determined to be one of the most distinct symptoms induced by B toxicity in plants (Tanaka and

Fujiwara, 2008; Aquea et al., 2012). In another model of tip growth–pollen tube, we found that B toxicity inhibited apple pollen tube elongation through [Ca^{2+}] signals and altered tube wall components (Fang et al., 2016). In the present study, we found the growth of pollen tubes were not affected by B toxicity significantly, but the tips of tubes bulged sharply, which was different from our previous studies of apple pollen tubes, and B toxicity induced smaller bulge in apple pollen tubes (Fang et al., 2016). In the study of *Arabidopsis* pollen tube, the over-expression of ANXUR receptor-like kinases (RLKs) inhibited growth and increased the width of pollen tubes by over-activating exocytosis and the over-accumulation of secreted wall materials (Boisson-Dernier et al., 2013). We speculated that B toxicity induced an increase in exocytosis and accumulated deposition of cell wall material to result in the bulge of the pollen tube tip. Also, in this study, we focused on changes in the pollen tube wall components induced by B toxicity with emphasis on ultrastructure. Our present work provides novel evidence for the effects of B toxicity on pollen tube wall components and ultrastructure.

As we mentioned above, B toxicity resulted in less agricultural production. While pollen tube development is critical for double fertilization, we speculate that the disorder of pollen tubes leads to less fruit production. Huang et al. (2016) reported that B toxicity led to the secondary deposition of cell-wall components in regions close to the pits of vessel elements in tolerant *Castanea sinensis* and poorly developed vessel elements in intolerant *Castanea grandis*. In the present research, B toxicity led to fibrous wall thickening at the tube tip and therefore swollen tip.

Effects of B toxicity on the deposition of cell wall components

As we mentioned above, the pollen tube wall consists of cellulose, callose, and pectins (Li et al., 1996, 2002; Ferguson et al., 1998). The interactions between pectins and B have been reported to be important for the assembly of the cell wall (Baluška et al., 2003). Two rhamnogalacturonan II (RG-II) chains of pectins could be linked with B by forming borate-diol ester bonds (Funakawa and Miwa, 2015), which is essential to cell wall formation (Dumont et al., 2014). The Golgi apparatus produces and transports esterified pectins to the pollen tube extreme tip (Hasegawa et al., 1998), where the enzyme pectin methyl-esterase could alter the esterified pectins to acid pectins (Li et al., 2002). The crosslinks between the acidic residue of acid pectins and Ca^{2+} ions form a semi-rigid pectate gel (Braccini and Perez, 2001). So the changes in B concentrations may cause a mechanical change in the cell wall. B toxicity has been reported to alter cell-wall polysaccharides as well as other cell-wall components in *Citrus* leaf veins and roots (Wu et al., 2019). In our previous research, B toxicity also induced changes in apple pollen tube wall components including acid pectins and esterified pectins (Fang et al., 2016). In the present research, cellulose was present throughout the control pollen tube wall except for the tip. However, B toxicity induced cellulose deposition at the pollen tube tip. Callose is one of the important components in the normal pollen tube walls (Li et al., 2002). In addition, callose is also found at the abnormal pollen tube tip (Hao et al., 2013). Our previous results demonstrated that B toxicity induced the deposition of the callose at the pollen tube tip of *Malus domestica* (Fang et al., 2016). In the present study, similar results were obtained. In the control pollen tube, callose was distributed along the entire pollen tube except for the tip, while B toxicity induced accumulation of callose at the pollen tube tip.

Effects of B toxicity on the relationship among pectins, cellulose, and callose

In apple pollen tubes, B toxicity had no obvious effect on cellulose distribution. On the contrary, B toxicity enhanced callose deposition at the pollen tube tip and increased acid pectins and esterified pectins at the pollen tube (Fang et al., 2016). In the present study, similar results were obtained. B toxicity induced accumulation of the cellulose and callose at the tip and increased esterified and acid pectins.

In the present study, to further study the effects of B toxicity on the relationship among pectins, cellulose, and callose, cellulase, pectinase, and β-1,3-glucanase were applied. Results from FTIR showed that treatment with cellulase, pectinase, and β-1,3-glucanase decreased chemical components of the pollen tube wall, suggesting the intimate relationship among cellulose, pectins, and callose. β-1,3-glucanase induced the disappearance of the pectins in pollen tubes, indicating that there existed closer relation between callose and pectins. Also, the pectin signals after cellulase treatment showed intermittent distribution, and disappeared after β-1,3-glucanase treatment, which suggested the crossliking relationship of cellulose, pectins, and callose of tube walls. And we speculated that the relationship between pectins and callose might be stronger than that between cellulose and pectins. However, B toxicity not only affected the morphology of the pollen tube but also affected the tube wall components. In addition, B toxicity strengthened the relationship among the pectins, cellulose, and callose with stronger fluorescence and higher peak of chemical components of the pollen tube wall.

Effect of B toxicity on pollen tube cell wall ultrastructure

B toxicity altered the cell wall structure. B toxicity thickened the cell wall in cork cells of *C. grandis* leaves (Huang et al.,

2014). B toxicity has been reported to alter the pectin network crosslinking structure of leaf tip and cell ultrastructure and architecture of components in leaf center and the tip of trifoliate orange (Wu et al., 2019). Although B is essential for pollen tube wall morphological formation, few investigations reported the effect of B toxicity on pollen tube wall ultrastructure. In our present study, B toxicity resulted in the thicker wall at the pollen tube tip and destruction of cell wall integrity leading to the swollen tip.

In brief, we found that boron toxicity disturbed cell wall components such as pectins, cellulose, callose, and ultrastructure. B toxicity also altered the relation among pectins, cellulose, and callose. Our investigation of the effects of boron toxicity on *C. mollissima* pollen tubes provides an extensive understanding of the role of boron in the cell wall component architecture of pollen tubes. These findings provide valuable information which enhances our current understanding of the mechanism regulating B in pollen tube growth.

Data availability statement

The original contributions presented in the study are included in the article/Supplementary material, further inquiries can be directed to the corresponding authors.

Author contributions

KF and LQ designed the research and edited the article. FK drafted the article. WZ performed the main experiments. QZ, QC, and YX were involved in data analysis. All authors have read and approved the final version of the manuscript.

Funding

This work was supported by the National Key Research and Development Program of China (2018YFD1000605), Beijing advanced innovation center for tree breeding by molecular design (2023210001) and the National Natural Science Foundation of China (31270719).

Conflict of interest

Author WZ was employed by Beijing Bei Nong Enterprise Management Co. Ltd.

The remaining authors declare that the research was conducted in the absence of any commercial or financial relationships that could be construed as a potential conflict of interest.

Publisher's note

All claims expressed in this article are solely those of the authors and do not necessarily represent those of their affiliated organizations, or those of the publisher, the editors and the reviewers. Any product that may be evaluated in this article, or claim that may be made by its manufacturer, is not guaranteed or endorsed by the publisher.

Supplementary material

The Supplementary Material for this article can be found online at: https://www.frontiersin.org/articles/10.3389/fpls.2022.946781/full#supplementary-material

References

Aquea, F., Federici, F., Moscoso, C., Vega, A., and Jullian, P., Heseloff, J., et al. (2012). A molecular framework for the inhibition of *Arabidopsis* root growth in response to boron toxicity. *Plant Cell Environ.* 35, 719–734. doi: 10.1111/j.1365-3040.2011.02446.x

Baluška, F., Šamaj, J., Wojtaszek, P., Volkmann, D., and Menzel, D. (2003). Cytoskeleton – plasma membrane – cell wall continuum in plants: emerging links revisited. *Plant Physiol.* 133, 482–491. doi: 10.1104/pp.103.027250

Behera, B., Kancheti, M., Raza, M. B., Shiv, A., Mangal, V., Rathod, G., et al. (2022). Mechanistic insight on boron-mediated toxicity in plant vis-a-vis its mitigation strategies: a review. *Int. J. Phytoremediat.* 17, 1–18. doi: 10.1080/15226514.2022.2049694

Boisson-Dernier, A., Lituiev, D. S., Nestorova, A., Franck, C. M., Thirugnanarajah, S., and Grossniklaus, U. (2013). ANXUR receptor-like kinases coordinate cell wall integrity with growth at the pollen tube tip via NADPH oxidases. *PLoS Biol.* 11, e1001719. doi: 10.1371/journal.pbio.1001719

Bou, D. F., and Geitmann, A. (2011). Actin is involved in pollen tube tropism through redefining the spatial targeting of secretory vesicles. *Traffic.* 12, 1537–1551. doi: 10.1111/j.1600-0854.2011.01256.x

Braccini, I., and Perez, S. (2001). Molecular basis of Ca^{2+} induced gelation in alginates and pectins: the egg-box model revisited. *Biomacromolecules.* 2, 1089–1096. doi: 10.1021/bm010008g

Brdar-Jokanović, M. (2020). Boron toxicity and deficiency in agricultural plants. *Int J Mol Sci.* 21, 1424. doi: 10.3390/ijms21041424

Cervilla, L. M., Blasco, B., Ríos, J. J., Romero, L., and Ruiz, J. M. (2007). Oxidative stress and antioxidants in tomato (*Solanum lycopersicum*) plants subjected to boron toxicity. *Ann. Bot.* 100, 747–756. doi: 10.1093/aob/mcm156

Dumont, M., Lehner, A., Bouton, S., Kiefer-Meyer, M. C., Voxeur, A., Pelloux, J., et al. (2014). The cell wall pectic polymer rhamnogalacturonan-II is required for proper pollen tube elongation: implications of a putative sialyltransferase-like protein. *Ann. Bot.* 114, 1177–1188. doi: 10.1093/aob/mcu093

Fang, K. F., Zhang, W. W., Xing, Y., Zhang, Q., Yang, L., Cao, Q. Q., et al. (2016). Boron toxicity causes multiple effects on *Malus Domestica* pollen tube growth. *Front. Plant Sci.* 7, 208. doi: 10.3389/fpls.2016.00208

Ferguson, C., Teeri, T. T., Siika-aho, M., Read, S. M., and Bacic, A. (1998). Location of cellulose and callose in pollen tubes and grains of *Nicotiana tabacum*. *Planta* 206, 452–460. doi: 10.1007/s004250050421

Funakawa, H., and Miwa, K. (2015). Synthesis of borate cross-linked rhamnogalacturonan II. *Front. Plant Sci.* 6, 223. doi: 10.3389/fpls.2015.00223

Geitmann, A., and Steer, M. (2006). *The architecture and properties of the pollen tube cell wall, [M]// R. Malhó. The pollen tube. Plant Cell Monographs, Vol 3.* Berlin, Heidelberg: Springer Verlag. p. 177–200. doi: 10.1007/7089_049

Hao, H. Q., Chen, T., Fan, L., Li, R. L., and Wang, X. H. (2013). 2, 6-dichlorobenzonitrile causes multiple effects on pollen tube growth beyond altering cellulose synthesis in *Pinus bungeana* Zucc. *PLoS ONE.* 8, e76660. doi: 10.1371/journal.pone.0076660

Hasegawa, Y., Nakamura, S., Kakizoe, S., Sato, M., and Nakamura, N. (1998). Immunocytochemical and chemical analyses of Golgi vesicles isolated from the germinated pollen of *Camellia japonica*. *J. Plant Res.* 111, 421–429. doi: 10.1007/BF02507807

Huang, J. H., Cai, Z. J., Wen, S. X., Guo, P., Ye, X., Lin, G. Z., et al. (2014). Effects of boron toxicity on root and leaf anatomy in two citrus species differing in boron tolerance. *Trees.* 28, 1653–1666. doi: 10.1007/s00468-014-1075-1

Huang, J. H., Qi, Y. P., Wen, S. X., Guo, P., Chen, X. M., and Chen, L. S. (2016). Illumina microRNA profiles reveal the involvement of miR397a in Citrus adaptation to long-term boron toxicity via modulating secondary cell-wall biosynthesis. *Sci. Rep.* 6, 22900. doi: 10.1038/srep22900

Keles, Y., and Öncel, I., Yenice, N. (2004). Relationship between boron content and antioxidant compounds in *Citrus* leaves taken from fields with different water source. *Plant Soil.* 265, 345–353. doi: 10.1007/s11104-005-0646-8

Landi, M., Margaritopoulou, T., Papadakis, T., and Araniti, F. (2019). Boron toxicity in higher plants: an update. *Planta.* 250, 1011–1032. doi: 10.1007/s00425-019-03220-4

Landi, M., Remorini, D., Pardossi, A., and Guidi, L. (2013). Boron excess affects photosynthesis and antioxidant apparatus of greenhouse *Cucurbita pepo* and *Cucumis sativus*. *J. Plant Res.* 126, 775–786. doi: 10.1007/s10265-013-0575-1

Li, Y. Q., Mareck, A., Faleri, C., Moscatelli, A., Liu, Q., and Cresti, M. (2002). Detection and localization of pectin methylesterase isoforms in pollen tubes of *Nicotiana tabacum* L. *Planta.* 214, 734–740. doi: 10.1007/s004250100664

Li, Y. Q., Zhang, H. Q., Pierson, E. S., Huang, F. Y., Linskens, H. F., Hepler, P. K., et al. (1996). Enforced growth-rate fluctuation causes pectin ring formation in the cell wall of *Lilium longiflorum* pollen tubes. *Planta.* 200, 41–49. doi: 10.1007/BF00196647

Matthes, M. S., Robil, J. M., and McSteen, P. (2020). From element to development: the power of the essential micronutrient boron to shape morphological processes in plants. *J. Exp. Bot.* 71, 1681–1693. doi: 10.1093/jxb/eraa042

Obermeyer, G., Kriechbaumer, R., Strasser, D., Maschessning, A., and Bentrup, F. W. (1996). Boric acid stimulates the plasma membrane H+-ATPase of ungerminated lily pollen grains. *Physiol. Plantarum.* 98, 281–290. doi: 10.1034/j.1399-3054.1996.980209.x

Papadakis, I. E., Tsiantas, P. I., Tsaniklidis, G., Landi, M., Psychoyou, M., and Fasseas, C. (2018). Changes in sugar metabolism associated to stem bark thickening partially assist young tissues of *Eriobotrya japonica* seedlings under boron stress. *J. Plant Physiol.* 231, 337–345. doi: 10.1016/j.jplph.2018.10.012

Ruiz, J. M., Rivero, R. M., and Romero, L. (2003). Preliminary studies on the involvement of biosynthesis of cysteine and glutathione concentration in the resistance to B toxicity in sunflower plants. *Plant Sci.* 165, 811–817. doi: 10.1016/S0168-9452(03)00276-0

Sakamoto, T., Inui, Y. T., Uraguchi, S., Yoshizumi, T., Matsunaga, S., Mastui, M., et al. (2011). Condensin II alleviates DNA damage and is essential for tolerance of boron overload stress in *Arabidopsis*. *Plant Cell.* 23, 3533–3546. doi: 10.1105/tpc.111.086314

Sang, W., Huang, Z. R., Yang, L. T., Guo, P., Ye, X., and Chen, L. S. (2017). Effects of high toxic boron concentration on protein profiles in roots of two citrus species differing in boron-tolerance revealed by a 2-DE based MS approach. *Front. Plant Sci.* 8, 180. doi: 10.3389/fpls.2017.00180

Seth, K., and Aery, N. C. (2017). Boron induced changes in biochemical constituents, enzymatic activities, and growth performance of wheat. *Acta Physiol. Plant.* 39, 244. doi: 10.1007/s11738-017-2541-3

Sotiras, M., Papadakis, I., Landi, M., Tsaniklidis, G., Tsiantas, P., and Psychoyou, M. (2019). Allocation pattern, photosynthetic performance and sugar metabolism in hydroponically grown seedlings of loquat (*Eriobotrya japonica* Lindl.) subjected to salinity. *Photosynthetica* 57, 258–267. doi: 10.32615/ps.2019.018

Tanaka, M., and Fujiwara, T. (2008). Physiological roles and transport mechanisms of boron: perspectives from plants. *Pflugers. Arch-Eur. J. Physiol.* 456, 671–677. doi: 10.1007/s00424-007-0370-8

Voxeur, A. A., and Fry, S. C. (2014). Glycosylinositol phosphorylceramides from Rosa cell cultures are boron-bridged in the plasma membrane and form complexes with rhamnogalacturonan II. *Plant J.* 79, 139–149. doi: 10.1111/tpj.12547

Warington, K. (1923). The effect of boric acid and borax on the broan bean and certain other plants. *Ann. Bot.* 37, 629–672. doi: 10.1093/oxfordjournals.aob.a089871

Wu, X., Lu, X., Riaz, M., Yan, L., and Jiang, C. C. (2018). Boron deficiency and toxicity altered the subcellular structure and cell wall composition architecture in two citrus rootstocks. *Sci. Hortic.* 238, 147–154. doi: 10.1016/j.scienta.2018.04.057

Wu, X. W., Lu, X. P., Ria, M., Yan, L., and Jiang, C. C. (2019). B toxicity induced specific changes of ultrastructure and architecture of components in leaf center and tip of trifoliate orange [*Poncirus trifoliate* (L.) Raf.]. *J. Environ. Manage.* 246, 426–433. doi: 10.1016/j.jenvman.2019.05.148

Zhang, Y., He, J., Lee, D., and McCormick, S. (2010). Interdependence of endomembrane trafficking and actin dynamics during polarized growth of *Arabidopsis* pollen tubes. *Plant Physiol.* 152, 2200–2210. doi: 10.1104/pp.109.142349

frontiers | Frontiers in Plant Science

TYPE Mini Review
PUBLISHED 15 September 2022
DOI 10.3389/fpls.2022.1022684

OPEN ACCESS

EDITED BY
Delia Fernández-González,
Universidad de León, Spain

REVIEWED BY
Jorge Lora,
Spanish National Research Council (CSIC), Spain

*CORRESPONDENCE
Daphne R. Goring
d.goring@utoronto.ca

†These authors have contributed equally to this work and share first authorship

SPECIALTY SECTION
This article was submitted to Plant Cell Biology, a section of the journal Frontiers in Plant Science

RECEIVED 18 August 2022
ACCEPTED 02 September 2022
PUBLISHED 15 September 2022

CITATION
Bordeleau SJ, Canales Sanchez LE and Goring DR (2022) Finding new *Arabidopsis* receptor kinases that regulate compatible pollen-pistil interactions. *Front. Plant Sci.* 13:1022684. doi: 10.3389/fpls.2022.1022684

Finding new *Arabidopsis* receptor kinases that regulate compatible pollen-pistil interactions

Stephen J. Bordeleau[1†], Laura E. Canales Sanchez[1†] and Daphne R. Goring[1,2*]

[1]Department of Cell and Systems Biology, University of Toronto, Toronto, ON, Canada, [2]Centre for the Analysis of Genome Evolution and Function, University of Toronto, Toronto, ON, Canada

Successful fertilization of a flowering plant requires tightly controlled cell-to-cell communication between the male pollen grain and the female pistil. Throughout *Arabidopsis* pollen-pistil interactions, ligand-receptor kinase signaling is utilized to mediate various checkpoints to promote compatible interactions. In *Arabidopsis*, the later stages of pollen tube growth, ovular guidance and reception in the pistil have been intensively studied, and thus the receptor kinases and the respective ligands in these stages are quite well understood. However, the components of the earlier stages, responsible for recognizing compatible pollen grains and pollen tubes in the upper reproductive tract are less clear. Recently, predicted receptor kinases have been implicated in the initial stages of regulating pollen hydration and supporting pollen tube growth through the upper regions of the reproductive tract in the pistil. The discovery of these additional signaling proteins at the earlier stages of pollen-pistil interactions has further elucidated the mechanisms that *Arabidopsis* employs to support compatible pollen. Despite these advances, many questions remain regarding their specific functions. Here, we review the roles of the different receptor kinases, integrate their proposed functions into a model covering all stages of pollen-pistil interactions, and discuss what remains elusive with regard to their functions, respective binding partners and signaling pathways.

KEYWORDS

***Arabidopsis*, pollen-pistil interactions, pollen tube, receptor kinases, ligands**

Introduction

The process leading to fertilization in flowering plants begins with the deposition of pollen, the male gametophyte, on the stigma, the receptive part of the female pistil. A general property of Brassicaceae pistils, including *Arabidopsis*, is the presence of dry stigmas which possess cellular signalling pathways for selective pollen hydration (reviewed in Abhinandan et al., 2022). Brassicaceae pollen grains carry a pollen coat on the surface with a number of small Pollen Coat Proteins (PCPs) that can serve as signalling peptides (Doughty et al., 1993; Wang et al., 2017). In *Arabidopsis*, the recognition of compatible pollen grains involves receptor kinases (RKs) on the surface stigmatic papillae and leads to the papillae releasing water for pollen hydration. Hydration of the desiccated pollen grains is a critical step as it is required to initiate pollen metabolism and germination of a pollen tube. In contrast, pistils with wet stigmas such as tomato (*Solanum lycopersicum*) have little control over pollen hydration, and RKs begin to regulate these interactions during pollen tube growth (Huang et al., 2014; reviewed in Dickinson, 1995; Kim et al., 2021). In *Arabidopsis*, once a pollen tube emerges, it grows down to the base of the stigmatic papilla where it continues to grow through the stigma and style to reach the transmitting tract. Using RK-mediated autocrine and paracrine signalling, the pollen tube will grow down the transmitting tract towards an unfertilized ovule where it emerges from the septum and grows along the funiculus of the ovule to enter the micropyle, ceasing growth as it reaches a receptive synergid cell (Figure 1A). The pollen tube then bursts to release the two sperm cells which fuse to the egg cell and central cell culminating in double fertilization. All these steps depend on tightly controlled cell-to-cell communication between male and female tissues to deliver the male gametophytes to an ovule (reviewed in Johnson et al., 2019; Hafidh and Honys, 2021; Kim et al., 2021; Robichaux and Wallace, 2021)

As is common with flowering plants, *Arabidopsis* has a large family of receptor-like kinase (RLK) genes, and an increasing number of these RLKs have been shown to encode true RKs with the associated ligand(s) identified; thus, serving as primary sensors in the perception of extracellular signals (reviewed in Escocard de Azevedo Manhaes et al., 2021). The predicted RLKs have been further subdivided in several different subgroups based on the type of domains identified in their predicted extracellular domains (Shiu and Bleecker, 2001; reviewed in Dievart et al., 2020). In the context of *Arabidopsis* reproduction, members of the *Catharanthus roseus* Receptor-Like Kinase 1-like (CrRLK1L) and the Leucine-Rich Repeat (LRR) RLK subfamilies have proven to be critical regulators, and they are involved at every stage of this complex, multifaceted process (reviewed in Hafidh and Honys, 2021; Kim et al., 2021). Much of these discoveries have centered on the later stages where receptor kinases and signaling events guide pollen tubes to unfertilized ovules, regulate pollen tube reception at the synergid cells, and prevent multiple pollen tubes from approaching an unfertilized ovule. More recently, additional RKs and RLKs have been discovered in the pistil that act at earlier stages of pollen-stigma interactions and pollen tube growth through the upper regions of the reproductive tract (Stuhrwohldt et al., 2015; Lee and Goring, 2021; Liu et al., 2021a). This review will integrate these recent discoveries to provide some context for where they function in compatible pollen-pistil interactions and highlight what remains elusive in terms of their proposed functions.

Negative and positive regulators at the pollen-stigma interface

In the absence of pollen, the stigma has been found to have high levels of reactive oxygen species (ROS) (McInnis et al., 2006; Zafra et al., 2016). Recently, high stigmatic ROS levels in *Arabidopsis* have been proposed to have an inhibitory effect on pollen hydration. A complex of two CrRLK1L members, ANJEA (ANJ) and FERONIA (FER), are proposed to establish an autocrine signalling cascade to maintain these ROS levels in *Arabidopsis* sigmatic papillae in the absence of pollen (Liu et al., 2021a). A connection between FER and a ROS pathway had been previously established in the context of root hair elongation (Duan et al., 2010) and pollen tube reception (described below; Duan et al., 2014). The extracellular domains of CrRLK1L family members contain two malectin-like domains which have been previously found to bind to secreted cysteine-rich peptides known as RAPID ALKALINIZATION FACTORs (RALFs) (reviewed in Galindo-Trigo et al., 2020b). In the context of the stigma, RALF33 which is proposed to be secreted by the stigma was shown to bind ANJ/FER. RALF33 perception by the stigmatic ANJ/FER complex then leads to the induction of a RAC/ROP-NADPH oxidase (RBOHD) pathway for ROS production. As the high ROS state is inhibitory to pollen hydration, it would need to be reversed for compatible pollen hydration. Pollen-Coat Protein Bs (PCP-Bs) have been previously found to be required for compatible pollen hydration (Wang et al., 2017) and these PCP-Bs were found to competitively bind ANJ/FER replacing RALF33 to shut down ROS production which would then allow for compatible pollen hydration (Liu et al., 2021a). Pollinating the *anj-1 fer-4* double-mutant stigmas with *pcp-bγ* mutant pollen resulted in increased *pcp-bγ* mutant pollen hydration compared to wild-type stigmas; thus supporting the model that ANJ/FER act in the stigma as negative regulators of pollen hydration (Figure 1B; (Liu et al., 2021a).

One would predict from the proposed model by Liu et al., (2021a) that the *pcp-bγ* mutant pollen hydration defect would also be rescued relative to wild-type pollen, but this was not observed suggesting that additional regulators are present in the stigma.

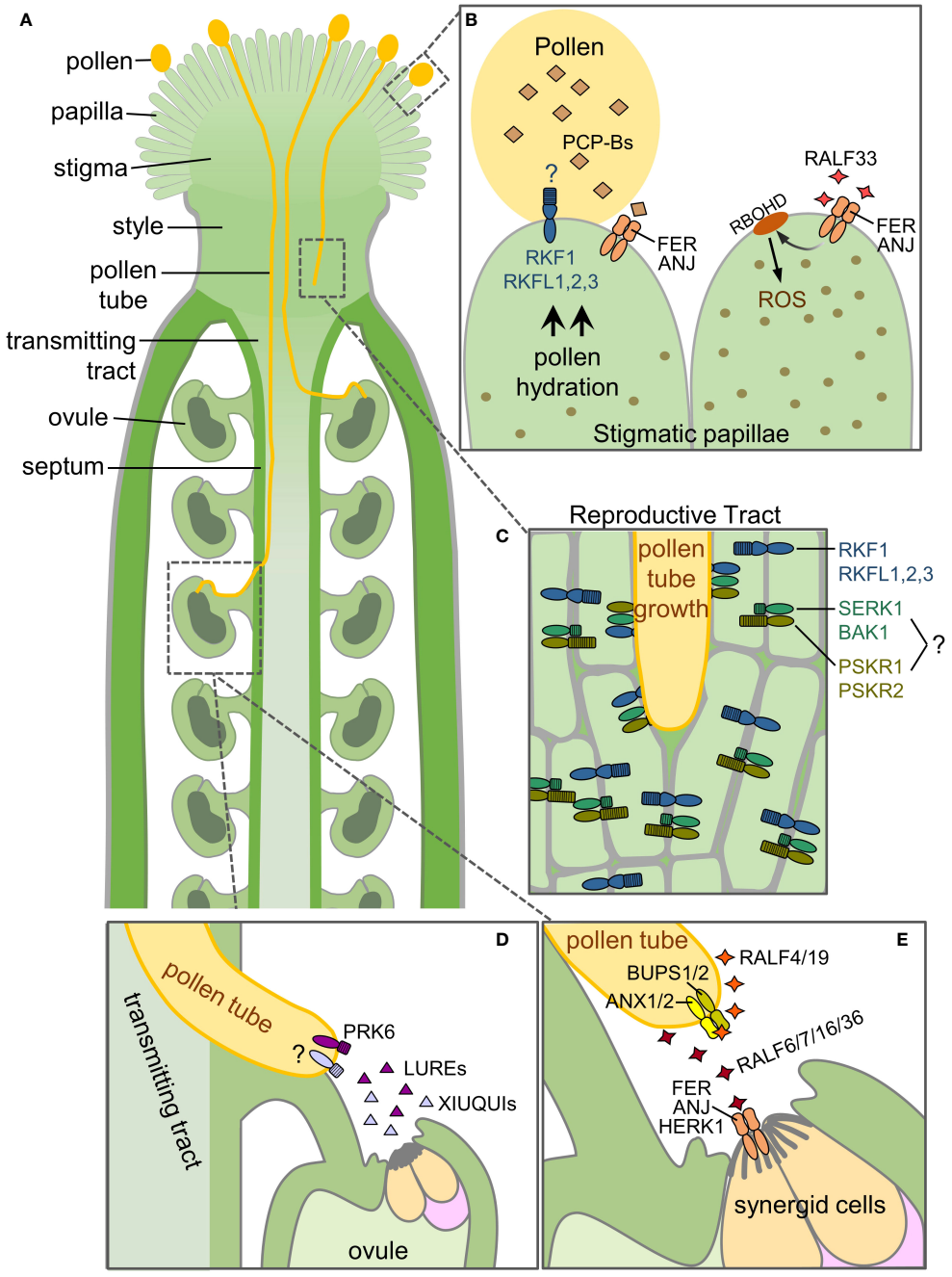

FIGURE 1
Receptor kinases and their respective ligands for compatible pollen-pistil interactions. This diagram illustrates the RLKs, RKs and their ligands functioning at different stages of the pollen-pistil interactions in *Arabidopsis*. **(A)** Overview of the different structures in a pollinated pistil. **(B)** Pollen reception at the stigmatic papilla. **(C)** Growth of the pollen tube through the reproductive tract (stigma, style, transmitting tissue). **(D)** Ovular guidance of the pollen tube to an unfertilized ovule. **(E)** Pollen tube reception at the ovule. See text for further details.

Recently, *Arabidopsis* LRR-VIII-2 RLK subgroup members have been identified as positive regulators in the stigma to promote pollen hydration and may be the missing link. RECEPTOR-LIKE KINASE IN FLOWERS 1 (RKF1) and its paralogue, RKF-LIKE 1 (RKFL1) were identified through a yeast two-hybrid screen to interact with a stigma-specific pseudokinase, BRASSIKIN 1 (BKN1; Doucet et al., 2019; Lee and Goring, 2021). These predicted RLKs have extracellular domains composed of a LRR

domain followed by a malectin domain (reviewed in Dievart et al., 2020). The *RKF1* and *RKFL1* genes are tandemly linked along with two other paralogs (*RKFL1-RKFL2-RKFL3-RKF1*), and the *RKF1* gene cluster has not been previously ascribed any function. CRISPR-Cas9 generated deletion mutants of the *RKF1* gene cluster (*rkfΔ* mutants) were found to display some phenotypic changes in pollen-stigma interactions (Lee and Goring, 2021). Pollinations of *rkfΔ* mutant pistils with wild-type pollen resulted in significantly slower pollen hydration rates compared to wild-type pistils indicating their role in the stigma as positive regulators of this process. Notably, single *rkf1* and *rkfl1* knockout mutant pistils supported wild-type levels of pollen hydration suggesting functional redundancy within the *RKF1* gene cluster. What remains unknown is what signals from the pollen are being perceived by the extracellular domains of RKF1 and the RKFLs in the stigmatic papillae. Malectin domains in the extracellular regions of CrRLK1Ls perceive RALF peptides for signal transduction (reviewed in Galindo-Trigo et al., 2020b), and ANJ/FER were found to bind PCP-Bs through the second malectin domain in their extracellular domain (Liu et al., 2021a). It is likely that RKF1/RKFLs are binding to other pollen coat signalling peptides to induce the necessary intracellular signals required to initiate water release for pollen hydration (Figure 1B).

Regulators of pollen tube growth in the upper reproductive tract

Immediately following pollen hydration, a pollen tube emerges and grows through the cell wall of the stigmatic papilla to the base of the cell where it continues to grow down between the cells of the stigma and style to reach the transmitting tract. The pollen tube will continue to grow down through the transmitting tract until it senses cues to exit to an unfertilized ovule. RLKs have been identified to function in the reproductive tract to support growth of the compatible pollen tubes. The yeast two-hybrid screen with the stigma-specific BKN1 yielded a second subgroup of RKs, SOMATIC EMBRYOGENESIS RECEPTOR KINASE 1 (SERK1) and BRI1-ASSOCIATED RECEPTOR KINASE 1 (BAK1/SERK3) (Lee and Goring, 2021). While pistils from a *serk1-1 bak1-4* double mutant promoted wild-type pollen hydration, a phenotype was observed for pollen tube growth. Wild-type pollen tubes grew more slowly through the *serk1-1 bak1-4* mutant reproductive tract, failing to grow to the same length as wild-type pollen tubes in wild-type pistils at 6-hours post-pollination. In contrast, there was no change for wild-type pollen tube growth lengths in the *rkfΔ* mutant pistils. However, when the *rkfΔ* mutation was crossed into the *serk1-1 bak1-4* mutant (*serk1-1 bak1-4 rkfΔ*), it exacerbated the phenotype significantly, resulting in further reductions in wild-type pollen tube growth through the mutant reproductive tract at 6 hours post-pollination. Ultimately, some of these pollen tubes failed to reach ovules, as denoted by decreased seed counts in fully developed mutant siliques (Lee and Goring, 2021). Overall, this work indicated that SERK1 and BAK1 in conjunction with the RKF1 cluster play a critical role in the reproductive tract to support pollen tube growth. Ascribing this new biological function to the RKF1 cluster and SERKs is an important step forward in understanding how the pistil sufficiently supports growing compatible pollen tubes (Figure 1C).

The SERKs are a subgroup of LRR-RKs with shorter extracellular domains that function as co-receptors with other LRR-RKs in many different processes during plant development and immunity (reviewed in Gou and Li, 2020; Escocard de Azevedo Manhaes et al., 2021). Acting as co-receptors to LRR-RKs, SERKs aid in receiving extracellular signals and transmitting them into the cell for downstream signalling cascades often involving Mitogen Activated Protein Kinases (MAPKs; reviewed in He et al., 2018). Whether SERK1 and BAK1 are forming complexes that include the RKF1/RKFLs in the reproductive tract is not known. However, it is also more likely that additional RKs are involved, given the pattern of SERKs acting as co-receptors for other LRR-RKs. PHYTOSULFOKINE RECEPTOR 1 and 2 (PSKR1 and PSKR2) have been implicated in pollen-pistil interactions (Stuhrwohldt et al., 2015), and these LRR-RKs are known to form complexes with SERK1 and BAK1 in other developmental processes (reviewed in Gou and Li, 2020). Using *pskr1-3 pskr2-1* double mutant pistils, wild-type pollen tubes were observed to grown more slowly through the upper reproductive tract resulting in an increased number of pollen tubes failing to reach an ovule (Stuhrwohldt et al., 2015), a phenotype also observed by Lee and Goring (2021). In addition, Stuhrwohldt et al. (2015) found that phytosulfokine signalling in the pollen tube also promoted pollen tube growth and ovular guidance. Thus, this study implicates phytosulfokine signalling in the reproductive tract to support pollen tube growth, and it would be interesting to see if they are connected to SERK1 and BAK1 in this proposed role (Figure 1C).

Regulators of pollen tube ovular guidance and reception

In order to achieve successful fertilization, the pollen tube needs to successfully exit from the transmitting tract to reach an unfertilized ovule for delivery of the immotile sperm cells for double fertilization of the egg cell and central cell. This is achieved by constant communication between both the male and female gametophytes. The ovule plays an important role in this process since it is responsible for guiding the pollen tube to transversely grow out of the transmitting tract and reach a viable ovule, a

process known as ovular guidance. Using both *in-vitro* and semi-*in vivo* experiments with *Torenia fournieri* ovules, it was shown that two cysteine-rich peptides, LURE1 and LURE2, expressed in the synergid cells, were able to attract pollen tubes towards the ovules (Okuda et al., 2009; Goto et al., 2010). This discovery led to the identification of the AtLURE1 peptides secreted by *Arabidopsis* ovules to attract pollen tubes (Takeuchi and Higashiyama, 2012). The pollen tube LRR-RK, POLLEN-SPECIFIC RECEPTOR-LIKE KINASE 6 (PRK6), was then shown to be the key LRR-RK for perceiving AtLURE1 (Takeuchi and Higashiyama, 2016; Zhang et al., 2017). Upon AtLURE1 perception, PRK6 orients the pollen tube tip through re-localization at the plasma membrane and interactions with intracellular signalling proteins such as RopGEFs (guanine nucleotide-exchange factors) for the activation of the ROP1 Rho GTPase (Takeuchi and Higashiyama, 2016). While AtLURE1 has a more species-specific role (Liu et al., 2021b), a second set of related cysteine-rich peptides, XIUQIUs, are also secreted from the synergid cells and play a more non-species-specific function in pollen tube attraction (Zhong et al., 2019). The receptor for perceiving the XIUQIUs is so far unknown (Figure 1D).

In the pollen tube, four members of the CrRLK1L family, BUDDHA'S PAPER SEAL (BUPS) 1 and 2, and ANXUR1 and ANXUR2 (ANX1 and 2) are responsible for maintaining pollen tube integrity as the pollen tube grows through the reproductive tract (Miyazaki et al., 2009; Ge et al., 2017; Zhu et al., 2018; reviewed in Hafidh and Honys, 2021; Robichaux and Wallace, 2021). BUPS1/2 form a heterodimeric complex with ANX1/2 to perceive autocrine signals from the pollen tube itself. The signals are secreted RALF4/19 peptides which are detected by the BUPS1/2-ANX1/2 complex to reinforced cell wall integrity and ensure that the pollen tube does not rupture prematurely before arriving at the synergid cells. Pollen tube reception occurs once the pollen tube has reached an ovule and enters the micropyle to come in contact with a receptive synergid cell where the pollen tube will rupture to release the sperm cells. Three additional CrRLK1L family members, FER, ANJ and HERCULES RECEPTOR KINASE 1 (HERK1) are present in the synergid cells for pollen tube reception, where they have a functionally redundant role in promoting pollen tube growth arrest and rupture (Escobar-Restrepo et al., 2007; Galindo-Trigo et al., 2020a) by perceiving several RALFs (RALF 6, 7, 16, 36 and 37) secreted by the pollen tube (Figure 1E; Zhong et al., 2022). FER is also proposed to increase ROS production for pollen tube rupture and sperm cell discharge (Duan et al., 2014). Prior to this final stage, FER, ANJ and HERK1 regulate the polytubey block which is proposed to take place at the septum (Figure 1A), where additional pollen tubes are prevented from exiting the transmitting tract adjacent to an ovule that has already attracted one pollen tube. FER, ANJ and HERK1 are proposed to carry out this function by perceiving the same pollen tube secreted RALF peptides, RALF 6, 7, 16, 36 and 37 (Zhong et al., 2022).

Conclusion and future perspectives

The regulation of compatible pollen-pistil interactions leading to fertilization in *Arabidopsis* involves an extensive network of RLKs, RKs and their corresponding ligands. While a number of these players have been identified, there are still many remaining gaps, particularly at the early stages. Starting with the stigmatic papilla regulation of pollen hydration, further work is needed to understand how the negative gating mechanism of the ANJ-FER complex in the papillae connects with the positive regulatory role proposed for the RKF1 cluster. Future investigations should seek to identify ligands for RKF1 and RKFLs as well as potential binding partners in the papilla plasma membrane. Similarly, does the same unknown ligands and binding partners function with RKF1 and the RKFLs in the reproductive tract. As discussed above, SERK1 and SERK3/BAK1 typically form complexes with other LRR-RKs (reviewed in Gou and Li, 2020), and thus future work should focus on identifying which RK complexes are formed in the transmitting tract to support pollen tube growth. Here we have proposed the PSKR1 and PSKR2 as excellent candidates as the *pskr1-3 pskr2-1* double mutant pistils supported displayed slower pollen tube growth through the style (Stuhrwohldt et al., 2015). Finally, downstream signaling pathways activated by these RKs in the reproductive tract will need to be elucidated. The identification of these new RLK players in the reproductive tract is an exciting and important step towards fully understanding this complex process and provides new grounds for additional research into the *Arabidopsis* reproductive processes.

Author contributions

SB, LC, and DG conceived the review, SB and LC wrote the first draft, SB, LC, and DG edited the review and approved the submitted version.

Funding

This work was supported by a grant from Natural Sciences and Engineering Research Council of Canada to DG (5010470).

Acknowledgments

We thank members of the Goring lab for critically reading this article.

Conflict of interest

The authors declare that the research was conducted in the absence of any commercial or financial relationships that could be construed as a potential conflict of interest.

Publisher's note

References

Abhinandan, K., Sankaranarayanan, S., Macgregor, S., Goring, D. R.Samuel, M. A. (2022). Cell-cell signaling during the brassicaceae self-incompatibility response. *Trends Plant Sci.* 27 (5), 472–487. doi: 10.1016/j.tplants.2021.10.011

Dickinson, H. (1995). Dry stigmas, water and self-incompatibility in *Brassica*. *Sex Plant Reprod.* 8 (1), 1–10. doi: 10.1007/BF00228756

Dievart, A., Gottin, C., Perin, C., Ranwez, V.Chantret, N. (2020). Origin and diversity of plant receptor-like kinases. *Annu. Rev. Plant Biol.* 71, 131–156. doi: 10.1146/annurev-arplant-073019-025927

Doucet, J., Lee, H. K., Udugama, N., Xu, J., Qi, B.Goring, D. R. (2019). Investigations into a putative role for the novel BRASSIKIN pseudokinases in compatible pollen-stigma interactions in *Arabidopsis thaliana*. *BMC Plant Biol.* 19 (1), 549. doi: 10.1186/s12870-019-2160-9

Doughty, J., Hedderson, F., McCubbin, A.Dickinson, H. (1993). Interaction between a coating-borne peptide of the brassica pollen grain and stigmatic s (self-incompatibility)-locus-specific glycoproteins. *Proc. Natl. Acad. Sci. U.S.A.* 90 (2), 467–471. doi: 10.1073/pnas.90.2.467

Duan, Q., Kita, D., Johnson, E. A., Aggarwal, M., Gates, L., Wu, H. M., et al. (2014). Reactive oxygen species mediate pollen tube rupture to release sperm for fertilization in *Arabidopsis*. *Nat. Commun.* 5 (3129), 1–10. doi: 10.1038/ncomms4129

Duan, Q., Kita, D., Li, C., Cheung, A. Y.Wu, H. M. (2010). FERONIA receptor-like kinase regulates RHO GTPase signaling of root hair development. *Proc. Natl. Acad. Sci. U.S.A.* 107 (41), 17821–17826. doi: 10.1073/pnas.1005366107

Escobar-Restrepo, J.-M., Huck, N., Kessler, S., Gagliardini, V., Gheyselinck, J., Yang, W.-C., et al. (2007). The FERONIA receptor-like kinase mediates Male-female interactions during pollen tube reception. *Science* 317 (5838), 656–660. doi: 10.1126/science.1143562

Escocard de Azevedo Manhaes, A. M., Ortiz-Morea, F. A., He, P.Shan, L. (2021). Plant plasma membrane-resident receptors: Surveillance for infections and coordination for growth and development. *J. Integr. Plant Biol.* 63 (1), 79–101. doi: 10.1111/jipb.13051

Galindo-Trigo, S., Blanco-Touriñán, N., DeFalco, T. A., Wells, E. S., Gray, J. E., Zipfel, C., et al. (2020a). CrRLK1L receptor-like kinases HERK1 and ANJEA are female determinants of pollen tube reception. *EMBO Rep.* 21 (2), e48466. doi: 10.15252/embr.201948466

Galindo-Trigo, S., Blumke, P., Simon, R.Butenko, M. A. (2020b). Emerging mechanisms to fine-tune receptor kinase signaling specificity. *Curr. Opin. Plant Biol.* 57, 41–51. doi: 10.1016/j.pbi.2020.05.010

Ge, Z., Bergonci, T., Zhao, Y., Zou, Y., Du, S., Liu, M.-C., et al. (2017). *Arabidopsis* pollen tube integrity and sperm release are regulated by RALF-mediated signaling. *Science* 358 (6370), 1596–1600. doi: 10.1126/science.aao3642

Goto, H., Okuda, S., Mizukami, A., Mori, H., Sasaki, N., Kurihara, D., et al. (2010). Chemical visualization of an attractant peptide, LURE. *Plant Cell Physiol.* 52 (1), 49–58. doi: 10.1093/pcp/pcq191

Gou, X.Li, J. (2020). Paired receptor and coreceptor kinases perceive extracellular signals to control plant development. *Plant Physiol.* 182 (4), 1667–1681. doi: 10.1104/pp.19.01343

Hafidh, S.Honys, D. (2021). Reproduction multitasking: The Male gametophyte. *Annu. Rev. Plant Biol.* 72, 581–614. doi: 10.1146/annurev-arplant-080620-021907

He, Y., Zhou, J., Shan, L.Meng, X. (2018). Plant cell surface receptor-mediated signaling – a common theme amid diversity. *J. Cell Sci.* 131 (12), jcs209353. doi: 10.1242/jcs.209353

Huang, W. J., Liu, H. K., McCormick, S.Tang, W. H. (2014). Tomato pistil factor STIG1 promotes in vivo pollen tube growth by binding to phosphatidylinositol 3-phosphate and the extracellular domain of the pollen receptor kinase LePRK2. *Plant Cell* 26 (6), 2505–2523. doi: 10.1105/tpc.114.123281

Johnson, M. A., Harper, J. F.Palanivelu, R. (2019). A fruitful journey: Pollen tube navigation from germination to fertilization. *Annu. Rev. Plant Biol.* 70, 809–837. doi: 10.1146/annurev-arplant-050718-100133

Kim, M. J., Jeon, B. W., Oh, E., Seo, P. J.Kim, J. (2021). Peptide signaling during plant reproduction. *Trends Plant Sci.* 26 (8), 822–835. doi: 10.1016/j.tplants.2021.02.008

Lee, H. K.Goring, D. R. (2021). Two subgroups of receptor-like kinases promote early compatible pollen responses in the *Arabidopsis thaliana* pistil. *J. Exp. Bot.* 72 (4), 1198–1211. doi: 10.1093/jxb/eraa496

Liu, C., Shen, L., Xiao, Y., Vyshedsky, D., Peng, C., Sun, X., et al. (2021a). Pollen PCP-b peptides unlock a stigma peptide-receptor kinase gating mechanism for pollination. *Science* 372 (6538), 171–175. doi: 10.1126/science.abc6107

Liu, M., Wang, Z., Hou, S., Wang, L., Huang, Q., Gu, H., et al. (2021b). AtLURE1/PRK6-mediated signaling promotes conspecific micropylar pollen tube guidance. *Plant Physiol.* 186 (2), 865–873. doi: 10.1093/plphys/kiab105

McInnis, S. M., Desikan, R., Hancock, J. T.Hiscock, S. J. (2006). Production of reactive oxygen species and reactive nitrogen species by angiosperm stigmas and pollen: potential signalling crosstalk? *N. Phytol.* 172 (2), 221–228. doi: 10.1111/j.1469-8137.2006.01875.x

Miyazaki, S., Murata, T., Sakurai-Ozato, N., Kubo, M., Demura, T., Fukuda, H., et al. (2009). ANXUR1 and 2, sister genes to FERONIA/SIRENE, are male factors for coordinated fertilization. *Curr. Biol.* 19 (15), 1327–1331. doi: 10.1016/j.cub.2009.06.064

Okuda, S., Tsutsui, H., Shiina, K., Sprunck, S., Takeuchi, H., Yui, R., et al. (2009). Defensin-like polypeptide LUREs are pollen tube attractants secreted from synergid cells. *Nature* 458 (7236), 357–361. doi: 10.1038/nature07882

Robichaux, K. J.Wallace, I. S. (2021). Signaling at physical barriers during pollen-pistil interactions. *Int. J. Mol. Sci.* 22 (22):12230, 1–17. doi: 10.3390/ijms222212230

Shiu, S. H.Bleecker, A. B. (2001). Receptor-like kinases from *Arabidopsis* form a monophyletic gene family related to animal receptor kinases. *Proc. Natl. Acad. Sci. U.S.A.* 98 (19), 10763–10768. doi: 10.1073/pnas.181141598

Stuhrwohldt, N., Dahlke, R. I., Kutschmar, A., Peng, X., Sun, M. X.Sauter, M. (2015). Phytosulfokine peptide signaling controls pollen tube growth and funicular pollen tube guidance in *Arabidopsis thaliana*. *Physiol. Plant* 153 (4), 643–653. doi: 10.1111/ppl.12270

Takeuchi, H.Higashiyama, T. (2012). A species-specific cluster of defensin-like genes encodes diffusible pollen tube attractants in *Arabidopsis*. *PloS Biol.* 10 (12), e1001449. doi: 10.1371/journal.pbio.1001449

Takeuchi, H.Higashiyama, T. (2016). Tip-localized receptors control pollen tube growth and LURE sensing in *Arabidopsis*. *Nature* 531 (7593), 245–248. doi: 10.1038/nature17413

Wang, L., Clarke, L. A., Eason, R. J., Parker, C. C., Qi, B., Scott, R. J., et al. (2017). PCP-b class pollen coat proteins are key regulators of the hydration checkpoint in *Arabidopsis thaliana* pollen–stigma interactions. *New Phytol.* 213 (2), 764–777. doi: 10.1111/nph.14162

Zafra, A., Rejon, J. D., Hiscock, S. J.Alche Jde, D. (2016). Patterns of ROS accumulation in the stigmas of angiosperms and visions into their multi-functionality in plant reproduction. *Front. Plant Sci.* 71112. doi: 10.3389/fpls.2016.01112

Zhang, X., Liu, W., Nagae, T. T., Takeuchi, H., Zhang, H., Han, Z., et al. (2017). Structural basis for receptor recognition of pollen tube attraction peptides. *Nat. Commun.* 8 (1), 1331. doi: 10.1038/s41467-017-01323-8

Zhong, S., Liu, M., Wang, Z., Huang, Q., Hou, S., Xu, Y. C., et al. (2019). Cysteine-rich peptides promote interspecific genetic isolation in *Arabidopsis*. *Science* 364 (6443):eaau9564, 1–8. doi: 10.1126/science.aau9564

Zhong, S., Li, L., Wang, Z., Ge, Z., Li, Q., Bleckmann, A., et al. (2022). RALF peptide signaling controls the polytubey block in *Arabidopsis*. *Science* 375 (6578), 290–296. doi: 10.1126/science.abl4683

Zhu, L., Chu, L. C., Liang, Y., Zhang, X. Q., Chen, L. Q.Ye, D. (2018). The *Arabidopsis* CrRLK1L protein kinases BUPS1 and BUPS2 are required for normal growth of pollen tubes in the pistil. *Plant J.* 95 (3), 474–486. doi: 10.1111/tpj.13963

frontiers | Frontiers in Plant Science

TYPE Original Research
PUBLISHED 08 November 2022
DOI 10.3389/fpls.2022.1028311

OPEN ACCESS

EDITED BY
Giampiero Cai,
University of Siena, Italy

REVIEWED BY
Liang Guo,
Huazhong Agricultural University, China
Hubert Schaller,
UPR2357 Institut de biologie moléculaire des plantes (IBMP), France

*CORRESPONDENCE
Martin Potocký
potocky@ueb.cas.cz

SPECIALTY SECTION
This article was submitted to Plant Cell Biology, a section of the journal Frontiers in Plant Science

RECEIVED 25 August 2022
ACCEPTED 11 October 2022
PUBLISHED 08 November 2022

CITATION
Serrano N, Pejchar P, Soukupová H, Hubálek M and Potocký M (2022) Comprehensive analysis of glycerolipid dynamics during tobacco pollen germination and pollen tube growth. *Front. Plant Sci.* 13:1028311. doi: 10.3389/fpls.2022.1028311

Comprehensive analysis of glycerolipid dynamics during tobacco pollen germination and pollen tube growth

Natalia Serrano[1], Přemysl Pejchar[1], Hana Soukupová[1], Martin Hubálek[2] and Martin Potocký[1]*

[1]Institute of Experimental Botany of the Czech Academy of Sciences, Prague, Czechia, [2]Institute of Organic Chemistry and Biochemistry of the Czech Academy of Sciences, Prague, Czechia

Pollen germination and subsequent pollen tube elongation are essential for successful land plant reproduction. These processes are achieved through well-documented activation of membrane trafficking and cell metabolism. Despite this, our knowledge of the dynamics of cellular phospholipids remains scarce. Here we present the turnover of the glycerolipid composition during the establishment of cell polarity and elongation processes in tobacco pollen and show the lipid composition of pollen plasma membrane-enriched fraction for the first time. To achieve this, we have combined several techniques, such as lipidomics, plasma membrane isolation, and live-cell microscopy, and performed a study with different time points during the pollen germination and pollen tube growth. Our results showed that tobacco pollen tubes undergo substantial changes in their whole-cell lipid composition during the pollen germination and growth, finding differences in most of the glycerolipids analyzed. Notably, while lysophospholipid levels decrease during germination and growth, phosphatidic acid increases significantly at cell polarity establishment and continues with similar abundance in cell elongation. We corroborated these findings by measuring several phospholipase activities *in situ*. We also observed that lysophospholipids and phosphatidic acid are more abundant in the plasma membrane-enriched fraction than that in the whole cell. Our results support the important role for the phosphatidic acid in the establishment and maintenance of cellular polarity in tobacco pollen tubes and indicate that plasma membrane lysophospholipids may be involved in pollen germination.

KEYWORDS

lipidomics, phosphatidic acid, phospholipid, plasma membrane, pollen, pollen tube, tip growth, tobacco

Introduction

In plant reproduction, the highly coordinated delivery of nonmotile sperm cells to the egg *via* a pollen tube represents a key innovation during the colonization of land by flowering plants because it allowed for sexual reproduction (Higashiyama and Takeuchi, 2015). Detailed knowledge of the mechanisms of sexual reproduction is critical for its obvious agronomic implications, but in addition, pollen germination and pollen tube growth are excellent model systems for understanding cell morphology. During pollen germination, processes determining the establishment of cellular polarity are overrepresented, and analogously, strictly apical elongation of pollen tubes involves many processes of cell polarity maintenance (Conze et al., 2017; Grobei et al., 2009; Hafidh and Honys, 2021). Typically, when pollen grain lands on the stigma (or is incubated in culturing medium), it rapidly hydrates to trigger a metabolic program for the germination stage. The hydration then switches on a signaling, metabolic and transcriptomic program that leads to the breakdown of energy stores, uptake of nutrients, reorganization of cytoskeleton and endomembrane organelles, cellular polarization, and buildup of vesicular trafficking machinery. After 30-60 min, this collectively leads to the emergence of a pollen tube from the germination pore, and a second developmental program focused on pollen tube growth gradually takes over (Wang et al., 2010).

There is tremendous membrane dynamics in germinating pollen and elongating pollen tubes, comprising both plasma membrane and various compartments of the endomembrane system (Zonia and Munnik, 2008). This coincides with the fact that pollen grains from all known species accumulate enormous amounts of glycerolipids, that are stored in endoplasmic reticulum-derived compartments termed lipid droplets (LD, Hernández et al., 2020). They provide ready-to-use material and the energy source for rapid membrane production and remodeling during germination and elongation of pollen tubes. It has been estimated that a pollen tube with a diameter of 10 µm would require around 2-3 pmol (corresponding to ~2 ng) of membrane lipids for each cm of length for the tonoplast and the plasma membrane alone (Ischebeck, 2016). All lipid classes, including sphingolipids, glycerophospholipids, galactolipids, triacylglycerols, sterols, and waxes, are present in pollen, where they are subject to tight regulation (Žárský et al., 2006; Ischebeck, 2016).

Glycerophospholipids are the most abundant type of phospholipids and constitute a crucial component of all eukaryotic membranes, including plants (Kerwin et al., 1994). Different glycerophospholipid families with distinct polar head groups bound to the sn-3 position of the glycerol backbone and diverse acyl-chain compositions are present in cell membranes. This headgroup and acyl chain composition of glycerophospholipids in various cell types, endomembrane compartments, and plasma membrane are quite distinct (Horn and Chapman, 2012; Nakamura et al., 2017). Based on the knowledge from mammalian and yeast studies, different lipid composition is also expected in the outer and inner leaflets of the plasma membrane (PM), with the glycerolipids dominating the in inner, cytoplasmic leaflet. However, direct evidence for PM asymmetry in plants is still missing (Cacas et al., 2016; Cassim et al., 2018). Importantly, this diversity and dynamic nature of membrane glycerolipids are not only due to *de novo* lipid biosynthesis in the ER and Golgi but also due to enzymatic activities of various phospholipases, lysophospholipid acyltransferases, and lipid kinases. This glycerolipid remodeling cycle thus contributes to the generation of membrane glycerophospholipid diversity and the production of lipid signaling molecules such as phosphatidic acid, phosphoinositides, lysophospholipids, diacylglycerol, and fatty acids (Colin and Jaillais, 2020; Heilmann and Heilmann, 2022).

Despite the apparent importance of membrane lipids in tip-growing pollen tubes, high-throughput lipidomic analyses in pollen are scarce compared to the wealth of data from sporophytic tissues. To some extent, pollen glycerolipids had been analyzed in rape seed (Piffanelli et al., 1997), lily (Nakamura et al., 2009), Arabidopsis (McDowell et al., 2013), wheat (Narayanan et al., 2018), tobacco (Krawczyk et al., 2022), and olive (Hernández et al., 2020). However, most of these studies studied non-germinated pollen grains or focused on pollen responses to heat stress. Here, we explored the glycerolipid composition of different stages of tobacco pollen germination and pollen tube elongation. Simultaneously, we analyzed the *in situ* activity dynamics of phospholipase A_2, phospholipase D, and non-specific phospholipase C. To provide a glimpse into the compartment-specific lipid composition, we investigated the glycerolipid composition of the plasma membrane-enriched fraction. Having the advantage of tobacco (*Nicotiana tabacum* L.) pollen tubes as a model, which combines easy cultivation in quantities needed for various -omics experiments with genetic transformation and relatively high *in vitro* growth rates of 50-100 nm/s (Hepler et al., 2001; Chen et al., 2002), we also followed the dynamic localization of phosphatidic acid marker between various subcellular compartments.

Materials and methods

Pollen *in vitro* germination and lipid extraction

Tobacco (*Nicotiana tabacum* L. cv. Samsun) pollen was collected from the greenhouse-grown flowers and long-term stored at –20°C. For the lipid isolation at dedicated timepoints, pollen was resuspended in simple pollen growth medium (10% sucrose, 0.01% boric acid) at 2 mg/mL concentration, and 1 mL samples were immediately collected (timepoint 0'). After 30 minutes of imbibition, we collected the second set of 1 mL samples (timepoint 30'). Finally, after 3 hours, we collected the

last set of 1mL samples (timepoint 3h). For each timepoint, five replicate cultures were cultivated.

Immediately after samples were collected, we performed the total lipid extraction using a slightly modified method of Bligh and Dyer (1959) using 4 mL of cooled (-20°C) methanol-chloroform 2:1 as described in Pejchar et al. (2010). The samples were centrifuged briefly and kept at room temperature for 30 minutes. Following, 1 M KCl was added to the mix, vortexed vigorously, and held at 4°C for 30 minutes. After 15 min centrifugation at 2000 x g, the organic phase was collected and transferred to a new 2 mL glass vial, dried with nitrogen, sealed with parafilm, and stored at -80°C.

Lipidome analysis was performed using an automated electrospray ionization-tandem mass spectrometry approach (Narayanan et al., 2016). The lipid extracts were introduced by continuous infusion into the ESI source on a triple quadrupole MS/MS (API 4000, Applied Biosystems, Foster City, CA). Samples were placed into the ESI using an autosampler compatible with the requirements of the ESI needle. Sequential precursor and neutral loss scans of the extracts generate a series of spectra with each spectrum revealing a set of lipid species containing a common head group. The background of each spectrum was subtracted, the data were smoothed, and peak areas integrated using an Applied Biosystems Analyst software (Xiao et al., 2010) in Kansas Lipidomics Research Center. The intensity values were calculated using a normalized intensity per mg pollen dry weight, and they were converted to the percentage of the total signal as it is the signal for each lipid species multiplied by 100 and divided by the total signal for the sample (Narayanan et al., 2018). All chemicals used were HPLC-grade.

Plasma membrane isolation and characterization

For the isolation of the PM-enriched fraction, 0.15 g of dry pollen was germinated for 3 hours, and pollen tubes were collected by gentle filtration using a vacuum pump with a Miracloth filter. The sample was then split into two fractions, and the PM-enriched fraction was isolated with the Minute™ Plant Plasma Membrane Protein Isolation Kit (Invent Biotechnologies, Inc.). During the isolation, cytosolic and organelle fractions were also collected for monitoring purposes.

The isolated PM-enriched fraction (together with the cytosolic and organelle fraction) was separated on 10% SDS-PAGE gel and transferred to the PVDF membrane. After overnight incubation in 5% nonfat milk blocking solution (TBS with 0.05% Tween-20), the membrane was probed for 1 h with the following compartment marker antibodies (Agrisera) using the recommended dilutions: Anti-H^+-ATPase (Plasma membrane maker, 90-95 kDa, AS07 260), Anti-UGPase (Cytoplasm marker, 52 kDa, AS14 2813), Anti-H3 (Nuclear marker, 17 kDa, AS10 710), Anti-BiP (Endoplasmic reticulum marker, 73.5/80 kDa, AS09 481), Anti-V-ATPase (Vacuolar marker, 26/31 kDa, AS07 213), and Anti-Arf1 (Golgi marker, 21 kDa, AS08 325). After washing, membranes were probed with the Anti-rabbit IgG secondary antibody (diluted 1:20000) conjugated with horseradish peroxidase (Promega). The detection was done with ECL™ Prime Western Blotting Detection Reagent (Cytiva) according to the manufacturer's instructions.

Sample preparation and mass spectrometry analysis

The samples for proteomic analysis were prepared in a 2% SDS buffer and heated up for 5 minutes at 95°C. The reduction was done using 100 mM Tris(2-carboxyethyl)phosphine (TCEP) for 30 minutes incubation at 37°C using the Microcon® Filter Unit (UF). The filter placed on a collection tube was spun at 14000 g for 25 minutes. The collection tube was changed and 200 µL of buffer A (800 mM urea, 0.5 mM Deoxycholic acid (DCA), and 100 mM Ammonium bicarbonate (ABC)) were added. Tube was spun at 14000 g for 30 minutes. For the alkylation, we added 15 µL of 100 mM of Iodoacetamide (IAA) and 85 µL of buffer A to the filter and incubated for 30 minutes in the dark. Afterwards it was spun at 14000 g for 30 minutes. Following three washes with 3x100 µL of buffer A, the filter was centrifuged at 14000 g for 20 minutes. Additionally, the filter was washed three times with 100 µL buffer B (0.5 mM DCA, 50mM ABC) and centrifuged at 14000 g for 20 minutes. 100 µL of buffer B with trypsin (Pierce™ Trypsin Protease, MS-Grade), added to the UF device, was used for the digestion, which proceeded for 8 h at 37°C. Peptides were recovered by transferring the UF filter into a new collection tube and spinning at 14000 g for 15 min. To recover the peptides from the filter, 50 µL of 50 mM ABC was used twice and spun at 14000g for 15 minutes at RT. 200 µL of ethyl acetate, and 2.5 µL of TFA were added to the peptides and vortexed for 1 minute, followed by the addition of 1 mL of ethyl acetate and vortexed again. The tubes were spun at 16000 g for 10 minutes at RT. The organic phase was discarded, and these last two steps were repeated two more times. Peptides were evaporated in Speedvac (Erde et al., 2014).

The resulting peptides were separated on an UltiMate 3000 RSLCnano system (Thermo Fisher Scientific, Waltham, MA, USA) coupled to a Mass Spectrometer Orbitrap Fusion Lumos (Thermo Fisher Scientific) as described previously (Keilhauer et al., 2015; Langerova et al., 2020). The peptides were trapped and desalted with 2% acetonitrile in 0.1% formic acid at a flow rate of 30 µL/min on an Acclaim PepMap100 column (5 µm, 5 mm by 300-µm internal diameter (ID); Thermo Fisher Scientific). Eluted peptides were separated using an Acclaim PepMap100 analytical column (2 µm, 50-cm by 75-µm ID; Thermo Fisher Scientific). The 125 minutes elution gradient at a constant flow rate of 300 nL/min was set to 5% phase B (0.1% formic acid in 99.9% acetonitrile) and 95% phase A

(0.1% formic acid) for the first 1 minute. Then, the content of acetonitrile increased gradually. The orbitrap mass range was set from m/z 350 to 2000 in the MS mode, and the instrument acquired fragmentation spectra for ions of m/z 100 to 2000. Proteome Discoverer 2.5 (Thermo Fisher Scientific) was used for peptide and protein identification using Sequest and Amanda as search engines against databases of tobacco downloaded from UNIPROT November 2021 and common contaminants. The mass spectrometry proteomics data have been deposited to the ProteomeXchange Consortium *via* the PRIDE (Perez-Riverol et al., 2022) partner repository with the dataset identifier PXD037046 and 10.6019/PXD037046.

Statistical analysis

Various statistical analyses (including PCA analysis, One-way ANOVA with the *post hoc* tests, hierarchical cluster, and heatmap analyses) were done by the MetaboAnalyst web service (http://www.metaboanalyst.ca/). Significance was analyzed using ANOVA, FDR-adjusted *p* values lower than 0.05 were considered significant, and Tukey's HSD was used as a *post hoc* test. We also used the web-based LipidSig tool for additional lipidomic data analysis and visualization of the plasma membrane and cell samples (Lin et al., 2021; http://chenglab.cmu.edu.tw/lipidsig/).

In situ lipase analyses

Two microliters of the solution of fluorescently-labeled substrate Bodipy-phosphatidylcholine (2-decanoyl-1-(O-(11-(4,4-difluoro-5,7-dimethyl-4-bora-3a,4a-diaza-s-indacene-3-propionyl) amino) undecyl) sn-glycero-3-phosphocholine) (Bodipy-PC, D-3771, Invitrogen) in ethanol was added to the pollen culture (2 mg/mL) at indicated times (final concentration of Bodipy-PC was 0.66 μg/mL). After incubation on an orbital shaker at RT for 10 min, lipids were extracted as described above, the organic phase was evaporated to dryness by a vacuum evaporator, redissolved in ethanol and analyzed using thin-layer chromatography as described earlier (Pejchar et al., 2010). Briefly, samples were applied on the HP-TLC silica plates by automatic sampler, plates were developed in a mobile phase chloroform: methanol: water 65: 25: 4 (v/v/v), dried and scanned by FLA-7000 (Fujifilm) laser scanner. Individual spots were identified based on the comparison with fluorescently-labeled lipid standards and quantified by Multi Gauge (Fujifilm) software.

Molecular cloning and stable tobacco transformation

Molecular cloning of the construct for genetically-encoded PA sensor (pUBQ::mCherry-NES-2xSpo20-PABD) was described previously (Kalachova et al., 2022). The final construct was transferred into *Agrobacterium tumefaciens* strain GV3101, which was used to transform tobacco (*N. tabacum* L. cv. "Petit Havana" SR1) plants by leaf-disk immersion method according to Horsch et al. (1985). Transformants were selected in kanamycin-containing medium.

Confocal microscopy

For live-cell imaging, pollen and pollen tubes were observed with a spinning disk confocal microscope (Yokogawa CSU-X1 on Nikon Ti-E platform) equipped with a 60x Plan Apochromat objective (WI, NA = 1.2) and Andor Zyla sCMOS camera. Laser excitation (561 nm, laser box Agilent MLC400) together with 607/36-nm single-band filter (Semrock Brightline) were used for mCherry fluorescence collection.

Results

For successful delivery of the sperm cells, two main developmental switches must happen (i) pollen germination, i.e., the hydration of mature pollen and activation of processes leading to the emergence of a pollen tube; (ii) pollen tube growth, i.e., the successful maintenance of polarity-related processes ensuring the rapid tip growth, like the proper balance of anterograde and retrograde membrane trafficking, proper organization of actin cytoskeleton and the correct positioning of the male-germ unit. To monitor pollen lipidome changes in these crucial developmental steps, we sampled the *in vitro* tobacco pollen culture immediately after imbibition (timepoint 0'), 30 minutes after imbibition (timepoint 30'), and finally, after 3h of *in vitro* growth (timepoint 3h). These timepoints are well established as the most representative for pollen hydration, pollen germination, and pollen tube growth, respectively (Mascarenhas, 1975; Dorne et al., 1988). The microscopic monitoring confirmed that at 0', >90% of pollen grains were correctly hydrated, germination was occurring *en masse* at 30', and almost all pollen grains developed nicely growing pollen tubes at 3h (Figure 1A).

Glycerolipidome undergoes substantial changes during tobacco pollen germination and pollen tube elongation

Recommended plant lipid isolation procedures typically involve solid samples (e.g., leaves), and great caution was made to prevent artificially high levels of phosphatidic acid (PA) caused by an uncontrolled release of phospholipase D (PLD). To inactivate PLD and other lipolytic enzymes, sample incubation in hot isopropanol with 0.01% BHT,

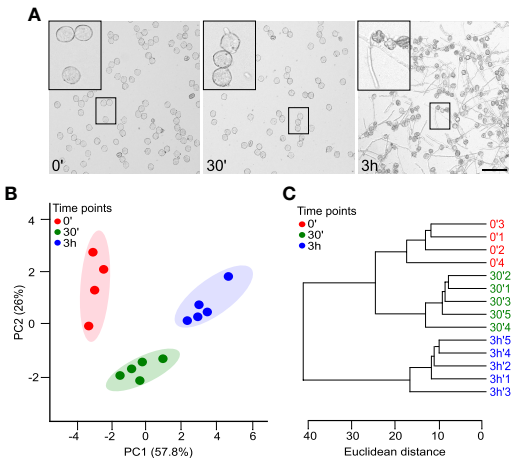

FIGURE 1
Tobacco pollen has a distinct whole-cell lipidome during the establishment and maintenance of cell polarity. **(A)** Time series of growing pollen tubes monitored at 0, 30 and 180 minutes after germination in liquid medium. Bar =100 µm. **(B)** Principal component analysis (PCA) of the glycerolipidome based on pollen tubes at 0, 30 and 180 minutes. The shaded areas indicate the 95% confidence regions. Samples are colored according to the time of collection 0' (red), 30' (green) and 3h (blue). **(C)** Dendrogram of hierarchical cluster analysis of individual glycerolipidome samples among pollen tubes at different times 0, 30 and 180 minutes. Both PCA and hierarchical clustering were done using the MetaboAnalyst package.

followed by a mixture of chloroform-methanol-water, is recommended as the first isolation step (Shiva et al., 2018). We initially attempted to isolate the lipids from liquid pollen tube culture using this protocol, which required the rapid removal of the medium prior to hot isopropanol addition. Unexpectedly, our pilot results showed atypically high levels of PA (~40%) at the expense of phosphatidylcholine (PC) and phosphatidylethanolamine (PE) levels, likely caused by the cell damage (Supplementary Figure 1). Therefore, we reverted to the classical lipid extraction technique that uses a 2:1 ratio of methanol: chloroform as a first step (Bligh and Dyer, 1959) and is compatible with the liquid cell culture samples. This isolation approach, followed by the electrospray ionization-tandem mass spectrometry, quantified 115 lipid analytes from 11 glycerolipid classes (Supplementary Table 1). These included two galactolipids class lipids – 8 species of monogalactosyldiacylglycerol (MGDG) and 9 digalactosyldiacylglycerols (DGDG). Among glycerophospholipids, we identified 4 species of lysophosphatidylglycerol (LPG), 6 lysophosphatidylcholines (LPC), 4 lysophosphatidylethanolamines (LPE), 18 phosphatidylcholines (PC), 21 phosphatidylethanolamines (PE), 10 phosphatidylglycerols (PG), 14 phosphatidylinositols (PI), 12 phosphatidylserines (PS) and 9 phosphatidic acids (PA).

To further explore the difference between the time points and get a comprehensive view of the lipidomic data, we performed a multivariate analysis on the dataset employing the MetaboAnalyst 5.0 pipeline (http://www.metaboanalyst.ca; Pang et al., 2022), which is also geared towards the processing of lipidomics data (Narayanan et al., 2018). Principal component analysis (PCA) of the pruned and scaled data (Supplementary Table 2) shows that replicates from each timepoint are grouped together and that the datasets from individual timepoints are well-separated, with the first two principal components explaining 84% of data variation (Figure 1B). In parallel with the PCA analysis, the hierarchical clustering of the data corroborated the similarity of the replicates for each timepoint and suggested that general glycerolipidome profiles for hydrated and germinated pollen are more closely related compared to pollen tubes (Figure 1C).

The overall analysis of the pollen glycerolipid classes showed that the non-charged zwitterionic phospholipids PC and PE constitute most of the pollen glycerolipids with ~50% and ~35%, respectively (Figure 2A). Among negatively charged phospholipids, PI species in pollen comprise ~10%, while the total PA levels reach 1.5%, the total amount of PG is 0.9%, and PS is present at <0.5%. Lysophospholipids LPC and LPE represent ~0.8% of total glycerolipids each, and LPG was found only in trace amounts. Finally, galactolipids MGDG and DGDG are the minor components of the pollen glycerolipidome, constituting 0.3% and 0.15%, respectively. These relative phospholipid proportions (i.e., PC~PE>PI>PA~PG>PS) corresponded somewhat to glycerolipid compositions in non-photosynthesizing sporophytic tissues, such as Arabidopsis or tomato roots (Devaiah et al., 2006; Pfaff et al., 2020). Similarly, the presence of low galactolipid levels is consistent with the previous reports showing that although pollen and pollen tubes do not develop photosynthesizing chloroplasts, MGDG and DGDG were also detected in Arabidopsis, lily, and wheat pollen (Nakamura et al., 2009; McDowell et al., 2013; Narayanan et al., 2018).

Notably, all analyzed pollen glycerolipid classes underwent significant and distinct changes during the pollen hydration-to-germination and/or pollen tube germination-to-elongation switch (Figure 2A). Surprisingly, this was also true for bulk phospholipids like PC and PE, which displayed the opposite trend during pollen tube growth. Also, both detected galactolipids (MGDG and DGDG) showed significant but unrelated changes, where total MGDG levels continuously increased with time while the amount of DGDG transiently decreased during germination. Inverse dynamics was also observed for anionic lipids PA and PI, where relative PA levels go up during the germination while PI decreases. The dynamics of PG strongly resembles that of MGDG, while PS shows a minor decrease during the germination phase. Finally, all

10.3389/fpls.2022.1028311

lysophospholipid levels seem to decrease during the germination and pollen tube phase, with LPC showing the most notable changes.

Next, we checked the general unsaturation index and the changes in saturated, monosaturated on polyunsaturated lipids in our datasets. We observed a significant decrease in unsaturation during both pollen germination and pollen tube elongation (Figure 2B), which is most prominent in glycerolipids with polyunsaturated fatty acids (PUFAs), i.e., those with the total number of double bonds >4 (Figure 2C). This is accompanied by an increase in monounsaturated lipids. Those general trends are driven by bulk phospholipids PC, PE, and PI, but they can also be seen in the extreme form in glycolipids, where DGDG and MGDG in hydrated pollen contain almost exclusively two PUFAs (i.e., containing 6 total double bonds) (Supplementary Figure 2). It is worth mentioning that these findings correspond well with the analysis of Arabidopsis cell culture when fast-growing cells also tended to accumulate monosaturated lipids and reduce the content of PUFAs (Meï et al., 2015).

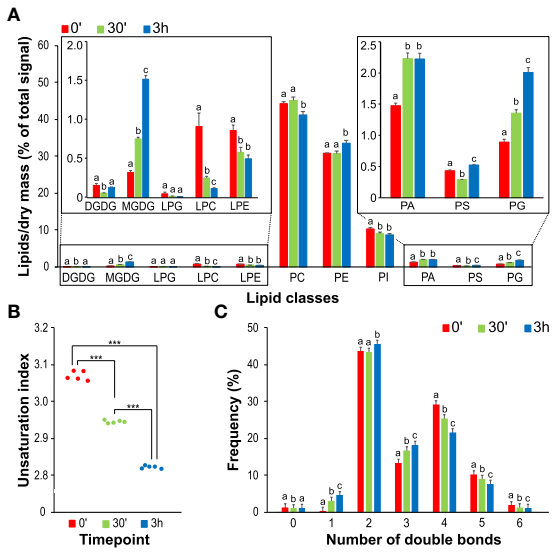

FIGURE 2
Changes in glycerolipid classes during the process of pollen germination and pollen tube elongation. **(A)** The composition of the main lipid classes (DGDG, MGDG, PG, PC, LPG, LPC, LPE, PE, PI, PS and PA) at different time points during the germination process of pollen tubes. The inset shows the composition of selected lipid classes in more detail. Data are presented as mean ± sd, n=4 (0') and n=5 (30' and 3h). Different letters indicate significant differences between samples at $p < 0.05$. **(B)** Changes of total unsaturation index during the different timepoints. **(C)** Double bonds distribution in the different time points. Asterisks (***) represent the significance between samples at $p < 0.001$.

Alteration of lipid species composition during pollen germination and pollen tube growth

To get more specific insight into the glycerolipid changes during the switch from hydrated to germinated pollen and elongated pollen tubes, we analyzed the changes in individual lipid species. The composition of phospholipids in all three stages was dominated by two species, 34:2 and 36:4 (Figure 3). Although our analysis did not allow for direct identification of individual fatty acids (FAs), based on the lysophospholipid profiles, we can estimate that 34:2 phospholipids predominantly contain palmitic (16:0) and linoleic (18:2) acids. At the same time, 36:4 lipids are composed primarily of two 18:2 FAs and, to a much lesser extent, of oleic (18:1) and linolenic (18:3) acids (Figure 3). Analogously, we can estimate the FA composition of other significantly occurring phospholipids; 34:3 contains mainly 16:0/18:3, 36:3 contains mainly18:1/18:2 or 18:0/18:3, and 36:5 consists of 18:2/18:3.

Regarding the dynamics of specific phospholipid species, complex patterns can be seen for most phospholipids. For example, the most abundant species of PC, 34:2 and 36:4, both gradually decrease in time, whereas PE 34:2 and PE 36:4 display opposite trends. The same pattern is evident for 34:3, where PE increases during pollen germination and tube elongation while levels of PC 34:3 go down. Thus, PE 34:2 and 34:3 are mainly responsible for the increase in total PE levels (Figures 2A, 3). Notably, both PC 34:1 and PE 34:1 are massively boosted during pollen germination (over 10-fold and 5-fold increase, respectively), and similar dynamics was recorded for PC 36:3 (5-fold accumulation). On the other hand, most PI species decreased, including the most abundant PI 34:3 and PI 34:2, and a slight increase was only observed for monosaturated PI 34:1 and for PI 36:3. PG species then all follow the same linearly increasing trend. Among minor signaling phospholipids, both dominant PA species, PA 34:2 and PA 36:4, show a modest but significant increase in the pollen germination phase, while their relative levels do not further increase during pollen tube growth. Conversely, PS molecular species show distinct trends in both acyl-chain composition and relative changes during pollen germination and growth, which are unapparelled with other tested glycerolipids (Figure 3). First, predominant PS species PS 40:2, PS 40:3, PS 42:2, and PS 42:3, containing very-long-chain fatty acids (VLCFAs), together constitute >90% of total pollen PS, which contrasts with reported values for Arabidopsis (McDowell et al., 2013), wheat (Narayanan et al., 2018) and tobacco (Krawczyk et al., 2022) pollen. Second, PS species show unique dual dynamics, where particularly shorter species (PS 34:3 and 34:2) are significantly upregulated in the pollen tube phase. In contrast, most VLCFA-containing PS species exhibit 30-50% drop during the pollen hydration-to-germination phase and increase again during pollen tube elongation.

Although they are present at low absolute values, lysophospholipids also displayed profound changes in the two

10.3389/fpls.2022.1028311

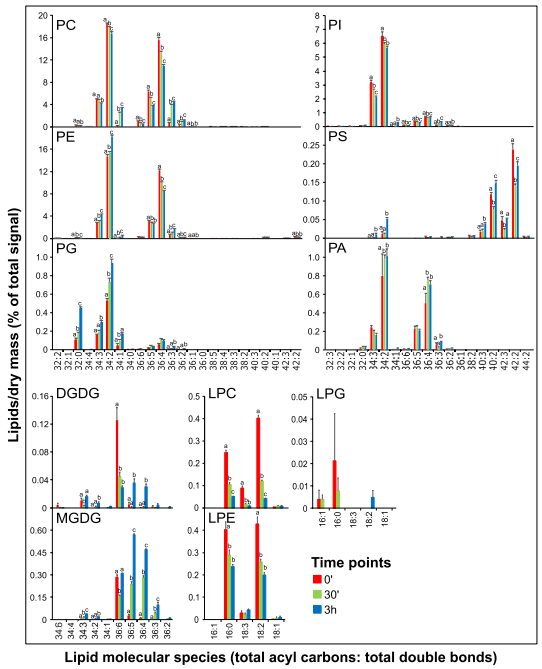

FIGURE 3
Changes in lipid molecular species during tobacco pollen germination and pollen tube elongation. Data are presented as mean ± s.e.m., n=4 (0') and n=5 (30' and 3h). Different letters indicate significant differences between samples at $p < 0.05$.

pollen developmental switches. Both major LPC and LPE species (16:0 and 18:2) decreased rapidly during pollen germination, partly reflecting the changes in PC and PE with 34:2 or 36:4 composition (Figure 3). Interestingly, while LPC 18:3 levels also sharply fall during the germination phase (5-fold decrease), LPE 18:3 remains constant in all three pollen phases, suggesting a distinct function of these polyunsaturated lysophospholipids species. Finally, despite the different behavior of the two detected galactolipids, MGDG and DGDG (Figure 2A), analysis of their molecular species during pollen germination and pollen tube growth suggested certain common trends. In hydrated pollen, single polyunsaturated species (MGDG 36:6 and DGDG 36:6) make up the absolute majority of galactolipids (85% and 90%, respectively), and they are progressively desaturated to 36:5, 36:4, and 36:3 (Figure 3).

Correlated lipid patterns through pollen germination and pollen tube elongation *in vitro*

To identify lipid clusters that follow specific patterns during the switch from hydrated pollen to the germinating one and/or growing pollen tube, all detected glycerolipids species were hierarchically clustered using the MetaboAnalyst service. We focused on eight different patterns representing different dynamic behaviors in the three time points (e.g., continuous increase or continuous decrease, etc., Supplementary Figure 3). In total, 70 lipids (i.e., 61%) showed some dynamic behavior, with the majority (43 or 37%) exhibiting upward trends. While this can be partly explained by an overall increase in overall metabolic activity, the lipid class population of these clusters differs significantly. PC, PE, and PG species make up most of the continuous increase cluster, while the abundant cluster (no change during germination followed by an increase in the pollen tube phase, 19 lipids) is populated predominantly by minor lipids like PS and DGDG (Supplementary Figure 3). PA, PC, and PE are then present in the cluster with an increase during germination and stable levels in the pollen tube phase. The three downward trends were followed by 23 lipids (20%); as suggested by Figures 2A, 3, lysophospholipid and PI species are strongly represented here. Finally, only 5 lipids (4.3%) displayed transient increase or decrease in the germination phase, with the PUFA-containing PS species being the most interesting lipids (Supplementary Figure 3).

Lysophospholipids and phosphatidic acid are enriched in pollen tube plasma membrane

After 3 hours, pollen tubes have significantly increased their surface, accompanied by a concomitant increase of cellular membranes, including the plasma membrane (Mascarenhas, 1975). We, therefore, set out to investigate the distinct lipidomic features of pollen tube plasma membrane (PM) isolated from the 3h-old cells and compared them to the whole cell samples. To achieve this, we prepared PM-enriched fractions, employing a commercially available kit that allows the isolation of PM even from relatively low starting points. We tested the quality of the obtained fractions with Western blot, utilizing the battery of compartmental markers. Our data demonstrate a significant enrichment of the plasma membrane in the isolated fractions, although the presence of some endomembranes, in particular, ER and Golgi, was also detected (Figure 4A). To further corroborate this, we analyzed our fractions using the proteomic approach. After filtering out cytoplasmic contaminants, we found 269 peripheral and integral membrane proteins reliably identified in both PM preparations (Supplementary Table 4). Gene ontology analysis of the identified membrane proteins has corroborated our Western-blot data and showed that plasma membrane-related GO terms were significantly overrepresented, demonstrating plasma membrane enrichment in the purified fractions (Figure 4B). We then isolated glycerolipids from the PM-enriched fractions (further shortened to PM for brevity) and performed a comparative analysis with the whole cell glycerolipidome, replicating the strategy described above.

PCA analysis demonstrated that replicates from PM fractions are separated from the whole cell replicates, with the first PC (principal component) explaining almost 89% of total variation (Figure 4C). Supplementary to the PCA analysis, results from the hierarchical clustering (Figure 4D) confirmed the resemblance between each set's replicates and the distance between the two datasets. The comparison of the lipid classes between the two datasets revealed no significant changes in galactolipids in PM-enriched fractions compared with the whole cell samples. Similarly, relative PS, PG, and PE levels remain the same in PM as in the whole cell membranes. While PI levels were only slightly increased in the PM, PA levels in the PM samples reached 7%, more than a three-fold increase compared to the whole cell membranes. Somewhat unexpectedly, all detected lysophospholipids were markedly increased in the PM dataset, with LPC showing seven-fold enrichment (Figure 5A). The unsaturation index of PM is significantly lower than the whole cell sample, in agreement with most eukaryotic systems (Figure 5B). Notably, an increase in saturated and a decrease in monounsaturated lipids is apparent in the PM dataset (Figure 5C). This is consistent with the lower propensity of general PM for extreme curvatures which is typical for endomembranes and is characterized by increasing monounsaturated lipids at the expense of saturated ones (Antonny et al., 2015).

A comparison of molecular lipid species between PM and whole cell samples did not reveal striking differences in the PM's galacto- and phospholipid composition, and majority of the most abundant species in each class show the same relative abundance (Figure 6). The increase of saturated lipids in the PM can be attributed to PG 34:0, which was not detected in the whole cell samples; similarly, the decrease of monosaturated phospholipids in the PM is due to PC 34:1 and PI 34:1. The distribution of phosphatidic acid species suggests that PA 34:2, PA 34:3, and PA 36:3 are boosted in the PM, with the relative abundance shifted from longer to shorter species (Figures 3, 6). Notable changes can be seen for lysophospholipids, where polyunsaturated LPCs (18:2 and 18:3) significantly increased in the PM (Figure 6).

In situ phospholipase A_2 and D activities alter during pollen germination

To independently study the dynamics of phospholipid turnover in the pollen germination and pollen tube elongation phases, we used a fluorescent derivative of PC (Bodipy-PC) as a phospholipase substrate, which we established in the pollen tube system previously (Pejchar et al., 2010). This experimental setup, based on short-term incubation of pollen culture with Bodipy-PC (at different times after the imbibition) and followed by lipid extraction and thin layer chromatography separation, allowed us to directly monitor the activities of phospholipases A_2 (PLA_2), phospholipases D (PLD) and non-specific phospholipases C (NPC), which generate LPC, PA, and diacylglycerol (DAG), respectively. Figure 7 shows that Bodipy-LPC production (reflecting PLA_2 activity) is indeed linked with pollen germination, peaking 30 minutes after imbibition, while PLD activity increases steadily in growing pollen tubes. Interestingly, the DAG levels produced by NPC family members remain constant during all germination and tip growth phases. Taken together, the *in situ* analysis of LPC and PA production independently corroborates the role of lysophospholipids in the first 30 minutes of pollen germination.

Spatiotemporal analysis of phosphatidic acid during pollen tube germination and elongation

Our results suggest that PA may be vital in establishing cellular polarity, exemplified by the process of pollen germination. Moreover, PA is quantitatively the most enriched glycerolipid in the PM, and almost 40% of the PA species are significantly higher in the PM fraction. To see which PA species are putatively linked with either pollen germination or pollen tube elongation, we reanalyzed data from Figure 3 and performed a clustering of all PA species in the three timepoint samples. This approach yielded three clusters and suggested that in addition to major PA species (PA 34:2, PA 36:4, and also PA 32:0) that increase mainly during germination, there is a cluster of minor PA species that are primarily produced during pollen tube growth (PA 36:2, PA 36:3, PA 36:6, and PA 34:1; Figure 8A).

Next, we tested the changes in global PA levels in the pollen germination and pollen tube elongation phases, using tobacco pollen stably expressing genetically-encoded PA sensor (NES-2xSpo20-PABD) fused to mCherry fluorescent protein. This allowed us to assess the changes in PA levels semi-quantitatively in time and analyze spatiotemporal dynamics of different subcellular PA pools. We noticed that in the hydrated pollen, PA decorated mainly the pollen endomembrane surrounding the generative cell and compartments associated with the vegetative nucleus (Figure 8B). Upon germination, the endomembrane signal was rapidly lost and/or relocalized to the subapical plasma membrane domain of the emerging pollen tube, where it remained relatively stable during the subsequent elongation. Interestingly, the quantification of the total fluorescence signal of the PA marker over time somewhat resembled the lipidomic data, suggesting that a major pool of plasma membrane PA is formed during the germination phase (Figure 8C).

10.3389/fpls.2022.1028311

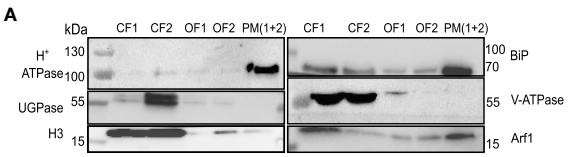

B

PANTHER GO-Slim Cellular Component	#	expected	Fold Enrichment	+/-	raw P value	FDR
plasma membrane respiratory chain complex I	4	0.03	> 100	+	3.34E-08	1.02E-06
plasma membrane protein complex	4	0.09	43.13	+	3.33E-06	9.47E-05
respiratory chain complex I	4	0.12	33.78	+	8.30E-06	2.20E-04
NADH dehydrogenase complex	4	0.13	31.67	+	1.06E-05	2.63E-04
respiratory chain complex	4	0.16	25.34	+	2.45E-05	5.73E-04
respirasome	4	0.17	24.13	+	2.94E-05	6.50E-04
transmembrane transporter complex	4	0.20	20.47	+	5.44E-05	1.14E-03
oxidoreductase complex	4	0.22	18.26	+	8.36E-05	1.58E-03
transporter complex	4	0.22	18.26	+	8.36E-05	1.66E-03
anchored component of plasma membrane	9	0.52	17.14	+	4.62E-09	1.67E-07
anchored component of membrane	9	0.52	17.14	+	4.62E-09	1.84E-07
intrinsic component of plasma membrane	13	0.79	16.55	+	2.27E-12	1.01E-10
integral component of plasma membrane	4	0.26	15.36	+	1.60E-04	2.89E-03
intrinsic component of membrane	27	1.95	13.85	+	8.61E-23	4.90E-21
integral component of membrane	18	1.40	12.85	+	7.08E-15	3.52E-13
cell-cell junction	5	0.52	9.63	+	2.00E-04	3.32E-03
anchoring junction	5	0.52	9.63	+	2.00E-04	3.47E-03
cell junction	5	0.52	9.56	+	2.07E-04	3.30E-03
plasma membrane	45	7.72	5.83	+	5.40E-23	3.58E-21
cell periphery	48	8.57	5.6	+	6.07E-24	4.84E-22
membrane	108	24.74	4.37	+	2.55E-59	3.39E-57
cellular anatomical entity	116	32.75	3.54	+	8.04E-59	8.00E-57

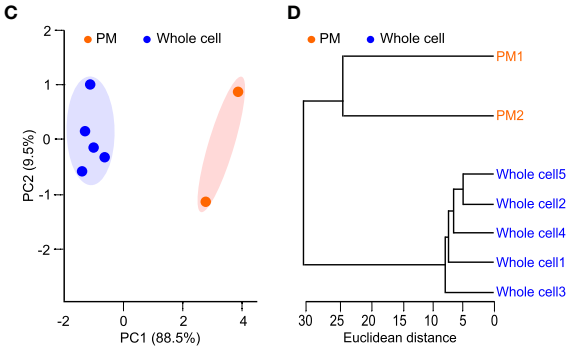

FIGURE 4
Proteomic and lipidomic characterization of plasma membrane-enriched fraction from tobacco pollen tubes. **(A)** Plasma membrane isolation. PM was isolated from germinated pollen tubes after 3h of germination in liquid medium. Western blots were performed to prove the enrichment of PM in the samples, using the different fractions obtained during the isolation protocol. CF represents cytosolic fraction (1 and 2), OF represents organelle membrane fraction (1 and 2) and PM represents the plasma membrane (combination of 1 and 2 fractions as suggested in the protocol). Cellular compartment markers used -H+-ATPase (Plasma membrane), UGPase (Cytoplasm), H3 (Nucleus), BiP (Endoplasmic reticulum), V-ATPase (Tonoplast-Vacuole) and Arf1 (Golgi apparatus). **(B)** Gene ontology (GO) analysis of the plasma membrane-enriched fraction showing the GO-slim cellular component significantly overexpressed in our proteomics results. **(C)** Principal component analysis (PCA) scores plot of the glycerolipidome extracted from whole-cell and PM enriched fraction. The explained variances are shown corresponding axes and the shaded areas indicate the 95% confidence regions. Samples are colored according to sample origin: whole cell (blue) and PM (orange). **(D)** Dendrogram of hierarchical cluster analysis of individual glycerolipidome from whole cell and PM. Both PCA and hierarchical clustering were done using the LipidSig package.

Discussion

In this study, we studied the changes in glycerolipid profiles of *Nicotiana tabacum* pollen during the two crucial developmental stages: the germination of the hydrated pollen grain and the subsequent tip growth of the elongating pollen tube (Kim et al., 2019; Scholz et al., 2020). We demonstrated a tremendous diversity in glycerolipid composition during the pollen hydration, germination, and elongation of the emerged pollen tube. While the lipid composition of dry pollen, which includes a mixture of unique galactolipids, glycerophospholipids, sphingolipids, and sterols, is well established across many plant species (Bashir et al., 2013; Ischebeck, 2016), the studies focused on the dynamical lipidome changes in non-stress conditions are still scarce (Dorne et al., 1988). Our data highlight the (apparent) importance of the pollen germination phase, which is often skipped or overlooked in functional pollen studies, especially those concerned with membrane-related processes. We argue that during pollen germination, an unparalleled combination of massive lipid metabolism activation and tremendous membrane trafficking, which also includes many lipid signaling pathways, coexists together for a relatively short time (Žárský et al., 2006; Sekereš et al., 2015). While it is evident that the *de novo* synthesis in the ER represents the main portion of structural phospholipids in every whole cell lipidomic study, our microscopic and *in situ* phospholipase activity data suggests that processes beyond lipid biosynthesis may be responsible for a significant portion of observable lipid changes.

In this regard, PA represents a great example of theoretical and methodological challenges connected with lipidomic studies: PA is a critical component of phospholipid biosynthesis and an important signaling molecule. In plant cells, PA is produced either in ER from glycerol-3-phosphate (G3P) by the sequential action of G3P-acyl transferase and lysophosphatidic acid acyl transferase (LPAAT) or at the plasma membrane (and/or Golgi or endosomal compartments) *via* the activity of PLD or DAG kinase (DGK) (Jenkins and Frohman, 2005). The biosynthetic pathway as the major PA route in pollen was suggested recently by Hernández et al. (2020) in olive, and pollen-abundant LPAAT3 was hypothesized to play a vital role in the Arabidopsis male gametophyte (Kim et al., 2005). Conversely, both PLD and DGK pathways were repeatedly implicated in PA-dependent polar growth of pollen tubes. Plasma membrane PA generated from structural phospholipids *via* PLD was implicated in tobacco pollen tube growth (Potocký et al., 2003), and tobacco PLDδ3 was proposed as the major PM-localized isoform (Pejchar et al., 2020). Multiple reports also pinpointed the role of several DGK isoforms: in Arabidopsis, ER-localized DGK2 and DGK4 are

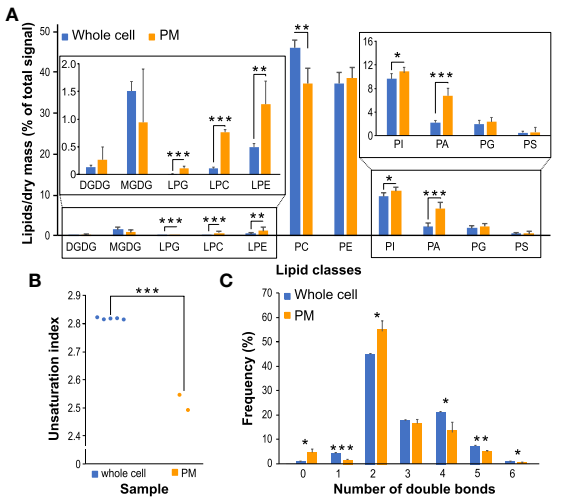

FIGURE 5
Changes in glycerolipid classes between PM-enriched fractions and corresponding whole cell samples. **(A)** The composition of the main lipid classes (DGDG, MGDG, PG, PC, LPG, LPC, LPE, PE, PI, PS and PA) for whole cell and PM samples. Data are presented as mean ± sd, n=5 (whole cell) and n=2 (PM). Asterisks (*), (**), (***) represent the significance between samples at $p < 0.05$, $p < 0.01$ and $p < 0.001$, respectively. **(B)** Total unsaturation index between PM and whole cell datasets. **(C)** Double bonds distribution between PM and whole cell datasets.

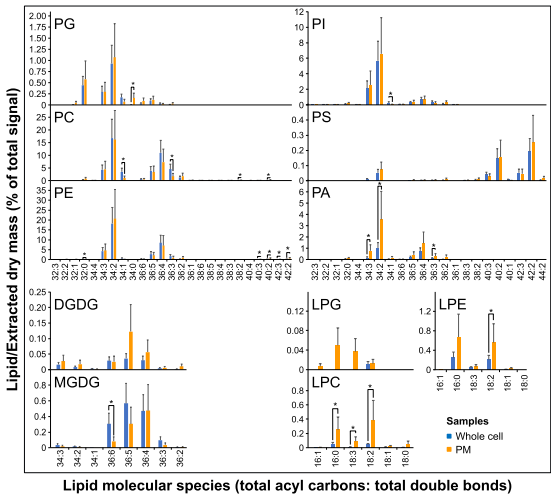

FIGURE 6
Changes in lipid molecular species between PM and the whole cell. The levels are normalized. Data are presented as mean ± s.e.m., n=5 (whole cell) and n=2 (PM). Asterisk represent the significance between samples at $p < 0.05$.

required for gametogenesis and pollen tube growth (Dias et al., 2019; Angkawijaya et al., 2020). Tobacco DGK5 is involved in the polar secretion of cell wall material to the pollen tube tip, possibly by regulating phosphoinositide-signaling pathways (Scholz et al., 2022). Our multifaceted data on PA generation and dynamics strongly suggest that in tobacco pollen, PA production comes mainly from PC and, to a lesser extent, from PE, as can be inferred from individual species profiles. We predict that this PA route represents a significant pathway and that PLD and NPC/DGK pathways generate distinct PA cellular pools. However, great caution must be taken in interpreting PA data from pollen lipidomic studies, as non-optimal lipid isolation may lead to artificially high PA levels due to PLD release and activation. Paradoxically, this is often the case when pollen tubes are separated from the medium without great care prior to hot isopropanol treatment. Seeming PA levels in whole cell samples may reach 20-60% of total glycerolipids, as was reported for soybean, tobacco, or Arabidopsis pollen (Djanaguiraman et al., 2013; McDowell et al., 2013; Krawczyk et al., 2022). Our data, reporting whole cell PA levels at 1.5-2.3% of total glycerolipids and PA levels in the PM at ~7% of total glycerolipids, agree with the data on wheat pollen and purified plasma membrane from tobacco cell culture (Cacas et al., 2016; Narayanan et al., 2018).

In a partial analogy to the PA, the surprisingly high dynamics of lysophospholipid levels (particularly LPC, but also LPE and perhaps even LPG) during the pollen germination phase can also be attributed to both metabolic and membrane signaling/remodeling pathways. LPC can be produced as a byproduct of the last step of triacylglycerol synthesis *via* phospholipid:diacylglycerol acyltransferase (PDAT) activity or generated from PC by PLA_2 activity. PDAT1 was indeed shown to be implicated in the proper development of Arabidopsis pollen together with diacylglycerol:acytransferase (Zhang et al., 2009). On the other hand, PDAT contribution to TAG synthesis

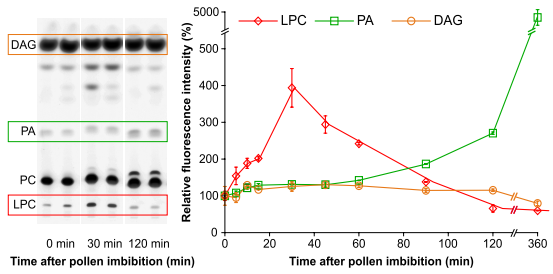

FIGURE 7
Lipid dynamics during pollen tube germination and pollen tube growth monitored by *in situ* analysis of PLD, PLA_2 and NPC activity. Left, profiles of Bodipy-labeled lipid products of pollen culture at 0, 30 and 120 minutes after imbibition. Lipids were extracted after 10 min of incubation and separated by high-performance thin layer chromatography (HP-TLC). LPC, PA and DAG are boxed. Representative cut-outs from 4 independent experiments performed in duplicates are shown. Right, quantification of individual Bodipy-labeled lipid products. Data are presented as mean ± s.e.m., n=8.

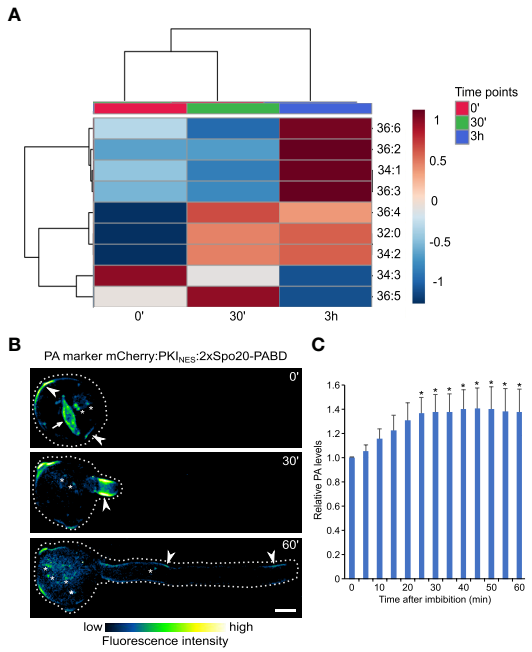

FIGURE 8
Distinct PA pools are mobilized during pollen germination and pollen tube growth. **(A)** Heatmap showing the correlation among phosphatidic acid (PA) species of germination and elongation of pollen tube samples. Data of the % of total signal of each species (identical to the data presented on Fig. 3) were normalized and analyzed using Spearman rank correlation analysis within MetaboAnalyst. Each colored cell on the map indicates the correlation coefficient, with the scale code shown on the top right corner. Blue and red colors on the heatmap indicate negative and positive correlations, respectively for increasing and decreasing species abundance relative to the mean of the 3 sample groups in the row for the 0', 30' and 3h sets, respectively; the color tint indicates fold-changes up to one and down to -1. The white color stands for no change, and gray for not detected. **(B)** During pollen germination and tube elongation, genetically-encoded PA markers relocalizes between different regions of pollen plasma membrane (arrowhead), nuclear membranes (arrow) and endomembranes (asterisk). Spinning disk confocal imaging (average Z-projections) of germinating tobacco pollen stably expressing PA marker mCherry-NES-2xSpo20-PABD under the control of UBQ10 promoter. Pollen was imaged at indicated times after imbibition and a cell exhibiting typical localization pattern (n=12) is shown. **(C)** Quantitative microscopic analysis of PA levels across all cellular pools during pollen germination and growth. Total fluorescence levels of PA marker were measured in ROIs encompassing the whole cell (dashed line) at indicated times after pollen imbibition. Relative fluorescence (normalized to time 0) is shown as mean ± SE (n=12 from three independent experiments), asterisk indicates time points different from time 0 (one-way Anova followed by Dunnet's test, $p<0.05$).

(and thus LPC production) in olive pollen is negligible (Hernández et al., 2020). On the other hand, activities of small secretory PLA_2 isoforms β, γ, and δ have been shown to control Arabidopsis pollen development, reportedly in the ER or Golgi. Notably, LPE was highlighted as the responsible lysophospholipid (Kim et al., 2011). Our results, showing high PLA_2 activity during the germination phase and demonstrating massive enrichment of lysophospholipids in PM fraction, also support the role of PLA_2 activity as the primary source of lysophospholipid production. However, our data paint a slightly different picture, as they place the site of the LPC action on the PM. Brown et al. (2003) proposed that PLA_2 hydrolyzes the phospholipids on the extraplasmatic leaflet of the membrane, generating a localized concentration of inverted cone-shaped lysophospholipids that drive the formation of positive membrane curvature. Indeed, mammalian PLA_2 and extracellular LPC were shown to regulate membrane-protein trafficking and exocytosis in concert with phosphatidic acid (Choukroun et al., 2000; Zeniou-Meyer et al., 2007). In plants, it has been found that LPC also contributes to the activation of the plasma membrane H^+-ATPases (Wielandt et al., 2015).

Although the lipidomic approaches and *in situ* phospholipase assays converged on the same lipid classes and biological processes, the temporal overlap was only partial (Figures 2, 7). Several, not mutually exclusive, explanations for this discrepancy can be drawn. First, both approaches tackle the lipid quantification from a slightly different angle: while lipidomics gathers steady-state levels of the lipids with great accuracy and distinguishes individual lipid species, *in situ* lipase analysis (or any other lipid pulse-labeling technique) uncovers immediate dynamical changes and fluxes (Kalachova et al., 2022). Second, the lipase activity analyses visualize specific enzyme activities, while the lipidomic approaches do not discriminate. It is thus possible that the high lysophospholipid levels detected in the imbibed pollen are either a remnant of the TAG synthesis during pollen maturation or products of phospholipase A_1, while the rapid production of Bodipy-LPC reflects only the activity of PLA_2. Similarly, increasing PLD activity, detected by the *in situ* approaches during pollen tube growth, may be counteracted by PA phosphatases that keep the steady state level of pollen tube PA constant.

Interestingly, the composition of galactolipids revealed distinct behavior of MGDG and DGDG (Figure 2). Although it is not clear if these galactolipids are strictly extraplastidial or are also present in pollen proplastids, both MGDG and DGDG are a common presence in pollen lipidomes from various species, e.g., Arabidopsis pollen contains 5% of MGDG and 2% of DGDG (McDowell et al., 2013), which roughly corresponds to our findings (1.5% for MGDG and 0.5% of DGDG in total membrane lipids). Significantly, both galactolipids were also detected in the enriched-PM fraction. While the specific function of MGDG and DGDG remain obscure, DGDG was reported to localize to the plasma membrane, and the chemical inhibition of MGDG synthase affects pollen tube growth but not germination (Botté et al., 2011). Moreover, increased galactolipid levels were linked to pollen tube growth in lily (Nakamura et al., 2009). This is consistent with our data showing the temporal decrease of DGDG during the germination phase, although the functional

significance remains to be established. The same holds true for PS, another lipid class showing temporal decrease during the germination phase.

The swap between the high abundance lipids PC and PE in the transition from the germination phase to the pollen tube growth phase is unclear. It is known that changes in PC/PE ratio in mammalian cells affect membrane integrity (Li et al., 2006). Alternatively, an increase of PE vs. PC in the pollen tube growth may be linked with its function in the electrostatic/hydrogen bond switch, by which the electrostatic interactions of peripheral membrane proteins with PA at the plasma membrane is regulated (Kooijman et al., 2007). Finally, PE was suggested as the primary glycerolipid regulator of membrane fluidity upon changes of cellular sterol contents (Dawaliby et al., 2016). Given that pollen sterols show remarkable diversity (Rotsch et al., 2017) and sterols were described to regulate cell polarity cues (Han et al., 2018), versatile PE levels might be required to maintain the proper balance that would allow the existence of sterol-induced membrane nanodomains and buffer the membrane fluidity required for rapid pollen tube growth.

Conclusions

In summary, we demonstrated that the establishment and maintenance of cellular polarity, exemplified here on the model of germinating pollen and tip-growing pollen tubes, are accompanied by complex changes in membrane glycerolipids. Such dynamics is likely an interplay of rapid metabolic changes needed by rapid cell expansion and concurrent anterograde and retrograde membrane trafficking regulated by phospholipid-derived signaling pathways. Our study thus provides a blueprint for future studies on the functional significance of individual lipids in different polarity processes and calls for analogous studies aimed at the dynamics of neutral lipids and sphingolipids.

Data availability statement

The mass spectrometry proteomics data generated in this study are available in the ProteomeXchange Consortium with the dataset identifier PXD037046 (https://www.ebi.ac.uk/pride/archive/projects/PXD037046).

Author contributions

MP conceived and designed the experiments. NS, PP, HS, MH, and MP carried out the experiments. MP and NS wrote the manuscript with the help of PP. All authors contributed to the discussion of the results and edited and approved the submitted version of the manuscript.

Funding

This work was supported by the Czech Science Foundation grants GA19-21758S and 21-09254S to MP, and 20-21547S to PP; NS was supported by the Postdoctoral Fellowship Program of the Czech Academy of Sciences (L200382051) and the Ministry of Education, Youth and Sports of the Czech Republic (MEYS CR)/Charles University (OP RDE, call no. 02_18_053). The Imaging Facility of the Institute of Experimental Botany of the Czech Academy of Sciences (IEB CAS) is supported by the MEYS CR LM2018129 Czech-Bioimaging and the IEB CAS.

Acknowledgments

The lipid analyses described in this work were performed at the Kansas Lipidomics Research Center Analytical Laboratory. Instrument acquisition and lipidomics method development were supported by the National Science Foundation (including support from the Major Research Instrumentation program; most recent award DBI-1726527), K-IDeA Networks of Biomedical Research Excellence (INBRE) of National Institute of Health (P20GM1013013), and Kansas State University.

Conflict of interest

The authors declare that the research was conducted in the absence of any commercial or financial relationships that could be construed as a potential conflict of interest.

Publisher's note

Supplementary material

The Supplementary Material for this article can be found online at: https://www.frontiersin.org/articles/10.3389/fpls.2022.1028311/full#supplementary-material

References

Angkawijaya, A. E., Nguyen, V. C., Gunawan, F., and Nakamura, Y. (2020). A pair of arabidopsis diacylglycerol kinases essential for gametogenesis and ER phospholipid metabolism in leaves and flowers. *Plant Cell.* 32, 2602–2620. doi: 10.1105/tpc.20.00251

Antonny, B., Vanni, S., Shindou, H., and Ferreira, T. (2015). From zero to six double bonds: phospholipid unsaturation and organelle function. *Trends Cell Biol.* 25, 427–436. doi: 10.1016/j.tcb.2015.03.004

Bashir, M. E. H., Lui, J. H., Palnivelu, R., Naclerio, R. M., and Preuss, D. (2013). Pollen lipidomics: Lipid profiling exposes a notable diversity in 22 allergenic pollen and potential biomarkers of the allergic immune response. *PLoS One* 8, e57566. doi: 10.1371/journal.pone.0057566

Bligh, E. G., and Dyer, W. J. (1959). A rapid method of total lipid extraction and purification. *Can. J. Biochem. Physiol.* 37 (8), 911–917. doi: 10.1139/o59-099

Botté, C. Y., Deligny, M., Roccia, A., Bonneau, A.-L., Saïdani, N., Hardré, H., et al. (2011). Chemical inhibitors of monogalactosyldiacylglycerol synthases in arabidopsis thaliana. *Nat. Chem. Biol.* 7, 834–842. doi: 10.1038/nchembio.658

Brown, W. J., Chambers, K., and Doody, A. (2003). Phospholipase A2 (PLA2) enzymes in membrane trafficking:mediators of membrane shape and function. *Traffic* 4, 214–221. doi: 10.1034/j.1600-0854.2003.00078.x

Cacas, J.-L., Buré, C., Grosjean, K., Gerbeau-Pissot, P., Lherminier, J., Rombouts, Y., et al. (2016). Revisiting plant plasma membrane lipids in tobacco: A focus on sphingolipids. *Plant Physiol.* 170, 367–384. doi: 10.1104/pp.15.00564

Cassim, A. M., Gouguet, P., Gronnier, J., Laurent, N., Germain, V., Grison, M., et al. (2018). Lant lipids: Key players of plasma membrane organization and function. *Prog. Lipid Res* 73, 1–27. doi: 10.1016/j.plipres.2018.11.002

Chen, C. Y., Wong, E. I., Vidali, L., Estavillo, A., Hepler, P. K., Wu, H. M., et al. (2002). The regulation of actin organization by actin-depolymerizing factor in elongation pollen tubes. *Plant Cell* 14, 2175–2190. doi: 10.1105/tpc.003038

Choukroun, G. J., Marshansky, V., Gustafson, C. E., McKee, M., Hajjar, R. J., Rosenzweig, A., et al. (2000). Cytosolic phospholipase a (2) regulates golgi structure and modulates intracellular trafficking of membrane proteins. *J. Clin. Invest.* 106, 983–993. doi: 10.1172/JCI8914

Colin, L. A., and Jaillais, Y. (2020). Phospholipids across scales: lipid patterns and plant development. *Curr. Opin. Plant Biol.* 53, 1–9. doi: 10.1016/j.pbi.2019.08.007

Conze, L. L., Berlin, S., Le Bail, A., and Kost, B. (2017). Transcriptome profiling of tobacco (*Nicotiana tabacum) pollen and pollen tubes*. *BMC Genomics* 18, 581. doi: 10.1186/s12864-017-3972-3

Dawaliby, R., Trubbia, C., Delporte, C., Noyon, C., Ruysschaert, J.-M., Van Antwerpen, P., et al. (2016). Phosphatidylethanolamine is a key regulator of membrane fluidity in eukaryotic cells*. *J. Biol. Chem.* 291, 3658–3667. doi: 10.1074/jbc.M115.706523

Devaiah, S. P., Roth, M. R., Baughman, E., Li, M., Tamura, P., Jeannotte, R., et al. (2006). Quantitative profiling of polar glycerolipid species from organs of wild-type arabidopsis and a PHOSPHOLIPASE Dα1 knockout mutant. *Phytochemistry* 67, 1907–1924. doi: 10.1016/j.phytochem.2006.06.005

Dias, F. V., Serrazina, S., Vitorino, M., Marchese, D., Heilmann, I., Godinho, M., et al. (2019). A role for diacylglycerol kinase 4 in signalling crosstalk during arabidopsis pollen tube growth. *New Phytol.* 222, 1434–1446. doi: 10.1111/nph.15674

Djanaguiraman, M., Prasad, P. V. V., and Schapaugh, W. T. (2013). High day- or nighttime temperature alters leaf assimilation, reproductive success, and phosphatidic acid of pollen grain in soybean [Glycine max (L.) merr.]. *Crop Sci.* 53, 1594–1604. doi: 10.2135/cropsci2012.07.0441

Dorne, A. J., Kappler, R., Kristen, U., and Heinz, E. (1988). Lipid metabolism during germination of tobacco pollen. *Phytochemistry* 27 (7), 2027–2031. doi: 10.1016/0031-9422(88)80090-6

Erde, J., Loo, R. R., and Loo, J. A. (2014). Enhanced FASP (eFASP) to increase proteome coverage and sample recovery for quantitative proteomic experiments. *J. Proteome Res.* 13 (4), 1885–1895. doi: 10.1021/pr4010019

Grobei, M.A., Qeli, E., Brunner, E., Rehrauer, H., Zhang, R., Roschitzki, B., et al (2009). Deterministic protein inference for shotgun proteomics data provides new insights into Arabidopsis pollen development and function. *Genome Res.* 19 (10), 1786–800. doi: 10.1101/gr.089060.108

Hafidh, S., and Honys, D. (2021). Reproduction multitasking: The male gametophyte. *Annu. Rev. Plant Biol.* 72, 581–614. doi: 10.1146/annurev-arplant-080620-021907

Han, B., Yang, N., Pu, H., and Wang, T. (2018). Quantitative proteomics and cytology of rice pollen sterol-rich membrane domains reveals pre-established cell polarity cues in mature pollen. *J. Proteome Res.* 17, 1532–1546. doi: 10.1021/acs.jproteome.7b00852

Heilmann, M., and Heilmann, I. (2022). Regulators regulated: Different layers of control for plasma membrane phosphoinositides in plants. *Curr. Opin. Plant Biol.* 67, 102218. doi: 10.1016/j.pbi.2022.102218

Hepler, P. K., Vidali, L., and Cheung, A. Y. (2001). Polarized cell growth in higher plants. *Annu. Rev. Cell. Dev. Biol.* 17, 159–187. doi: 10.1146/annurev.cellbio.17.1.159

Hernández, M. L., Lima-Cabello, E., Alché, J., de, D., Martínez-Rivas, J. M., and Castro, A. J. (2020). Lipid composition and associated gene expression patterns during pollen germination and pollen tube growth in olive (Olea europaea l.). *Plant Cell Physiol.* 61, 1348–1364. doi: 10.1093/pcp/pcaa063

Higashiyama, T., and Takeuchi, H. (2015). The mechanism and key molecules involved in pollen tube guidance. *Annu. Rev. Plant Biol.* 66, 393–413. doi: 10.1146/annurev-arplant-043014-115635

Horn, P. J., and Chapman, K. D. (2012). Lipidomics in tissues, cells and subcellular compartments. *Plant J.* 70, 69–80. doi: 10.1111/j.1365-313X.2011.04868.x

Horsch, R. B., Fry, J. E., Hoffmann, N. L., Wallroth, M., Eichholtz, D., Rogers, S. G., et al. (1985). A simple and general method for transferring genes into plants. *Science* 227, 1229–1231. doi: 10.1126/science.227.4691.1229

Ischebeck, T. (2016). "Lipid composition of arabidopsis thaliana pollen," in *Encyclopedia of lipidomics*. Ed. M. Wenk (Dordrecht: Springer). doi: 10.1007/978-94-007-7864-1_122-1

Jenkins, G. M., and Frohman, M. A. (2005). Phospholipase d: a lipid centric review. *Cell. Mol. Life Sci.* 62, 2305–2316. doi: 10.1007/s00018-005-5195-z

Kalachova, T., Škrabálková, E., Pateyron, S., Soubigou-Taconnat, L., Djafi, N., Collin, S., et al. (2022). DIACYLGLYCEROL KINASE 5 participates in flagellin-induced signaling in arabidopsis. *Plant Physiol.*, kiac354. doi: 10.1093/plphys/kiac354

Keilhauer, E. C., Hein, M. Y., and Mann, M. (2015). Accurate protein complex retrieval by affinity enrichment mass spectrometry (AE-MS) rather than affinity purification mass spectrometry (AP-MS). *Mol. Cell Proteomics* 14, 120–135. doi: 10.1074/mcp.M114.041012

Kerwin, J. L., Tuininga, A. R., and Ericsson, L. H. (1994). Identification of molecular species of glycerophospholipids and sphingomyelin using electrospray mass spectrometry. *J. Lipid Res.* 35, 1102–1114.

Kim, H. U., Li, Y., and Huang, A. H. C. (2005). Ubiquitous and endoplasmic reticulum–located lysophosphatidyl acyltransferase, LPAT2, is essential for female but not Male gametophyte development in arabidopsis. *Plant Cell.* 17, 1073–1089. doi: 10.1105/tpc.104.030403

Kim, H. J., Ok, S. H., Bahn, S. C., Jang, J., Oh, S. A., Park, S. K., et al. (2011). Endoplasmic reticulum– and golgi-localized phospholipase A2 plays critical roles in arabidopsis pollen development and germination. *Plant Cell.* 23, 94–110. doi: 10.1105/tpc.110.074799

Kim, Y.-J., Zhang, D., and Jung, K.-H. (2019). Molecular basis of pollen germination in cereals. *Trends Plant Sci.* 24, 1126–36 doi: 10.1016/j.tplants.2019.08.005

Kooijman, E. E., Tieleman, D. P., Testerink, C., Munnik, T., Rijkers, D. T. S., Burger, K. N. J., et al. (2007). An Electrostatic/Hydrogen bond switch as the basis for the specific interaction of phosphatidic acid with proteins. *J. Biol. Chem.* 282, 11356–11364. doi: 10.1074/jbc.M609737200

Krawczyk, H. E., Rotsch, A. H., Herrfurth, C., Scholz, P., Shomroni, O., Salinas-Riester, G., et al. (2022). Heat stress leads to rapid lipid remodelling and transcriptional adaptations in nicotiana tabacum pollen tubes. *Plant Physiol.* 189, 490–515. doi: 10.1093/plphys/kiac127

Langerova, H., Lubyova, B., Zabransky, A., Hubalek, M., Glendova, K., Aillot, L., et al. (2020). Hepatitis b core protein is post-translationally modified through K29-linked ubiquitination. *Cells* 9, 2547. doi: 10.3390/cells9122547

Li, Z., Agellon, L. B., Allen, T. M., Umeda, M., Jewell, L., Mason, A., et al. (2006). The ratio of phosphatidylcholine to phosphatidylethanolamine influences membrane integrity and steatohepatitis. *Cell Metab.* 3, 321–331. doi: 10.1016/j.cmet.2006.03.007

Lin, W. J., Shen, P. C., Liu, H. C., Cho, Y. C., Hsu, M. K., Lin, I. C., et al. (2021). LipidSig: a web-based tool for lipidomic data analysis. *Nucleic Acid Res.* 49 (W1), W336–W345. doi: 10.1093/nar/gkab419

Mascarenhas, J. P. (1975). The biochemistry of angiosperm pollen development. *Bot. Rev.* 41, 259–314. doi: 10.1007/BF02860839

McDowell, S. C., Lopez-Marques, R. L., Poulsen, L. R., Palmgren, M. G., and Harper, J. F. (2013). Loss of the arabidopsis thaliana P(4)-ATPase ALA3 reduces

adaptability to temperature stresses and impairs vegetative, pollen and ovule development. *PloS One* 8, e62577. doi: 10.1371/journal.pone.0062577

Meï, C., Michaud, M., Cussac, M., Albrieux, C., Gros, V., Maréchal, E., et al. (2015). Levels of polyunsaturated fatty acids correlate with growth rate in plant cell cultures. *Sci. Rep.* 5, 15207. doi: 10.1038/srep15207

Nakamura, Y. (2017). Plant phospholipid diversity: Emerging functions in metabolism and protein–lipid interactions. *Trends Plant Sci.* 22, 1027–1040. doi: 10.1016/j.tplants.2017.09.002

Nakamura, Y., Kobayashi, K., and Ohta, H. (2009). Activation of galactolipid biosynthesis in development of pistils and pollen tubes. *Plant Physiol. Biochem.* 47, 535–539. doi: 10.1016/j.plaphy.2008.12.018

Narayanan, S., Prasad, P. V. V., and Welti, R. (2018). Alterations in wheat pollen lipidome during high day and night temperature stress. *Plant Cell Environ.* 41, 1749–1761. doi: 10.1111/pce.13156

Narayanan, S., Tamura, P. J., Roth, M. R., Prasad, P. V. V., and Welti, R. (2016). Wheat leaf lipids during heat stress: I. high day and night temperatures result in major lipid alterations. *Plant Cell Environ.* 39, 787–803. doi: 10.1111/pce.12649

Pang, Z., Zhou, G., Ewald, J., Chang, L., Hacariz, O., Basu, N., et al. (2022). Using MetaboAnalyst 5.0 for LC–HRMS spectra processing, multi-omics integration and covariate adjustment of global metabolomics data. *Nat. Protoc.* 17, 1735–1761. doi: 10.1038/s41596-022-00710-w

Pejchar, P., Potocký, M., Novotná, Z., Veselková, Š., Kocourková, D., Valentová, O., et al. (2010). Aluminum ions inhibit the formation of diacylglycerol generated by phosphatidylcholine-hydrolysing phospholipase c in tobacco cells. *New Phytol.* 188, 150–160. doi: 10.1111/j.1469-8137.2010.03349.x

Pejchar, P., Sekereš, J., Novotný, O., Žárský, V., and Potocký, M. (2020). Functional analysis of phospholipase Dδ family in tobacco pollen tubes. *Plant J.* 103, 212–226. doi: 10.1111/tpj.14720

Perez-Riverol, Y., Bai, J., Bandla, C., Hewapathirana, S., García-Seisdedos, D., Kamatchinathan, S., et al. (2022). The PRIDE database resources in 2022: A hub for mass spectrometry-based proteomics evidences. *Nucleic Acids Res.* 50, D543–D552. doi: 10.1093/nar/gkab1038

Pfaff, J., Denton, A. K., Usadel, B., and Pfaff, C. (2020). Phosphate starvation causes different stress responses in the lipid metabolism of tomato leaves and roots. *Biochim. Biophys. Acta Mol. Cell Biol. Lipids* 1865, 158763. doi: 10.1016/j.bbalip.2020.158763

Piffanelli, P., Ross, J. H. E., and Murphy, D. J. (1997). Intra- and extracellular lipid composition and associated gene expression patterns during pollen development in *Brassica napus*. *Plant J.* 11, 549–562. doi: 10.1046/j.1365-313x.1997.11030549.x

Potocký, M., Eliáš, M., Profotová, B., Novotná, Z., Valentová, O., Žárský, V., et al. (2003). Phosphatidic acid produced by phospholipase d is required for tobacco pollen tube growth. *Planta* 217, 122–130. doi: 10.1007/s00425-002-0965-4

Rotsch, A. H., Kopka, J., Feussner, I., and Ischebeck, T. (2017). Central metabolite and sterol profiling divides tobacco male gametophyte development and pollen tube growth into eight metabolic phases. *Plant J.* 92, 129–146. doi: 10.1111/tpj.13633

Scholz, P., Anstatt, J., Krawczyk, H. E., and Ischebeck, T. (2020). Signalling pinpointed to the tip: The complex regulatory network that allows pollen tube growth. *Plants* 9, 1098. doi: 10.3390/plants9091098

Scholz, P., Pejchar, P., Fernkorn, M., Škrabálková, E., Pleskot, R., Blersch, K., et al. (2022). DIACYLGLYCEROL KINASE 5 regulates polar tip growth of tobacco pollen tubes. *New Phytol* 233, 2185–2202. doi: 10.1111/nph.17930

Sekereš, J., Pleskot, R., Pejchar, P., Žárský, V., and Potocký, M. (2015). The song of lipids and proteins: dynamic lipid-protein interfaces in the regulation of plant cell polarity at different scales. *J. Exp. Bot.* 66, 1587–1598. doi: 10.1093/jxb/erv052

Shiva, S., Enninful, R., Roth, M. R., Tamura, P., Jagadish, K., and Welti, R. (2018). An efficient modified method for plant leaf lipid extraction results in improved recovery of phosphatidic acid. *Plant Methods* 14, 14. doi: 10.1186/s13007-018-0282-y

Wang, H.-J., Huang, J.-C., and and Jauh, G.-Y. (2010). "Pollen Germination and Tube Growth," in Advances in Botanical Research. Eds. J.-C. Kader and M. Delseny (Elsevier), 1–52. doi: 10.1016/S0065-2296(10)54001-1

Wielandt, A. G., Pedersen, J. T., Falhof, J., Kemmer, G. C., Lund, A., Ekberg, K., et al. (2015). Specific activation of the plant p-type plasma membrane h+-ATPase by lysophospholipids depends on the autoinhibitory n- and c-terminal domains*. *J. Biol. Chem.* 290, 16281–16291. doi: 10.1074/jbc.M114.617746

Xiao, S., Gao, W., Chen, Q. F., Chan, S. W., Zheng, S. X., Ma, J., et al. (2010). Overexpression of arabidopsis acyl-CoA binding protein ACBP3 promotes starvation-induced and age-dependent leaf senescence. *Plant Cell* 22, 1463–1482. doi: 10.1105/tpc.110.075333

Žárský, V., Potocký, M., Baluška, F., and Cvrčková, F. (2006). "Lipid metabolism, compartmentalization and signalling in the regulation of pollen tube growth," in *The pollen tube: A cellular and molecular perspective plant cell monographs*. Ed. R. Malhó (Berlin, Heidelberg: Springer), 117–138. doi: 10.1007/7089_046

Zeniou-Meyer, M., Zabari, N., Ashery, U., Chasserot-Golaz, S., Haeberle, A.-M., Demais, V., et al. (2007). Phospholipase D1 production of phosphatidic acid at the plasma membrane promotes exocytosis of Large dense-core granules at a late stage. *J. Biol. Chem.* 282, 21746–21757. doi: 10.1074/jbc.M702968200

Zhang, M., Fan, J., Taylor, D. C., and Ohlrogge, J. B. (2009). DGAT1 and PDAT1 acyltransferases have overlapping functions in arabidopsis triacylglycerol biosynthesis and are essential for normal pollen and seed development. *Plant Cell* 21, 3885–3901. doi: 10.1105/tpc.109.071795

Zonia, L., and Munnik, T. (2008). Vesicle trafficking dynamics and visualization of zones of exocytosis and endocytosis in tobacco pollen tubes. *J. Exp. Bot.* 59, 861–873. doi: 10.1093/jxb/ern007

frontiers | Frontiers in Plant Science

TYPE Perspective
PUBLISHED 24 November 2022
DOI 10.3389/fpls.2022.1020306

OPEN ACCESS

EDITED BY
Giampiero Cai,
University of Siena, Italy

REVIEWED BY
Said Hafidh,
Institute of Experimental Botany,
Czechia

*CORRESPONDENCE
Kazuki Motomura
kazuki-m@fc.ritsumei.ac.jp
Daisuke Maruyama
dmaru@yokohama-cu.ac.jp

SPECIALTY SECTION
This article was submitted to Plant Cell Biology, a section of the journal Frontiers in Plant Science

RECEIVED 16 August 2022
ACCEPTED 04 November 2022
PUBLISHED 24 November 2022

CITATION
Motomura K, Sugi N, Takeda A, Yamaoka S and Maruyama D (2022) Possible molecular mechanisms of persistent pollen tube growth without *de novo* transcription. *Front. Plant Sci.* 13:1020306. doi: 10.3389/fpls.2022.1020306

Possible molecular mechanisms of persistent pollen tube growth without *de novo* transcription

Kazuki Motomura[1,2,3]*, Naoya Sugi[4], Atsushi Takeda[1], Shohei Yamaoka[5] and Daisuke Maruyama[4]*

[1]College of Life Sciences, Ritsumeikan University, Kusatsu, Japan, [2]Japanese Science and Technology Agency, PRESTO, Kawaguchi, Japan, [3]Institute of Transformative Bio-Molecules, Nagoya University, Nagoya, Japan, [4]Kihara Institute for Biological Research, Yokohama City University, Yokohama, Japan, [5]Graduate School of Biostudies, Kyoto University, Kyoto, Japan

The vegetative cell nucleus proceeds ahead of a pair of sperm cells located beneath the pollen tube tip during germination. The tip-localized vegetative nucleus had been considered to play a pivotal role in the control of directional pollen tube growth and double fertilization. However, we recently reported the female-targeting behavior of pollen tubes from mutant plants, of which the vegetative nucleus and sperm nuclei were artificially immotile. We showed that the apical region of the mutant pollen tubes became physiologically enucleated after the first callose plug formation, indicating the autonomously growing nature of pollen tubes without the vegetative nucleus and sperm cells. Thus, in this study, we further analyzed another *Arabidopsis thaliana* mutant producing physiologically enucleated pollen tubes and discussed the mechanism by which a pollen tube can grow without *de novo* transcription from the vegetative nucleus. We propose several possible molecular mechanisms for persistent pollen tube growth, such as the contribution of transcripts before and immediately after germination and the use of persistent transcripts, which may be important for a competitive race among pollen tubes.

KEYWORDS

pollen tube growth, pollen tube guidance, male germ unit, vegetative nucleus, plant reproduction, gene expression

Introduction

A pollen is a small male gametophyte produced by flowering plants. *Arabidopsis thaliana* produces tricellular pollen grains consisting of vegetative cells that contain an eyeglasses-shaped pair of sperm cells. The two sperm cells are enclosed by the inner vegetative plasma membrane (IVPM), an endomembrane that originates from the plasma membrane of the host vegetative cell. This reflects the phagocytic

internalization of the sperm cell precursor during male gametogenesis. In addition to the symbiotic feature, the male germ unit (MGU) is formed by a complex of vegetative nuclei and sperm cells, representing the uniqueness of pollen cell biology (Mogensen, 1992). After pollen tube germination, the MGU is localized in the apical area approximately 50–100 μm away from the tip of the pollen tube and maintains the triplet structure, keeping the vegetative nucleus ahead of the sperm cells. The directional growth of the pollen tube in response to various guidance cues in the pistil is a complex process. Regardless, the apical MGU localization ensures precise sperm cell delivery before its double fertilization by rupturing the tip of the pollen tube inside the ovule (Hamamura et al., 2011; McCue et al., 2011; Denninger et al., 2014; Higashiyama and Takeuchi, 2015).

Although the molecular mechanisms of the apical MGU transport are poorly understood, available genetic evidence supports that the vegetative nucleus and sperm cells in the MGU have their respective motive forces in the pollen tube. For example, the linker of the nucleoskeleton and cytoskeleton (LINC) complex plays a key role in vegetative nucleus transport. This nuclear envelope complex regulates nucleus morphology and migration in various plant cells *via* mechanical force transmission, which is generated by motor proteins and cytoskeletons in the cytosol (Tatout et al., 2014). Zhou and Meier (2014) reported that in *A. thaliana*, simultaneous loss of the functionally redundant LINC complex proteins, WPP domain-interacting tail-anchored protein 1 (WIT1) and WIT2, on the outer nuclear envelopes causes the passive migration of the vegetative nucleus dragged by the sperm cells (Zhou and Meier, 2014). In a parallel study, we observed over-accumulation of callose (β-1,3-glucan) at the cell wall of sperm cells expressing the gain-of-function mutant protein, CALLOSE SYNTHASE 3 (*cals3m*), fused with the sperm cell-specific *HTR10* promoter (*pHTR10:cals3m*) (Motomura et al., 2021). These abnormal sperm cells are usually observed at the basal region of the pollen tube, probably due to the loss of sperm cell motility (Motomura et al., 2021).

The decreased motilities of the vegetative nucleus and the sperm cells observed in the *wit1 wit2* double mutant and *pHTR10:cals3m* (hereafter referred to as *SC-cal*)-expressing *Arabidopsis* plants enabled us to better understand the hidden potential of the pollen tube to grow autonomously irrespective of the MGU. Interestingly, the *wit1 wit2* mutant expressing *SC-cal* produced pollen tubes with the vegetative nucleus and sperm nuclei located behind the callose plugs in its basal region (Motomura et al., 2021). Callose plugs are callose-rich cell wall partitions specifically found in pollen tubes, where phasing formation maintains most of the protoplasm at its apical region (Franklin-Tong, 1999). The first callose plug formation isolates immotile MGUs, leading to physiologically anucleated growth of the pollen tubes in *wit1 wit2 SC-cal* plants within 3 h after germination. Surprisingly, *wit1 wit2 SC-cal* pollen tubes not only displayed continuous growth but also responded to pollen tube-attractant signals and reached the ovule. These results suggest that the pollen tube is a robust stand-alone system that can work even without the *de novo* transcript supply from the MGU (Motomura et al., 2021).

DROP1 and *DROP2*, also known as *LRL1* and *LRL2*, respectively, are members of subfamily XI of the basic helix-loop-helix (bHLH) transcription factors. The *drop1 drop2* double mutant showed loss of sperm cells in pollen grains, exhibiting normal directional growth toward attractant peptides and pollen tube discharge in the ovule (Zhang et al., 2017). This mutant is an excellent material to demonstrate the irrelevance of sperm cells in various pollen tube behaviors, elucidating the significance of the vegetative nucleus. A similar sperm cell-absent phenotype was also induced by double mutations in *BONOBO1* (*BNB1*) and *BNB2*, which encode subfamily VIIIa bHLH proteins that are putative partners of DROP1 and DROP2 (Yamaoka et al., 2018). In the present study, we further investigated whether *wit1 wit2* double mutations abolished the apical transport of the vegetative nucleus in the *bnb1 bnb2* double mutant. We show that most sperm cell-absent pollen tubes carrying *bnb1 bnb2 wit1 wit2* quadruple mutations retain the vegetative nucleus in their basal regions. Importantly, these pollen tubes maintain the capabilities of tip-growth and attraction to an ovule after isolation of the vegetative nucleus despite their anucleated condition, supporting the stand-alone behavior of the *wit1 wit2 SC-cal* pollen tubes (Motomura et al., 2021). Based on these results, we discuss when and how pollen tubes obtain their versatile abilities concerning *de novo* gene expression in the vegetative nucleus.

Materials and methods

Plant material and growth conditions

A. thaliana Columbia-0 (Col-0) was used as the wildtype (WT) plant and the background of all the mutants. The *pRPS5A:H2B-tdTomato* plasmid was provided by Dr. Kurihara (Maruyama et al., 2013). The *wit1-1 wit2-1* double mutant was kindly provided by Dr. Meier and Dr. Tamura (Zhou and Meier, 2014). The *bnb1* (GK-277A11) and *bnb2* (SALK_031573) mutants have been previously described (Yamaoka et al., 2018). Plants were grown in soil at 22°C under continuous light conditions. *Agrobacterium*-mediated plant transformation was performed by the floral dipping method using *Agrobacterium* strain GV3101 (Clough and Bent, 1998).

Pollen grain analysis

Mature pollen grains from opened flowers were mounted on a 5% sucrose solution for further imaging analysis. Differential

interference contrast (DIC) and fluorescence images were acquired using a confocal laser-scanning microscope (Leica TCS SP8, Wetzlar, Germany).

Pollen tube analyses

For the *in-vitro* pollen tube growth assay, pollen grains were incubated on pollen germination medium (0.01% boric acid, 5 mM $CaCl_2$, 5 mM KCl, 1 mM $MgSO_4$, 10% sucrose, adjusted pH to 7.5 with 1 N KOH, and 1.5% NuSieve GTG agarose) supplemented with 10 µM epibrassinolide (Muro et al., 2018). Pollen tubes 3 h after germination (HAG) were observed using an Axio Imager M1 (Zeiss, Jera, Germany). For the *in-vivo* single pollen tube guidance assay, a single pollen grain was picked up by an eyelash under an MVX10 macro zoom microscope (Olympus, Tokyo, Japan) and attached to the stigma of a WT pistil, as previously described (Zhang et al., 2017). In the case of the quadruple mutant pollen, teardrop-shaped pollen grains were selected from pollen from the +/*bnb1 bnb2 wit1 wit2* mutant. The pistils one day after pollination were dissected in aniline blue solution (0.1% [w/v] aniline blue, 0.1 M K_3PO_4) and observed using the Axio Imager M1.

Results

To examine the motility of the vegetative nucleus in the pollen tubes of the *bnb1 bnb2 wit1 wit2* quadruple mutant, we generated an *A. thaliana* mutant that was heterozygous for *bnb1* (+/*bnb1*) and homozygous for *bnb2*, *wit1*, and *wit2* since *bnb1 bnb2* double homozygous plants cannot be recovered due to severe male lethality (Yamaoka et al., 2018). All mutant and WT plants were transformed with the *pRPS5A:H2B-tdTomato* (*RHT*) ubiquitous nuclear marker gene (Maruyama et al., 2013). The results showed that most pollen grains had tricellular MGUs containing two condensed sperm nuclei and a relatively dispersed single vegetative nucleus in the WT-*RHT*, *wit1 wit2* double mutant, and *bnb2 wit1 wit2* triple mutant (Figures 1A,B). However, in the +/*bnb1 bnb2 wit1 wit2* mutant, only approximately 60% of the pollen was trinucleate, while the remaining pollen showed aberrant uninucleate or binucleate cells (Figures 1A,B). Notably, unicellular pollen contained a single vegetative nucleus and usually showed abnormal teardrop-shaped morphology with tiny protrusions due to the abortion of the male germ cells. These pollen phenotypes were comparable to those observed in a previous study with +/*bnb1 bnb2* plants (Yamaoka et al., 2018), suggesting little or no effect on *wit1 wit2* double mutations during pollen formation. The +/*bnb1 bnb2 wit1 wit2* mutant should produce *bnb2 wit1 wit2* triple mutant pollen and *bnb1 bnb2 wit1 wit2* quadruple mutant pollen in a 1:1 ratio. Thus, we concluded that aberrant unicellular or bicellular pollen reflects defects in male gametogenesis caused by *bnb1 bnb2 wit1 wit2* quadruple mutations.

Thereafter, we analyzed *in-vitro* germinated pollen tubes. In the WT-*RHT* line, the MGU was found at the apical region of the pollen tube, with the vegetative nucleus ahead of the two sperm nuclei (Figures 1C, D). However, the vegetative nuclei of *wit1 wit2* double mutant and *bnb2 wit1 wit2* triple mutant plants were frequently separated from sperm nuclei and located in the base of the pollen tube (Figures 1C–E). This phenotype indicates a loss of motive force in the vegetative nucleus. The remaining approximately half of the pollen tubes showed apical transport of MGU in *wit1 wit2* and *bnb2 wit1 wit2* mutants (Figure 1D). In this type of apical MGU transport, however, almost all the sperm nuclei preceded the vegetative nucleus (Figure 1E). Given that the sperm cells and vegetative nuclei are physically connected in the pollen tubes, we suggested that in the MGUs of these pollen tubes, this connection remains unbroken, resulting in the immotile vegetative nuclei being passively pulled by the sperm cells that proceed ahead of them. Thus, the absence of sperm cells is expected to deprive the motility of the vegetative nucleus in *wit1 wit2* mutant pollen tubes. Consistently, we found that the vegetative nucleus was at the basal region in 97% of the unicellular *bnb1 bnb2 wit1 wit2* quadruple mutant pollen tubes segregated from +/*bnb1 bnb2 wit1 wit2* mutant lines (n = 65, Figures 1C, D).

The unicellular *bnb1 bnb2 wit1 wit2* mutant pollen tube is an ideal material to investigate how vegetative nuclei function during pollen tube growth because we can exclude the possible contribution of the sperm cells. The first callose plug formation would block the *de novo* transcript supply from the immotile vegetative nucleus to the growing tip region (Figure 1C). An analysis of the length of the pollen tubes at 3 HAG demonstrated that the growth of the unicellular *bnb1 bnb2 wit1 wit2* quadruple mutant pollen tubes was comparable with those of the WT pollen tubes, *wit1 wit2* double mutant pollen tubes, and *bnb2 wit1 wit2* triple mutant pollen tubes (Figure 1F). To clarify the ability of pollen tubes to respond to attraction signals from the ovule, we pollinated a WT pistil with a single pollen grain and performed aniline blue staining one day after pollination. Among pollen grains from +/*bnb1 bnb2 wit1 wit2* mutant, we distinguished the unicellular *bnb1 bnb2 wit1 wit2* mutant pollen from *bnb2 wit1 wit2* pollen by its unique teardrop morphology under a microscope (Figure 1A, lower-left panel). In the single pollen tube guidance assay, the *bnb1 bnb2 wit1 wit2* pollen with tear-drop morphology showed normal germination rate (42.2%) that was comparable with that of WT-Col-0 pollen tubes (63.6%, $p = 0.085$, compared to *bnb1 bnb2 wit1 wit2*) or *bnb2 wit1 wit2* pollen tubes (59.0%, $p = 0.120$, compared to *bnb1 bnb2 wit1 wit2*). Strikingly, we found that *bnb1 bnb2 wit1 wit2* mutant pollen tubes could reach the ovule despite the nuclear-absent condition (Figure 1G), albeit the ovule-insertion rate (9.4%) was

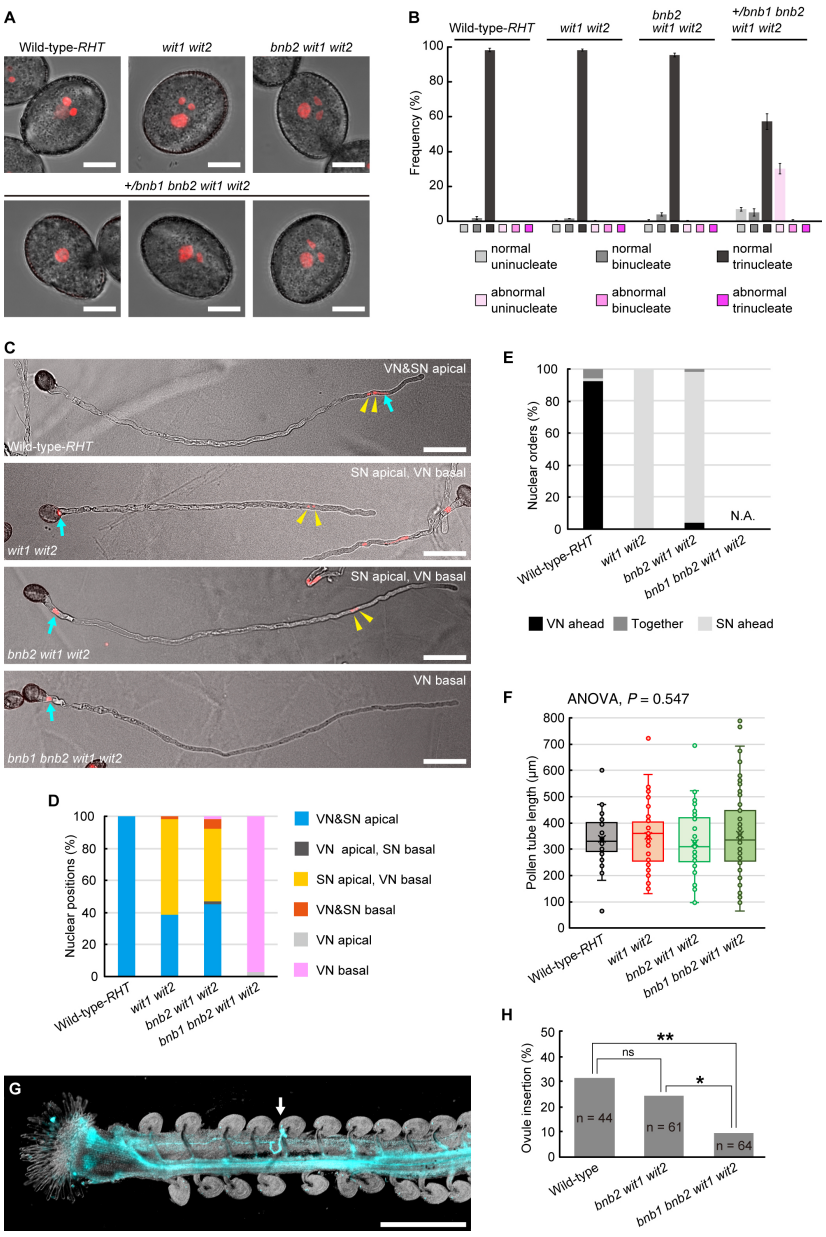

FIGURE 1
Pollen tube behavior in +/*bnb1 bnb2 wit1 wit2* mutant plants. **(A)** Representative images of mature transgenic pollen carrying the *pRPS5A:H2B-tdTomato* (*RHT*) plasmid of the wildtype (WT) Col-0 plant (WT-*RHT*), *wit1 wit2* double homozygous mutant, *bnb2 wit1 wit2* triple homozygous mutant or +/*bnb1* heterozygous, and *bnb2 wit1 wit2* triple homozygous mutant (+/*bnb1 bnb2 wit1 wit2*). The three images represent an abnormal uninucleate (left), a normal binucleate (center), and a normal trinucleate (right) pollen from the +/*bnb1 bnb2 wit1 wit2* mutant. Scale bars: 10 μm. **(B)** Pollen nucleation frequencies in the four genotypes observed in **(A)**, considering both the number of nuclei and shape of pollen grains. Normal indicates pollen of normal contour. At least three independent observations were conducted, with a total of 572 to 1,160 pollen grains. **(C)** Representative images of WT-*RHT*, *wit1 wit2*, *bnb2 wit1 wit2*, and *bnb1 bnb2 wit1 wit2* pollen tubes 3 h post-germination *in vitro*. Blue arrows and yellow arrowheads indicate vegetative nuclei (VN) and sperm nuclei (SN) pairs, respectively. Scale bars: 50 μm. **(D, E)** Nuclear positions **(D)** and nuclear orders **(E)** analyzed in the WT-*RHT*, *wit1 wit2*, *bnb2 wit1 wit2*, and *bnb1 bnb2 wit1 wit2* mutant pollen tubes. For each plant genotype, 51 to 65 pollen tubes were observed. **(F)** Box-and-whisker plots of pollen tube length analyzed in the same samples as in **(D)** and **(E)**. Note that we observed only *bnb1 bnb2 wit1 wit2* quadruple pollen tubes with one nucleus out of 65 pollen grains from +/*bnb1 bnb2 wit1 wit2* mutants in **(C)** to **(F)**. **(G)** Representative image of an ovule penetrated by a *bnb1 bnb2 wit1 wit2* quadruple mutant pollen tube (white arrow). In the *in-vivo* single-pollen-tube guidance assay, a pistil was harvested one day after pollination and observed after aniline blue staining. Scale bar: 500 μm. **(H)** Ovule-insertion analyzed in the *in-vivo* single pollen tube guidance assay of the WT, *bnb2 wit1 wit2*, and *bnb1 bnb2 wit1 wit2* mutant pollen. Statistics: Chi-square test with a *p*-value adjustment by the Hochberg algorithm. ns, not significant. *P = 0.0459. **P = 0.0095.

significantly lower than those of WT pollen (31.8%) and *bnb2 wit1 wit2* pollen tubes (24.6%) (Figure 1H). A long pollen tube journey elucidated the functional limitation of enucleated pollen tubes. However, it was clear that some enucleated pollen tubes obtained the capability to reach the ovule. This finding indicates the robustness of the pollen tube to function without the *de novo* transcript supply from the vegetative nucleus, which supports our previous findings on *wit1 wit2 SC-cal* pollen tubes (Motomura et al., 2021).

Discussion

It is widely believed that a vegetative nucleus is required for pollen tube growth. However, the pollen tubes of the *bnb1 bnb2 wit1 wit2* quadruple mutant and the *wit1 wit2 SC-cal* mutant could grow and even showed targeting behavior towards the ovule after enucleation by the first callose plug formation (Motomura et al., 2021) (Figure 1). Based on these findings and other cumulative evidence, we propose plausible mechanisms responsible for the persistent directional growth capability of pollen tubes.

Precocious gene expression required for persistent pollen tube growth

We assume that early acquisition of persistent pollen tube growth capability depends on a combination of mRNA storage in mature pollen and *de novo* transcription in a short period of time after germination. The mRNAs accumulated in mature pollen are sufficient to induce germination because various species can germinate their pollen tubes on media containing transcription inhibitors, such as actinomycin D (Honys and Twell, 2004; Hao et al., 2005). Pollen grains may have a special mRNA storage system. In *Nicotiana tabacum* and *A. thaliana*, mature pollen contains mRNA-protein complexes (mRNPs) (Honys et al., 2009; Scarpin et al., 2017; Hafidh et al., 2018). These mRNPs resemble stress granules that isolate mRNA from ribosomes, preventing *de novo* protein synthesis in somatic tissues under stress conditions. Recently, Sze et al. (2021) proposed that pollen accumulates transcripts in a quiescent form of mRNP and release the transcripts during rehydration, prior to pollen tube germination (Figure 2, 0 h).

Precocious mRNA accumulation alone appears to be insufficient for persistent pollen tube growth. Pollen tubes germinated on a medium containing a transcriptional inhibitor showed growth retardation in various species, including *Tradescantia*, *Lobelia*, *Aeschynanthus*, *Iris*, *Hippeastrum*, *Narcissus*, and *Endymion*, indicating the importance of the transcripts synthesized after pollen tube germination (Mascarenhas, 1975). In contrast, the pollen tubes of the +/*bnb1 bnb2 wit1 wit2* quadruple mutant and *wit1 wit2 SC-cal* mutant showed normal pollen tube growth without any retardation (Motomura et al., 2021) (Figure 1). The difference between these two observations may be because of the presence of *de novo* transcripts supplied immediately after germination. The pollen tubes of the *bnb1 bnb2 wit1 wit2* quadruple mutant and *wit1 wit2 SC-cal* mutant have vegetative nuclei at the basal region; thus, these pollen tubes can transport *de novo* transcripts into their apical growing region (Figure 2, 0.5 h). This mRNA transport continues until the first callose plug formation, which occurs approximately a few hours after germination. In transcriptome analyses, pollen tubes growing through a style 4 h after pollination show a very different gene expression pattern from that of mature pollen grains (Qin et al., 2009; Chen et al., 2014). Although the functions of most of the induced genes remain unknown, an R2R3-type MYB transcription factor, MYB120, starts to accumulate after pollen tube germination and regulates pollen tube discharge in the ovules with its paralogs MYB97 and MYB101 redundantly (Leydon et al., 2013). These reports indicate that a subset of genes expressed after germination is required for the functional maturation of pollen tubes. We anticipate that these genes play key roles in the persistent directional growth capability of pollen tubes.

Stability and transport of transcripts in pollen tubes

In addition to the production of sufficient transcripts, mRNA stability would also be important for robust pollen tube growth after enucleation. The pollen tubes may be able to recycle mRNA molecules and continue to use them for long periods compared to somatic cells (Figure 2). RNA exosomes or decapping proteins are key enzymes of RNA metabolism that are ubiquitously expressed during the transition of cell identity and function through RNA degradation. Mutants of these factors show severe developmental defects during gametogenesis and embryogenesis (Motomura et al., 2012; Kumakura et al., 2013; Motomura et al., 2020). Pollen tube growth also accompanies drastic changes in the gene expression profile and morphology; however, no phenotypes have been reported in these mutant pollen tubes. Moreover, gene sets with an ontology term RNA metabolic process are less expressed in pollen tubes (Poidevin et al., 2021). These findings support the low RNA metabolic activity in the pollen tubes (Figure 2, 0.5 h).

Not only the suppression of mRNA degradation but also the directional mRNA transport and local activation of protein synthesis may be the key mechanisms responsible for the robustness of pollen tube growth. Axon guidance in animal neurons is often compared to pollen tube growth because of

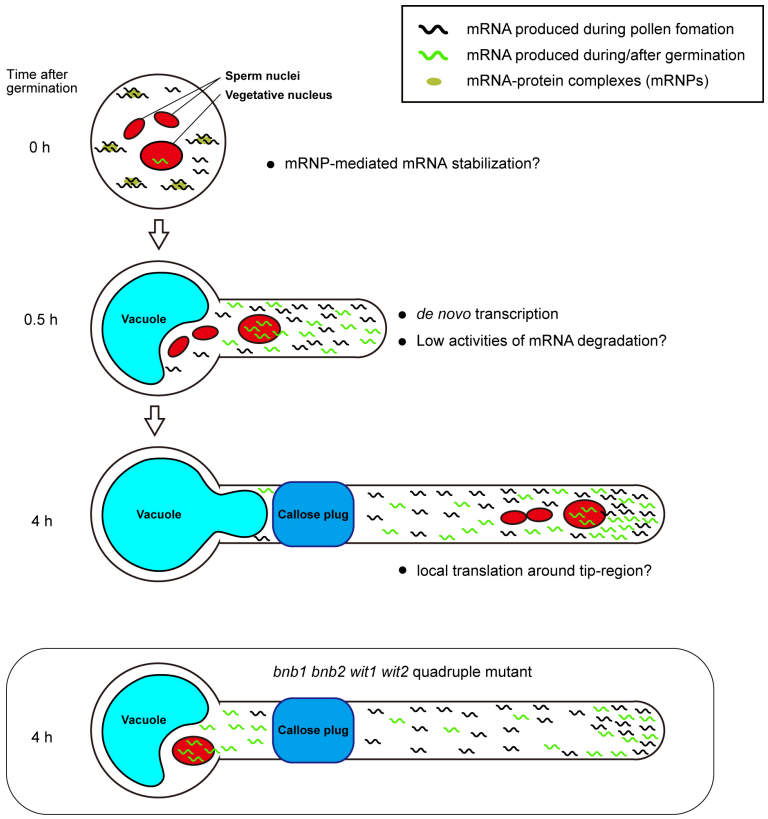

FIGURE 2
Plausible mechanism for persistent pollen tube growth based on gene expression. Pollen tubes generate many transcripts for their germination and short-time pollen tube growth during pollen tube development. Mature pollen may conserve large amounts of mRNAs in the quiescent mRNP form (0 h). When pollen tubes are ready to germinate, they begin to germinate with the transcription of *de novo* mRNAs within a short period of time. In the germinating pollen tube, reduced mRNA degradation activity may contribute to the accumulation of a large amount of transcripts (0.5 h). In *Arabidopsis* Col-0 accession, the first callose plug is formed at the basal part of the pollen tube within 3 h after germination. Subcellular localization bias of mRNA in pollen tubes is not known; however, local translation at the pollen tube tip may contribute to active pollen tube growth (4 h). In *bnb1 bnb2 wit1 wit2* quadruple mutant pollen tubes, the vegetative nucleus is left at the basal area, implying that *de novo* transcripts are not supplied to the apical region. However, transcripts that accumulate in the apical region by riding the cytoplasm flow prior to the formation of the first callose plug may maintain persistent pollen tube growth (*bnb1 bnb2 wit1 wit2* quadruple mutant).

similarities in the active tip growth and the response behavior against directional cues. Neurons produce mRNA in the nucleus at the cell body and then transport them to the growth cone (Rodriguez et al., 2008). During axonal mRNA transport, mRNAs form RNPs and are most likely to repress translation. In contrast, mRNAs become translationally active at the growth cone. Interestingly, abnormal neurite outgrowth was observed when local translation was impaired, indicating the importance of axonal mRNA transport and local protein synthesis in neurons (Rodriguez et al., 2008). The active transport of specific mRNA and local protein synthesis in the pollen tube have not been reported so far; however, a recent study has uncovered a regulatory mechanism of local protein synthesis in *A. thaliana* root hairs, which are tip-growing cells (Zhu et al., 2020). These studies improve the understanding of the biology of RNA binding proteins in the pollen tube and enable the exploration of possible mechanistic links to the animal axon guidance (Billey et al., 2021; Duarte-Conde et al., 2022) (Figure 2, 4 h).

Future directions for the study of pollen tube capability

The duration of pollen tube growth varies in different organisms and is sometimes more than 24 h (O'Neill, 1997; Borgardt and Nixon, 2003). Precocious mRNA production as well as stabilization of mRNA will provide unusual and persistent growth capabilities to pollen tubes. The mechanisms of mRNA transport may also have positive effects on pollen tube germination by saving transcription time and facilitating germination and tip growth, thereby providing an opportunity

to win a competitive race among pollen tubes and increase reproductive fitness (Erbar, 2003). Moreover, mRNA reservoirs in pollen tubes possibly contribute toward the quick response against biotic and/or abiotic environmental stresses, as the expression of genes involved in DNA repair and defense response is upregulated in pollen tubes growing through a style (Qin et al., 2009). In the context of pollen biology, enucleated pollen tubes from the *+/bnb1 bnb2 wit1 wit2* mutant are valuable for analyzing the persistent growth of pollen tubes and illuminating the functional limitation of the early set of transcripts.

Data availability statement

The original contributions presented in the study are included in the article/supplementary material. Further inquiries can be directed to the corresponding authors.

Author contributions

KM and DM designed the study, conducted the experiments, analyzed pollen tube growth, and drafted the manuscript. NS analyzed the pollen phenotypes of the mutants. AT and SY provided critical advice and reviewed the manuscript. All authors have contributed to the manuscript and approved the submitted version.

Funding

This work was supported by JSPS KAKENHI (Grant nos. JP19H04869, JP20H03280, JP20K21432, JP20H05422, JP20H05778, and JP20H05781 awarded to DM; and Grant nos. JP19K23759, JP20K15822, and JP22K15147 awarded to KM; JP20H05780 awarded to SY); Asahi Glass Foundation (Research Grant to SY); JST PRESTO (Grant no. JPMJPR20D9 awarded to KM); Yokohama City University (Academic Research Grant to DM; Development Fund to DM; and Strategic Research Promotion Grant no. SK1903 to DM); Japan Science Society (Sasakawa Scientific Research Grant to KM); Takeda Science Foundation (research Grant to KM); and Ritsumeikan Global Innovation Research Organization, Ritsumeikan University (Third-Phase R-GIRO Research Grant to KM and AT).

Acknowledgments

We thank K. Tamura and I. Mayer for providing the *wit1 wit2* mutant; D. Kurihara for providing the *pRPS5A:H2B-tdTomato*; K. Matsuura-Tokita for performing the *in-vitro* germination assay; T. Kinosita for various support; and M. Tsukatani, H. Ikeda, H. Kakizaki, A. Matsumoto, A. Saito, and R. Shibayama for their technical support. We would like to thank Editage (www.editage.com) for English language editing.

Conflict of interest

The authors declare that the research was conducted in the absence of any commercial or financial relationships that could be construed as a potential conflict of interest.

Publisher's note

References

Billey, E., Hafidh, S., Cruz-Gallardo, I., Litholdo, C. G., Jean, V., Carpentier, M.-C., et al. (2021). LARP6C orchestrates posttranscriptional reprogramming of gene expression during hydration to promote pollen tube guidance. *Plant Cell.* 33, 2637–2661. doi: 10.1093/plcell/koab131

Borgardt, S. J., and Nixon, K. C. (2003). A comparative flower and fruit anatomical study of quercus acutissima, a biennial-fruiting oak from the cerris group (Fagaceae). *Am. J. Bot.* 90, 1567–1584. doi: 10.3732/ajb.90.11.1567

Chen, Y., Zou, M., and Cao, Y. (2014). Transcriptome analysis of the arabidopsis semi-*in vivo* pollen tube guidance system uncovers a distinct gene expression profile. *J. Plant Biol.* 57, 93–105. doi: 10.1007/s12374-013-0272-6

Clough, S. J., and Bent, A. F. (1998). Floral dip: A simplified method for agrobacterium-mediated transformation of arabidopsis thaliana. *Plant J.* 16, 735–743. doi: 10.1046/j.1365-313x.1998.00343.x

Denninger, P., Bleckmann, A., Lausser, A., Vogler, F., Ott, T., Ehrhardt, D. W., et al. (2014). Male-Female communication triggers calcium signatures during fertilization in arabidopsis. *Nat. Commun.* 5, 4645. doi: 10.1038/ncomms5645

Duarte-Conde, J. A., Sans-Coll, G., and Merchante, C. (2022). RNA-Binding proteins and their role in translational regulation in plants. *Essays. Biochem* 66, 87–97. doi: 10.1042/EBC20210069

Erbar, C. (2003). Pollen tube transmitting tissue: Place of competition of male gametophytes. *Int. J. Plant Sci.* 164, S265–S277. doi: 10.1086/377061

Franklin-Tong, V. E. (1999). Signaling and the modulation of pollen tube growth. *Plant Cell.* 11, 727–738. doi: 10.1105/tpc.11.4.727

Hafidh, S., Potěšil, D., Müller, K., Fíla, J., Michailidis, C., Herrmannová, A., et al. (2018). Dynamics of the pollen sequestrome defined by subcellular coupled omics. *Plant Physiol.* 178, 258–282. doi: 10.1104/pp.18.00648

Hamamura, Y., Saito, C., Awai, C., Kurihara, D., Miyawaki, A., Nakagawa, T., et al. (2011). Live-cell imaging reveals the dynamics of two sperm cells during double fertilization in arabidopsis thaliana. *Curr. Biol.* 21, 497–502. doi: 10.1016/j.cub.2011.02.013

Hao, H., Li, Y., Hu, Y., and Lin, J. (2005). Inhibition of RNA and protein synthesis in pollen tube development of pinus bungeana by actinomycin d and cycloheximide. *New Phytol.* 165, 721–729. doi: 10.1111/j.1469-8137.2004.01290.x

Higashiyama, T., and Takeuchi, H. (2015). The mechanism and key molecules involved in pollen tube guidance. *Annu. Rev. Plant Biol.* 66, 393–413. doi: 10.1146/annurev-arplant-043014-115635

Honys, D., Rěnák, D., Feciková, J., Jedelský, P. L., Nebesárová, J., Dobrev, P., et al. (2009). Cytoskeleton-associated large RNP complexes in tobacco male gametophyte (EPPs) are associated with ribosomes and are involved in protein synthesis, processing, and localization. *J. Proteome Res.* 8, 2015–2031. doi: 10.1021/pr8009897

Honys, D., and Twell, D. (2004). Transcriptome analysis of haploid male gametophyte development in arabidopsis. *Genome Biol.* 5, R85. doi: 10.1186/gb-2004-5-11-r85

Kumakura, N., Otsuki, H., Tsuzuki, M., Takeda, A., and Watanabe, Y. (2013). Arabidopsis AtRRP44A is the functional homolog of Rrp44/Dis3, an exosome component, is essential for viability and is required for RNA processing and degradation. *PloS One* 8, e79219. doi: 10.1371/journal.pone.0079219

Leydon, A. R., Beale, K. M., Woroniecka, K., Castner, E., Chen, J., Horgan, C., et al. (2013). Three MYB transcription factors control pollen tube differentiation required for sperm release. *Curr. Biol.* 23, 1209–1214. doi: 10.1016/j.cub.2013.05.021

Maruyama, D., Hamamura, Y., Takeuchi, H., Susaki, D., Nishimaki, M., Kurihara, D., et al. (2013). Independent control by each female gamete prevents the attraction of multiple pollen tubes. *Dev. Cell.* 25, 317–323. doi: 10.1016/j.devcel.2013.03.013

Mascarenhas, J. P. (1975). The biochemistry of angiosperm pollen development. *Bot. Rev.* 41, 259–314. doi: 10.1007/BF02860839

McCue, A. D., Cresti, M., Feijó, J. A., and Slotkin, R. K. (2011). Cytoplasmic connection of sperm cells to the pollen vegetative cell nucleus: potential roles of the male germ unit revisited. *J. Exp. Bot.* 62, 1621–1631. doi: 10.1093/jxb/err032

Mogensen, H. L. (1992). "The Male germ unit: Concept, composition, and significance," in *International review of cytology*. Eds. S. D. Russell and C. Dumas (Cambridge, Massachusetts: Academic Press), 129–147.

Motomura, K., Arae, T., Araki-Uramoto, H., Suzuki, Y., Takeuchi, H., Suzuki, T., et al. (2020). AtNOT1 is a novel regulator of gene expression during pollen development. *Plant Cell Physiol.* 61, 712–721. doi: 10.1093/pcp/pcz235

Motomura, K., Le, Q. T., Kumakura, N., Fukaya, T., Takeda, A., and Watanabe, Y. (2012). The role of decapping proteins in the miRNA accumulation in arabidopsis thaliana. *RNA Biol.* 9, 644–652. doi: 10.4161/rna.19877

Motomura, K., Takeuchi, H., Notaguchi, M., Tsuchi, H., Takeda, A., Kinoshita, T., et al. (2021). Persistent directional growth capability in arabidopsis thaliana pollen tubes after nuclear elimination from the apex. *Nat. Commun.* 12, 2331. doi: 10.1038/s41467-021-22661-8

Muro, K., Matsuura-Tokita, K., Tsukamoto, R., Kanaoka, M. M., Ebine, K., Higashiyama, T., et al. (2018). ANTH domain-containing proteins are required for the pollen tube plasma membrane integrity *via* recycling ANXUR kinases. *Commun. Biol.* 1, 152. doi: 10.1038/s42003-018-0158-8

O'Neill, S. D. (1997). Pollination regulation of flower development. *Annu. Rev. Plant Physiol. Plant Mol. Biol.* 48, 547–574. doi: 10.1146/annurev.arplant.48.1.547

Poidevin, L., Forment, J., Unal, D., and Ferrando, A. (2021). Transcriptome and translatome changes in germinated pollen under heat stress uncover roles of transporter genes involved in pollen tube growth. *Plant Cell Environ.* 44, 2167–2184. doi: 10.1111/pce.13972

Qin, Y., Leydon, A. R., Manziello, A., Pandey, R., Mount, D., Denic, S., et al. (2009). Penetration of the stigma and style elicits a novel transcriptome in pollen tubes, pointing to genes critical for growth in a pistil. *PloS Genet.* 5, e1000621. doi: 10.1371/journal.pgen.1000621

Rodriguez, A. J., Czaplinski, K., Condeelis, J. S., and Singer, R. H. (2008). Mechanisms and cellular roles of local protein synthesis in mammalian cells. *Curr. Opin. Cell Biol.* 20, 144–149. doi: 10.1016/j.ceb.2008.02.004

Scarpin, M. R., Sigaut, L., Temprana, S. G., Boccaccio, G. L., Pietrasanta, L. I., and Muschietti, J. P. (2017). Two arabidopsis late pollen transcripts are detected in cytoplasmic granules. *Plant Direct.* 1, e00012. doi: 10.1002/pld3.12

Sze, H., Palanivelu, R., Harper, J. F., and Johnson, M. A. (2021). Holistic insights from pollen omics: Co-opting stress-responsive genes and ER-mediated proteostasis for male fertility. *Plant Physiol.* 187, 2361–2380. doi: 10.1093/plphys/kiab463

Tatout, C., Evans, D. E., Vanrobays, E., Probst, A. V., and Graumann, K. (2014). The plant LINC complex at the nuclear envelope. *Chromosome Res.* 22, 241–252. doi: 10.1007/s10577-014-9419-7

Yamaoka, S., Nishihama, R., Yoshitake, Y., Ishida, S., Inoue, K., Saito, M., et al. (2018). Generative cell specification requires transcription factors evolutionarily conserved in land plants. *Curr. Biol.* 28, 479–486.e5. doi: 10.1016/j.cub.2017.12.053

Zhang, J., Huang, Q., Zhong, S., Bleckmann, A., Huang, J., Guo, X., et al. (2017). Sperm cells are passive cargo of the pollen tube in plant fertilization. *Nat. Plants.* 3, 17079. doi: 10.1038/nplants.2017.79

Zhou, X., and Meier, I. (2014). Efficient plant male fertility depends on vegetative nuclear movement mediated by two families of plant outer nuclear membrane proteins. *Proc. Natl. Acad. Sci. U. S. A.* 111, 11900–11905. doi: 10.1073/pnas.1323104111

Zhu, S., Estévez, J. M., Liao, H., Zhu, Y., Yang, T., Li, C., et al. (2020). The RALF1-FERONIA complex phosphorylates eif4e1 to promote protein synthesis and polar root hair growth. *Mol. Plant* 13, 698–716. doi: 10.1016/j.molp.2019.12.014

frontiers | Frontiers in Plant Science

TYPE Review
PUBLISHED 15 December 2022
DOI 10.3389/fpls.2022.1090836

OPEN ACCESS

EDITED BY
Giampiero Cai,
University of Siena, Italy

REVIEWED BY
Hidenori Takeuchi,
Nagoya University, Japan
Jorge Lora,
Spanish National Research Council (CSIC), Spain

*CORRESPONDENCE
Tian-Ying Yu
tyyu@ytu.edu.cn

SPECIALTY SECTION
This article was submitted to Plant Cell Biology, a section of the journal Frontiers in Plant Science

RECEIVED 15 November 2022
ACCEPTED 02 December 2022
PUBLISHED 15 December 2022

CITATION
Yu T-Y, Xu C-X, Li W-J and Wang B (2022) Peptides/receptors signaling during plant fertilization. *Front. Plant Sci.* 13:1090836. doi: 10.3389/fpls.2022.1090836

Peptides/receptors signaling during plant fertilization

Tian-Ying Yu*, Chun-Xia Xu, Wen-Jia Li and Bo Wang

College of Life Sciences, Yantai University, Yantai, China

Double fertilization is a unique and particularly complicated process for the generation alternation of angiosperms. Sperm cells of angiosperms lose the motility compared with that of gymnosperms. The sperm cells are passively carried and transported by the pollen tube for a long journey before targeting the ovule. Two sperm cells are released at the cleft between the egg and the central cell and fused with two female gametes to produce a zygote and endosperm, respectively, to accomplish the so-called double fertilization process. In this process, extensive communication and interaction occur between the male (pollen or pollen tube) and the female (ovule). It is suggested that small peptides and receptor kinases play critical roles in orchestrating this cell-cell communication. Here, we illuminate the understanding of phases in the process, such as pollen-stigma recognition, the hydration and germination of pollen grains, the growth, guidance, and rupture of tubes, the release of sperm cells, and the fusion of gametes, by reviewing increasing data recently. The roles of peptides and receptor kinases in signaling mechanisms underlying cell-cell communication were focused on, and directions of future studies were perspected in this review.

KEYWORDS

double-fertilization, peptide, kinase, pollen tube guidance, polytubey block, cell-cell communication

Introduction

The life cycle alternates between the diploid sporophytic generation and the haploid gametophytic generation in flowering plants. Meiosis and double fertilization are indispensable and crucial programs for the alternation of generations (Hater et al., 2020; Hafidh and Honys, 2021). The mature gametophyte, the pollen grain, is a cell-in-cell structure, which means that two small sperm cells are embedded in the cytoplasm of a big vegetative cell. The polygonum-type embryo sac is found in the majority of flowering plants. It is a polarized structure with two synergids, one egg, one central cell that contains two nuclei, and three antipodals arranged from the micropyle to the chalazal end. In contrast to animal sperms, the immobile sperm cells of angiosperms are transmitted passively for long distances by pollen tubes that target the female gametes

for double fertilization (Bleckmann et al., 2014). Germination and the subsequent elongation of the pollen tubes for transmission of sperm cells are initiated as the recognition of compatible grains and papillar cells. Pollen tubes penetrate the transmitting tract and are guided to the funiculus, then the micropyle of the ovule. The sperm cells will be released when the tube enters the embryo sac through the micropyle (Dresselhaus and Franklin-Tong, 2013). Complicated and extensive communication or interaction is involved during the process mentioned above. In the guiding signaling network, it is indicated that small peptide ligands and receptor kinases play essential roles (Chevalier et al., 2011; Kawashima and Berger, 2011; Dresselhaus et al., 2016; Zhou and Dresselhaus, 2019; Hafidh and Honys, 2021; Kim et al., 2021).

The plant receptor-like kinases (RLKs) are classified as the largest RLKs/Pelle family, with more than 610 and 1130 members in *Arabidopsis thaliana* and *Oryza sativa L.*, respectively (Shiu et al., 2004). RLKs are characterized into various subfamilies according to the different extracellular domains (ECDs), including Leucine-rich repeat RLKs, lysine motifs (LysM) RLKs (Franck et al., 2018a; Yu et al., 2021a), wall-associated kinases (WAKs), lectin RLKs, proline-rich receptor kinases (PERK), and others. There is also a class of co-receptors that are featured with basic structures similar to that of receptor kinases and facilitate the recognition of ligands (Kirkbride et al., 2005; Hohmann et al., 2017). Small peptides act as signals to bind to the ECDs of receptor kinases/co-receptors to induce multimerization and *trans*-phosphorylation, and further activate downstream signaling cascades. Currently, most of the small peptide signals identified in plant reproduction are small cysteine-rich peptides, defensin-like peptides, or rapid alkalinization factors (RALFs) (Okuda et al., 2009; Amien et al., 2010; Takeuchi and Higashiyama, 2012; Kanaoka, 2018; Somoza et al., 2021). Due to the remarkable diversity of peptide/receptor/co-receptor pairs, this communicating mechanism of peptide-receptor interaction is fundamental to many signaling pathways.

The communication of pollen-pistil during fertilization is involved in the five stages mentioned above. The signaling pathways orchestrated by peptide/receptor kinases in angiosperm fertilization are reviewed and discussed here. Peptides, receptors, and their functions are summarized in Table 1.

Recognition of pollen and stigma

The first checkpoint for plant fertilization is at the beginning of pollen-papilla interaction. The mature pollen grains (male gametophytes) land on the stigmatic papillae at the top of the pistil. The male and female are adhered to and recognized by each other. In self-incompatible plants, only the compatible grains can proceed with the subsequent hydration and germination (Rozier et al., 2020). The alien pollens from unrelated species or the self-incompatible (SI) ones are ineffective. In about half of the species in flowering plants, self-incompatibility and cross-pollination are applied to maintain genetic diversity within species populations (Murase et al., 2004; Zhang et al., 2021). Accumulating data indicate that this self/non-self-recognition in *Brassica* is triggered by *S*-haplotype-specific interaction between the male and female determinants. The *S*-haplotype consists of two or more closely linked polymorphic *S* loci. The pistil and pollen will show self-incompatibility given that the same *S* allele is present in the male and female. Rejection of pollen for the same individual *Brassica* plant is due to sporophytic self-incompatibility (Jany et al., 2019). The male determinant factor is a small peptide ligand, *S*-locus cysteine-rich protein/*S*-locus protein 11 (SCR/SP11), which is secreted from the anther tapetum cells, and diffused to the pollen wall and stored there. The female determinant factor is the *S*-locus receptor kinase (SRK) localized in the papillar cell membrane (Scandola and Samuel, 2019). The SI response is initiated by the haplotype-specific interaction between SCR/SP11 and SRK, the interaction through which the reciprocal communication between the pollen and papillar cells is regulated (Scandola and Samuel, 2019). SCR/SP11-SRK is involved in the self-incompatibility signal pathway in *Brassica*, as shown in Figure 1. In the stigma, SRK exists as a preassembled homodimer at the plasma membrane of papillae and remains inactive until pollination. SRK is activated by the *S*-haplotype-specific SCR/SP11 binding to its ECD and the autophosphorylation of its intracellular kinase. The intracellular serine/threonine M-LOCUS PROTEIN KINASEs (MLPKs) is anchored at the membrane of papillae, and acts as a downstream target for SRK (Murase et al., 2004). THL1 and THL2 are members of the thioredoxin-H family and function as negative effectors (Bower et al., 1996). The stigma-expressed E3 ubiquitin ligase ARMADILLO-REPEAT-CONTAINING1 (ARC1) is a positive regulator in the pistil for the rejection of self-incompatible pollen in *Brassica napus*, *Arabidopsis lyrata*, and *Arabidopsis thaliana* (Stone et al., 2003; Goring et al., 2014). All these players mentioned above are involved in the self-incompatibility response.

In *Brassica*, in the absence of self-pollen, THL1/2 interacts with the intracellular domain of SRK to form a heterodimer that prevents SRK from homodimerization and activation (Bower et al., 1996; Mazzurco et al., 2001). In the presence of self-pollen, SCR/SP11 interacts with the ECD of SRK to promote SRK homodimerization and consequently results in the release of THL1 and THL2 from SRK. The active SRK recruits and phosphorylates MLPK (Murase et al., 2004; Liang and Zhou, 2018). The cytoplasmic kinase MLPK subsequently phosphorylates and activates ARC1 (Stone et al., 2003; Goring et al., 2014) to transduce the SI signaling. Phosphorylated ARC1 mediates ubiquitination and degradation of a series of downstream substrates involved in pollen hydration,

TABLE 1 peptides, receptors, functions during plant fertilization.

Process	Peptides	Peptides derived from	Receptors	Receptor localizationcell	Functions	Species	ref
Pollen-stigma recognition	SCR/SP11	anther tapetum cells	SRK MLKS THL1/2	papillae	Self-incompatible response	*Brassica*	Bower et al., 1996; Murase et al., 2004; Scandola and Samuel, 2019
	PCP-Bs	Pollen coat	FER ANJ HERK1	Papillae	pollen hydration and germination	*Arabidopsis*	Liu et al., 2021a; Wang et al., 2017; Galindo-Trigo et al., 2020
	RALF23 RALF33	papilla cells	FER ANJ LLG1	papillae	Maintenance of high levels of ROS in the stigma papillae	*Arabidopsis*	Liu et al., 2021a
	LAT52	anther	LePRK1/2	pollen	Inhibition of pollen germination before pollination	*Solanum Lycopersicum*	Tang et al., 2002; Johnson and Preuss, 2003
Pollen tubes growth in transmitting tract	LeSTIG1	stigma	LePRK1/2	pollen	Pollen tube growth	*Solanum Lycopersicum*	Tang et al., 2004; Zhang et al., 2008
	RALF4/19	Pollen tubes	BUPS1/2 ANX1/2 LLG2/3 MRI AUN1/2	Pollen tubes	Pollen tube growth and integrity	*Arabidopsis*	Boisson-Dernier et al., 2015; Ge et al., 2017; Ge et al., 2019; Franck, 2018b; Zhou et al., 2021
	RALF4	Pollen tubes	LRX8/9/10/11	Pollen tubes	Pollen tube growth and integrity	*Arabidopsis*	Mecchia et al., 2017; Fabrice et al., 2018
Pollen tubes guidance	TfLURE1/2	synergid cell	N.D.	N.D.	pollen tube guidance and attraction at the micropyle	*Torenia fournieri*	Okuda et al., 2009
	AtLURE1.1-1.5 AtLURE1.7 AtLURE1.8	synergid cell	PRK6 MDIS1/2 MIK1/2	Pollen tubes	Species-specific pollen tubes attraction and guidance in the septum and micropyle	*Arabidopsis*	Takeuchi and Higashiyama, 2012; Takeuchi and Higashiyama, 2016; Wang et al., 2016; Zhong et al., 2019; Liu et al., 2021b
	XIUQIU1/2 XIUQIU3/4	synergid cell	N.D.	N.D.	Species-indiscriminate pollen tubes attraction and guidance	*Arabidopsis*	Zhong et al., 2019; Liu et al., 2021b
	ZmEA1	egg apparatus	N.D.	N.D.	Pollen tubes attraction and guidance	*Zea Mays*	Marton et al., 2005; Marton et al., 2012
	RALF6/7/16/36/37	pollen tube	FER-ANJ-HERK1 LLG1	Transmission track and septum of pistil	Polyspermy block at the septum and the micropyle	*Arabidopsis*	Zhong et al., 2022
Pollen tube reception and rupture	RALF6/7/16/36/37	pollen tube	FER-ANJ-HERK1 LLG1 NORTIA	micropyle	Polyspermy block at the micropyle	*Arabidopsis*	Ju et al. 2021; Huck et al., 2003; Zhong et al., 2022
	RALF4/19	Pollen tubes	BUPS1/2 ANX1/2 LLG2/3	Pollen tubes	Pollen tube growth and integrity	*Arabidopsis*	Ge et al., 2017; Ge et al., 2019
	RALF34	inner integument	BUPS1/2 ANX1/2 LLG2/3	Pollen tubes	Pollen tubes rupture	*Arabidopsis*	Ge et al., 2017; Ge et al., 2019
	ZmES1-4	synergid cell	N.D.	N.D.	Pollen tube rupture and sperm release	*Zea Mays*	Cordts et al., 2001; Amien et al., 2010
Gamete fusion and double fertilization	EC1s	egg cell			Guidance of HAP2/GCS1 of sperm cells to the membrane and gametes fusion	*Arabidopsis*	Sprunck et al., 2012; Hamamura et al., 2012

exocytosis, and germination. For example, the factor for stigmatic compatibility: Exo70A1, is involved in pollen hydration (Kitashiba et al., 2011; Li et al., 2013; Zhang et al., 2016); the phospholipase D-1 protein (PLD1) plays role in germination (Scandola and Samuel, 2019). The glyoxalase 1 (GLO1) is required to detoxify plants' methylglyoxal (MG) cytotoxicity. ARC1 was shown to ubiquitinate GLO1 effectively (Sankaranarayanan et al., 2015). In self-incompatible pollination, less GLO1 was found in stigma. It was suggested that the factors involved in compatible reactions were modified and disrupted by the enriched methylglyoxal. Eventually, the 'self-pollen' is rejected, and the papillae are degenerated (Sankaranarayanan et al., 2015).

In model plant *A. thaliana*, the acceptance of self-pollen by the stigma is attributed to the malfunction of self-incompatible genes *SCRs* and *SRKs* (Boggs et al., 2009). The *Brassica* pollen coat protein class B (PCP-B) are small cysteine-rich proteins (CRPs). Both PCP-Bs and SCRs are CRP proteins with eight conserved cysteines. However, it is shown that they belong to different small branches according to the phylogenetic analysis, and they are specialized for compatible pollination and self-incompatibility, respectively (Wang et al., 2017). In *A. thaliana*, defective pollen hydration and delay of tube growth are observed due to the disruption of genes for *PCP-Bs* (Wang et al., 2017). PCP-Bs serve as male factors for molecular dialogues of stigma—pollen to orchestrate pollen hydration, adhesion, and pollen tube growth (Wang et al., 2017). The reduction of reactive oxygen species (ROS) in papillar cells is closely correlated with the hydration and adhesion of pollen, especially at the adhesion sites (McInnis et al., 2006). When landed on the wild-type stigma, pollen from *pcp-bγ* and *pcp-bβ/γ* mutants showed markedly slow hydration because of severe suppression of the ROS reduction, in contrast to the response of wild-type pollen (Liu et al., 2021a). Wild-type stigmas treated with mature peptide PCP-Bγ exhibited a dose dependence on ROS reduction (Liu et al., 2021a). Fed with ROS inhibitor and ROS scavengers, the pistil with reduced ROS showed a significant acceleration of pollen hydration 10 minutes after pollination (Liu et al., 2021a).

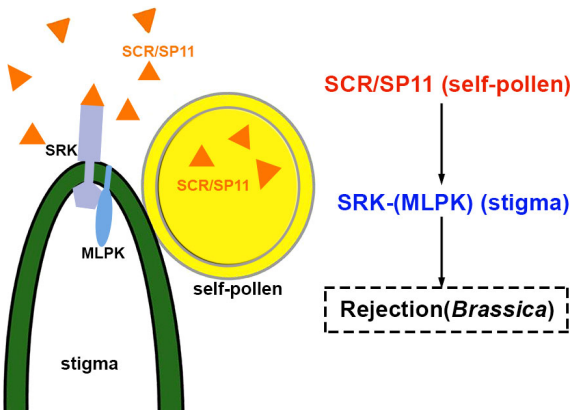

FIGURE 1
Schematic diagram of SCR/SP11 and SRK grouped for pollen-stigma interactions of *Brassica* self-incompatibility. The peptide triggering inhibition of signaling pathways is highlighted in red. The blue represents receptor complexes and the co-receptors are shown in parentheses. The source of peptides and receptors is shown in parentheses. Abbreviations for all small peptides and receptors are elucidated in the text.

The well-known receptor kinase FERONIA (FER) is expressed in various tissues and plays diverse essential roles (Escobar-Restrepo et al., 2007; Deslauriers and Larsen, 2010; Duan et al., 2010; Stegmann et al., 2017). In *Arabidopsis*, both receptor kinases ANJEA (ANJ) (Galindo-Trigo et al., 2020) and FER belong to *Catharanthus roseus* receptor-like kinase 1–like (CrRLK1L) family and are strongly expressed in stigma. The ANJ-FER receptor complexes act as essential female factors. They are involved in pollen—papilla communication by interacting with PCP-Bs for pollen hydration and germination (Liu et al., 2021a). When pollinated with wild-type pollen, rapid hydration phenotype was observed on the mutants pistil of *fer-4*, *anj-1*, and *fer-4 anj-1*, which was opposite to that of *pcp-bs* mutants. The phenotype was rescued in the complementation test (McInnis et al., 2006; Liu et al., 2021a).

The autocrine RALF23/33 peptides interact with the ECDs of FER and ANJ in stigma. Mutant *ralf33* showed a similar phenotype to *fer-4* and *anj-1* at reduced ROS accumulation in stigmatic papillae and accelerated pollen hydration (Liu et al., 2021a). LORELEI-like-GPI-anchored proteins (LLG)1, the co-receptor of FER-ANJ, is one of the members of the LORELEI (LRE) family (Feng et al., 2019). Loss of LLG1 function also resulted in reduced ROS accumulation in papillae. The guanine nucleotide exchange factors (GEFs) of Rho-like GTPases (RAC/ROP) and NADPH oxidases (RESPIRATORY BURST OXIDASE HOMOLOG D, RBOHD) act downstream of FER-ANJ-LLG1 to regulate ROS generation. Data from ROS-producing mutants suggested that autocrine RALF23/33 induces ROS generation through the ROP2-RBOHD pathway (Liu et al., 2021a).

The dissociation constants (K_d) of PCP-Bγ and RALF33 binding FER ectodomain (FERecd) were 0.34 μM and 0.1604 μM, respectively (Liu et al., 2021a). It means that RALF33 has a greater affinity for FERecd than PCP-Bγ does. However, the inhibition constant (K_i) that PCP-Bγ competed to bind FERecd in the mixture of RALF33-FERecd was 2.5099 μM (Liu et al., 2021a). It seems that the results are somewhat contradictory. Without compatible pollen, RALF23 and RALF33 are secreted from stigmatic papillary cells and facilitate ANJ-FER and its co-receptor LLG1 to form polymer complexes that stimulate ROP2 to trigger RBOHD activity, which leads to maintaining the high level of ROS in papillae before pollination. (Liu et al., 2021a; Kou et al., 2022). It was proposed that after the landing of compatible pollen grains on the stigma, the pollen coat protein PCP-Bs competed with and replaced RALF23/33 to interact with the

ANJ-FER receptor complexes in papilla cells. Consequently, the RALF23/33-initiated ROS signaling pathway was shut down. The ROS decreased rapidly in papillae to promote the hydration and germination of pollen grains. The maintenance of ROS content in papillar cells might be regulated through distinct signaling pathways stimulated by autocrine and paracrine peptides. The model is shown in Figure 2. These speculations need to be supported and verified by further experimental data.

Coincidentally, ligands exchange also occurs in the process of pollen growth and germination in tomato. The signaling pathway is triggered by receptor kinases at the pollen surface but not from female tissue. In *Solanum Lycopersicum*, cysteine-rich late-anther tomato 52 (LAT52), the male player, interacts with pollen-specific receptor kinase 2 (LePRK2) and prevents pollen from germination before pollination (Tang et al., 2002; Johnson and Preuss, 2003). After germination, another cysteine-rich peptide, stigma-specific protein 1 (LeSTIG1), is secreted and matured to a 7-kD peptide as the female player. LeSTIG1 accumulates on the pollen tube surface and binds the LePRK1/2 receptor complexes to promote pollen tube growth (Tang et al., 2004; Zhang et al., 2008; Huang et al., 2014). The ligand of the LePRK1/2 complexes, LAT52, is substituted by LeSTIG1. The signals could be switched from repression to activation of germination and tube growth, as shown in Figure 2 (Tang et al., 2004). LeSTIG1-LePRK2 orchestrates ROS levels through phosphatidylinositol 3-phosphate PI(3)P signaling to promote pollen tube growth (Huang et al., 2014). The Kinase partner protein (KPP) of *S. lycopersicum* is a Rop-GEF that interacts with the cytoplasmic kinase domains of LePRK1 and LePRK2 through its C-terminus. It recruits Actin-Related Protein 2/3 (ARP2/3, actin nucleators) complexes to the membrane of the pollen tube tip and coordinates actin and cytoskeleton to enhance tube growth (Huang et al., 2014; Liu et al., 2020). It may also be in an essential manner through which tomato LeSTIG1 regulates the growth of pollen tubes in the transmitting tract. It is required to investigate whether LeSTIG1 is strongly expressed and localized in the stylar transmitting tract.

Pollen tubes grow in the transmitting tract

In *Rosaceae*'s Gametophytic Self-Incompatibility (GSI) pollination, the pollen germinates and grows on the stigma. The growth of pollen tube arrests at one-third distance through the stylar transmitting tract (Franklin-Tong and Franklin, 2003). The GSI of *Rosaceae* is jointly regulated by the products of *S* locus, *S*-RNase of pistil determinants and *S*-haplotype specific F-box proteins/*S* locus F-box brothers (SFB/SFBB) of pollen

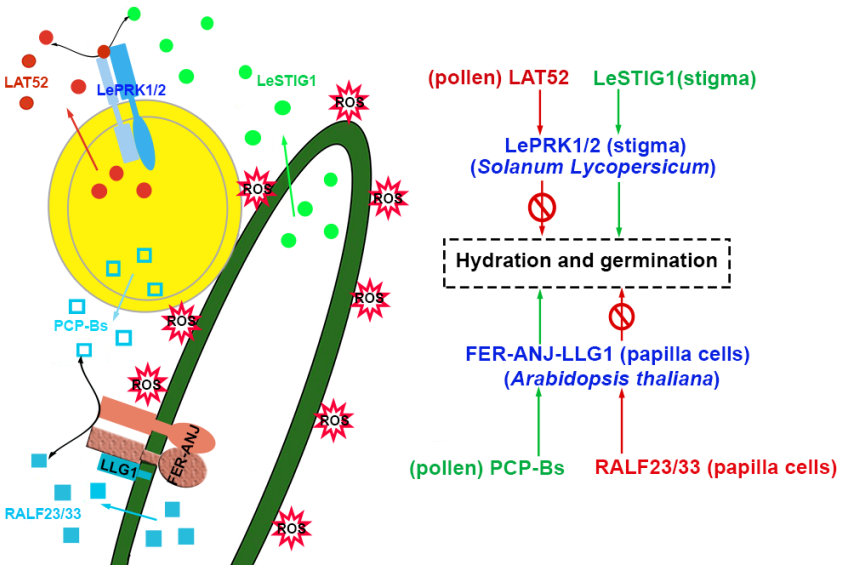

FIGURE 2
Pollen and stigma recognize each other to initiate the hydration and germination of pollen. In *Solanum Lycopersicum*, LAT52 interacts with LePRK1/2 to inhibit hydration and germination, and LeSTIG1 interacts with LePRK1/2 to facilitate hydration and germination. However, in *Arabidopsis*, pollen-specific PCP-Bs bind to FER/ANJ-LLG1 to promote hydration and germination, and stigmatic RALF23/33 interacts with FER/ANJ-LLG1 to maintain ROS accumulation and repress hydration of pollen. The peptides involved in the activation and inhibition of signaling pathways are highlighted in green and red, respectively. The receptor complexes are marked in blue and the co-receptors are shown in parentheses. The source of peptides and receptors is shown in parentheses. Abbreviations for all small peptides and receptors are elucidated in the text.

determinant (Sassa, 2016; Sun et al., 2018; Matsumoto and Tao, 2019). In the transmitting tract, pistil *S*-RNases penetrate the pollen tube to interact with the male determinants. Pollen SFB/SFBB recognizes each a subset of non-self *S*-RNases, ubiquitinates them, and mediates their degradation by 26S proteasome (Entani et al., 2014). Self-*S*-RNase disrupted tip-localized ROS and decreased the Ca^{2+} current, inducing nuclear DNA degradation and pollen tube disintegration (Wang and Kao, 2012; Del Duca et al., 2019).

The compatible pollen germinates, penetrates the papillae (Iwano et al., 2014), and continues to grow through the transmitting tract. The pollen tubes elongate considerably in style, and their integrity is maintained to prevent premature rupture. There are at least two signaling networks for the integrity of the pollen tube in the transmitting tract and the burst upon arrival at its destination.

RALF is a class of small peptide ligands widely known in various signaling pathways. The pollen tube-specific tomato (*S. lycopersicum*) RALF (SlPRALF) small peptides are responsible for pollen tube growth in different developmental windows (Covey et al., 2010). Eight pollen specifically expressed RALFs are clustered into three phylogenetic clades among the 37 RALFs in *A. thaliana*. RALF4 and RALF19 are grouped into one clade. The pollen tube of the homozygous and pollen-specific-promoter-*amiRRALF4/19* transgenic plants fails to grow in the transmitting tract and cannot reach the ovule *in vivo* (Mecchia et al., 2017). Nearly 70% of pollen tubes from the *amiRRALF4/19* plants burst *in vitro* germination of pollen tube assay (Mecchia et al., 2017). In the *ralf4-1*mutant, fertilization could occur, but 47% of pollen tubes burst *in vitro* germination (Mecchia et al., 2017). It is suggested that RALF4/19 plays a crucial and redundant role for pollen tube integrity and growth. Disruption of ANXUR1(ANX) and ANXUR2, the closest members to FERONIA in the CrRLK1L subfamily, phenocopies *amiRRALF4/19* lines in pollen tube dehiscence and elongation repression (Boisson-Dernier et al., 2009; Miyazaki et al., 2009). The rupture of tubes in *amiRRALF4/19* cannot be rescued with overexpression of *ANX1/2* (Mecchia et al., 2017). It is indicated that ANX1/2 is the downstream receptor of RALFs, which might coordinate other components to regulate tube integrity.

Meanwhile, Mecchia et al., 2017 found that premature tube rupture resulted from the repression of pollen-specific ANX1 and ANX2 *in vitro* germination assay. A similar phenotype was also observed when *BUDDHA'S PAPER SEAL (BUPS) 1/2* was knocked out (Ge et al., 2017). The T-DNA or knock-down mutant of *bups1* showed apical rupture after exiting the style and cessation of growth at the apex of the transmission tract (Ge et al., 2017). It is demonstrated that the mutants failed to maintain the integrity of the pollen tube. BUPS1 is involved in the perception and response to mechanical stress when tubes pass through style. It is suggested that BUPS1 activates ROP1 GTPase signals directly to promote exocytosis that accelerates BUPS1-dependent secretion of RALF4 (Ge et al., 2019; Kou et al., 2022). RALF4, acting as a cognate ligand for BUPS1, activates BUPS1 to amplify signaling and strengthen the rigidification of the cell wall (Zhou et al., 2021). It is proposed that these four receptor kinases are involved in maintaining pollen tube integrity in *Arabidopsis*.

The pollen-tube-expressed glycosylphosphatidylinositol-anchored proteins (GPI-APs), LORELEI-like-GPI-anchored protein 2/3 (LLG2/3), are engaged in maintaining tube integrity. Early rupture of pollen tubes and severe fertility defects result from *LLG2/3* disruption (Ge et al., 2019). LLG2/3 interacts with the extracellular domains of BUPS1/2 and ANX1/2 *in vitro* pull-down assay, and the interaction is enhanced by RALF4/19 (Ge et al., 2019). It is suggested that LLG2 and LLG3 act as co-receptors of the BUPSs/ANXs to regulate pollen tube integrity. RALF4 interacts with LLG3 and BUPSs/ANXs *via* different N-terminal domains. The N-terminal YISY motif of RALF4 is independent of the interaction but responsible for pollen tube integrity (Ge et al., 2019). It means that other proteins or receptors may interact with the N-terminal YISY domain of RALF4, which plays an essential role in pollen tube integrity in *Arabidopsis*.

LRX (LEUCINE-RICH REPEAT EXTENSIN) is the partner of RALFs in tomato. The pollen-specific LRX8/9/10/11 regulates the integrity of pollen tubes in *Arabidopsis* (Mecchia et al., 2017; Fabrice et al., 2018). LRXs play critical roles in maintaining cell wall rigidity during pollen tube growth and play essential roles in physical links between the intra- and extracellular components. The *lrx* multiple mutants showed premature rupture of pollen tubes and sterility to different extents (Mecchia et al., 2017). This phenotype was similar to that of mutants with the disruption of *BUPSs* and *ANXs*, and could not respond to the RALF4-triggered pollen tube growth. LRXs are linked through disulfide bonds to form dimers, and their N-terminal region physically interacts with RALF4 (Mecchia et al., 2017; Fabrice et al., 2018). RALF4/19 directly interacted with ANX1/2-BUPS1/2 to orchestrate the growth and integrity of pollen tubes (Ge et al., 2017). In addition, the N-terminal domains of LRX1/2/4/5 were discovered to interact with FER in vegetative tissues physically (Herger et al., 2020). It is very significant to explore whether LRX8/9/10/11 interacts with the ANX1/2-BUPS1/2 complexes in maintaining the integrity of pollen tubes. It is unknown whether LRXs interact with RALF4 through the N-terminal YISY motif of RALF4.

The coordination between RALF4-LRX8 and RALF4/19-ANX1/2-BUPS1/2 was identified *via* the downstream factors of the signaling cascade. The *mri-3D* was obtained in the *anx1anx2* mutagenesis screening for repression of pollen tube rupture (Boisson-Dernier et al., 2015). Due to the R240C nonsynonymous replacement in the kinase activation loop of MARIS (MRI) resulting in excessive kinase activity, *mri-3D* showed the opposite phenotype. MRI is a member of the receptor-like cytoplasmic kinases (RLCKs) localized at the

plasma membrane. MRI functions as the downstream player of ANX1/ANX2 to maintain the integrity of pollen tubes (Boisson-Dernier et al., 2015). ANX1/2 acts upstream of NADPH oxidase (RESPIRATORY BURST OXIDASE HOMOLOG H/J, RBOHH/RBOHJ) of the pollen tube membrane and affects the matrix exocytosis of cell wall for the tube integrity. NADPH oxidase generates tip-accumulated ROS to maintain the calcium gradient at the apex, ultimately regulating the growth and integrity of pollen tubes (Boisson-Dernier et al., 2013). MRI^{R240C} displayed hyperactive and could partially rescue the phenotype of pollen tubes burst of *anx1anx2* (Boisson-Dernier et al., 2015). It is proposed that MRI might function downstream of RBOHH/J. It is shown that both ANX1 and MRI cannot rescue the rupture of pollen tubes of *amiRRALF4/19* when ANX1-YFP and MRI-YFP are exclusively expressed in pollen tubes (Mecchia et al., 2017). Therefore, it is proved that two parallel signaling pathways are activated by the cysteine-rich peptides RALF4/19 that are secreted by pollen tubes.

The protein phosphatase ATUNIS1/2 (AUN1/2) is discovered to act downstream of ANX1/2 *via* screening for suppression to untimely rupture of the *anx1anx2* pollen tube (Franck et al., 2018b). However, it is the activity of $AUN1^{D94N}$, but not the expression of MRI^{R240C}, sufficient to attenuate male sterility and pollen burst phenotype in *lrx8-11* quadruple mutants (Franck et al., 2018b). It is suggested that AUN1/2 phosphatases may equilibrate MRI kinase activity and regulate the phosphorylation status of target substrates for the growth and integrity of the tubes (Vogler et al., 2019).

Therefore, the integrity of pollen tubes is regulated jointly by parallel pathways, RALF4/19-LRX8/9/10/11-AUN1/2 and RALF4/19-ANXs/BUPSs-MRI signaling pathway, as shown in Figure 3. The phosphorylation status of downstream substrates is equilibrated and maintained by negative regulator AUN1/2 *via* the RALF4/19-LRX8/9/10/11-AUN1/2 signaling pathway. The positive effector MRI facilitates the phosphorylation of downstream targets by RALF4/19-ANXs/BUPSs-MRI pathway (Ge et al., 2017; Mecchia et al., 2017). However, RALF4/19 is allocated by an unknown mechanism. As mentioned previously, BUPS1-activated ROP1 promotes BUPS1-dependent secretion of RALF4. It was suggested that RALF4/19 triggered ANX1/2-BUPS1/2-MRI, and activated the kinase activity of MRI. Simultaneously, RALF4/19 activated LRX8/9/10/11-AUX1/2 signaling pathway, exerting the phosphatase activity of AUX1/2 to balance MRI kinase activity. These two pathways jointly coordinated and regulated tube growth and integrity.

It is suggested that the abundant extracellular matrix protein, arabinogalactan protein AGP is involved in tube elongation in the transmitting tract (Leszczuk et al., 2019). AGP is a hydroxyproline-rich glycoprotein that can adhere to the surface of the pollen tube. AGP can be integrated into the cell wall matrix of the pollen tubes and decrease after hydrolyzation by deglycosylase (Coimbra et al., 2008; Jia et al., 2015). Continuous adhesion and integration of AGP are necessary to promote tube elongation. The slow growth of pollen tubes resulted from decreased AGPs in the surface of pollen tubes from *Arabidopsis agp6 agp11* mutants (Levitin et al., 2008; Costa et al., 2013). In addition, the growth and elongation of pollen tubes are also associated with the glutamate-derived signaling molecule GABA (Ramesh et al., 2015). Low-concentration GABA stimulates pollen tube growth *in vitro*; however, gradually increasing GABA is required for tube guidance in the transmission tract (Ma, 2003; Palanivelu et al., 2003). The role of AGP and GABA, especially AGP, as physiological signals still needs to be determined.

Pollen tube guidance and polytubey block

Chemoattractants emitted by the ovule (especially synergids) direct the growth of the pollen tube along the funiculus towards the micropyle. In *Torenia fournieri* (*Linden. ex Fourn*), four cells in a mature embryo sac, including a central cell, an egg cell, and two synergid cells, were ablated individually or in groups. The capability of pollen tube attraction is lost in the ovule with two ablated synergids (Higashiyama et al., 2001). It indicates that the synergid cell produces signals to attract the pollen tube growth toward the ovule. The synergid cells from *T. fournieri* were isolated and studied to identify the chemoattractant. A class of small cysteine-rich defensin-like peptides, abundantly and predominantly expressed in synergid cells, were determined. Mature peptides of LUREs (LURE1 and LURE2) produced in *E. coli* showed guiding activity for pollen tube targeting *in vitro* assay for pollen tube attraction (Okuda et al., 2009). AtLURE1 peptides were secreted merely from synergid cells and diffused along the funicular surface, guiding the growth of pollen tubes to micropyle (Takeuchi and Higashiyama, 2012). The AtLURE1s' variants were inefficient in reorienting the pollen tube under the semi-*in vivo* pollen tube attraction assay (Zhong et al., 2019). Mutants of 23 pollen-specific receptor kinases were used to study the attraction capability of the AtLURE1s peptide. Pollen tubes from *prk6* ignored attractants and could not be redirected toward AtLRUE1.2 (Takeuchi and Higashiyama, 2016). PRK6 served as a vital receptor for AtLURE1 signals *in vitro* attraction assay. PRK6-mRuby2 was asymmetrically localized at the surface of pollen tubes, with the attraction of AtLURE1.2. It was suggested that PRK6 acted as the male player to sense AtLURE1s signaling from synergid cells to guide pollen tube growth toward the micropyle (Takeuchi and Higashiyama, 2016).

Lost in Pollen tube guidance 1 and 2 (LIP1 and LIP2) are cytoplasmic receptor kinases localized at the membrane of tube tips through palmitoylation at the N-terminal cysteine site. *In vivo*, 46% of *lip1 lip2* pollen tubes showed guidance defects to the micropyle. The transmitting effciency of male gametes was 43% in *lip1 lip2*. Thirty percent of *lip1 lip2* pollen tubes were

insensitive to the female attractant AtLURE1.2 *in vitro* attraction assay, although 95% of the wild-type pollen tubes were attracted (Liu et al., 2013). LIP1/2 interacted with tip-localized PRK6 and was involved in response to the AtLURE1s (Liu et al., 2013). It was demonstrated that LIP1 and LIP2 were not necessary components of the PRK6 receptor complexes in micropylar guidance signaling pathways (Liu et al., 2013; Takeuchi and Higashiyama, 2016).

Wang et al. reported that LUREs specifically interacted with the ECDs of three receptor kinases, MALE DISCOVERER1 (MDIS1), MDIS1-INTERACTING RECEPTORS LIKE KINASE1 (MIK1), and MIK2, to attract pollen tubes in a self-favorite way (Wang et al., 2016). PRK6 contains six LRRs in its ectodomain to form a solenoid structure. AtLURE1s, which act as female participants of pollen tube guidance, bind directly to the juxta-membrane region of PRK6, despite the extracellular LRR domains that interact specifically with ligands (Takeuchi and Higashiyama, 2016). It was proposed that other ligands might interact with the LRR domain of PRK6 to initiate pollen tube guidance. In addition to PRK6, MDIS1/MIK1/MIK2 acted as other receptors for AtLURE1s.

LUREs' attraction to pollen tubes was based on conspecific preferential principles so that the interspecific genetic isolation and maintaining of species specificity are promoted. Recombinant AtLURE1.3 peptides preferentially attracted *A. thaliana* but not *A. lyrata* pollen tubes *in vitro* (Takeuchi and Higashiyama, 2012; Zhong et al., 2019). Consistently, AtLURE1 expressed in *T. fournieri* synergids fascinated *A.thaliana* pollen tubes to *T. fournieri* ovule (Takeuchi and Higashiyama, 2012). It is suggested that LURE1s are species-specific pollen attractants for interspecies specificity and reproductive isolation. It implies that additional and common pollen-tube attractants might be released from ovules.

In addition, loss-of-function *atlure1* septuple mutant and null *prk6* showed natural fertility (Zhong et al., 2019). The *A. lyrata* pollen tubes were attracted to pass through the septum to the micropyles of ovules in null *atlure1* pistil. It is proposed that general genus attractants are present in *atlure1* ovules. The XIUQIUs, a close relative of AtLURE1 in *Brassicaceae*, are small cysteine-rich peptides secreted from synergid cells to accumulate near the filiform apparatus. The recombinant XIUQIUs indiscriminately attract the pollen tubes of *A.thaliana* and *A. lyrata* under semi-*in vivo* assay for pollen tube attraction (Zhong et al., 2019). XIUQIUs take roles as female players, and their pollen tube-localized receptors still need to be identified. Compared with non-species-specific XIUQIUs, AtLURE1s-PRK6 and AtLURE1s-MDIS1/MIK1/MIK2 control conspecific pollen tube-preferred signaling pathways at septum and micropyle, as shown in Figure 4 (Liu et al., 2021b).

Besides XIUQIUs and LUREs, there are 73 other CRP proteins expressed exclusively in synergid cells of *Arabidopsis*, and the roles of these CRPs are still unknown (Takeuchi and Higashiyama, 2012). The mutants showed an abortion rate of 20% in the seed sets after the knockout of all clade genes (CRP810), including XIUQIUs and LUREs (Liu et al., 2021b).

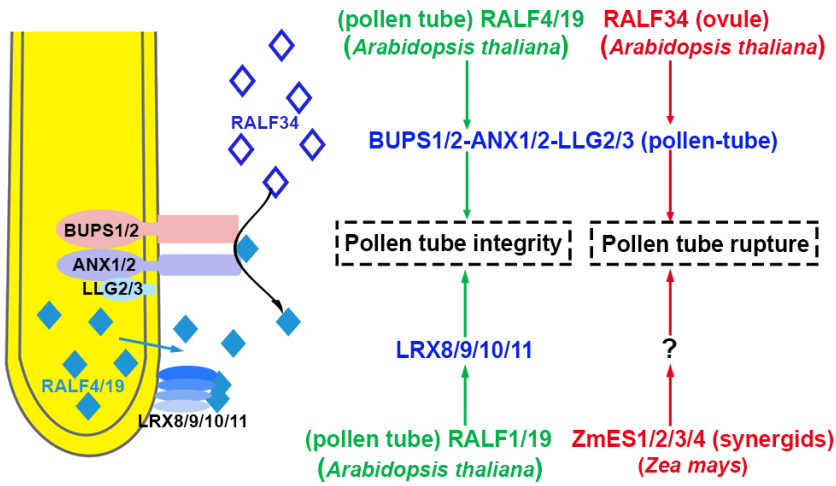

FIGURE 3
The integrity of pollen tube growth is maintained, and pollen tubes rupture In *Arabidopsis thaliana*, pollen-specific RALF4/19 orchestrates pollen tube receptor complexes BUPS1/2-ANX1/2-LLG2/3 and LRX8/9/10/11 to maintain pollen tube growth and integrity in the transmitting tract. After the pollen tube enters the ovule, the ovule-specific RALF34 interacts with BUPS1/2-ANX1/2-LLG2/3, resulting in pollen tube rupture. In *Zea Mays*, ZmES1/2/3/4 secreted from synergid cells causes pollen tube rupture. The peptides involved in the activation and inhibition of signaling pathways are highlighted in green and red, respectively. The blue represents receptor complexes and the co-receptors are shown in parentheses. Question marks indicate unidentified signal components. The source of peptides and receptors is shown in parentheses. Abbreviations for all small peptides and receptors are elucidated in the text.

It is suggested that attraction for the oriented growth of pollen tubes is lost incompletely. It indicates that there must be additional attractants of pollen tubes in synergids or other female gametophytic cells (Hater et al., 2020).

For instance, the capability of pollen tubes for chemotropic response to LURE is induced and enhanced by methyl-glucuronosyl arabinogalactan (AMOR) in *T. fournieri* ovules (Mizukami et al., 2016). As tube guiding attractants in maize, ZmEA1 is exclusively expressed in the egg apparatus, subsequently diffused toward the filiform apparatus, and finally localized at the nucellar cell wall below the micropylar end (Marton et al., 2005; Marton et al., 2012). The pollen tube-specific cognate receptor for the ZmEA1 has yet to be discovered. Coincidentally, the glycoproteins secreted into the obturator pore of the apple embryo sac were reported to direct the pollen tube toward the ovule (*Malus* × *domestica*) (Losada and Herrero, 2017).

Polytubey block occurs at the micropyle and the pistil's septum. It is indispensable to ensure that only one conspecific pollen tube passes through the septum and grows along the funiculus to target the micropyle. GENERATIVE CELL SPECIFIC 1 (GCS1)/HAPLESS 2 (HAP2) is specifically expressed in sperm cells and plays a vital role in membrane fusion during double fertilization (Mori et al., 2006; von Besser et al., 2006). In null *hap2*, the double fertilization failure resulted from impaired membrane fusion. However, fertilization recovery is successful when the second pollen tube comes 7 hours after pollination. However, multiple pollen tubes crossed out of the septum for fertilization recovery since the polytubey block was disrupted in mutants. RNA-seq data from the transmission tract and septum of the pistil indicated that FER, ANJEA (ANJ), and HERCULES RECEPTOR KINASE 1 (HERK1), malectin-like domain-containing receptor-like kinase (MLD-RLK) (also known as *C. roseus* RLK1-LIKE or CrRLK1L), were highly expressed. Multiple pollen tubes grew along the funiculus 5 hrs after pollination in the pistils of *fer-4*, *anj herk1*, or *fer anj herk1* (Zhong et al., 2022). These three CrRLK1L receptor kinases functioned as female players to communicate with pollen tube signals. In pollen-specific MYB mutants, *myb97myb101myb120*, the polytubey phenotype similar to the three null receptors was identified. The expression profiling data demonstrated that five *RALFs* (*RALF6*, *RALF7*, *RALF16*, *RALF36*, and *RALF 37*) were downregulated. Mutants of multiple combinations of *RALFs* knockout exhibited polytubey when pollinated to wild-type pistil. It is indicated that five RALFs (pollen tube-specific RALF6/7/16/36/37 peptides) function as ligands to be perceived and interact with the FER-ANJ-HERK1 receptor complexes (Zhong et al., 2022). It was speculated that a polyspermy block might be established through RALFs-FER/ANJ/HERK1 at the septum until tubes burst in the ovule after the removal of RALFs signaling as shown in Figures 4, 5. Polyspermy block initiated upon the exit of pollen tubes from the septum and ended up at the vanishing of RALFs signaling after tube discharge. The mechanisms underlying polytubey block might play roles in the recognition between pollen tubes and synergids. The particular block should be precisely restricted in an appropriate spatial and temporal window. If fertilization fails, the persisting synergid cell would be responsible for secreting signals to attract additional pollen tubes for fertilization recovery.

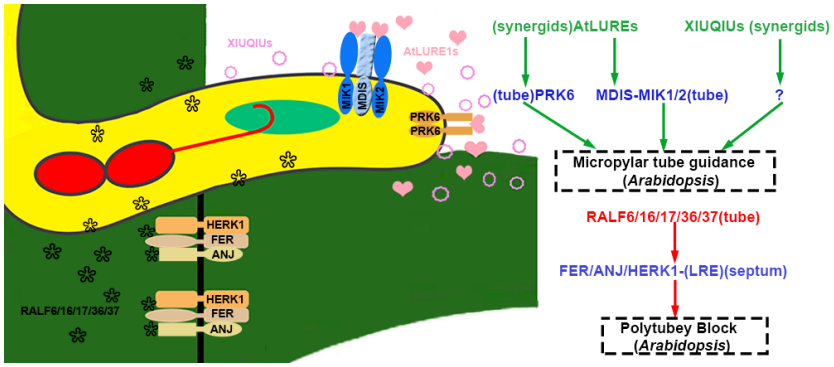

FIGURE 4
The micropyle guidance and polytubey block of pollen tubes. In *Arabidopsis thaliana*, pollen tubes penetrate the septum, and the RALF6/16/17/36/37 secreted by the pollen tube interacts with the septum-specific FER/ANJ/HERK1 to initiate the polytubey block. XIUQIUs and AtLURE1s secreted by synergid cells diffuse along the funiculus. AtLURE1s interact with PRK6 and/or MIK1/2-MDIS of the pollen tube to guide the pollen tube to grow towards the micropyle. The peptides are highlighted in green and red to represent activation or suppression, respectively. The blue represents receptor complexes and the co-receptors are shown in parentheses. Question marks indicate unidentified signal components. The source of peptides and receptors is shown in parentheses. Abbreviations for all small peptides and receptors are elucidated in the text.

Discharge of sperm cells from pollen tubes

After arrival at the micropyle, the pollen tube is recognized by one of the two synergid cells, and the following communication occurs. Subsequently, the synergid cell undergoes programmed cell death, and the tube bursts to release two sperm cells. Two sperms fuse with two female gametes to form a zygote and primary endosperm, respectively. The persistent synergid cell undergoes degeneration and nourishes primary endosperm, preventing the attraction of excessive pollen tubes. Pollen tube reception and growth termination are tightly controlled by cell-cell communication between pollen tubes and synergid cells. The rupture of pollen tubes is also elaborately regulated through molecular communication of signals from the inner integuments and pollen tubes.

In *fer*, two or more pollen tubes enter a single ovule. It is demonstrated that the *fer* female gametophyte keeps attracting more tubes to enter the same ovule after the reception of the first tube. The polyspermy block mechanism is ineffective in *fer* (Pereira et al., 2016b). FER is localized at the membrane of the filiform apparatus and functions as receptor kinase to sense peptide signals in cell-cell communication. FER participates in receiving the first pollen tube and hinders extra tubes from polytubey and polyspermy (Huck et al., 2003; Escobar-Restrepo et al., 2007). The overgrowth of pollen tubes occurs when the A.thaliana fer is pollinated with pollen from A. lyrata or C. flexuosa (Escobar-Restrepo et al., 2007). It is suggested that FER plays an essential role in receiving signals from conspecific pollen tubes to maintain reproductive barriers.

HERK1 and ANJ are homologs of FER and localized in the filiform apparatus of the synergids. In *anj herk1*, a similar phenotype of tube overgrowth and failure of fertilization was identified, indicating that HERK1 and ANJ were functionally redundant regulators for pollen tube reception. (Galindo-Trigo et al., 2020). In *fer anj herk1*, pollen tubes were not able to be recognized and overgrown at the surface of the ovule, resulting in various rates of seed set abortion (Zhong et al., 2022). It was concluded that HERK1 and ANJ, as well as FER, served as the female participants for pollen tube reception and took roles in polytubey block at the micropyle. As pollen from different *ralfs* (*ralf36 ralf37, and ralf6 ralf7 ralf16 ralf36 ralf37*) were pollinated to the stigma of wild type, the phenotype of pollen tube overgrowth and seed set abortion were more severe as the increase of the disrupted RALFs. The phenotype was similar to that of *fer anj herk1* (Zhong et al., 2022). The data were consistent with the physical interaction of RALFs with FER-ANJ-HERK1 in an *in vitro* pull-down assay.

The co-receptor LORELEI (LRE) is involved in the interaction between RALF6/7/16/36/37 and FER-ANJ-HERK1. FER-ANJ-HERK1 received pollen tube signals at the micropyle, leading to polar accumulation of the downstream NORTIA (MLO protein) at filiform apparatus. Conversely, NORTIA promotes the perception of pollen tubes to ensure the polytubey block for double fertilization (Ju et al., 2021).

Now it is known that mechanisms underlying the recognition of pollen tubes at the septum and filiform apparatus are triggered by the above players coordinately. RALFs and FER-ANJ-HERK1 take critical roles in the reception of pollen tubes at the filiform apparatus of synergids and act as the second tier of the polytubey barrier as shown in Figures 4, 5 (Zhong et al., 2022). Once the pollen tube rupture in the ovule, the RALFs derived from tubes are diluted and diffuse into embryo sac. The interaction between RALFs and FER-ANJ-HERK1 receptor complexes is disrupted, so the polytubey barrier controlled by RALFs-FER/ANJ/HERK1 is removed at the septum and micropyle.

RNAi knock-down of *ZmES4* or *in vitro* treatment with ZmES4 (Zea mays Embryo Sac), the polymorphic defensin-like cysteine-rich protein from maize, induced tube rupture to release sperm cells in a species-preferred manner, as presented in Figure 5 (Amien et al., 2010). ZmES4 is accumulated in vesicles of mature synergid cells and released upon the arrival of pollen tubes. The subsequent interaction between ZmES4 and KZM1(K^+ channel Zea mays 1) leads to channel opening, K^+ influxion, plasma membrane depolarization, water uptake, and eventual osmotic pollen tube burst (Cordts et al., 2001; Philippar et al., 2003; Amien et al., 2010).

It was speculated that the pollen tube entered the degenerated synergid cell and continued to grow and release sperm cells at the cleft between the egg and central cell. Another class of ligands should shut down the signaling pathways mentioned above for pollen tube integrity and growth. Pollen-tube localized receptors ANX1/2-BUPS1/2 would perceive RALF4/19 peptides secreted from pollen to regulate the tube growth integrity (Ge et al., 2017; Mecchia et al., 2017). However, an antagonistic signal would be required to disengage signaling pathways triggered by RALF4/19-ANX1/2-BUPS1/2 in ovules. This signal for the rupture of pollen tubes might be derived from the female tissue and received by receptors on the pollen tubes.

In contrast to RALF4, required for maintaining pollen tube integrity, a low concentration (2nM) of RALF34 caused the rupture of 23% of pollen tubes, and almost 70% of tubes are ruptured when treated with 20 mM RALF34 (Ge et al., 2017). Before fertilization, RALF34 accumulates in the ovule, especially in the inner integument. After the pollen tube's arrival, it diffuses toward the micropyle/synergid cell region. The *ralf34* mutant did not display fertility defects, suggesting that other RALFs in female reproductive tissue are involved in the burst of pollen tubes and release of sperm cells (Ge et al., 2017). RALF34 binds the ECD of ANX1/2 and BUPS1/2 by competing with RALF4/19. The interaction between RALF34 and ANX1/2-BUPS1/2 shut off RALF4/19 signaling pathways for the maintenance of tube integrity. The model is shown in Figure 5. The pollen tube releases sperm cells subsequently (Ge et al., 2017). The same

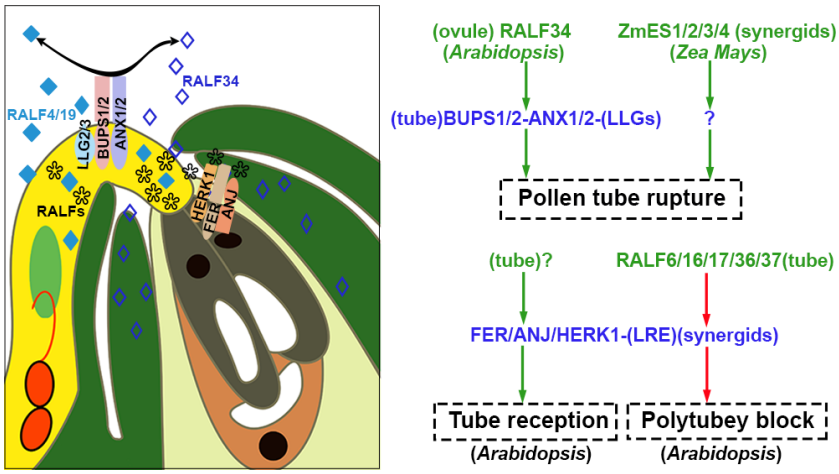

FIGURE 5
Pollen tube is received, polytubey block, and rupture. At the micropyle, FER/ANJ/HERK1-LLG1 derived from synergid cells is involved in the recognition and reception of pollen tube; they also interact with tube-specific RALF6/16/17/36/37 to cause polytubey block. After the pollen tube enters the ovule, the interaction between ovule-specific RALF34 and BUPS1/2-ANX1/2-LLGs of the pollen tube results in the rupture of the tube in *Arabidopsis*. ZmES1/2/3/4 secreted by synergids is related to the rupture of the pollen tube in *Zea Mays*. The peptides are highlighted in green and red to represent activation or suppression, respectively. The receptor complexes are marked in blue and the co-receptors are shown in parentheses. Question marks indicate unidentified signal components. The source of peptides and receptors is shown in parentheses. Abbreviations for all small peptides and receptors are elucidated in the text.

receptor complexes realize different biological processes by simply substituting the autocrine signal with the paracrine signal in the different spatiotemporal windows.

Gamete fusion and double fertilization

Two sperm cells released from the pollen tube are activated. Plasma membrane adhesion and nuclear fusion of male and female gametes occur consequently. In the process mentioned above, the cysteine-rich peptide EC1 (Egg cell 1) secreted by the egg cell plays an important role (Sprunck et al., 2012). Sprunck et al., 2012 found that EC1 is accumulated and constrained in spherical vesicle-like structures within unfertilized egg cells by observation of EC1-GFP fusion. During double fertilization, once sperm cells arrive, EC1 is detected outside the egg cell, especially in the apical region of the degenerated synergid (Sprunck et al., 2012), where gametes fusion occurs (Hamamura et al., 2012). It was shown quantitatively that the intensity of GFP signal gradually increased toward the egg cell membrane during the interaction and fusion of gametes. There are five EC1-encoding genes in *Arabidopsis* that are specifically expressed in egg cells. The recognition receptors in sperm cells or tubes are unknown. However, under the action of EC1, the potential viral-like Fusogen (HAP2/GCS1 that is related in structure to certain viral fusogens to promote the fusion of gamete cell membranes), was redistributed to the surface of sperm cells to regulate their adhesion and separation. (Sprunck et al., 2012; Cyprys et al., 2019). Gamete membrane fusion is promoted by sperm cell-specific expression of DUF679 membrane proteins, DMP8 and DMP9 (Takahashi et al., 2018; Cyprys et al., 2019).

Multiple pollen tubes are directed into one ovule for fertilization compensation in *hap2*$^{-/-}$, a mutant with gamete fusion disorder (Mori et al., 2006; von Besser et al., 2006; Zhong et al., 2022). However, polyspermy block initiates rapidly after the completion of double fertilization. It is correlated with the clearance or degradation of pollen tube attractants and programmed cell death of the synergids. To prevent the attraction to excessive pollen tubes, the persistent synergid fused with primary endosperm is selectively disorganized during endosperm proliferation. The attractants pre-secreted are rapidly diluted and modified (Maruyama et al., 2015; Sprunck and Dresselhaus, 2015; Motomura et al., 2018). Ethylene signaling is activated by fertilization of egg and leads to nucleus disintegration of the synergid (Maruyama et al., 2015; Sprunck and Dresselhaus, 2015). In *Arabidopsis*, the ethylene-free mutants, knocked out five ethylene biosynthetic 1-aminocyclopropane-1-carboxylate oxidase (ACO) genes by CRISPR/Cas9 technology, were investigated (Li et al., 2022). It was indicated that specific components of ethylene signaling pathways, such as the transcription factors ethylene-insensitive 3 (EIN3) (Abozeid et al., 2017) and EIN3-LIKE 1 (EIL1) (Xiao et al., 2021), but not ethylene itself, are required for directing the death of persistent synergid (Li et al., 2022). It is necessary that the persistent synergid undergoes programmed cell death. It

seems that the egg and central cell control independent signaling pathways to eliminate the persistent synergid cell and prevent polytubey fertilization (Pereira et al., 2016a). The molecular mechanism is unclear.

The arrival of the first pollen tube at the ovule leads to nitric oxide accumulation in the filiform apparatus. The process depends on de-esterified pectin that is mediated and maintained by FER. Nitric oxide nitrosates the precursor and the mature forms of the attractant AtLURE1 to impede AtLURE1 secretion and interaction with its receptors, and inhibit additional pollen tubes from entering the ovule for polytubey block (Duan et al., 2020). In addition to nitrosation of chemoattractants, AtLURE1s are also digested by egg cell-specific peptidases. The aspartate endopeptidases, EGG CELL-SPECIFIC1/2 (ECS1/2), are expressed specifically in egg cells. The transcripts are degraded immediately after gamete fusion. Once fertilization is completed, ECS1 and ECS2 are secreted from the cortical network at the apical region of *Arabidopsis* egg cell into extracellular space or to the persistent synergid, where it cleaves exclusively and decomposes AtLURE1 (Yu et al., 2021b). The clearing mechanism of XIUQIUs has yet to be discovered. If double fertilization fails, pollen tube attractors will be secreted from the persistent synergid to attract the second pollen tube for fertilization.

Conclusion remarks

In flowering plants, the cell-cell communication and the signaling network dominated by ligands/receptors are most vividly manifested in the process of fertilization. However, many signal pathways governed by ligand-receptor are still unclear. (1) When the pollen tube grows in the transmitting tract, are there peptide signals secreted by female tissue for rapid tube elongation? How can the two distinct signaling pathways of ANX1/2-BUPS1/2 and LRXs be selected by RALF4/19 for regulating the growth and integrity of pollen tubes? (2) Which factors regulate RALF34 to ensure the timely replacement of RALF4/19 to induce pollen tube rupture at the appropriate spatiotemporal window? (3) The arrest of pollen tube growth and synergid burst resulted from recognition of RALF6/7/16/36/37 by the FER-ANJ-HERK1 receptor. Whether FER-ANJ-HERK1 receives ligand signals secreted by synergid to replace RALF6/7/16/36/37 derived from pollen tubes, triggers the rupture of synergid cells that received pollen tubes? (4) What are the cognate receptors of XIUQIUs during micropylar guidance for pollen tubes? Is there a class of highly conserved receptors that recognize XIUQIUs during their evolution? (5) The EC1 secreted by the egg cell directs the sperm cells to be released at the cleft between the egg and central cell, and promotes gamete fusion and double fertilization. So, does EC1 have a cognate receptor of sperm cells?

With further advances in study, more signaling pathways directly provoked during the plant reproductive process will be discovered and investigated. However, due to the functional redundancy and homology in the genome, it is not easy to identify the phenotype of mutation in a homologous gene. It is suggested that unexpected difficulties in discovering ligands and receptors may be inevitable. Significant progress has been made since the application of CRISPR-Cas9 technology in knocking out multiple homologous genes simultaneously, and obtaining relevant functional mutants is greatly favored as a consequence. It is imperative to develop technologies for high-throughput protein expression and localization. It is expected to integrate high-throughput protein localization and efficient CRISPR-Cas9 knockout technology to leverage forward genetics and elucidate the molecular mechanism of functionally redundant receptor kinases and small peptide ligands in the future. Undoubtedly, the network for cell-cell communication will be dissected with the aid of the coming biotechnologies and ideas.

Author contributions

C-XX, W-JL, and BW performed the literature search and data analysis. C-XX and T-YY prepared the figure. T-YY drafted and revised the manuscript. All authors contributed to the article and approved the submitted version.

Funding

This work was supported by the National Natural Science Foundation of China (31871450), the Natural Science Foundation of Shandong (ZR2022MC217), and the Yantai University Top Talent Project (2220011).

Acknowledgments

We appreciate Dr. Dongqiao Shi from the Institute of Genetics and Developmental Biology, Chinese Academy of Sciences for her kind advice and revision on the manuscript.

Conflict of interest

The authors declare that the research was conducted in the absence of any commercial or financial relationships that could be construed as a potential conflict of interest.

Publisher's note

References

Abozeid, A., Ying, Z., Lin, Y., Liu, J., Zhang, Z., and Tang, Z. (2017). Ethylene improves root system development under cadmium stress by modulating superoxide anion concentration in arabidopsis thaliana. *Front. Plant Sci.* 8. doi: 10.3389/fpls.2017.00253

Amien, S., Kliwer, I., Marton, M. L., Debener, T., Geiger, D., Becker, D., et al. (2010). Defensin-like ZmES4 mediates pollen tube burst in maize *via* opening of the potassium channel KZM1. *PloS Biol.* 8 (6), e1000388. doi: 10.1371/journal.pbio.1000388

Bleckmann, A., Alter, S., and Dresselhaus, T. (2014). The beginning of a seed: regulatory mechanisms of double fertilization. *Front. Plant Sci.* 5. doi: 10.3389/fpls.2014.00452

Boggs, N. A., Nasrallah, J. B., and Nasrallah, M. E. (2009). Independent s-locus mutations caused self-fertility in arabidopsis thaliana. *PloS Genet.* 5 (3), e1000426. doi: 10.1371/journal.pgen.1000426

Boisson-Dernier, A., Franck, C. M., Lituiev, D. S., and Grossniklaus, U. (2015). Receptor-like cytoplasmic kinase MARIS functions downstream of CrRLK1L-dependent signaling during tip growth. *Proc. Natl. Acad. Sci. U.S.A.* 112 (39), 12211–12216. doi: 10.1073/pnas.1512375112

Boisson-Dernier, A., Lituiev, D. S., Nestorova, A., Franck, C. M., Thirugnanarajah, S., and Grossniklaus, U. (2013). ANXUR receptor-like kinases coordinate cell wall integrity with growth at the pollen tube tip *via* NADPH oxidases. *PloS Biol.* 11 (11), e1001719–e1001719. doi: 10.1371/journal.pbio.1001719

Boisson-Dernier, A., Roy, S., Kritsas, K., Grobei, M., Jaciubek, M., Schroeder, J., et al. (2009). Disruption of the pollen-expressed FERONIA homologs ANXUR1 and ANXUR2 triggers pollen tube discharge. *Development* 136, 3279–3288. doi: 10.1242/dev.040071

Bower, M. S., Matias, D. D., Fernandes-Carvalho, E., Mazzurco, M., Gu, T., Rothstein, S. J., et al. (1996). Two members of the thioredoxin-h family interact with the kinase domain of a brassica s locus receptor kinase. *Plant Cell* 8 (9), 1641–1650. doi: 10.1105/tpc.8.9.1641

Chevalier, E., Loubert-Hudon, A., Zimmerman, E. L., and Matton, D. P. (2011). Cell-cell communication and signalling pathways within the ovule: From its inception to fertilization. *New Phytol.* 192 (1), 13–28. doi: 10.1111/j.1469-8137.2011.03836.x

Coimbra, S., Jones, B., and Pereira, L. G. (2008). Arabinogalactan proteins (AGPs) related to pollen tube guidance into the embryo sac in arabidopsis. *Plant Signal Behav.* 3 (7), 455–456. doi: 10.4161/psb.3.7.5601

Cordts, S., Bantin, J., Wittich, P. E., Kranz, E., Lorz, H., and Dresselhaus, T. (2001). ZmES genes encode peptides with structural homology to defensins and are specifically expressed in the female gametophyte of maize. *Plant J.* 25 (1), 103–114. doi: 10.1046/j.0960-7412.2000.00944.x

Costa, M., Nobre, M. S., Becker, J. D., Masiero, S., Amorim, M. I., Pereira, L. G., et al. (2013). Expression-based and co-localization detection of arabinogalactan protein 6 and arabinogalactan protein 11 interactors in arabidopsis pollen and pollen tubes. *BMC Plant Biol.* 13, 7. doi: 10.1186/1471-2229-13-7

Covey, P. A., Subbaiah, C. C., Parsons, R. L., Pearce, G., Lay, F. T., Anderson, M. A., et al. (2010). A pollen-specific RALF from tomato that regulates pollen tube elongation. *Plant Physiol.* 153 (2), 703–715. doi: 10.1104/pp.110.155457

Cyprys, P., Lindemeier, M., and Sprunck, S. (2019). Gamete fusion is facilitated by two sperm cell-expressed DUF679 membrane proteins. *Nat. Plants* 5 (3), 253–257. doi: 10.1038/s41477-019-0382-3

Del Duca, S., Aloisi, I., Parrotta, L., and Cai, G. (2019). Cytoskeleton, transglutaminase and gametophytic self-incompatibility in the malinae (Rosaceae). *Int. J. Mol. Sci.* 20 (1), 209. doi: 10.3390/ijms20010209

Deslauriers, S. D., and Larsen, P. B. (2010). FERONIA is a key modulator of brassinosteroid and ethylene responsiveness in arabidopsis hypocotyls. *Mol. Plant* 3 (3), 626–640. doi: 10.1093/mp/ssq015

Dresselhaus, T., and Franklin-Tong, N. (2013). Male-Female crosstalk during pollen germination, tube growth and guidance, and double fertilization. *Mol. Plant* 6 (4), 1018–1036. doi: 10.1093/mp/sst061

Dresselhaus, T., Sprunck, S., and Wessel, G. M. (2016). Fertilization mechanisms in flowering plants. *Curr. Biol.* 26(3) R125–R139. doi: 10.1016/j.cub.2015.12.032

Duan, Q., Kita, D., Li, C., Cheung, A. Y., and Wu, H. M. (2010). FERONIA receptor-like kinase regulates RHO GTPase signaling of root hair development. *Proc. Natl. Acad. Sci. U.S.A.* 107 (41), 17821–17826. doi: 10.1073/pnas.1005366107

Duan, Q., Liu, M. J., Kita, D., Jordan, S. S., Yeh, F. J., Yvon, R., et al. (2020). FERONIA controls pectin- and nitric oxide-mediated male-female interaction. *Nature* 579 (7800), 561–566. doi: 10.1038/s41586-020-2106-2

Entani, T., Kubo, K., Isogai, S., Fukao, Y., Shirakawa, M., Isogai, A., et al. (2014). Ubiquitin-proteasome-mediated degradation of s-RNase in a solanaceous cross-compatibility reaction. *Plant J.* 78, 1014–1021. doi: 10.1111/tpj.12528

Escobar-Restrepo, J. M., Huck, N., Kessler, S., Gagliardini, V., Gheyselinck, J., Yang, W. C., et al. (2007). The FERONIA receptor-like kinase mediates male-female interactions during pollen tube reception. *Science* 317 (5838), 656–660. doi: 10.1126/science.1143562

Fabrice, T. N., Vogler, H., Draeger, C., Munglani, G., Gupta, S., Herger, A. G., et al. (2018). LRX proteins play a crucial role in pollen grain and pollen tube cell wall development. *Plant Physiol.* 176 (3), 1981–1992. doi: 10.1104/pp.17.01374

Feng, F., Sun, J., Radhakrishnan, G., Lee, T., Bozsoki, Z., Fort, S., et al. (2019). A combination of chitooligosaccharide and lipochitooligosaccharide recognition promotes arbuscular mycorrhizal associations in medicago truncatula. *Nat. Commun.* 10, 5047. doi: 10.1038/s41467-019-12999-5

Franck, C. M., Westermann, J., and Boisson-Dernier, A. (2018a). Plant malectin-like receptor kinases: From cell wall integrity to immunity and beyond. *Annu. Rev. Plant Biol.* 69, 301–328. doi: 10.1146/annurev-arplant-042817-040557

Franck, C. M., Westermann, J., Burssner, S., Lentz, R., Lituiev, D. S., and Boisson-Dernier, A. (2018b). The protein phosphatases ATUNIS1 and ATUNIS2 regulate cell wall integrity in tip-growing cells. *Plant Cell* 30 (8), 1906–1923. doi: 10.1105/tpc.18.00284

Franklin-Tong, N., and Franklin, F. (2003). Gametophytic self-incompatibility inhibits pollen tube growth using different mechanisms. *Trends Plant Sci.* 8, 598–605. doi: 10.1016/j.tplants.2003.10.008

Galindo-Trigo, S., Blanco-Tourinan, N., DeFalco, T. A., Wells, E. S., Gray, J. E., Zipfel, C., et al. (2020). CrRLK1L receptor-like kinases HERK1 and ANJEA are female determinants of pollen tube reception. *EMBO Rep.* 21 (2), e48466. doi: 10.15252/embr.201948466

Ge, Z., Bergonci, T., Zhao, Y., Zou, Y., Du, S., Liu, M. C., et al. (2017). Arabidopsis pollen tube integrity and sperm release are regulated by RALF-mediated signaling. *Science* 358 (6370), 1596–1600. doi: 10.1126/science.aao3642

Ge, Z., Zhao, Y., Liu, M. C., Zhou, L. Z., Wang, L., Zhong, S., et al. (2019). LLG2/3 are Co-receptors in BUPS/ANX-RALF signaling to regulate arabidopsis pollen tube integrity. *Curr. Biol.* 29 (19), 3256–3265.e3255. doi: 10.1016/j.cub.2019.08.032

Goring, D. R., Indriolo, E., and Samuel, M. A. (2014). The ARC1 E3 ligase promotes a strong and stable self-incompatibility response in arabidopsis species: Response to the nasrallah and nasrallah commentary. *Plant Cell* 26 (10), 3842–3846. doi: 10.1105/tpc.114.131243

Hafidh, S., and Honys, D. (2021). Reproduction multitasking: The Male gametophyte. *Annu. Rev. Plant Biol.* 72, 581–614. doi: 10.1146/annurev-arplant-080620-021907

Hamamura, Y., Nagahara, S., and Higashiyama, T. (2012). Double fertilization on the move. *Curr. Opin. Plant Biol.* 15 (1), 70–77. doi: 10.1016/j.pbi.2011.11.001

Hater, F., Nakel, T., and Gross-Hardt, R. (2020). Reproductive multitasking: The female gametophyte. *Annu. Rev. Plant Biol.* 71, 517–546. doi: 10.1146/annurev-arplant-081519-035943

Herger, A., Gupta, S., Kadler, G., Franck, C. M., Boisson-Dernier, A., and Ringli, C. (2020). Overlapping functions and protein-protein interactions of LRR-extensins in arabidopsis. *PloS Genet.* 16 (6), e1008847. doi: 10.1371/journal.pgen.1008847

Higashiyama, T., Yabe, S., Sasaki, N., Nishimura, Y., Miyagishima, S., Kuroiwa, H., et al. (2001). Pollen tube attraction by the synergid cell. *Science* 293 (5534), 1480–1483. doi: 10.1126/science.1062429

Hohmann, U., Lau, K., and Hothorn, M. (2017). The structural basis of ligand perception and signal activation by receptor kinases. *Annu. Rev. Plant Biol.* 68, 109–137. doi: 10.1146/annurev-arplant-042916-040957

Huang, W. J., Liu, H. K., McCormick, S., and Tang, W. H. (2014). Tomato pistil factor STIG1 promotes in vivo pollen tube growth by binding to phosphatidylinositol 3-phosphate and the extracellular domain of the pollen receptor kinase LePRK2. *Plant Cell* 26 (6), 2505–2523. doi: 10.1105/tpc.114.123281

Huck, N., Moore, J. M., Federer, M., and Grossniklaus, U. (2003). The arabidopsis mutant feronia disrupts the female gametophytic control of pollen tube reception. *Development* 130 (10), 2149–2159. doi: 10.1242/dev.00458

Iwano, M., Igarashi, M., Tarutani, Y., Kaothien-Nakayama, P., Nakayama, H., Moriyama, H., et al. (2014). A pollen coat-inducible autoinhibited Ca2+-ATPase expressed in stigmatic papilla cells is required for compatible pollination in the brassicaceae. *Plant Cell* 26 (2), 636–649. doi: 10.1105/tpc.113.121350

Jany, E., Nelles, H., and Goring, D. R. (2019). The molecular and cellular regulation of brassicaceae self-incompatibility and self-pollen rejection. *Int. Rev. Cell Mol. Biol.* 343, 1–35. doi: 10.1016/bs.ircmb.2018.05.011

Jia, Q. S., Zhu, J., Xu, X. F., Lou, Y., Zhang, Z. L., Zhang, Z. P., et al. (2015). Arabidopsis AT-hook protein TEK positively regulates the expression of arabinogalactan proteins for nexine formation. *Mol. Plant* 8 (2), 251–260. doi: 10.1016/j.molp.2014.10.001

Johnson, M. A., and Preuss, D. (2003). On your mark, get set, GROW! LePRK2-LAT52 interactions regulate pollen tube growth. *Trends Plant Sci.* 8 (3), 97–99. doi: 10.1016/S1360-1385(03)00009-8

Ju, Y., Yuan, J., Jones, D. S., Zhang, W., Staiger, C. J., and Kessler, S. A. (2021). Polarized NORTIA accumulation in response to pollen tube arrival at synergids promotes fertilization. *Dev. Cell* 56 (21), 2938–2951 e2936. doi: 10.1016/j.devcel.2021.09.026

Kanaoka, M. M. (2018). Cell-cell communications and molecular mechanisms in plant sexual reproduction. *J. Plant Res.* 131 (1), 37–47. doi: 10.1007/s10265-017-0997-2

Kawashima, T., and Berger, F. (2011). Green love talks; cell-cell communication during double fertilization in flowering plants. *AoB Plants* 2011, plr015. doi: 10.1093/aobpla/plr015

Kim, M. J., Jeon, B. W., Oh, E., Seo, P. J., and Kim, J. (2021). Peptide signaling during plant reproduction. *Trends Plant Sci.* 26 (8), 822–835. doi: 10.1016/j.tplants.2021.02.008

Kirkbride, K., Ray, B., and Blobe, G. (2005). Cell-surface co-receptors: Emerging roles in signaling and human disease. *Trends Biochem. Sci.* 30, 611–621. doi: 10.1016/j.tibs.2005.09.003

Kitashiba, H., Liu, P., Nishio, T., Nasrallah, J. B., and Nasrallah, M. E. (2011). Functional test of brassica self-incompatibility modifiers in arabidopsis thaliana. *Proc. Natl. Acad. Sci. U.S.A.* 108 (44), 18173–18178. doi: 10.1073/pnas.1115283108

Kou, X., Cao, P., He, Q., Wang, P., Zhang, S., and Wu, J. (2022). PbrROP1/2-elicited imbalance of cellulose deposition is mediated by a CrRLK1L-ROPGEF module in the pollen tube of pyrus. *Hortic. Res* 6511232. doi: 10.1093/hr/uhab034

Leszczuk, A., Szczuka, E., and Zdunek, A. (2019). Arabinogalactan proteins: Distribution during the development of male and female gametophytes. *Plant Physiol. Biochem.* 135, 9–18. doi: 10.1016/j.plaphy.2018.11.023

Levitin, B., Richter, D., Markovich, I., and Zik, M. (2008). Arabinogalactan proteins 6 and 11 are required for stamen and pollen function in arabidopsis. *Plant J.* 56 (3), 351–363. doi: 10.1111/j.1365-313X.2008.03607.x

Liang, X., and Zhou, J. M. (2018). Receptor-like cytoplasmic kinases: Central players in plant receptor kinase-mediated signaling. *Annu. Rev. Plant Biol.* 69, 267–299. doi: 10.1146/annurev-arplant-042817-040540

Li, S., Chen, M., Yu, D., Ren, S., Sun, S., Liu, L., et al. (2013). EXO70A1-mediated vesicle trafficking is critical for tracheary element development in arabidopsis. *Plant Cell* 25 (5), 1774–1786. doi: 10.1105/tpc.113.112144

Li, W., Li, Q., Lyu, M., Wang, Z., Song, Z., Zhong, S., et al. (2022). Lack of ethylene does not affect reproductive success and synergid cell death in arabidopsis. *Mol. Plant* 15 (2), 354–362. doi: 10.1016/j.molp.2021.11.001

Liu, H. K., Li, Y. J., Wang, S. J., Yuan, T. L., Huang, W. J., Dong, X., et al. (2020). Kinase partner protein plays a key role in controlling the speed and shape of pollen tube growth in tomato. *Plant Physiol.* 184 (4), 1853–1869. doi: 10.1104/pp.20.01081

Liu, C., Shen, L., Xiao, Y., Vyshedsky, D., Peng, C., Sun, X., et al. (2021a). Pollen PCP-b peptides unlock a stigma peptide-receptor kinase gating mechanism for pollination. *Science* 372 (6538), 171–175. doi: 10.1126/science.abc6107

Liu, M., Wang, Z., Hou, S., Wang, L., Huang, Q., Gu, H., et al. (2021b). AtLURE1/PRK6-mediated signaling promotes conspecific micropylar pollen tube guidance. *Plant Physiol.* 186 (2), 865–873. doi: 10.1093/plphys/kiab105

Liu, J., Zhong, S., Guo, X., Hao, L., Wei, X., Huang, Q., et al. (2013). Membrane-bound RLCKs LIP1 and LIP2 are essential Male factors controlling Male-female attraction in arabidopsis. *Curr. Biol.* 23 (11), 993–998. doi: 10.1016/j.cub.2013.04.043

Losada, J. M., and Herrero, M. (2017). Pollen tube access to the ovule is mediated by glycoprotein secretion on the obturator of apple (Malus × domestica, borkh). *Ann. Bot.* 119 (6), 989–1000. doi: 10.1093/aob/mcw276

Ma, H. (2003). Plant reproduction: GABA gradient, guidance and growth. *Curr. Biol.* 13 (21), R834–R836. doi: 10.1016/j.cub.2003.10.015

Marton, M. L., Cordts, S., Broadhvest, J., and Dresselhaus, T. (2005). Micropylar pollen tube guidance by egg apparatus 1 of maize. *Science* 307 (5709), 573–576. doi: 10.1126/science.1104954

Marton, M. L., Fastner, A., Uebler, S., and Dresselhaus, T. (2012). Overcoming hybridization barriers by the secretion of the maize pollen tube attractant ZmEA1 from arabidopsis ovules. *Curr. Biol.* 22 (13), 1194–1198. doi: 10.1016/j.cub.2012.04.061

Maruyama, D., Volz, R., Takeuchi, H., Mori, T., Igawa, T., Kurihara, D., et al. (2015). Rapid elimination of the persistent synergid through a cell fusion mechanism. *Cell* 161 (4), 907–918. doi: 10.1016/j.cell.2015.03.018

Matsumoto, D., and Tao, R. (2019). Recognition of s-RNases by an s locus f-box like protein and an s haplotype-specific f-box like protein in the prunus-specific self-incompatibility system. *Plant Mol. Biol.* 100, 367–378. doi: 10.1007/s11103-019-00860-8

Mazzurco, M., Sulaman, W., Elina, H., Cock, J., and Goring, D. (2001). Further analysis of the interactions between the brassica s receptor kinase and three interacting proteins (ARC1, THL1 and THL2) in the yeast two-hybrid system. *Plant Mol. Biol.* 45, 365–376. doi: 10.1023/a:1006412329934

McInnis, S. M., Desikan, R., Hancock, J. T., and Hiscock, S. J. (2006). Production of reactive oxygen species and reactive nitrogen species by angiosperm stigmas and pollen: potential signalling crosstalk? *New Phytol.* 172 (2), 221–228. doi: 10.1111/j.1469-8137.2006.01875.x

Mecchia, M. A., Santos-Fernandez, G., Duss, N. N., Somoza, S. C., Boisson-Dernier, A., Gagliardini, V., et al. (2017). RALF4/19 peptides interact with LRX proteins to control pollen tube growth in arabidopsis. *Science* 358 (6370), 1600–1603. doi: 10.1126/science.aao5467

Miyazaki, S., Murata, T., Sakurai-Ozato, N., Kubo, M., Demura, T., Fukuda, H., et al. (2009). ANXUR1 and 2, sister genes to FERONIA/SIRENE, are male factors for coordinated fertilization. *Curr. Biol.* 19, 1327–1331. doi: 10.1016/j.cub.2009.06.064

Mizukami, A. G., Inatsugi, R., Jiao, J., Kotake, T., Kuwata, K., Ootani, K., et al. (2016). The AMOR arabinogalactan sugar chain induces pollen-tube competency to respond to ovular guidance. *Curr. Biol.* 26 (8), 1091–1097. doi: 10.1016/j.cub.2016.02.040

Mori, T., Kuroiwa, H., Higashiyama, T., and Kuroiwa, T. (2006). GENERATIVE CELL SPECIFIC 1 is essential for angiosperm fertilization. *Nat. Cell Biol.* 8 (1), 64–71. doi: 10.1038/ncb1345

Motomura, K., Kawashima, T., Berger, F., Kinoshita, T., Higashiyama, T., and Maruyama, D. (2018). A pharmacological study of arabidopsis cell fusion between the persistent synergid and endosperm. *J. Cell Sci.* 131 (2), jcs204123. doi: 10.1242/jcs.204123

Murase, K., Shiba, H., Iwano, M., Che, F. S., Watanabe, M., Isogai, A., et al. (2004). A membrane-anchored protein kinase involved in brassica self-incompatibility signaling. *Science* 303 (5663), 1516–1519. doi: 10.1126/science.1093586

Okuda, S., Tsutsui, H., Shiina, K., Sprunck, S., Takeuchi, H., Yui, R., et al. (2009). Defensin-like polypeptide LUREs are pollen tube attractants secreted from synergid cells. *Nature* 458 (7236), 357–361. doi: 10.1038/nature07882

Palanivelu, R., Brass, L., Edlund, A. F., and Preuss, D. (2003). Pollen tube growth and guidance is regulated by POP2, an arabidopsis gene that controls GABA levels. *Cell* 114 (1), 47–59. doi: 10.1016/s0092-8674(03)00479-3

Pereira, A. M., Lopes, A. L., and Coimbra, S. (2016a). JAGGER, an AGP essential for persistent synergid degeneration and polytubey block in arabidopsis. *Plant Signal Behav.* 11 (8), e1209616. doi: 10.1080/15592324.2016.1209616

Pereira, A. M., Nobre, M. S., Pinto, S. C., Lopes, A. L., Costa, M. L., Masiero, S., et al. (2016b). "Love is strong, and you're so sweet": JAGGER is essential for persistent synergid degeneration and polytubey block in arabidopsis thaliana. *Mol. Plant* 9 (4), 601–614. doi: 10.1016/j.molp.2016.01.002

Philippar, K., Büchsenschutz, K., Abshagen, M., Fuchs, I., Geiger, D., Lacombe, B., et al. (2003). The k+ channel KZM1 mediates potassium uptake into the phloem and guard cells of the C4 grass zea mays. *J. Biol. Chem.* 278 (19), 16973–16981. doi: 10.1074/jbc.M212720200

Ramesh, S. A., Tyerman, S. D., Xu, B., Bose, J., Kaur, S., Conn, V., et al. (2015). GABA signalling modulates plant growth by directly regulating the activity of plant-specific anion transporters. *Nat. Commun.* 6, 7879. doi: 10.1038/ncomms8879

Rozier, F., Riglet, L., Kodera, C., Bayle, V., Durand, E., Schnabel, J., et al. (2020). Live-cell imaging of early events following pollen perception in self-incompatible arabidopsis thaliana. *J. Exp. Bot.* 71, 2513–2526. doi: 10.1093/jxb/eraa008

Sankaranarayanan, S., Jamshed, M., and Samuel, M. A. (2015). Degradation of glyoxalase I in brassica napus stigma leads to self-incompatibility response. *Nat. Plants* 1, 15185. doi: 10.1038/nplants.2015.185

Sassa, H. (2016). Molecular mechanism of the s-RNase-based gametophytic self-incompatibility in fruit trees of rosaceae. *Breed Sci.* 66, 116–121. doi: 10.1270/jsbbs.66.116

Scandola, S., and Samuel, M. A. (2019). A flower-specific phospholipase d is a stigmatic compatibility factor targeted by the self-incompatibility response in brassica napus. *Curr. Biol.* 29 (3), 506–512.e504. doi: 10.1016/j.cub.2018.12.037

Shiu, S. H., Karlowski, W. M., Pan, R., Tzeng, Y. H., Mayer, K. F., and Li, W. H. (2004). Comparative analysis of the receptor-like kinase family in arabidopsis and rice. *Plant Cell* 16 (5), 1220–1234. doi: 10.1105/tpc.020834

Somoza, S. C., Sede, A. R., Boccardo, N. A., and Muschietti, J. P. (2021). Keeping up with the RALFs: How these small peptides control pollen-pistil interactions in arabidopsis. *New Phytol.* 229 (1), 14–18. doi: 10.1111/nph.16817

Sprunck, S., and Dresselhaus, T. (2015). Three cell fusions during double fertilization. *Cell* 161 (4), 708–709. doi: 10.1016/j.cell.2015.04.032

Sprunck, S., Rademacher, S., Vogler, F., Gheyselinck, J., Grossniklaus, U., and Dresselhaus, T. (2012). Egg cell-secreted EC1 triggers sperm cell activation during double fertilization. *Science* 338 (6110), 1093–1097. doi: 10.1126/science.1223944

Stegmann, M., Monaghan, J., Smakowska-Luzan, E., Rovenich, H., Lehner, A., Holton, N., et al. (2017). The receptor kinase FER is a RALF-regulated scaffold controlling plant immune signaling. *Science* 355 (6322), 287–289. doi: 10.1126/science.aal2541

Stone, S. L., Anderson, E. M., Mullen, R. T., and Goring, D. R. (2003). ARC1 is an E3 ubiquitin ligase and promotes the ubiquitination of proteins during the rejection of self-incompatible brassica pollen. *Plant Cell* 15 (4), 885–898. doi: 10.1105/tpc.009845

Sun, L., Williams, J., Li, S., Wu, L., Khatri, W., Stone, P., et al. (2018). S-locus f-box proteins are solely responsible for s-RNase-Based self-incompatibility of petunia pollen. *Plant Cell* 30, 2959–2972. doi: 10.1105/tpc.18.00615

Takahashi, T., Mori, T., Ueda, K., Yamada, L., Nagahara, S., Higashiyama, T., et al. (2018). The male gamete membrane protein DMP9/DAU2 is required for double fertilization in flowering plants. *Dev. (Cambridge England)* 145 (23), dev170076. doi: 10.1242/dev.170076

Takeuchi, H., and Higashiyama, T. (2012). A species-specific cluster of defensin-like genes encodes diffusible pollen tube attractants in arabidopsis. *PloS Biol.* 10 (12), e1001449. doi: 10.1371/journal.pbio.1001449

Takeuchi, H., and Higashiyama, T. (2016). Tip-localized receptors control pollen tube growth and LURE sensing in arabidopsis. *Nature* 531 (7593), 245–248. doi: 10.1038/nature17413

Tang, W., Ezcurra, I., Muschietti, J., and McCormick, S. (2002). A cysteine-rich extracellular protein, LAT52, interacts with the extracellular domain of the pollen receptor kinase LePRK2. *Plant Cell* 14 (9), 2277–2287. doi: 10.1105/tpc.003103

Tang, W., Kelley, D., Ezcurra, I., Cotter, R., and McCormick, S. (2004). LeSTIG1, an extracellular binding partner for the pollen receptor kinases LePRK1 and LePRK2, promotes pollen tube growth *in vitro*. *Plant J.* 39 (3), 343–353. doi: 10.1111/j.1365-313X.2004.02139.x

Vogler, H., Santos-Fernandez, G., Mecchia, M. A., and Grossniklaus, U. (2019). To preserve or to destroy, that is the question: the role of the cell wall integrity pathway in pollen tube growth. *Curr. Opin. Plant Biol.* 52, 131–139. doi: 10.1016/j.pbi.2019.09.002

von Besser, K., Frank, A. C., Johnson, M. A., and Preuss, D. (2006). Arabidopsis HAP2 (GCS1) is a sperm-specific gene required for pollen tube guidance and fertilization. *Development* 133 (23), 4761–4769. doi: 10.1242/dev.02683

Wang, L., Clarke, L. A., Eason, R. J., Parker, C. C., Qi, B., Scott, R. J., et al. (2017). PCP-b class pollen coat proteins are key regulators of the hydration checkpoint in arabidopsis thaliana pollen-stigma interactions. *New Phytol.* 213 (2), 764–777. doi: 10.1111/nph.14162

Wang, N., and Kao, T. (2012). Self-incompatibility in petunia: a self/nonself-recognition mechanism employing s-locus f-box proteins and s-RNase to prevent inbreeding. *Wiley Interdiscip. Rev. Dev. Biol.* 1, 267–275. doi: 10.1002/wdev.10

Wang, T., Liang, L., Xue, Y., Jia, P. F., Chen, W., Zhang, M. X., et al. (2016). A receptor heteromer mediates the male perception of female attractants in plants. *Nature* 531 (7593), 241–244. doi: 10.1038/nature16975

Xiao, D., Li, X., Zhou, Y. Y., Wei, L., Keovongkod, C., He, H., et al. (2021). Transcriptome analysis reveals significant difference in gene expression and pathways between two peanut cultivars under Al stress. *Gene* 781, 145535. doi: 10.1016/j.gene.2021.145535

Yu, T. Y., Sun, M. K., and Liang, L. K. (2021a). Receptors in the induction of the plant innate immunity. *Mol. Plant Microbe Interact.* 34 (6), 587–601. doi: 10.1094/MPMI-07-20-0173-CR

Yu, X., Zhang, X., Zhao, P., Peng, X., Chen, H., Bleckmann, A., et al. (2021b). Fertilized egg cells secrete endopeptidases to avoid polytubey. *Nature* 592 (7854), 433–437. doi: 10.1038/s41586-021-03387-5

Zhang, C., Brown, M. Q., van de Ven, W., Zhang, Z. M., Wu, B., Young, M. C., et al. (2016). Endosidin2 targets conserved exocyst complex subunit EXO70 to inhibit exocytosis. *Proc. Natl. Acad. Sci. U.S.A.* 113 (1), E41–E50. doi: 10.1073/pnas.1521248112

Zhang, L., Huang, J., Su, S., Wei, X., Yang, L., Zhao, H., et al. (2021). FERONIA receptor kinase-regulated reactive oxygen species mediate self-incompatibility in brassica rapa. *Curr. Biol.* 31 (14), 3004–3016.e3004. doi: 10.1016/j.cub.2021.04.060

Zhang, D., Wengier, D., Shuai, B., Gui, C. P., Muschietti, J., McCormick, S., et al. (2008). The pollen receptor kinase LePRK2 mediates growth-promoting signals and positively regulates pollen germination and tube growth. *Plant Physiol.* 148 (3), 1368–1379. doi: 10.1104/pp.108.124420

Zhong, S., Liu, M., Wang, Z., Huang, Q., Hou, S., Xu, Y. C., et al. (2019). Cysteine-rich peptides promote interspecific genetic isolation in arabidopsis. *Science*, 364(6443), eaau9564. doi: 10.1126/science.aau9564

Zhong, S., Li, L., Wang, Z., Ge, Z., Li, Q., Bleckmann, A., et al. (2022). RALF peptide signaling controls the polytubey block in arabidopsis. *Science* 375 (6578), 290–296. doi: 10.1126/science.abl4683

Zhou, L. Z., and Dresselhaus, T. (2019). Friend or foe: Signaling mechanisms during double fertilization in flowering seed plants. *Curr. Top. Dev. Biol.* 131, 453–496. doi: 10.1016/bs.ctdb.2018.11.013

Zhou, X., Lu, J., Zhang, Y., Guo, J., Lin, W., Van Norman, J. M., et al. (2021). Membrane receptor-mediated mechano-transduction maintains cell integrity during pollen tube growth within the pistil. *Dev. Cell* 56 (7), 1030–1042.e1036. doi: 10.1016/j.devcel.2021.02.030

frontiers | Frontiers in Plant Science

TYPE Original Research
PUBLISHED 25 January 2023
DOI 10.3389/fpls.2023.1090026

OPEN ACCESS

EDITED BY
Gerald Alan Berkowitz,
University of Connecticut, United States

REVIEWED BY
Tong Chen,
Institute of Botany (CAS), China
Juan de Dios Alché,
Experimental Station of Zaidín (CSIC), Spain

*CORRESPONDENCE
Iris Aloisi
iris.aloisi2@unibo.it

SPECIALTY SECTION
This article was submitted to Plant Membrane Traffic and Transport, a section of the journal Frontiers in Plant Science

RECEIVED 04 November 2022
ACCEPTED 02 January 2023
PUBLISHED 25 January 2023

CITATION
Suanno C, Tonoli E, Fornari E, Savoca MP, Aloisi I, Parrotta L, Faleri C, Cai G, Coveney C, Boocock DJ, Verderio EAM and Del Duca S (2023) Small extracellular vesicles released from germinated kiwi pollen (pollensomes) present characteristics similar to mammalian exosomes and carry a plant homolog of ALIX.
Front. Plant Sci. 14:1090026.
doi: 10.3389/fpls.2023.1090026

Small extracellular vesicles released from germinated kiwi pollen (pollensomes) present characteristics similar to mammalian exosomes and carry a plant homolog of ALIX

Chiara Suanno[1], Elisa Tonoli[2], Enzo Fornari[3], Maria P. Savoca[2], Iris Aloisi[1]*, Luigi Parrotta[1,4], Claudia Faleri[5], Giampiero Cai[5], Clare Coveney[6,7], David J. Boocock[6,7], Elisabetta A. M. Verderio[1,2] and Stefano Del Duca[1,4]

[1]University of Bologna, Department of Biological, Geological, and Environmental Sciences, Bologna, Italy, [2]Nottingham Trent University, Interdisciplinary Biomedical Research Centre, School of Science and Technology, Nottingham, United Kingdom, [3]Chrysalis Health & Beauty Creation House, Nottingham, United Kingdom, [4]University of Bologna, Interdepartmental Centre for Agri-Food Industrial Research, Cesena, Italy, [5]University of Siena, Department of Life Sciences, Siena, Italy, [6]Nottingham Trent University, Department of Biosciences, Centre for Health, Ageing and Understanding Disease (CHAUD), School of Science and Technology, Nottingham, United Kingdom, [7]Nottingham Trent University, John van Geest Cancer Research Centre, Centre for Health, Ageing and Understanding Disease (CHAUD), School of Science and Technology, Nottingham, United Kingdom

Introduction: In the last decade, it has been discovered that allergen-bearing extracellular nanovesicles, termed "pollensomes", are released by pollen during germination. These extracellular vesicles (EVs) may play an important role in pollen-pistil interaction during fertilization, stabilizing the secreted bioactive molecules and allowing long-distance signaling. However, the molecular composition and the biological role of these EVs are still unclear. The present study had two main aims: (I) to clarify whether pollen germination is needed to release pollensomes, or if they can be secreted also in high humidity conditions; and (II) to investigate the molecular features of pollensomes following the most recent guidelines for EVs isolation and identification.

Methods: To do so, pollensomes were isolated from hydrated and germinated kiwi (*Actinidia chinensis* Planch.) pollen, and characterized using imaging techniques, immunoblotting, and proteomics.

Results: These analyses revealed that only germinated kiwi pollen released detectable concentrations of nanoparticles compatible with small EVs for shape and protein content. Moreover, a plant homolog of ALIX, which is a well-recognized and accepted marker of small EVs and exosomes in mammals, was found in pollensomes.

Discussion: The presence of this protein, along with other proteins involved in endocytosis, is consistent with the hypothesis that pollensomes could comprehend a prominent subpopulation of plant exosome-like vesicles.

KEYWORDS

pollensomes, nanovesicles, pollen tube, pollination, exosomes, signaling, ALIX, EVs

1 Introduction

It is widely known that protein secretion is needed for pollen-pistil communication during spermatophyte sexual reproduction, from the species-specific recognition, to the self-compatibility or incompatibility, to the pollen tube elongation (Cheung and Wu, 2008; Hafidh et al., 2014; Mandrone et al., 2019). However, proof that extracellular vesicles (EVs) are involved in such communication has been found only in the last two decades. Initially, Grote and colleagues demonstrated that allergenic pollen, when hydrated in rainwater, can release nanoparticles bearing pollen allergens (Grote et al., 2000; Grote et al., 2003). In 2014, Prado and colleagues proved that allergen-bearing nanoparticles released by germinated pollen grains are extracellular nanovesicles, with diameter ranging from 28 to 60 nm, which they named "pollensomes" (Prado et al., 2014; Prado et al., 2015). Since pollensomes were isolated using a protocol designed for mammalian exosomes, and because they were comparable in size with known exosomes, the researchers speculated that pollensomes could be plant exosomes (or small EVs, according with recent nomenclature) (Prado et al., 2014). EVs are a relatively new concept in biology and especially in plant science (Théry et al., 2018). They were first discovered in mammals and the bulk of knowledge about them derives from the study of mammalian cells, but they have also been described in other animals, yeasts, and plants (Rutter and Innes, 2017; Kurian et al., 2021). Exosomes can be defined as small EVs between 30 and 200 nm in diameter, with a lipidic double-layered membrane and endocytic origins. These features distinguish them from other known extracellular vesicles: nanovesicles derived by exocyst-positive organelles (EXPOs) have single-layered lipidic membranes (Wang et al., 2010), while extracellular microvesicles and apoptotic bodies are on average larger in size (50-1000 nm and 500-2000 nm, respectively) and originate by outward budding from the plasma membrane (Kurian et al., 2021), a phenomenon that has not been demonstrated for plants to date (Woith et al., 2021). Exosomes instead have a peculiar biogenesis, since they are produced by invagination of the late endosome membrane. At this first stage, exosomes are called intraluminal vesicles (ILVs), and the organelle including them is called multivesicular body (MVB). The membrane of the MVB then fuses to the plasma membrane, releasing the ILVs in the extracellular environment as exosomes (Johnstone, 2006; Javeed and Mukhopadhyay, 2017). While exosomes are known to mediate cellular signaling and several other biological functions in mammals (Javeed and Mukhopadhyay, 2017), their role in plants is yet to be fully understood. It is however ascertained that plant exosomes are involved in stress responses and defense signaling, and they may also mediate intercellular communication (An et al., 2007; Hansen and Nielsen, 2017; Rutter and Innes, 2017; Woith et al., 2021). Moreover, there is evidence that stigmatic papillae of Brassica napus L. secrete exosomes to communicate with pollen during pollen hydration and pollen tube entry (Goring, 2017). It is reasonable to wonder whether this type of communication might be adopted by the pollen too, since exosomes are known to enhance the effectiveness of signaling by protecting their cargo from degradation in the extracellular environment (Akuma et al., 2019).

According to recent literature, EVs can be defined exosomes if all the following criteria are met: (I) they can be isolated by ultracentrifugation at 100000 × g, (II) their dimensions fall within the accepted range for exosomes (30-200 nm), (III) they are released by MVBs, (IV) they contain accepted molecular markers for exosomes (Gurung et al., 2021; Kurian et al., 2021). Throughout the years, several molecular markers have been used to define mammalian exosomes, such as ALIX (Apoptosis-Linked gene-2 Interacting protein X), Tsg101 (Tumor Susceptibility Gene 101), tetraspanins (CD81, CD63, CD9), and flotillin; while for plant exosomes no universal molecular marker has been described yet, although some attempts have been made (Regente et al., 2009; Hafidh et al., 2016; Rutter and Innes, 2017; Woith et al., 2021). However, in the last years the International Society for Extracellular Vesicles has pointed out that proteins commonly regarded as molecular markers for exosomes are also enriched in small EVs of various origins, thus their presence cannot be correlated to a specific EVs subtype (Théry et al., 2018). For this reason, to date it is not possible to describe small EVs as exosomes without certain proof of their biogenesis.

The aim of this study was to deepen the knowledge on pollensomes, assessing (I) whether they could be secreted also by non-germinated pollen, under high humidity conditions; and (II) if they could be considered plant exosomes-like vesicles, i.e. if they met the most recent criteria to be defined small EVs, while having a protein content compatible with an endocytic origin. In particular, the presence of plant homologs of ALIX in pollensomes was investigated, since ALIX domain Bro1 is highly preserved in the evolution of eukaryotic organisms, and Bro1 domain-containing proteins are present in yeasts and plants, where they are known to be involved in the formation of ILVs and in the sorting of their cargo (Bissig and Gruenberg, 2014; Kalinowska et al., 2015; García-León and Rubio, 2020). In the present study, kiwi (Actinidia chinensis Planch.) pollen was used to investigate both the conditions that stimulate pollensomes release and the molecular content of these EVs, using a combination of imaging techniques, immunoblotting, and proteomic analysis that is required to gain insight on and to formally define small EVs.

2 Materials and methods

2.1 Plant material

Kiwi pollen has been chosen as a model for this study because it is easily available, it shows a high in vitro germination rate in only two hours, and it can be stored for several years without a significant decrease in viability and germinability. Kiwi pollen used in these experiments was purchased in 2019 from Azienda Agricola Tabanelli Pierino, Mirko e C. (Castel Bolognese, Bologna, Italy). Pollen was then dried and stored at -20°C.

2.2 Sample treatment

Each sample was made of 10 mg dry pollen for particle tracking analysis, atomic force microscopy, immunofluorescence, and

Abbreviations: AFM, Atomic force microscopy; BP, Biological Process; CC, Cellular Component; EVF, vesicle-free supernatant; EVs, extracellular vesicles; EXPO, Exocyst-Postive Organelle; GKP, Germinated kiwi pollen; GO, Gene ontology; HKP, Hydrated kiwi pollen; ILV, Intraluminal vesicle; NTA, Nanoparticle tracking analysis; MF, Molecular function; MVB, Multivesicular body; PKP, PBS-hydrated kiwi pollen; TL, Total Lysate.

immunogold. For FM4-64™ staining, samples were made of 20 mg dry pollen for each treatment, whereas 40 mg dry pollen samples were used for total proteomics and Western blot analysis. All the samples were initially rehydrated for 30 min at 30°C in a humid chamber with 100% relative humidity, and their viability was checked by MTT assay (Paris et al., 2017). Pollen was then resuspended in germination medium (10% sucrose, 324 μM H_3BO_3, 1.27 mM $Ca(NO_3)_2$) at concentrations of 1 mg/mL, and incubated in a Petri dish for 2 h at 30°C (germinated kiwi pollen, GKP); alternatively, pollen was hydrated in the humid chamber, under the same conditions and for the same time of GKP, and it was eventually resuspended in particle-free PBS at concentrations of 0.5 mg/mL (hydrated kiwi pollen, HKP). For FM4-64 staining, a third treatment group was added (PBS-hydrated kiwi pollen, PKP), by resuspending the rehydrated pollen in particle-free PBS (Dubecco's PBS 1x, Capricorn Scientific, Italy) at concentrations of 1 mg/mL, and incubating it in a Petri dish for 2 h at 30°C. PKP was used as control only in the FM4-64 experiment, since the extended incubation in a liquid medium without the promotion of germination represents a stressful condition for pollen grains (Siriwattanakul et al., 2019; Božič and Šiber, 2022), hence cannot be assumed as a neutral treatment for a negative control. For all groups, viability and germinability were estimated in bright field microscopy with a Leica DM750 microscope, equipped with a Leica ICC50 W camera, using Leica AirLab software. Only pollen that had a viability rate over 80%, a germination rate over 60% for GKP, and a germination rate of 0% for HKP and PKP was used for subsequent analyses.

2.3 Extracellular vesicles isolation

EVs isolation was carried out as previously described (Prado et al., 2014; Prado et al., 2015; Furini et al., 2018), with minor modifications. Briefly, pollen grains were pelleted at 5000 × g for 15 min at 4°C. Pelleted pollen was stored at 4°C until protein extraction, while the supernatant was filtered twice in 0.22 μm syringe filters, and then EVs were pelleted by ultra-centrifuge at 100000 × g at 4°C for 1h. The resulting vesicle-free supernatant (EVF) was stored at 4°C until further analysis.

2.4 Protein isolation and quantification

Total proteins were isolated from whole pollen grains as shown in literature (Mandrone et al., 2019), with minor modifications. Briefly, pelleted pollen was resuspended in pollen extraction buffer (PEB) (Tris-HCl 20 mM pH 8.5, DTT 2 mM, protease inhibitors cocktail 1:100) and pottered 80 times. Pollen wall debris were discarded afterwards by spinning the samples at 1000 × g for 10 min, and the supernatant (total lysate, TL) was then collected.

Total proteins were extracted from the pelleted EVs by resuspending them in PEB.

Proteins in the EVF were precipitated with 10% TCA and washed with acetone at -20°C, pelleted by centrifuge at 15000 × g for 5 min at 4°C, and then resuspended in PEB (Furini et al., 2018).

Protein content was quantified by Bradford assay (Bradford Reagent, Sigma-Aldrich, Italy).

2.5 Immunoblotting

Total proteins from TLs, EVs, and EVFs fractions of both treatment and control groups were resolved in one-dimensional SDS-PAGE and blotted onto nitrocellulose membrane. For each pollen sample (40 mg), the total protein content for EVs and EVFs fractions was loaded into the gel for both treatments. Instead, for TLs only 50 μg of total proteins were used, to avoid overloading. The membrane was incubated for 10 min with Ponceau staining to visualize protein profiles and loadings for all the fractions. The membrane was then blocked in 5% Blotting Grade Blocker (BioRad, Italy) in TBS for 30 min, and thus incubated at 4°C overnight with one of the following rabbit polyclonal antibodies: 1:2000 dilution of anti-clathrin heavy chain (Agrisera), 1:5000 dilution of anti-H+ATPase (Agrisera, Italy), 1:500 dilution of anti-COXII (Agrisera, Italy), 1:5000 dilution of anti-UGPase (Agrisera, Italy), 1:1000 dilution of anti-ARF1 (Agrisera, Italy), or 1:1000 dilution of anti-ALIX (Covalab, Italy). All membranes were then washed in TBS-Tween (0.05% v/v) and TBS, and they were incubated at room temperature for 2 h with 1:5000 goat polyclonal anti-rabbit IgG peroxidase conjugated (Sigma-Aldrich, Italy). Finally, the membranes were developed with Amersham™ ECL Prime Western Blotting Reagents (GE Healthcare, Italy) and read in chemiluminescence with Azure 280 (Azure Biosystems, California). Experiments were repeated in triplicate for each target protein. Comparison between proteins bands was performed using ImageJ (Schneider et al., 2012).

The existence of plant homologs for human ALIX in Actinidia chinensis Planch. was assessed using BLAST (Altschul et al., 1990; Boratyn et al., 2012) to compare human ALIX sequence to published protein sequences in Actinidia chinensis var chinensis.

2.6 Proteomics

EVs from 3 germinated samples were lysed in RIPA buffer (25 mM TrisHCl pH 7.2, 150 mM NaCl, 2 mM EDTA, 5% (w/v) Sodium deoxycholate, 1% (v/v) NP40, 0.1% (w/v) SDS), and their protein content was quantified by Bradford assay, BCA assay, and 2-D Quant Kit (GE Healthcare, Italy), resulting in an average of 40 μg per sample. Proteins were lyophilized and stored at -80°C until analysis. EVs protein lysates were processed (reduced and alkyklated) and trypsinized using S-trap micro methodology (Protifi, USA). Samples were resuspended to 1 μg/μL in 5% acetonitrile (v/v) and 0.1% formic acid (v/v) in a two-stage process.

Individual samples and a pool of all three samples were analysed by RP-HPLC-ESI-MS/MS using a TripleTOF 6600+ mass spectrometer (MS) in data dependent acquisition mode (Top 30), according to literature (Furini et al., 2018) with some modifications. RP-HPLC mobile phases were solvent A (0.1% (v/v) formic acid in LC/MS grade water) and solvent B (LC/MS grade acetonitrile containing 0.1% (v/v) formic acid). Samples were injected (trap/elute via 5 x 0.3 μm YMC Triart C18 trap column) onto a YMC Triart-C18 column (15 cm, 3 μm, 300-um ID) at 5 μL/min using a microflow LC system (Eksigent ekspert nano LC 425) with an increasing linear gradient of B going from 3% to 30% in 68 min; to 40% at 73 min then washing to 80% for 3 min before re-equilibration in a total time of 87 min. Datafiles were searched both individually

and together using ProteinPilot 5.0.3 (Sciex) against the Actinidia chinensis Swissprot database with iodoacetamide selected as the alkylation method with the parameters of ID focus: Biological modifications and thorough ID. Protein families, cellular localizations and functions were drawn from UniProtKB (The UniProt Consortium, 2021) and from literature (Kawai and Uchimiya, 1995; Anderson et al., 2004; Tiwari et al., 2005; Al-Whaibi, 2011; Olvera-Carrillo et al., 2011; Lu et al., 2012; Suhandono et al., 2014; Dumont et al., 2016; Kuttiyatveetil and Sanders, 2017; Saqib et al., 2019). Gene ontology (GO) analysis was performed using the overrepresentation test of Panther Classification System (Thomas et al., 2022) version 17.0, with Fisher's exact test and False Discovery Rate correction. GO terms were clustered and summarized using REVIGO with simRel as semantic similarity measure (Supek et al., 2011). Protein-protein networks were elaborated in STRING version 11.5 (Szklarczyk et al., 2021).

2.7 Nanoparticle tracking analysis

Nanoparticle tracking analysis (NTA) was performed using ZetaView® Basic-NTA (Particle Metrix, Germany). Pelleted EVs were resuspended in particle-free PBS and analyzed in measurement mode "Size Distribution", 2 Cycles, 11 Positions. Germination medium and particle-free PBS were used as blank for the treatment and the control group respectively, and the measurements were performed in triplicate for each group. Eventually, particle concentrations of the blank controls were subtracted from the particle concentrations of the samples.

2.8 Atomic force microscopy

Atomic force microscopy (AFM) was performed using a Dimension ICON atomic force microscope equipped with a Nanoscope V controller operating in ScanAsyst tapping mode air environment. Standard silicon nitride triangular cantilevers (ScanAsyst-air, Bruker, U.K.), with resonant frequencies ranging between 45 and 95 kHz, and spring constants ranging between 0.2 and 0.8 N/m, were used. Imaging was performed at a rate of 0.7 Hz. All measurements were performed in temperature (23°C ± 1°C) controlled laboratories.

EVs fractions from GKP and HKP were resuspended in particle-free PBS at concentrations of 10.4 ·104 particles/µL (calculated using ZetaView™) for both treatment and control group. Particle-free PBS and germination medium were used as blank control to rule out contamination, following the same protocol used for EVs samples. Slides were then prepared under laminar flow hood according to literature (Sebaihi et al., 2017), with some modifications. 35 µL of sample were added on a 5 cm^2 polylysine-coated MICA. After 1 h of incubation the samples were gently rinsed with ultrapure water and let dry overnight at room temperature. 2 x 2 μm^2, 10 × 10 μm^2, and 500 x 500 nm^2 AFM images were recorded at 512 sample lines. All the images were analyzed using Nanoscope software. A first order flattening was applied to AFM images and the section analysis function of Nanoscope software was used to detect and measure the size of the particles.

2.9 Fluorescence microscopy

Fluorescence microscopy was performed using a NEXCOPE NE920 microscope equipped with a mercury short-arc lamp Osram HBO 103 and a 20 Mpx cooled color camera with C-MOS 1" sensor (TiEsseLab, Italy).

To prove the vesicular nature of the isolated nanoparticles, both whole germinated pollen grains and the EVs fractions from GKP, PKP, and HKP were resuspended in PBS added with 2 µM FM™ 4-64 (also known as SynaptoRed™ C2) fluorescent dye (Tocris, Italy) and observed at the fluorescence microscope using TRIC filter. Intact pollen grains hydrated in humid chamber or in PBS were not considered for this analysis, since the pollen wall would not allow the visualization of the fluorescent signal inside the cytoplasm.

For fluorescence immunolocalization of ALIX-homologs, only germinated pollen samples were analyzed. Germination medium was discarded after a light centrifugation (1000 × g), and pelleted pollen grains were then processed as described in literature (Parrotta et al., 2018; Mandrone et al., 2019), with some modifications. Briefly, pelleted pollen grains were fixed with PME buffer (4% formaldehyde, 50 mM PIPES pH 6.8, 1 mM $MgSO_4$, 5 mM EDTA) for 1 h, digested by pectinase and cellulase for 7 min, permeabilized with 0.5% Triton X-100 for 30 min, and eventually dehydrated in cold methanol (-20°C) for 10 min. Samples were blocked with 3% BSA in PBS, and then incubated with a 1:50 dilution of anti-ALIX in PBS at 4°C overnight. Samples used as negative controls were incubated with PBS only. All samples were thus incubated with a goat polyclonal anti-rabbit IgG, FITC-conjugated (dilution 1:200, SouthernBiotech, Italy), and 3% BSA in PBS, for 2 h at room temperature, in the dark. Finally, samples were washed in PBS, added with 10% glycerol, and mounted on glass slides. Fluorescence was observed at 600X magnification using the FITC filter.

2.10 Electron microscopy

For electron microscopy, the transmission electron microscope (TEM) Philips Morgagni 268 D set at 80 kV was employed, and images were captured with a MegaView II CCD Camera (Philips Electronics, The Netherlands) and analyzed with the microscope software (AnaliSYS). Immunogold labeling was carried out following literature (Parrotta et al., 2019). Briefly, germinated pollen was dehydrated in growing concentrations of ethanol, and then infiltrated with LR white resin (Sigma-Aldrich, Italy). Thus, the resin was encapsulated and polymerized in an oven at 40°C for 2 days. The resin was then sectioned, and the sections were blocked in 5% normal goat serum (Invitrogen, Italy) for 20 min and then incubated in a 1:50 dilution of the anti-ALIX antibody for 1 h. Three sections were selected as negative controls and they were not incubated with the primary antibody. Finally, the excess of primary antibody was washed in 50 mM Tris–HCl pH 7.6, 0.9% NaCl, 0.1% Tween, and all the sections were incubated for 45 min with a dilution 1:20 of goat anti-rabbit secondary antibody conjugated with 15 nm gold particles (BioCell, Italy). Sections were washed with distilled water and counterstained first with 2% uranyl acetate for 10 min, and then with lead citrate for 5 min. No osmium was employed in the preparation of the samples. At least 50 pollen tubes and grains were analyzed per sample.

2.11 Statistical analysis

Statistical analysis was carried out in RStudio (RStudio Team, 2020). To test datasets for normality, Shapiro-Wilk test was applied, using the "shapiro.test" function. To evaluate the statistical significance (p-value <0.05) of the differences between GKP and HKP samples, t-test and two-way ANOVA were performed on protein concentrations, using "t.test", "lm", and "anova" functions with default settings, followed by a post-hoc pairwise t-test with Bonferroni correction using "pairwise.t.test" function.

3 Results

3.1 Visualization and measurement of EVs

Nanoparticles ranging between 15 and 266 nm in diameter were present in the EVs fractions of both GKP and HKP when assessed by NTA. However, the majority of particles (>95%) had a diameter in the range between 120 and 209 nm. While median and modal diameters did not vary considerably between the two groups, nanoparticles in GKP EVs fraction showed a trend increase in concentration than those isolated from HKP (Figure 1).

In AFM analysis, nanoparticles compatible with EVs were visible in both GKP and HKP EVs fractions, while in the blank controls only smaller particles were present, with dimensions well below the range of published EVs (Supplementary Figure 1). Many particles appeared to be aggregated (Figure 2), having diameter and height of respectively 40.4 nm ± 60.4 nm and 10.7 ± 2.2 nm for HKP, and of 78.1 nm ± 57.4 nm and 9.8 ± 3.7 nm for GKP.

GKP EVs emitted a clear fluorescent signal after FM4-64™ staining (Figure 3A), indicating the presence of vesicles with double-layered lipidic membranes in this fraction. Excessive dimensions of the fluorescent spots compared to the maximum expected (266 nm) was likely due to aggregation of the vesicles (as also shown by AFM) and to the diffusion of fluorescent light. In fact, while the aggregation itself does not affect the FM4-64™ staining, the presence of closely associated vesicles marked with fluorescence and observed at the optical microscope can produce larger fluorescent spots than those expected on the basis of NTA and AFM analyses, and of the filtrations employed in the isolation protocol. On the contrary, EVs fractions from HKP and PKP did not show any fluorescence after FM4-64™ dyeing (Figures 3B, C), along with the blank controls (Supplementary Figure 2). Intact germinated pollen grains were stained with FM4-64™ as a positive control (Figures 3D, E), showing uniform fluorescent spotting along the pollen tube (Figure 3E), and the characteristic intense coloration on the tube apex (Figure 3D), due to vesicle accumulation (Parton et al., 2003).

3.2 Characterization of the proteins isolated from EVs

Total protein concentration of GKP EVs fraction resulted significantly higher (p-value<0.02) than the ones of HKP EVs fraction and EVFs fractions from both groups; while protein concentration of GKP EVFs, GHP EVFs, and GHP EVs fractions was comparable (Figure 4).

A Western blot analysis was carried out to identify the subcellular origin of the pollensomes and to rule out the presence of contaminations due to possible pollen tube ruptures during EVs isolation. Ponceau staining (Supplementary Figure 3) revealed different protein profiles for all three fractions of GKP, with distinct bands in the EVs fraction between 60 and 45 kDa, and between 35 and 25 kDa. Since protein quantification and Ponceau staining (Supplementary Figure 3) indicated a negligible protein content in both EVF fractions and in HKP EVs fraction, only TL and EVs from GKP were analyzed by immunoblotting. Clathrin heavy chain was chosen as a marker for vesicular compartments, H+ATPase as plasma membrane marker, COXII (Plant Cytochrome oxidase subunit II) as mitochondrial marker, UGPase (UDP-glucose phosphorylase) as cytoplasmic marker, and ARF1 (ADP-ribosylation factor 1) as a marker for the Golgi membrane. All the markers were found in GKP TL, which was expected, but only clathrin heavy chain was present in GKP EVs fraction (Figure 5).

A preliminary BLAST analysis revealed the presence of a Bro-1 domain containing protein (encoded by the gene CEY00_Acc28537) in the genome of Actinidia chinensis Planch., which showed 93.78% sequence identity with human ALIX. Western blot analysis using anti-human ALIX polyclonal antibodies revealed the presence of a possible plant homolog of ALIX, with a molecular weight around 43 kDa, in both TLs and in GKP EVs. Moreover, this protein showed a four to fivefold band intensity in the KPG EVs fraction when compared to the TLs, even though the protein content of the former was half the one of the latter (Figure 6).

The RP-HPLC-ESI-MS/MS provided a list of 2903 accession numbers matching with the peptides sequenced from GKP EVs, corresponding to 1170 different protein IDs (Supplementary Table 1). Among these, there were two tetraspanins (tetraspanin-8 like and tetraspanin-15 like), which are multi-pass membrane proteins, confirming the presence of membrane-bound particles in the GKP EVs fraction. ESCRT-related proteins, which have membrane-binding activity and allow the EVs to fuse with membranes, and heat-shock proteins (Hsp70 and Hsp90), which are cytosolic proteins commonly incorporated in EVs, were also present (Supplementary Table 1).

To ensure a better accuracy of the protein identification, only the accession numbers present in all three replicas, identified using at least 2 peptides, and with a 95% confidence coverage over 70% of the peptide length were selected for GO analysis, obtaining a list of 97 accession numbers, corresponding to 51 different protein IDs (Supplementary Table 2). In fact, some of the proteins listed in Supplementary Table 1 are unlikely to be secreted (e.g. ATP-synthase subunit beta, enzymes from the TCA cycle, nuclear proteins), and represent possible misidentifications. According to STRING, the 97 proteins selected had significantly more interactions (p-value<0.01) than a comparable random group of proteins drawn from kiwi genome, implying their biological connection and possible common role (Supplementary Figure 4). The majority of the accession numbers examined were involved in biological processes (BP) related to cellular component organization or biogenesis, and in metabolic processes of phosphorus and carbohydrates (Figure 7; Supplementary Figure 5), which is compatible with the high metabolic activity in the pollen cytoplasm

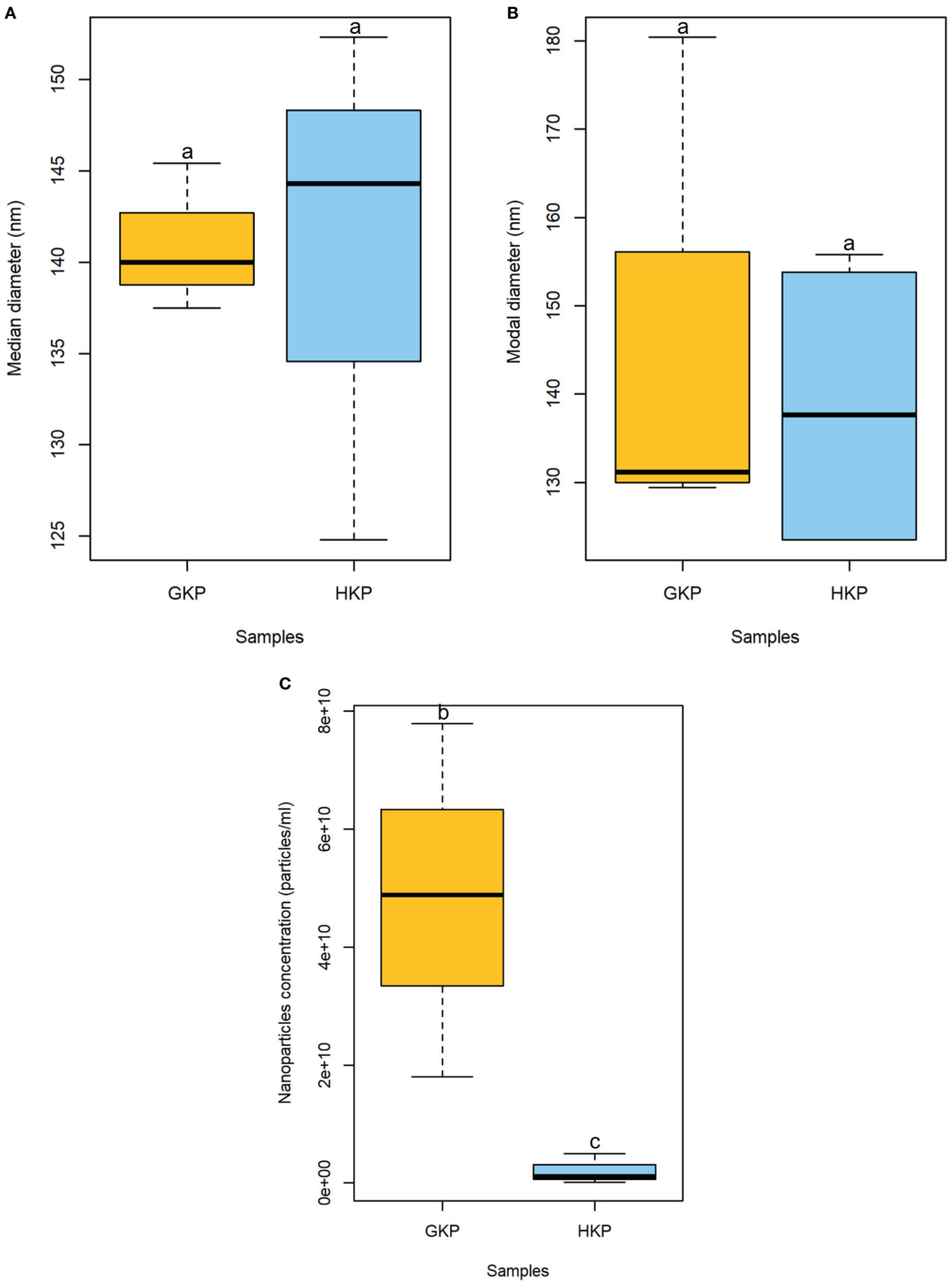

FIGURE 1
Boxplot representation (± SD) of median **(A)** and modal **(B)** diameters (nm), and concentration (particle/mL) **(C)** of nanoparticles in EVs fractions from GKP and HKP. Samples with different superscript letters differed with a weak significance (p-value<0.1) by one-way ANOVA.

during pollen tube elongation. Panther results indicated that, out of 78 GO terms in the BP category, 77 were overrepresented when compared to Actinidia chinensis proteome in UniProt database, with nucleoside metabolic processes and glycolytic processes having the highest fold enrichment (Figure 7; Supplementary Figure 5). Three proteins among those analyzed are also involved in stress response: the late embryogenesis abundant protein, the stress-induced protein, and the Hsp70. Others are involved in transport and signaling, like the guanosine nucleotide diphosphate dissociation inhibitor, and the clathrin heavy chain like protein (The UniProt Consortium, 2021). Furthermore, this analysis revealed the presence in GKP EVs of Ole e 1, a major pollen allergen with the biological function of trypsin inhibitor, also regarded as a pollensome marker (Prado et al., 2014; Prado et al., 2015). The most frequent Molecular Functions (MF) among the analyzed accession numbers were catalytic and binding activities, in line with the BP results (Figure 8; Supplementary Figure 6). While all

10.3389/fpls.2023.1090026

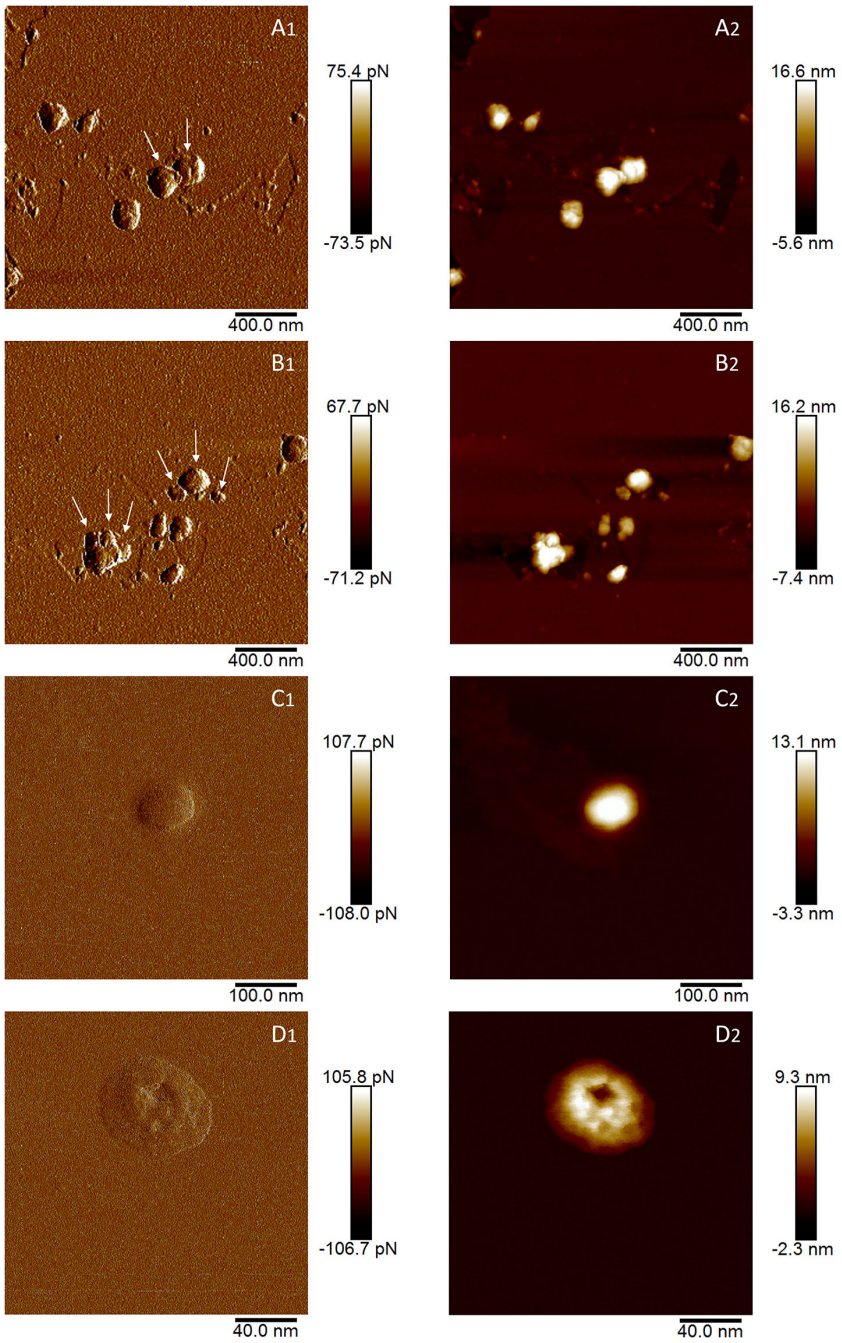

FIGURE 2
AFM images of EVs isolated from germinated **(A, B)** and hydrated **(C, D)** kiwi pollen. Images indexed with 1 (A1, B1, C1, D1) are captured in height mode, while images indexed with 2 (A2, B2, C2, D2) are captured in peak force error. In A1 and B1, arrows indicate plausible individual vesicles in vesicle aggregates.

the identified GO were overrepresented in the sample, "fructose-bisphosphate aldolase activity" and "structural constituent of cytoskeleton" were the GO terms with the highest fold enrichment (>75). Proteins involved in the cell wall remodeling, like α-L-arabinofuranosidase, glucosidases, galactosidases, and pectinases have been identified as well (Supplementary Tables 1, 2). Concerning the subcellular origin of the analyzed proteins, the majority of them belonged to the cytoplasm or to a protein-containing complex, while the most overrepresented GO terms for Cellular Components (CC) were the "lid subcomplex of the proteasome regulatory particle" and the "proteasome complex" (Supplementary Figure 7).

3.3 Localization of ALIX-homologs in the pollen tube

Immunofluorescence labeling revealed the presence of ALIX-homologs in the pollen tube, localized almost homogeneously in its

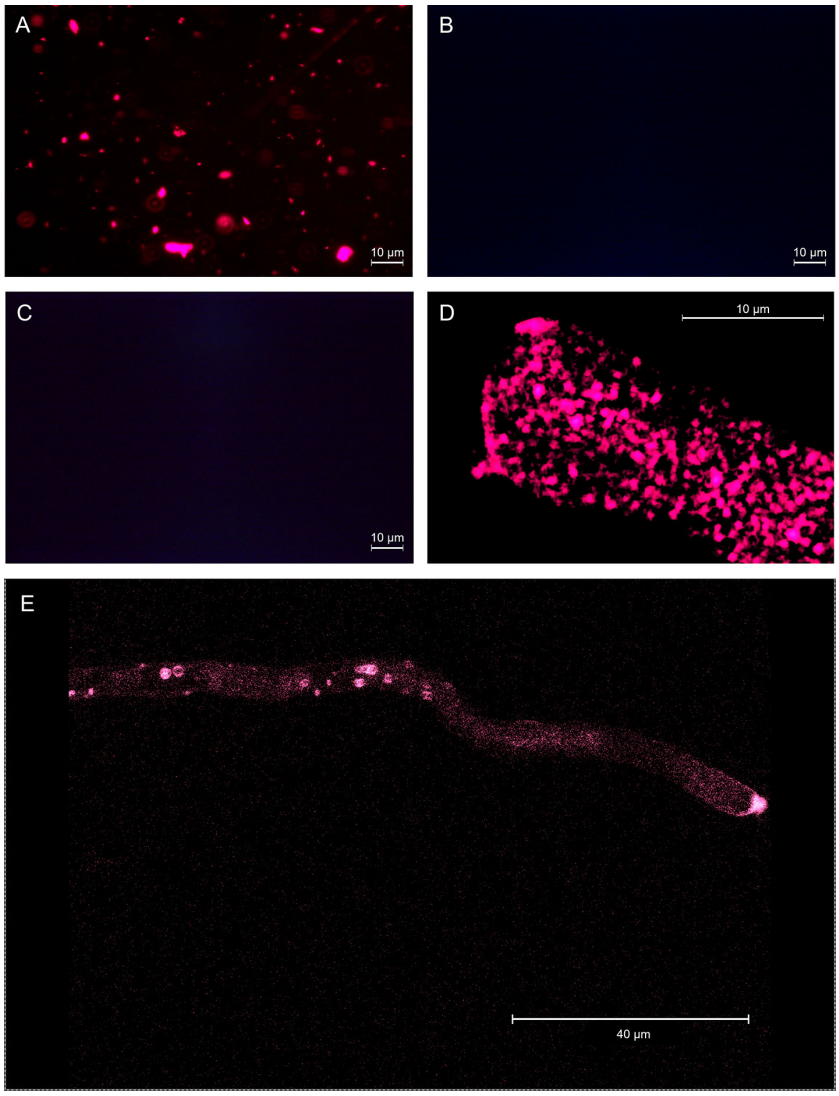

FIGURE 3
EVs from germinated kiwi pollen **(A)**, EVs from kiwi pollen hydrated in a humid chamber **(B)**, and EVs from kiwi pollen hydrated in PBS **(C)**, dyed with FM4-64^{TM} to enhance the presence of double-layered vesicles. **(D, E)** show FM4-64^{TM} staining on the pollen tube apical region at different magnifications, as a positive control.

metabolically active portions (Figures 9A–C), with a slight increase towards the apical region (Figures 9A, B). The negative control excluded nonspecific fluorescence for the pollen tube (Supplementary Figure 8).

The distribution of ALIX homologues was also studied by immunogold electron microscopy. Figures 9D–G show that these proteins were distributed in two different ways: in the cytoplasm of pollen tubes, and in association with rounded/tubular membrane-bounded structures. Since the images in Figure 9 were collected primarily at the apex and subapex of pollen tubes, it is likely that the membrane structures correspond to secretory or recycling vesicles, but other intermediate compartments cannot be excluded. In some cases, the signal was also found in association with the plasma membrane, although it was not a consistent trait, while it was never found in association with the cell wall. The negative control (Supplementary Figure 8) confirmed that nonspecific binding of gold-conjugated secondary antibodies did not impair the analysis.

4 Discussion

4.1 Nanoparticles can be isolated from kiwi pollen by ultracentrifugation

This study demonstrated that nanoparticles can be isolated from kiwi pollen samples after ultracentrifugation at 100000 × g (Figures 1, 2). While this has already been established for germinated pollen of other species (Prado et al., 2014; Prado et al., 2015), it is to our knowledge the first time that such nanoparticles have been also isolated from hydrated pollen, although Grote and colleagues described similar nanoparticles released after hydration in rainwater by birch, alder, hazel, and ryegrass pollen, using electron microscopy (Grote et al., 2000; Grote et al., 2003). However, while pollen types studied by Grote and colleagues underwent germinative abortion during hydration, kiwi pollen used in this study showed 0%

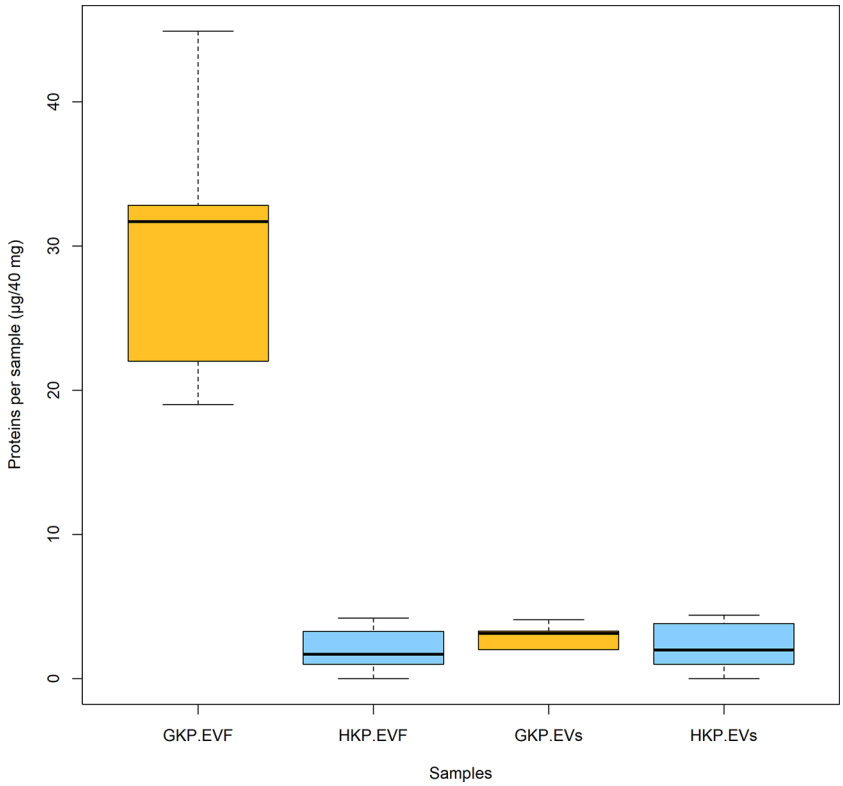

FIGURE 4
Mean protein content (± SD) for EVs and EVF from germinated and hydrated samples. Samples with different superscript letters were significantly different (p-value<0.05) by two-way ANOVA and Student t-test.

germination rate after hydration, performed either in humid chamber or in PBS. It is clear that hydrated kiwi pollen releases a considerably smaller amount of nanoparticles than germinated kiwi pollen (Figure 1). When samples containing the same concentration of nanoparticles isolated from HKP and GKP were visualized in AFM, it was possible to appreciate rounded, vesicle-like structures (Figure 2) in both groups, compatible for dimensions and shape with small EVs (Prado et al., 2014; Prado et al., 2015; Kurian et al., 2021).

4.2 Nanoparticles released by germinated kiwi pollen are EVs

When the nanoparticles (EVs fraction) isolated from the same sample size of GKP, HKP, and PKP were stained with FM4-64^{TM}, only the GKP preparation showed a detectable fluorescent signal, meaning that the nanoparticles isolated were EVs with a double-layered lipidic membrane (Figures 3A, B). The absence of a fluorescent signal in PKP nanoparticles indicates that the secretion of such vesicles is not promoted by the resuspension of pollen in a liquid medium, but rather by the germination process itself (Figure 3C). The relatively high protein content of GKP EVs fraction (Figure 4) corroborates the idea that GKP secretes nanovesicles, and the low protein concentrations in EVF fractions seem to exclude the possibility of a significant contamination of the EVs fraction by secreted proteins. Although in the light of NTA and AFM results (Figures 1, 2) it is not possible to rule out that HKP can secrete EVs, it is apparent that, if present, its secretion rate is very low and almost undetectable. Hence, while kiwi pollen hydration is necessary to reactivate pollen metabolism and promote the pollen tube growth, the hydration itself does not seem to activate any secretion pathway unless it is associated with stigmatic stimuli. This is in line with the current theory that pollen-pistil interactions during hydration are driven by proteins already present on the pollen surface, and specifically in the pollen coat (Wang et al., 2017). Cases in which the secretion of EVs-like nanoparticles has been documented as a consequence of pollen rehydration (Grote et al., 2000; Grote et al., 2003) always involved species in which pollen germination can be triggered by the resuspension in a liquid medium, while the present paper suggests that pollen rehydration caused by high relative humidity cannot trigger any relevant EVs secretion.

To furtherly assess that proteins and membranes found in GKP EVs fraction did not derive from pollen tube rupture and cell debris, total protein content of TL and EVs fractions from GKP samples was probed for known molecular markers of different organelles. The immunoblotting analysis excluded the presence of contaminations from plasma membrane, mitochondria, cytoplasm, and Golgi apparatus in EVs fractions (Figure 5), confirming that pollen integrity was preserved throughout the EVs isolation process. Moreover, proteomic analysis assessed the presence of tetraspanins, ESCRT-related proteins, and Hsp (Supplementary Table 1) fulfilling the technical requirement of the presence of specific transmembrane and cytosolic proteins to correctly identify EVs (Théry et al., 2018). The presence in all three replicas of Ole e 1 (Supplementary Table 1), which was described as a pollensome molecular marker by Prado and colleagues (Prado et al., 2014; Hafidh et al., 2016), furtherly validate

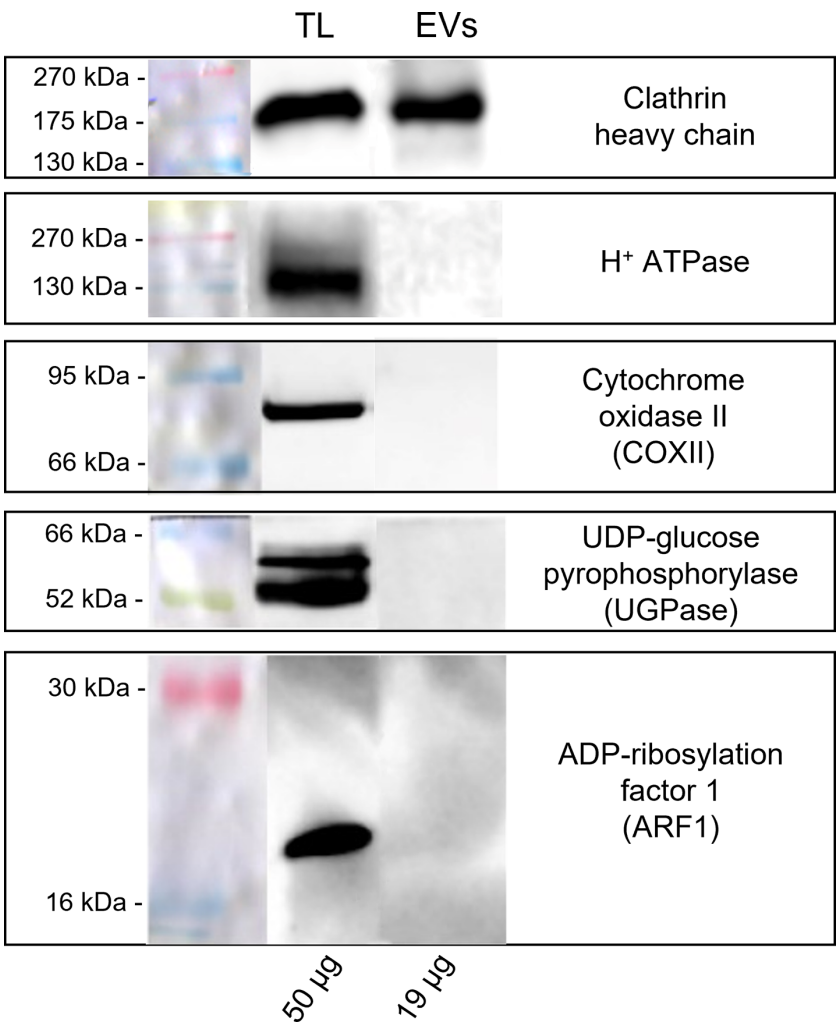

FIGURE 5
Western blot analysis of pollen total lysate (TL) and nanovesicles (EVs) fractions from germinated kiwi pollen (GKP). Samples were probed for the presence of molecular markers of different cell compartments with the following rabbit polyclonal antibodies: 1:2000 dilution of anti-clathrin heavy chain, 1:5000 dilution of anti-H+ATPase, 1:500 dilution of anti-COXII, 1:5000 dilution of anti-UGPase, 1:1000 dilution of anti-ARF1. The membranes were developed with ECL and read in chemiluminescence. On the left are reported the molecular weights of the pre-stained ladder, while on the bottom are reported the protein amounts loaded per lane.

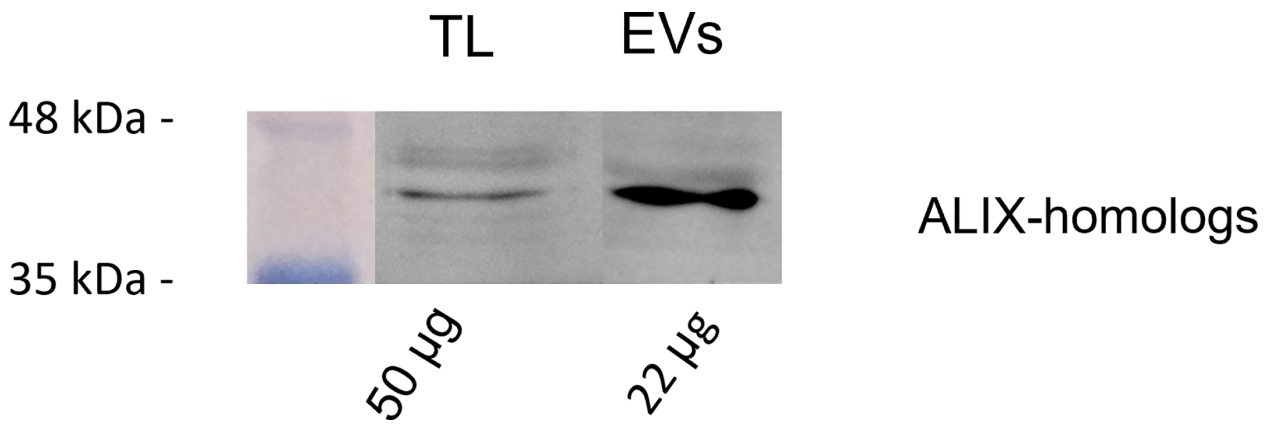

FIGURE 6
Western blot analysis of pollen total lysate (TL) and nanovesicles (EVs) fractions from germinated kiwi pollen (GKP), probed with a 1:1000 dilution of anti-ALIX rabbit polyclonal. The membranes were developed with ECL and read in chemiluminescence. On the left are reported the molecular weights of the pre-stained ladder, while on the bottom are reported the protein amounts loaded per lane.

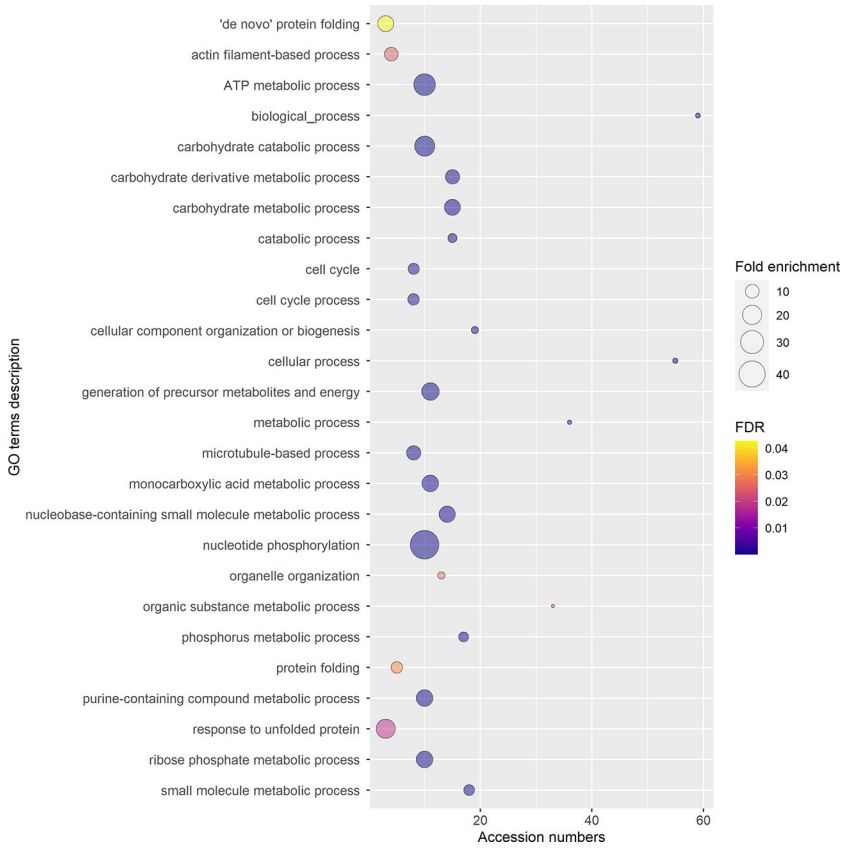

FIGURE 7
Gene Ontology (GO) terms for Biological Process, relative to the 97 selected accession numbers identified in extracellular nanovesicles from germinated pollen of *Actinidia chinensis* Planch. GO terms were provided by Panther Classification System version 17.0 and shortened by REVIGO using SimRel similarity measure. The diameter of the bubbles indicates the overrepresentation of the term when compared to the whole Actinidia chinensis Planch. genome (Fold enrichment), while the color indicates the False Detection Rate (FDR) value. GO terms with FDR>0.05 are not shown.

the presence of extracellular nanovesicles in the GKP EVs. Similarly to those found in pollensomes (Prado et al., 2014), many proteins from GKP EVs are involved in metabolic and biosynthetic processes, cell signaling, vesicular trafficking, cytoskeletal movements, and stress response (see Supplementary Materials). Moreover, enzymes thought to be involved in the cell wall reorganization needed for vesicles secretion (Woith et al., 2021) have been identified in GKP EVs as well (Supplementary Table 1).

4.3 EVs secreted by germinated kiwi pollen could be plant exosomes

The EVs isolation employed hereby was originally designed for mammalian exosomes (Prado et al., 2014; Furini et al., 2018; Kurian et al., 2021). The nanoparticles isolated in this study resulted on average larger in size than those described as pollensomes (Prado et al., 2014), but nonetheless their modal and median diameters fell within the accepted range for exosomes (Figure 1) and are compatible with published plant exosomes dimensions (Rutter and Innes, 2017). The tendency to aggregation shown by these particles during NTA, AFM, and FM4-64^{TM} staining (Figures 2, 3) and previously reported in literature (Linares et al., 2015) might explain the difference with the published pollensomes dimensions. In fact, ZetaView camera tends to consider the whole aggregate as a single particle, possibly overestimating mean and mode values of the diameter, and underestimating particle concentrations.

Most of the enzymes present in GKP EVs were involved in catabolic processes, especially in the energetic metabolism, with glycolytic activity and nucleoside metabolic activity (Supplementary Figures 4, 5). Since pollen tube elongation must be sustained by an intense metabolic activity, the cytoplasmic concentrations of metabolism-related enzymes are particularly high in this phase (Wang et al., 2022), hence they are more likely to be randomly internalized during EVs formation. Moreover, some of them, such as the pectinesterases or the pollen-specific leucine-rich repeat extensin-like protein (Supplementary Table 1), can cooperate in the degradation of female tissues to open a passage for the pollen tube through the style (Chae and Lord, 2011), and they might be released in a membranous compartment to extend their extracellular half-life. Another important feature of these vesicles, that emerged from the GO and interaction analyses, is the presence of interconnected proteasome subunits, 26S proteasome regulatory subunits, and proteasome inhibitors and activators, which are unlikely to have been randomly sorted into the vesicles (see Supplementary Materials). In fact, the EVs also contained various kinases, ubiquitin, and ubiquitin-related enzymes. It is known that proteasome plays a pivotal role in regulating the phosphoproteome

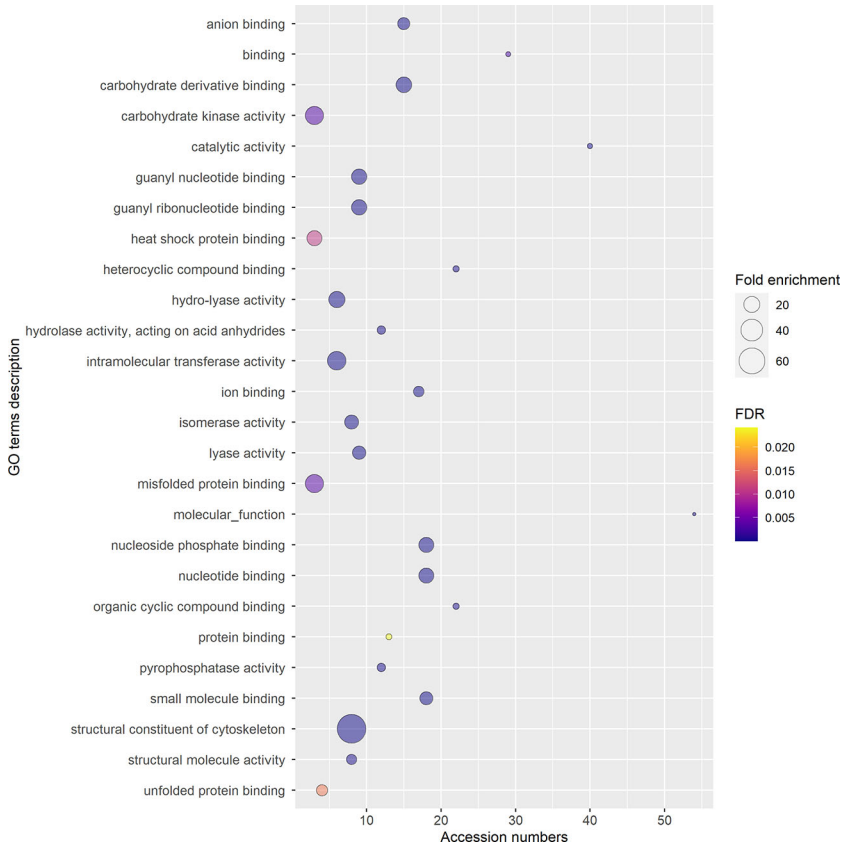

FIGURE 8
Gene Ontology (GO) terms for Molecular Functions, relative to the 97 selected accession numbers identified in extracellular nanovesicles from germinated pollen of *Actinidia chinensis* Planch. GO terms were provided by Panther Classification System version 17.0 and shortened by REVIGO using SimRel similarity measure. The diameter of the bubbles indicates the overrepresentation of the term when compared to the whole Actinidia chinensis Planch. genome (Fold enrichment), while the color indicates the False Detection Rate (FDR) value. GO terms with FDR>0.05 are not shown.

of kiwi pollen during the tube formation and growth, also affecting endocytosis and vesicular trafficking (Vannini et al., 2019). However, the extracellular role of the proteasome has been extensively studied only in mammals, where its presence in EVs, and especially exosome-like vesicles, appears to be related to pathological conditions, possibly targeting misfolded proteins in neighboring cells or in extracellular fluids (Ben-Nissan et al., 2022).

Ubiquitin-like proteins and ubiquitin-related enzymes are also common in both plant and mammalian exosomes, along with other proteins revealed by the proteomic analysis of GKP EVs, such as HSP70, chaperones, syntaxins, actin, and tetraspanins (Supplementary Tables 1, 2) (Johnstone, 2006; Rutter and Innes, 2017; Jeppesen et al., 2019; Kurian et al., 2021; Boccia et al., 2022). Ras-related Rab proteins (Supplementary Table 1), which have been considered as possible markers for plant exosomes (Regente et al., 2009), were also found. Moreover, using a polyclonal anti-ALIX antibody it was possible to detect the presence of a putative ALIX-homolog in GKP EVs (Figure 6). This protein was clearly more concentrated in EVs than in TL, suggesting a potential role of this protein in the formation or secretion of the nanovesicles. In fact, plant homologs of ALIX are known to participate in the differentiation of MVBs and to be involved in vesicular trafficking (Kalinowska et al., 2015; Cui et al., 2016; García-León and Rubio, 2020). The protein band had a molecular weight of about 43 kDa, that is compatible with the molecular weight estimated for ALIX-homolog encoded by the gene CEY00_Acc28537 of Actinidia chinensis var. chinensis (The UniProt Consortium, 2021). The immunofluorescence labeling of ALIX-homologs allowed to visualize their homogeneous distribution in the metabolically active portion of the elongating pollen tube (Figures 9A–C). This was confirmed by immunogold labeling that localized the proteins both in the cytoplasm and associated with vesicle-like structures near the pollen tube membrane (Figures 9D–G), which is compatible with the known subcellular localization and mechanisms of ALIX and Bro1 domain-containing proteins (Bissig and Gruenberg, 2014; García-León and Rubio, 2020), and with the observed localization of Ole e 1 in the pollen tubes (Prado et al., 2014).

Immunoblotting also revealed the presence of clathrin heavy chain in GKP EVs fraction (Figure 5). Clathrin light and heavy chains, clathrin heavy chain like proteins, clathrin coat assembly proteins, and clathrin interactors EPSIN like were also identified in GKP EVs by RP-HPLC-ESI-MS/MS analysis (Supplementary Tables 1, 2). Since clathrin mediates endocytic processes during the pollen tube elongation (Blackbourn and Jackson, 1996; Narasimhan et al., 2020), its presence in the EVs fraction may support the hypothesis of Prado and collaborators that these extracellular nanovesicles could have an endocytic origin (An et al., 2007; Prado et al., 2014). In fact, while it is not considered an exosome marker, clathrin heavy chain is often found in exosomes (Woith et al., 2021). It

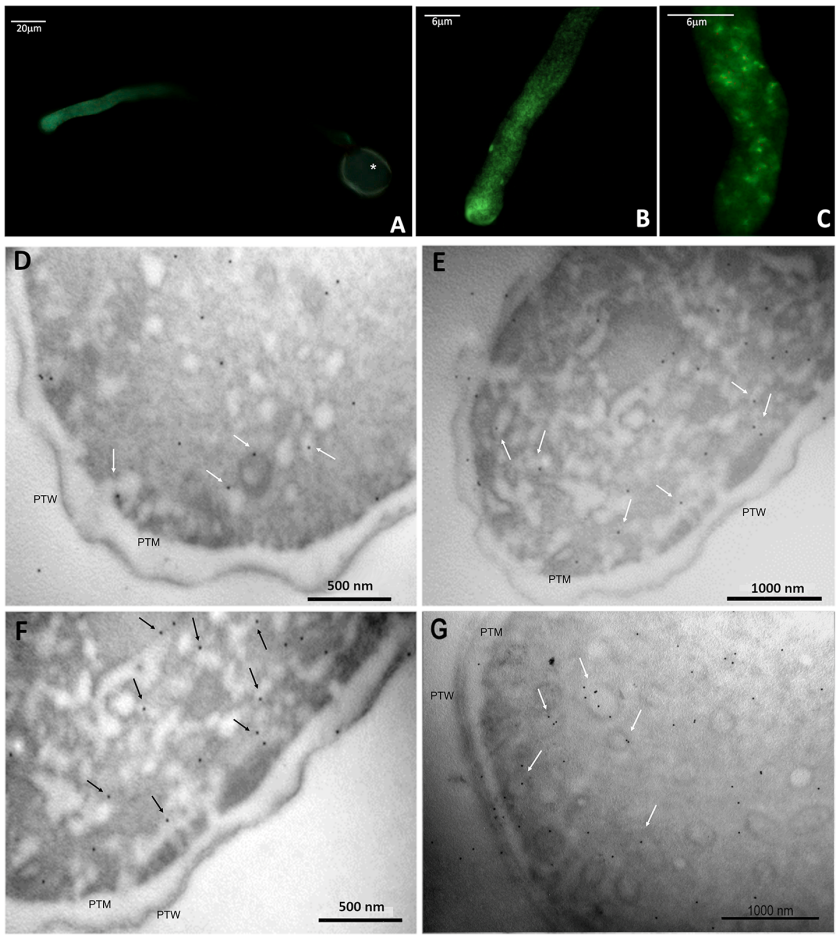

FIGURE 9
Immunolocalization of ALIX-homologs in kiwi pollen tube. **(A–C)**: indirect immunofluorescence labeling with FITC-conjugated secondary antibodies, probed for ALIX-homologs, at different magnifications.Tthe fluorescent labeling of the target proteins is pictured in green. In A, the autofluorescence of the pollen wall is visible (*). **(D–F)**: immunogold labeling of ALIX-homologs in transverse sections of kiwi pollen tube. Images were taken at the level of apex and subapex. Some of the proteins appear associated with subcellular structures compatible with vesicles (arrows), near the plasma membrane. PTW, pollen tube wall; PTM, pollen tube plasma membrane.

is possible that during the formation of exosomes, clathrin triskelions derived from the disassembly of endocytic vesicles coatings are still present in the cytoplasm near the endosome, and they might be incorporated in the ILVs lumen, as it happens for other cytoplasmic molecules (Kurian et al., 2021). In fact, dynamin and dynamin-related protein like, which are involved in the removal of clathrin coating from endocytic vesicles, were also identified in the GKP EVs proteome (Supplementary Table 1).

While proteomic analysis identified the presence of ARFs, ARF-GAPs, and ARF-GEFs in GKP EVs (Supplementary Table 1), ARF1, which is considered a molecular marker for Golgi membranes (Robinson et al., 2011), was not detected in EVs by immunoblotting (Figure 5). The absence of Golgi markers in GKP EVs could imply that these nanovesicles bypassed the Golgi apparatus and underwent unconventional secretion (Del Duca et al., 2013; Hafidh et al., 2016; Rabouille, 2017), which is in line with the exosome hypothesis. In fact, the proteomic analysis revealed the presence of proteins that have been found to be unconventionally secreted during pollen tube growth, such as actin, adenosine kinase (ADK), ARF/ARFGAP, Gp-dh-C domain containing proteins, HSP70, proteasome subunits, Ras, ribonucleoside-diphosphate reductase large subunit (RRM1), UDP-arabinopyranose mutase, and the translationally controlled tumor protein (NtTCTP) which is thought to be involved in pollen tube guidance and ovule targeting (Supplementary Tables 1, 2). Contrarily, only few proteins known to be conventionally secreted and abundant in germinated pollen secretome were found in EVs proteome (Hafidh et al., 2016). An exocyst subunit Exo70 was identified in the GKP EVs (Supplementary Table 1), but their staining with FM4-64^{TM} (Figure 3) indicates the presence of a lipidic bilayer, excluding the unconventional secretion by EXPOs, which produces single-layered extracellular vesicles (Wang et al., 2010; Hafidh et al., 2016). EVs proteomic analysis also identified proteins involved in signal transduction, e.g. a total of 277 kinases, and a cysteine protease family protein that could act as a ligand (Hafidh et al., 2016), and this is consistent with the role of exosomes in cell-cell communication.

However, as for Prado and colleagues (Prado et al., 2014) it was not possible in this study to visualize putative ILVs inside the vesicle-like structures associated with ALIX-homologs, and thus it was not possible to assess the presence of an MVB with the imaging techniques employed hereby. Nonetheless, the presence of ESCRT-related proteins in GKP EVs proteome reinforces the idea that at least

a prominent subpopulation of the isolated pollen extracellular nanovesicles could derive from MVBs, since ESCRT known functions in plant cells are related to the ILVs formation and possibly to the MVB fusion with the plasma membrane (Gao et al., 2017).

5 Conclusions

Pollen-pistil interactions have always been a fascinating yet elusive topic in plant molecular biology. Studies on pollen secretome are starting to shade light on the molecules involved in pollen hydration, pollen-stigma compatibility, pollen tube entrance, and tube guidance through the style (Del Duca et al., 2010; Hafidh et al., 2014; Hafidh et al., 2016; Mandrone et al., 2019). Since intercellular communication is fundamental for a successful fertilization, it is plausible that bioactive molecules might be secreted by pollen through vesicles, to stabilize them during their journey towards their target. In this study, a population of EVs released by kiwi pollen during in vitro germination was isolated and characterized using different proxies. These vesicles appeared to be consistent with the pollensomes described by Prado and colleagues (Prado et al., 2014; Prado et al., 2015), and also met several criteria in the definition of small EVs and exosomes (Suhandono et al., 2014; Théry et al., 2018; Kurian et al., 2021). In fact, they were isolated by centrifugation at 100000 × g, had an average diameter under 150 nm, a rounded shape, and a double-layered lipidic membrane. They also carried proteins involved in endocytosis such as clathrin, ESCRT-related proteins, and dynamin, suggesting an endocytic origin. This thesis is supported by the presence in their proteome of proteins that are usually unconventionally secreted, and the absence of the TGN marker ARF1, hinting that they followed an unconventional secretion route. Several proteins and protein families known to be common in exosomes were found, including Ras-related Rab proteins, one of which has been proposed as a possible plant exosome marker (Regente et al., 2009). Moreover, immunoblotting revealed an enrichment in a plant homolog of a well-known mammalian EVs marker, ALIX, that is proven to be involved in ILVs formation and cargo sorting. Immunolocalization revealed the presence of ALIX homologs along the growing pollen tube, and they were associated with vesicle-like organelles localized near the pollen tube wall. However, it was not possible to visualize MVBs in electron microscopy, hence it is still difficult to assess the exact biogenesis of these EVs.

On the other hand, the present study suggests that hydration in humid atmosphere does not seem to promote EVs secretion, averting the possibility for these small vesicles to represent airborne carriers of pollen allergens in humid environmental conditions.

While further investigation into these vesicles is surely needed to confirm their biogenesis and secretion route, this work contributes to deepen the still scarce knowledge on pollen EVs, and on the proteins that are possibly involved in their formation, release, and biological function.

Data availability statement

The data presented in this study are deposited in the PRIDE repository, accession number PXD039037.

Author contributions

EAMV and SDD conceived the presented idea and supervised the project. CS and IA developed the theory. CS planned and performed the experiments and wrote the manuscript. CC performed the proteomic analysis and analyzed the proteomic data. DJB supervised proteomic analysis and uploaded proteomic data to PRIDE. LP, ET, and MPS participated in performing the experiments and validating the results. Atomic force microscopy was carried out by EF, while GC and CF performed the electron microscopy. All authors contributed to the manuscript critique.

Funding

This work was supported by funds from the University of Bologna [Ricerca Fondamentale Orientata 19deldu and 20deldu] to SDD.

Acknowledgments

The authors would like to thank Professor Francesco Francia (University of Bologna) for the kind help with lab equipment.

Conflict of interest

The authors declare that the research was conducted in the absence of any commercial or financial relationships that could be construed as a potential conflict of interest.

Publisher's note

Supplementary material

The Supplementary Material for this article can be found online at: https://www.frontiersin.org/articles/10.3389/fpls.2023.1090026/full#supplementary-material

References

Akuma, P., Okagu, O. D., and Udenigwe, C. C. (2019). Naturally occurring exosome vesicles as potential delivery vehicle for bioactive compounds. *Front. Sustain. Food Syst.* 3. doi: 10.3389/fsufs.2019.00023

Altschul, S. F., Gish, W., Miller, W., Myers, E. W., and Lipman, D. J. (1990). Basic local alignment search tool. *J. Mol. Biol.* 215, 403–410. doi: 10.1016/S0022-2836(05)80360-2

Al-Whaibi, M. H. (2011). Plant heat-shock proteins: A mini review. *J. King Saud Univ. - Sci.* 23, 139–150. doi: 10.1016/J.JKSUS.2010.06.022

Anderson, L. E., Bryant, J. A., and Carol, A. A. (2004). Both chloroplastic and cytosolic phosphoglycerate kinase isozymes are present in the pea leaf nucleus. *Protoplasma* 2232 223, 103–110. doi: 10.1007/S00709-004-0041-Y

An, Q., Van Bel, A. J. E., and Hückelhoven, R. (2007). Do plant cells secrete exosomes derived from multivesicular bodies? *Plant Signal. Behav.* 2, 4–7. doi: 10.4161/psb.2.1.3596

Ben-Nissan, G., Katzir, N., Füzesi-Levi, M. G., and Sharon, M. (2022). Biology of the extracellular proteasome. *Biomolecules* 12, 619. doi: 10.3390/BIOM12050619/S1

Bissig, C., and Gruenberg, J. (2014). ALIX and the multivesicular endosome: ALIX in wonderland. *Trends Cell Biol.* 24, 19–25. doi: 10.1016/J.TCB.2013.10.009

Blackbourn, H. D., and Jackson, A. P. (1996). Plant clathrin heavy chain: Sequence analysis and restricted localisation in growing pollen tubes. *J. Cell Sci.* 109, 777–787. doi: 10.1242/jcs.109.4.777

Boccia, E., Alfieri, M., Belvedere, R., Santoro, V., Colella, M., Del Gaudio, P., et al. (2022). Plant hairy roots for the production of extracellular vesicles with antitumor bioactivity. *Commun. Biol.* 51 (5), 1–10. doi: 10.1038/s42003-022-03781-3

Boratyn, G. M., Schäffer, A. A., Agarwala, R., Altschul, S. F., Lipman, D. J., and Madden, T. L. (2012). Domain enhanced lookup time accelerated BLAST. *Biol. Direct* 7, 12. doi: 10.1186/1745-6150-7-12

Božič, A., and Šiber, A. (2022). Mechanics of inactive swelling and bursting of porate pollen grains. *Biophys. J.* 121, 782–792. doi: 10.1016/J.BPJ.2022.01.019

Chae, K., and Lord, E. M. (2011). Pollen tube growth and guidance: roles of small, secreted proteins. *Ann. Bot.* 108, 627. doi: 10.1093/AOB/MCR015

Cheung, A. Y., and Wu, H. M. (2008). Structural and signaling networks for the polar cell growth machinery in pollen tubes. *Annu. Rev. Plant Biol.* 59, 547–572. doi: 10.1146/annurev.arplant.59.032607.092921

Cui, Y., Shen, J., Gao, C., Zhuang, X., Wang, J., and Jiang, L. (2016). Biogenesis of plant prevacuolar multivesicular bodies. *Mol. Plant* 9, 774–786. doi: 10.1016/j.molp.2016.01.011

Del Duca, S., Cai, G., Di Sandro, A., and Serafini-Fracassini, D. (2010). Compatible and self-incompatible pollination in pyrus communis displays different polyamine levels and transglutaminase activity. *Amino Acids* 38, 659–667. doi: 10.1007/S00726-009-0426-5

Del Duca, S., Serafini-Fracassini, D., and Cai, G. (2013). An unconventional road for the secretion of transglutaminase in pollen tubes? *Plant Signal. Behav.* 8, 8–11. doi: 10.4161/psb.24446

Dumont, S., Bykova, N. V., Pelletier, G., Dorion, S., and Rivoal, J. (2016). Cytosolic triosephosphate isomerase from arabidopsis thaliana is reversibly modified by glutathione on cysteines 127 and 218. *Front. Plant Sci.* 7. doi: 10.3389/FPLS.2016.01942/BIBTEX

Furini, G., Schroeder, N., Huang, L., Boocock, D., Scarpellini, A., Coveney, C., et al. (2018). Proteomic profiling reveals the transglutaminase-2 externalization pathway in kidneys after unilateral ureteric obstruction. *J. Am. Soc Nephrol.* 29, 880–905. doi: 10.1681/ASN.2017050479

Gao, C., Zhuang, X., Shen, J., and Jiang, L. (2017). Plant ESCRT complexes: Moving beyond endosomal sorting. *Trends Plant Sci.* 22, 986–998. doi: 10.1016/J.TPLANTS.2017.08.003/ATTACHMENT/C7A3A70E-8C86-4FBC-90E0-E335130913E1/MMC1.MP4

García-León, M., and Rubio, V. (2020). Biochemical and imaging analysis of ALIX function in endosomal trafficking of arabidopsis protein cargoes. *Methods Mol. Biol.* 2177, 49–58. doi: 10.1007/978-1-0716-0767-1_5

Goring, D. R. (2017). Exocyst, exosomes, and autophagy in the regulation of brassicaceae pollen-stigma interactions. *J. Exp. Bot.* 69, 69–78. doi: 10.1093/jxb/erx340

Grote, M., Valenta, R., and Reichelt, R. (2003). Abortive pollen germination: A mechanism of allergen release in birch, alder, and hazel revealed by immunogold electron microscopy. *J. Allergy Clin. Immunol.* 111, 1017–1023. doi: 10.1067/mai.2003.1452

Grote, M., Vrtala, S., Niederberger, V., Valenta, R., and Reichelt, R. (2000). Expulsion of allergen-containing materials from hydrated rye grass (Lolium perenne) pollen revealed by using immunogold field emission scanning and transmission electron microscopy. *J. Allergy Clin. Immunol.* 105, 1140–1145. doi: 10.1067/mai.2000.107044

Gurung, S., Perocheau, D., Touramanidou, L., and Baruteau, J. (2021). The exosome journey: from biogenesis to uptake and intracellular signalling. *Cell Commun. Signal.* 19, 47. doi: 10.1186/S12964-021-00730-1

Hafidh, S., Potěšil, D., Fíla, J., Čapková, V., Zdráhal, Z., and Honys, D. (2016). Quantitative proteomics of the tobacco pollen tube secretome identifies novel pollen tube guidance proteins important for fertilization. *Genome Biol.* 17, 1–29. doi: 10.1186/s13059-016-0928-x

Hafidh, S., Potěšil, D., Fíla, J., Feciková, J., Čapková, V., Zdráhal, Z., et al. (2014). In search of ligands and receptors of the pollen tube: The missing link in pollen tube perception. *Biochem. Soc Trans.* 42, 388–394. doi: 10.1042/BST20130204

Hansen, L. L., and Nielsen, M. E. (2017). Plant exosomes: Using an unconventional exit to prevent pathogen entry? *J. Exp. Bot.* 69, 59–68. doi: 10.1093/jxb/erx319

Javeed, N., and Mukhopadhyay, D. (2017). Exosomes and their role in the micro-/macro-environment: A comprehensive review. *J. Biomed. Res.* 31, 386–394. doi: 10.7555/JBR.30.20150162

Jeppesen, D. K., Fenix, A. M., Franklin, J. L., Higginbotham, J. N., Zhang, Q., Zimmerman, L. J., et al. (2019). Reassessment of exosome composition. *Cell* 177, 428–445.e18. doi: 10.1016/J.CELL.2019.02.029

Johnstone, R. M. (2006). Exosomes biological significance: A concise review. *Blood Cells Mol. Dis.* 36, 315–321. doi: 10.1016/j.bcmd.2005.12.001

Kalinowska, K., Nagel, M. K., Goodman, K., Cuyas, L., Anzenberger, F., Alkofer, A., et al. (2015). Arabidopsis ALIX is required for the endosomal localization of the deubiquitinating enzyme AMSH3. *Proc. Natl. Acad. Sci. U. S. A.* 112, E5543–E5551. doi: 10.1073/PNAS.1510516112/-/DCSUPPLEMENTAL

Kawai, M., and Uchimiya, H. (1995). Biochemical properties of rice adenylate kinase and subcellular location in plant cells. *Plant Mol. Biol.* 27, 943–951. doi: 10.1007/BF00037022

Kurian, T. K., Banik, S., Gopal, D., Chakrabarti, S., and Mazumder, N. (2021). Elucidating methods for isolation and quantification of exosomes: A review. *Mol. Biotechnol.* 63, 249–266. doi: 10.1007/s12033-021-00300-3

Kuttiyatveetil, J. R. A., and Sanders, D. A. R. (2017). Analysis of plant UDP-arabinopyranose mutase (UAM): Role of divalent metals and structure prediction. *Biochim. Biophys. Acta - Proteins Proteomics* 1865, 510–519. doi: 10.1016/J.BBAPAP.2017.02.005

Linares, R., Tan, S., Gounou, C., Arraud, N., and Brisson, A. R. (2015). High-speed centrifugation induces aggregation of extracellular vesicles. *J. Extracell. Vesicles* 4. doi: 10.3402/JEV.V4.29509

Lu, W., Tang, X., Huo, Y., Xu, R., Qi, S., Huang, J., et al. (2012). Identification and characterization of fructose 1,6-bisphosphate aldolase genes in arabidopsis reveal a gene family with diverse responses to abiotic stresses. *Gene* 503, 65–74. doi: 10.1016/J.GENE.2012.04.042

Mandrone, M., Antognoni, F., Aloisi, I., Potente, G., Poli, F., Cai, G., et al. (2019). Compatible and incompatible pollen-styles interaction in pyrus communis l. show different transglutaminase features, polyamine pattern and metabolomics profiles. *Front. Plant Sci.* 10. doi: 10.3389/FPLS.2019.00741/BIBTEX

Narasimhan, M., Johnson, A., Prizak, R., Kaufmann, W. A., Tan, S., Casillas-Pérez, B., et al. (2020). Evolutionarily unique mechanistic framework of clathrin-mediated endocytosis in plants. *Elife* 9. doi: 10.7554/ELIFE.52067

Olvera-Carrillo, Y., Reyes, J. L., and Covarrubias, A. A. (2011). Late embryogenesis abundant proteins: Versatile players in the plant adaptation to water limiting environments. *Plant Signal. Behav.* 6, 586. doi: 10.4161/PSB.6.4.15042

Paris, R., Pagliarani, G., Savazzini, F., Aloisi, I., Iorio, R. A., Tartarini, S., et al. (2017). Comparative analysis of allergen genes and pro-inflammatory factors in pollen and fruit of apple varieties. *Plant Sci.* 264, 57–68. doi: 10.1016/J.PLANTSCI.2017.08.006

Parrotta, L., Aloisi, I., Suanno, C., Faleri, C., Kiełbowicz-Matuk, A., Bini, L., et al. (2019). A low molecular-weight cyclophilin localizes in different cell compartments of pyrus communis pollen and is released *in vitro* under Ca2+ depletion. *Plant Physiol. Biochem.* 144, 197–206. doi: 10.1016/J.PLAPHY.2019.09.045

Parrotta, L., Faleri, C., Del Duca, S., and Cai, G. (2018). Depletion of sucrose induces changes in the tip growth mechanism of tobacco pollen tubes. *Ann. Bot.* 122, 23–43. doi: 10.1093/aob/mcy043

Parton, R. M., Fischer-Parton, S., Trewavas, A. J., and Watahiki, M. K. (2003). Pollen tubes exhibit regular periodic membrane trafficking events in the absence of apical extension. *J. Cell Sci.* 116, 2707–2719. doi: 10.1242/jcs.00468

Prado, N., De Dios Alché, J., Casado-Vela, J., Mas, S., Villalba, M., Rodríguez, R., et al. (2014). Nanovesicles are secreted during pollen germination and pollen tube growth: A possible role in fertilization. *Mol. Plant* 7, 573–577. doi: 10.1093/mp/sst153

Prado, N., De Linares, C., Sanz, M. L., Gamboa, P., Villalba, M., Rodríguez, R., et al. (2015). Pollensomes as natural vehicles for pollen allergens. *J. Immunol.* 195, 445–449. doi: 10.4049/jimmunol.1500452

Rabouille, C. (2017). Pathways of unconventional protein secretion. *Trends Cell Biol.* 27, 230–240. doi: 10.1016/J.TCB.2016.11.007

Regente, M., Corti-Monzón, G., Maldonado, A. M., Pinedo, M., Jorrín, J., and de la Canal, L. (2009). Vesicular fractions of sunflower apoplastic fluids are associated with potential exosome marker proteins. *FEBS Lett.* 583, 3363–3366. doi: 10.1016/j.febslet.2009.09.041

Robinson, D. G., Scheuring, D., Naramoto, S., and Friml, J. (2011). ARF1 localizes to the golgi and the trans-golgi network. *Plant Cell* 23, 846. doi: 10.1105/TPC.110.082099

RStudio Team (2020) *RStudio: Integrated development for r*. Available at: http://www.rstudio.com/.

Rutter, B. D., and Innes, R. W. (2017). Extracellular vesicles isolated from the leaf apoplast carry stress-response proteins. *Plant Physiol.* 173, 728–741. doi: 10.1104/pp.16.01253

Saqib, A., Scheller, H. V., Fredslund, F., and Welner, D. H. (2019). Molecular characteristics of plant UDP-arabinopyranose mutases. *Glycobiology* 29, 839. doi: 10.1093/GLYCOB/CWZ067

Schneider, C. A., Rasband, W. S., and Eliceiri, K. W. (2012). NIH Image to image J: 25 years of image analysis. *Nat. Methods* 97 9, 671–675. doi: 10.1038/nmeth.2089

Sebaihi, N., De Boeck, B., Yuana, Y., Nieuwland, R., and Pétry, J. (2017). Dimensional characterization of extracellular vesicles using atomic force microscopy. *Meas. Sci. Technol.* 28, 1–8. doi: 10.1088/1361-6501/28/3/034006

Siriwattanakul, U., Piboonpocanun, S., and Songnuan, W. (2019). Rapid pollen rupture and release of pollen cytoplasmic granules upon hydration of allergenic grass and weed species commonly found in subtropical regions. *Aerobiologia (Bologna).* 35, 719–730. doi: 10.1007/s10453-019-09611-0

Suhandono, S., Apriyanto, A., and Ihsani, N. (2014). Isolation and characterization of three cassava elongation factor 1 alpha (MeEF1A) promoters. *PLoS One* 9. doi: 10.1371/JOURNAL.PONE.0084692

Supek, F., Bošnjak, M., Škunca, N., and Šmuc, T. (2011). REVIGO summarizes and visualizes long lists of gene ontology terms. *PLoS One* 6, e21800. doi: 10.1371/JOURNAL.PONE.0021800

Szklarczyk, D., Gable, A. L., Nastou, K. C., Lyon, D., Kirsch, R., Pyysalo, S., et al. (2021). The STRING database in 2021: customizable protein–protein networks, and functional characterization of user-uploaded gene/measurement sets. *Nucleic Acids Res.* 49, D605–D612. doi: 10.1093/NAR/GKAA1074

Théry, C., Witwer, K. W., Aikawa, E., Alcaraz, M. J., Anderson, J. D., Andriantsitohaina, R., et al. (2018). Minimal information for studies of extracellular vesicles 2018 (MISEV2018): A position statement of the international society for extracellular vesicles and update of the MISEV2014 guidelines. *J. Extracell. Vesicles* 7, 1–43. doi: 10.1080/20013078.2018.1535750

The UniProt Consortium (2021). UniProt : The universal protein knowledgebase in 2021. *Nucleic Acids Res.* 49, 480–489. doi: 10.1093/nar/gkaa1100

Thomas, P. D., Ebert, D., Muruganujan, A., Mushayahama, T., Albou, L. P., and Mi, H. (2022). PANTHER: Making genome-scale phylogenetics accessible to all. *Protein Sci.* 31, 8–22. doi: 10.1002/PRO.4218

Tiwari, A., Kumar, P., Singh, S., and Ansari, S. A. (2005). Carbonic anhydrase in relation to higher plants. *Photosynthetica* 43, 1–11. doi: 10.1007/s11099-005-1011-0

Vannini, C., Marsoni, M., Scoccianti, V., Ceccarini, C., Domingo, G., Bracale, M., et al. (2019). Proteasome-mediated remodeling of the proteome and phosphoproteome during kiwifruit pollen germination. *J. Proteomics* 192, 334–345. doi: 10.1016/J.JPROT.2018.09.014

Wang, L., Clarke, L. A., Eason, R. J., Parker, C. C., Qi, B., Scott, R. J., et al. (2017). PCP-b class pollen coat proteins are key regulators of the hydration checkpoint in arabidopsis thaliana pollen–stigma interactions. *New Phytol.* 213, 764–777. doi: 10.1111/NPH.14162

Wang, J., Ding, Y., Wang, J., Hillmer, S., Miao, Y., Lo, S. W., et al. (2010). EXPO, an exocyst-positive organelle distinct from multivesicular endosomes and autophagosomes, mediates cytosol to cell wall exocytosis in arabidopsis and tobacco cells. *Plant Cell* 22, 4009–4030. doi: 10.1105/TPC.110.080697

Wang, J., Kambhampati, S., Allen, D. K., and Chen, L. Q. (2022). Comparative metabolic analysis reveals a metabolic switch in mature, hydrated, and germinated pollen in arabidopsis thaliana. *Front. Plant Sci.* 13. doi: 10.3389/FPLS.2022.836665/BIBTEX

Woith, E., Guerriero, G., Hausman, J. F., Renaut, J., Leclercq, C. C., Weise, C., et al. (2021). Plant extracellular vesicles and nanovesicles: Focus on secondary metabolites, proteins and lipids with perspectives on their potential and sources. *Int. J. Mol. Sci.* 22, 1–20. doi: 10.3390/ijms22073719

frontiers | Frontiers in Plant Science

TYPE Perspective
PUBLISHED 26 January 2023
DOI 10.3389/fpls.2023.1116289

OPEN ACCESS

EDITED BY
Giampiero Cai,
University of Siena, Italy

REVIEWED BY
Xiongbo Peng,
Wuhan University, China

*CORRESPONDENCE
Daisuke Maruyama,
dmaru@yokohama-cu.ac.jp

SPECIALTY SECTION
This article was submitted to Plant Cell Biology, a section of the journal Frontiers in Plant Science

RECEIVED 05 December 2022
ACCEPTED 17 January 2023
PUBLISHED 26 January 2023

CITATION
Sugi N, Izumi R, Tomomi S, Susaki D, Kinoshita T and Maruyama D (2023) Removal of the endoplasma membrane upon sperm cell activation after pollen tube discharge.
Front. Plant Sci. 14:1116289.
doi: 10.3389/fpls.2023.1116289

Removal of the endoplasma membrane upon sperm cell activation after pollen tube discharge

Naoya Sugi, Rie Izumi, Shun Tomomi, Daichi Susaki, Tetsu Kinoshita and Daisuke Maruyama*

Kihara Institute for Biological Research, Yokohama City University, Yokohama, Japan

In pollen and pollen tubes, immotile sperm cells are enclosed by an inner vegetative plasma membrane (IVPM), a single endomembrane originating from the vegetative-cell plasma membrane. It is widely believed that sperm cells must be removed from the IVPM prior to gamete associations and fusions; however, details of the timing and morphological changes upon IVPM dissociation remain elusive. Here, we report a rapid IVPM breakdown immediately before double fertilization in *Arabidopsis thaliana*. The IVPM was stably observed in coiling pollen tubes when pollen tube discharge was prevented using *lorelei* mutant ovules. In contrast, a semi-*in vivo* fertilization assay in wild-type ovules demonstrated fragmented IVPM around sperm nuclei 1 min after pollen tube discharge. These observations revealed the dynamic alteration of released sperm cells and provided new insights into double fertilization in flowering plants. With a summary of recent findings on IVPM lipid composition, we discussed the possible physiological signals controlling IVPM breakdown.

KEYWORDS

pollen tube, sperm cell, vegetative nucleus, male germ unit (MGU), double fertilization

1 Introduction

A rapidly growing pollen tube transports immotile sperm cells to female gametes. Analyzing the dynamic morphological changes of sperm cells is important in understanding the unique reproduction of flowering plants. During male gametogenesis, pollen microspores undergo mitosis twice. The first asymmetric division (pollen mitosis I) produces a vegetative cell and a generative cell. Generative cells are enveloped within vegetative cells. Generative cells undergo symmetrical mitotic division (pollen mitosis II), producing two sperm cells. Following these unusual internalization events, a single membrane derived from the vegetative cell membrane encloses the generative and sperm cells. Electron micrographs of mature pollen demonstrated that the sperm-enclosing endoplasma membrane—inner vegetative plasma membrane (IVPM)—is closely apposed to the plasma membrane in several organisms as symbiotic organelle membranes, such as the inner and outer membranes of mitochondria (Jensen and Fisher, 1970; Russell and Cass,

1981; Dumas et al., 1985). A tail-like protrusion extending from one of the sperm cells tightly connects to the vegetative cell nucleus. This trinuclear assemblage is termed the male germ unit (MGU) (Figure 1) (Dumas et al., 1985).

The MGU is maintained in the apical region during pollen tube growth. When the pollen tube reaches the ovule, it discharges the MGU with its cytoplasmic contents deep inside the pistils, where double fertilization occurs: two sperm cells fertilize the egg and central cells. Thus, early studies often used histochemical approaches to investigate reproductive events in pollinated pistils. However, snapshots of fixed samples rarely capture rapid fertilization events, particularly a series of sperm cell behaviors after pollen tube discharge. A detailed time course of double fertilization anticipates the establishment of a semi-*in vivo* fertilization assay in *Arabidopsis thaliana* (Hamamura et al., 2011). Released sperm cells immediately reach the egg cell (8.8 ± 5.5 s), and double fertilization occurs within 7.4 ± 3.3 min. This observation raised new questions about how essential gamete interactions occur in plants within this short period. It has been postulated that IVPM removal and sperm plasma membrane exposure occur immediately after pollen tube discharge to ensure rapid gamete interactions (Sprunck, 2020).

IVPM and sperm plasma membrane are morphologically similar in intact pollen grains and tubes (Li et al., 2013; Billey et al., 2021; Gilles et al., 2021; Motomura et al., 2021). However, it was recently discovered that previously reported IVPM marker proteins are expressed in vegetative cells and exhibit peripheral membrane

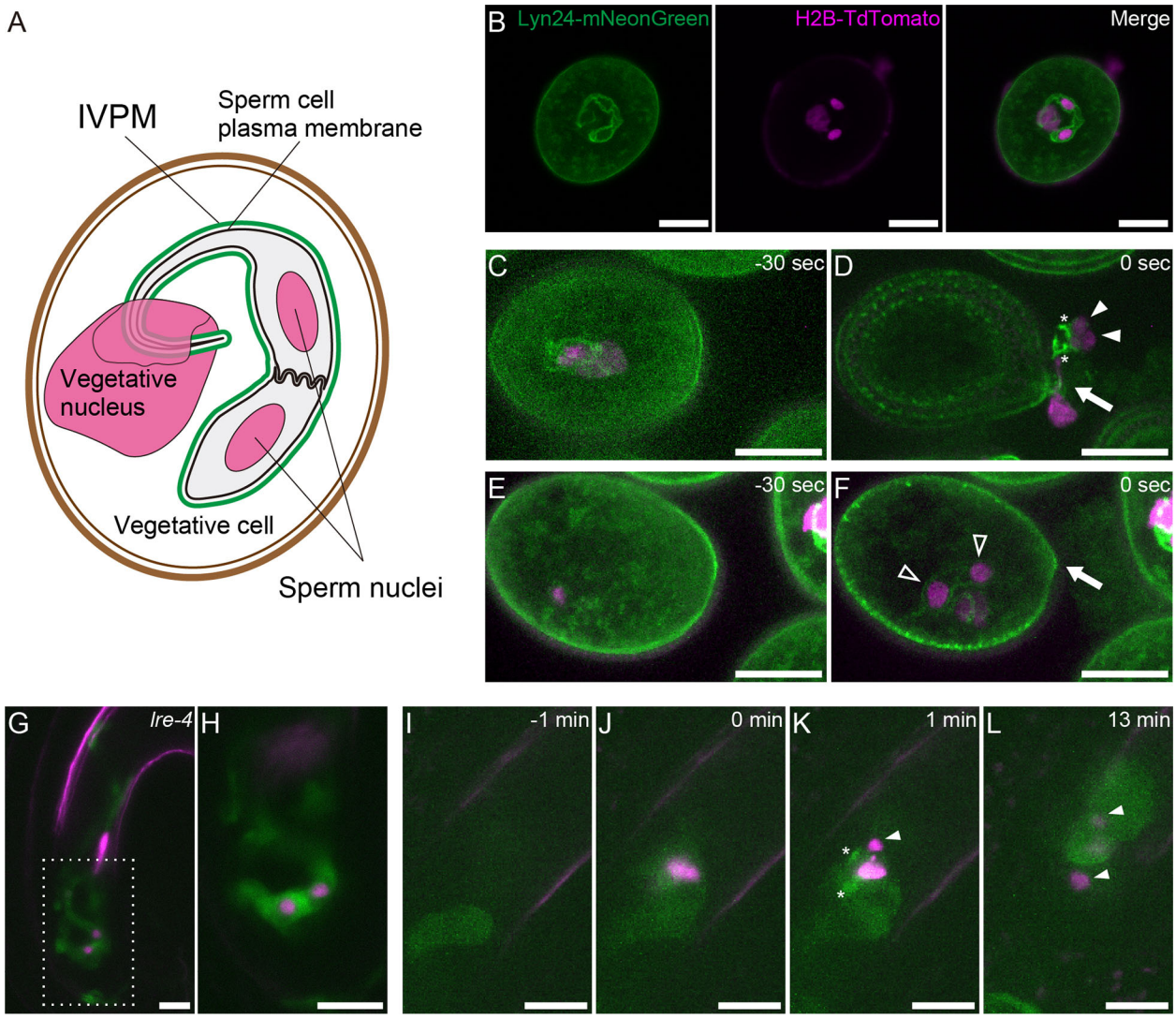

FIGURE 1
Structure and dynamics of IVPM. **(A)** Schematic drawings of the male germ unit (MGU) in *Arabidopsis* mature pollen. **(B)** Confocal images of a pollen grain in the *pACA3:Lyn24- mNeonGreen; pRPS5A:H2B-tdTomato* double marker. **(C–F)** Maximum intensity projections of *in vitro*-cultured *anx1/2* mutant pollen carrying the *pACA3:Lyn24-mNeonGreen; pRPS5A:H2B-tdTomato* double maker. Rapid transition from sperm cell-enclosing IVPM **(C)** to fragmented IVPM **(D)** occurred within 30 sec during sperm cell release. In contrast, sperm cell-enclosing IVPM was persistently observed before **(E)** or after **(F)** pollen tube rupture when the sperm failed to exit the pollen grain. Arrows indicate breaks of germinating pollen tubes; filled arrowheads, sperm nuclei dissociated from IVPM; open arrowheads, sperm nuclei within IVPM; and asterisks, fragmented IVPM. See also Supplementary Figure 1. **(G)** Representative projection image of a pollen tube growing in the *lre-4* mutant ovule 12–18 h after pollination. **(H)** Single plane confocal image of the dashed area in **(G)**. **(I–L)** Time-lapse imaging of IVPM breakdown during fertilization. Discharging of the *pACA3:Lyn24-mNeonGreen; pRPS5A:H2B-tdTomato* double marker pollen tube in the wild-type ovule was analyzed using semi-*in vivo* fertilization assay. Arrowheads indicate sperm nuclei. Asterisks indicate fragmented IVPM. See also Supplementary Movie 1. Scale bars: 10 µm.

associations with IVPM. According to the analysis of an IVPM-localized patatin-like phospholipase MATRILINEAL/ZmPHOSPHOLIPASE A1/NOT LIKE DAD (MTL/ZmPLA1/NLD) in maize, IVPM dissociates from sperm cells in both *in vitro* and *in vivo* conditions, such as after osmotic shock-induced pollen tube rupture and in the pollen tube receiving ovules, respectively (Gilles et al., 2021). However, the timing and morphological changes of IVPM breakdown remain elusive. We report the observation of rapid IVPM breakdown after pollen tube discharge, the mechanisms underlying IVPM stability, trigger signals of IVPM breakdown, and future directions of cell biology focusing on IVPM.

2 Material and methods

2.1 Plant materials and growth conditions

Arabidopsis thaliana Columbia-0 was used as the wild-type (WT) plant. The *pRPS5A:H2B-tdTomato pACA3:Lyn24-mNeonGreen* double marker has been previously described (Motomura et al., 2021). The *lorelei-4* (*lre-4*) mutant (SAIL_8_D07) was provided by Dr. Palanivelu (Univ. Arizona) (Tsukamoto et al., 2010). The double mutant of *anxur1-1* (*anx1-1*) and *anx2-2* was provided by Dr. Miyazaki through Dr. Mizuta (Nagoya Univ.) (*anx1-1*: SALK_016179, *anx2-2*: SALK_133057). Seeds were germinated on Murashige-Skoog medium and transferred to soil. Plants were grown at 22°C under continuous lighting conditions.

2.2 Microscopy

Mature pollen grains and *lre-4* ovules were mounted in 5% sucrose solution. Samples were observed using a confocal laser-scanning microscope equipped with a 63× objective lens (Leica TCS SP8; Leica, Wetzlar, Germany). The mNeonGreen was excited at 506 nm laser irradiation of the white light laser, and the fluorescence was detected using a Hybrid Detector (HyD) with a range of 511–553 nm. The tdTomato was excited at 554 or 558 nm laser irradiation of the white light laser, and the fluorescence was detected using an HyD with a range of 559–670 nm. Time-lapse images of the semi-*in vivo* fertilization assay was acquired every minute using the G/R split mode of an inverted microscope (IX-73; Olympus, Tokyo, Japan) equipped with a 60× objective lens, a spinning disk confocal scanning unit (CSU-W1; Yokogawa, Tokyo, Japan), and an sCMOS camera (Zyla 4.2; Andor, Belfast, Northern Ireland).

2.3 Observation of *in vitro* pollen tube rupture

The pollen grains were placed on pollen tube growth medium (0.01% boric acid, 5 mM $CaCl_2$, 5 mM KCl, 1 mM $MgSO_4$, 10% sucrose, 10 µM epibrassinolide, 1.5% NuSieve GTG agarose, pH7.5) solidified on a glass bottom dish (D11130H; Matsunami Glass, Osaka, Japan). Pollen tube rupture was observed using the spinning disk confocal microscopy during incubation at 22°C.

2.4 Semi-*in vivo* fertilization assay

Semi-*in vivo* fertilization assays were performed as previously described with minor modifications (Susaki et al., 2017). Emasculated WT pistils were cut beneath the style using a 27-gauged needle. The pistils were placed on pollen tube growth medium (0.001% boric acid, 1.27 mM Ca $(NO_3)_2$, 0.4 mM $MgSO_4$, 14% sucrose, 10 µM epibrassinolide, 1.5% NuSieve GTG agarose, pH7.0) solidified on a glass bottom dish (D11130H; Matsunami Glass, Osaka, Japan). Afterward, the stigma was pollinated with pollen from the *pRPS5A:H2B-tdTomato pACA3:Lyn24-mNeonGreen* plant. WT ovules were dissected from the emasculated pistils and aligned in front of the pollinated style. After 3 h of incubation at 22°C, pollen tubes reaching the ovules were observed using spinning disk confocal microscopy.

3 Results

To visualize IVPM dynamics, we used *pACA3:Lyn24-mNeonGreen*; *pRPS5A:H2B-tdTomato* double marker line (Motomura et al., 2021). The *pRPS5A:H2B-tdTomato* is a ubiquitous nuclear marker (Maruyama et al., 2013). Lyn24 is an N-terminal 24 amino acid of the murine Lyn protein that employs myristoylation and palmitoylation signals. The Lyn24-mNeonGreen fusion protein expressed from the vegetative cell–specific *ACA3* promoter efficiently labels the IVPM (Li et al., 2013). Confocal images of mature pollen grains showed eyeglass-shaped IVPM encasing two sperm nuclei and a tail structure connected to the vegetative nucleus (Figure 1). To observe the dynamics of IVPM during pollen tube discharge, we first performed *in vitro* assay of the *anx1-1 anx2-2* mutant (*anx1/2*) harboring *pACA3:Lyn24-mNeonGreen pRPS5A:H2B-tdTomato* markers with 30-s intervals. ANX1 and ANX2 are *Catharanthus roseus* receptor-like kinase 1-like (CrRLK1L)-type receptors that regulate the integrity of growing pollen tubes (Boisson-Dernier et al., 2009; Miyazaki et al., 2009). The *anx1/2* mutant pollen tubes ruptured soon after germination on the medium, which is expected to mimic the physiological state of native pollen tube reception. Among 13 cases of spontaneous discharge, nine showed immediate IVPM fragmentation and sperm cell separation after the release of MGUs from pollen grains (Figures 1C, Supplementary Figure 1A). In the other four cases, however, MGUs remained in the pollen and IVPM fragmentation was not observed (Figures 1E, Supplementary Figure 1B). These *in vitro* observations suggest that IVPM integrity is maintained until complete sperm cell release, and IVPM breakdown occurs through rapid IVPM fragmentation.

To examine IVPM in ovules prior to pollen tube reception, we analyzed *lre-4* mutant pistils pollinated with the double marker pollen. LORELEI is a GPI-anchored protein expressed in synergid cells and regulates pollen tube reception (Capron et al., 2008; Tsukamoto et al., 2010). As reported previously, the pollen tube exhibited overgrowth in the synergid cells of *lre-4* mutant ovules 12–18 h after pollination (Figures 1G). Notably, we observed an eyeglass-shaped IVPM pattern in coiling pollen tubes (n = 21), confirming a stable IVPM just before pollen tube discharge.

We then performed a semi-*in vivo* fertilization assay to monitor native IVPM breakdown in ovules. In this assay, WT ovules and pistils pollinated with the double marker pollen were incubated together on a medium, and the pollen tube discharge and double fertilization were captured using time-lapse imaging with 1-minute intervals (Figures 1I). Among 13 ovules analyzed, mNeonGreen signal of intact IVPM was detected around sperm nuclei before pollen tube discharge in five ovules (Supplementary Movie 1 ovule #2 and #3). However, the IVPM signal became fragmented or ambiguous within one min after pollen tube rupture, suggesting that rapid IVPM breakdown coincided with sperm cell release (Figures 1J, Supplementary Movie 1 ovule #1, #2). Thereafter, two sperm nuclei migrated in different directions, indicating a decisive feature of plasmogamy that showed the beginning of the nuclear congression stage in the egg and central cells (Figure 1). Overall, we observed a dynamic transition in IVPM stability upon pollen tube discharge.

4 Discussion

4.1 Pollen tube discharge triggers rapid transition in IVPM stability

IVPM is supposed to dissociate from sperm cells to allow quick gamete associations after discharge; although, membrane dynamics remain elusive (Sprunck, 2020). Through *in vitro* and semi-*in vivo* assays, we observed immediate IVPM fragmentation after sperm cell release. IVPM breakdown displayed good contrast to IVPM robustness before pollen tube discharge. These observations highlighted the rapid transition in IVPM stability.

WT pollen tubes maintained an eyeglass-like IVPM morphology throughout the growth phase (Figures 1G). In the pollen tube, the MGU is continuously exposed to mechanical stresses: stretching, twisting, and moving back and forth in intense protoplasmic flow (Schattner et al., 2020). The MGU structure, particularly the tail-like connection, becomes fragile after reducing cellular stiffness by disrupting the coordination of motility between a pair of sperm cells and the vegetative nucleus (Zhou and Meier, 2014; Motomura et al., 2021). We assume that IVPM has sophisticated homeostasis systems that maintain membrane integrity to resist excess mechanical forces and spontaneous membrane breaks. For example, the ESCRT-III complex is a good candidate for controlling IVPM integrity because it promotes membrane repair in a variety of organelles (Gatta and Carlton, 2019; Isono, 2021). The coordination of lipid biosynthesis and proper membrane trafficking would also contribute to IVPM integrity by maintaining the tight membrane association between IVPM and sperm plasma membrane.

Released sperm cells immediately showed IVPM fragmentation and separated from each other (Figures 1C, D). Such a finding was reported in earlier studies, where sperm cells were isolated from mature pollen grains or pollen tubes (Russell, 1986; Zhang et al., 1992; Borges et al., 2008; Russell et al., 2017). It is still unclear whether these *in vitro* sperm cell separations reflect native IVPM breakdown because mechanistic damage by homogenization or osmotic shock could induce artificial IVPM removal during the isolation procedures. By contrast, we directly observed IVPM breakdown using systems closer to the *in vivo* conditions, which clarified the timing of IVPM breakdown unanswered by the analyses of pollinated pistil in *Plumbago* and maize (Russell, 1983; Gilles et al., 2021). According to the original study of *Arabidopsis* imaging of double fertilization, gamete mergers occur within 7.4 ± 3.3 min after pollen tube discharge (Hamamura et al., 2011). During a short period, sperm cells must complete various events, including fine adjustment of sperm cell position (Huang et al., 2015) and consecutive interactions of male and female gametes, including adhesion, recognition, and fusion (Igawa et al., 2013; Sprunck, 2020). Furthermore, recent studies have depicted a scenario of sperm cell activation prior to gamete fusion, in which egg cell-secreted EC1 family peptides trigger the relocation of the *bona fide* fusogenic factor GCS1-HAP2 on the surface of the sperm plasma membrane in a tetra-spanning membrane proteins DMP8 and DMP9 dependent manner (Sprunck et al., 2012; Cyprys et al., 2019; Wang et al., 2022). Rapid IVPM breakdown could be the initial step in sperm cell activation, which exposes the sperm cell surface and allows EC1-mediated activation and subsequent gamete interactions. Thus, analyzing the two opposing states of IVPM (Figure 2)—stable and vulnerable—and understanding the transition mechanisms of IVPM stability will become important issues for future research on double fertilization.

4.2 Possible trigger signal of IVPM breakdown

Plants must control the timing of IVPM breakdown because even a slight delay or precocious IVPM disappearance from sperm cells could compromise double fertilization and reduce reproductive fitness. Abiotic stimuli upon pollen tube discharge, including osmotic shock or abrasion on cell wall surface, may explain such a timing control. Intact sperm cell pairs were obtained from various species by employing moderate isolation protocols; some studies detected IVPM capsule (Taylor et al., 1991; Southworth and Kwiatkowski, 1996; Sprunck et al., 2012; Gilles et al., 2021). IVPM behavior in *anx1/2* mutant was also consistent with the abiotic stimulation hypothesis (Figures 1C). However, these *ex vivo* releases would provide non-native physiological conditions to the sperm cells. Moreover, this hypothesis does not explain well the distinctive selectivity of IVPM breakdown discussed below. Hence, current data cannot exclude the relevance of other signaling cues at peak during intimate male–female interaction.

Putative signals that trigger IVPM breakdown should be temporarily elevated at the time of pollen tube rupture. Pollen tube cell wall integrity is regulated using an autocrine system, in which CrRLK1L-type receptors, ANX1, ANX2, BUDDHA'S PAPER SEAL 1 (BUPS1), and BUPS2 receive RAPID ALKALINIZATION FACTOR 4 (RALF4) and RALF19 peptides at the pollen tube tips (Boisson-Dernier et al., 2009; Miyazaki et al., 2009; Ge et al., 2017; Mecchia et al., 2017; Zhou et al., 2021). A competitive RALF34 ligand expressed in the ovules disrupts cell wall integrity before tube discharge. However, there is little evidence that the maximum signal of RALF34 can accurately determine the timing of IVPM breakdown *via* the ANX/BUPS pathway. Because *anx1/2* mutant did not show IVPM fragmentation before MGU release, the ANX/BUPS pathway unlikely determines the timing of IVPM breakdown (Figures 1C, Supplementary Figure 1).

Inorganic environmental changes surrounding the MGU could possibly trigger IVPM breakdown. Reactive oxygen species (ROS),

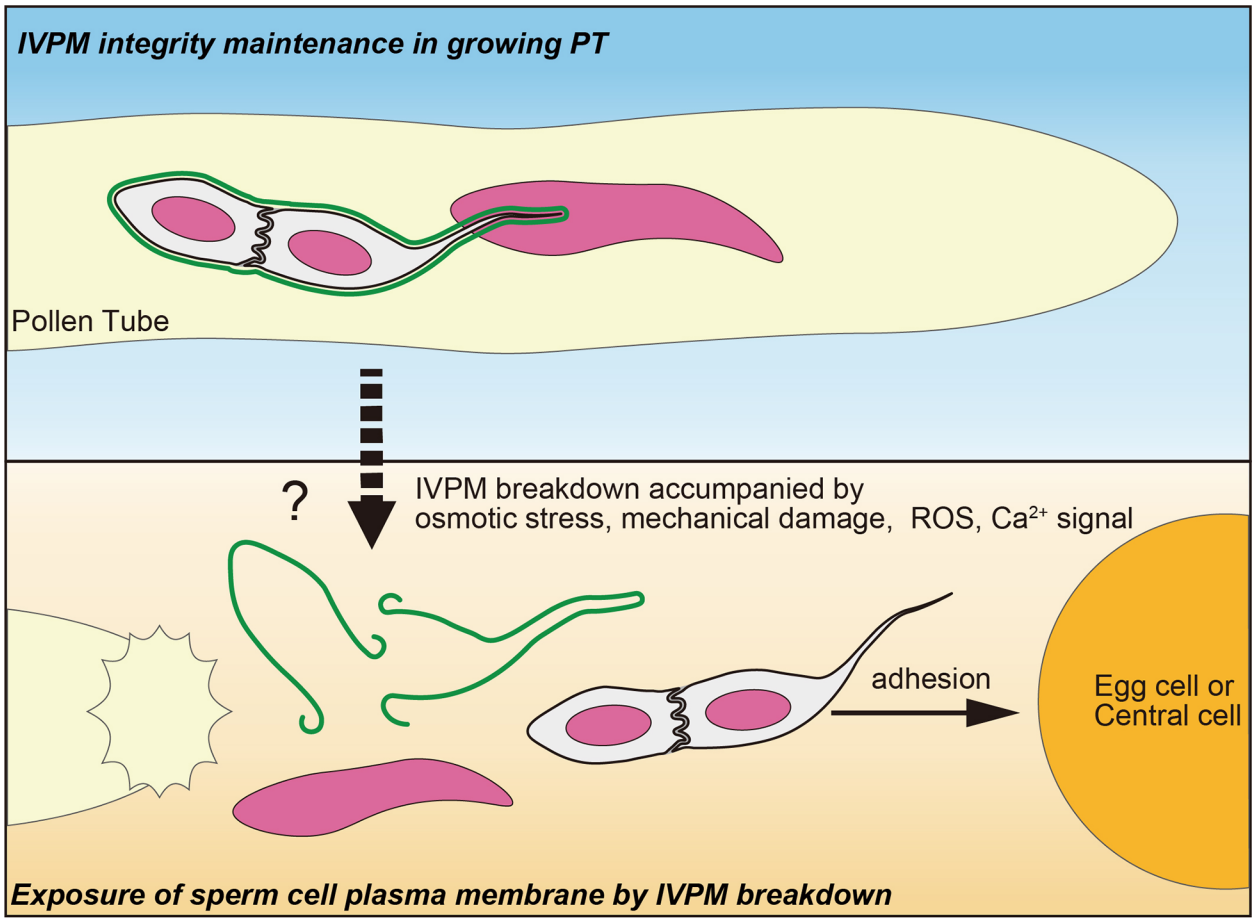

FIGURE 2
A fine control of IVPM breakdown prior to gamete interaction. Upper panel indicates stable IVPM whose integrity is maintained until pollen tube (PT) discharge. Lower panel shows selective elimination of IVPM after PT discharge. Trigger signal(s) of the IVPM breakdown would arise simultaneously with PT discharge, and thus may be caused by osmotic stress, mechanical damage, ROS and/or Ca^{2+} signal. Due to IVPM breakdown, sperm cells must expose their plasma membranes beforehand to adhere, recognize, and fuse with the egg or central cells.

most likely nitric oxide, are produced at high concentrations in synergid cells; *lre* mutants exhibit lower ROS levels than that of the WT (Duan et al., 2014; Duan et al., 2020). The characteristic pollen tube overgrowth phenotype in *lre* mutant ovules can be phenocopied *via* scavenger treatment in WT pistils, suggesting an important role of ROS in pollen tube rupture (Duan et al., 2014). However, these observations are insufficient to predict the ROS-dependent IVPM breakdown mechanism, as dynamic changes in ROS levels during fertilization remain to be analyzed. If synergid cells exhibited a clear oxidative burst upon pollen tube reception, highly membrane-permeable ROS would be an ideal intercellular signal controlling the delicate spatiotemporal activation of sperm cells and/or IVPM breakdown.

Compared with other signaling molecules, the dynamics of signal change were best characterized in cytoplasmic Ca^{2+} during double fertilization. In the time-lapse imaging of semi-*in vivo* fertilization assay using genetically encoded Ca^{2+} sensors, two synergid cells began to show Ca^{2+} oscillation immediately after pollen tube arrival (Ngo et al., 2014). The synergid cells and pollen tube produce a steep cytoplasmic Ca^{2+} elevation upon pollen tube rupture (Iwano et al., 2012; Ngo et al., 2014). Moreover, Ca^{2+} is considered as a putative gamete activator because Ca^{2+} spikes were also observed in the egg and central cells upon pollen tube discharge (Denninger et al., 2014; Hamamura et al., 2014). However, the inhibition of Ca^{2+} influx severely affects pollen tube growth and discharge (Duan et al., 2014). Simple pharmacological and genetic approaches are not applicable to semi-*in vivo* fertilization assays. Thus, decoding the physiological role of Ca^{2+} spikes in IVPM breakdown would be challenging without considerable technical advances in the future.

4.3 Molecules required for selective IVPM elimination

One of the most striking features of IVPM breakdown is its high membrane selectivity: IVPM breakdown must occur without damaging the sperm plasma membrane closely apposed with IVPM until pollen tube rupture. This selectivity may be because of its unique phospholipid composition: enriched phosphatidylserine and phosphatidylinositol 4,5-bisphosphate (Gilles et al., 2021). Anionic phospholipids are also enriched in the tips of pollen tube plasma membrane and play an important role in pollen tube growth (Helling et al., 2006; Zhou et al., 2020). It is interesting if membrane-degenerating factors are recruited to the anionic phospholipid–rich membrane domains and induce selective and simultaneous

membrane rupture at the pollen tube tip and IVPM. Among the limited number of IVPM proteins reported recently, Rho of Plant (ROP) proteins and MTL/ZmPLA1/NLD exhibit peripheral membrane localization *via* post-translational protein modifications such as palmitoylation or myristoylation (Li et al., 2013; Gilles et al., 2021). MTL/ZmPLA1/NLD also contains positively charged amino acids around the acyl modification motif, which reinforce the association with negatively charged phospholipids in IVPM. Understanding the basis of the protein-localization mechanism of IVPM would be an important clue to narrowing down the candidates for putative membrane-degenerating factors.

4.4 Future direction for the study of IVPM breakdown and double fertilization

s the correct subcellular localization of the MTL/ZmPLA1/NLD, an agronomically important haploid inducer protein, has been identified as IVPM, the unique sperm-enclosing membrane has come into the spotlight (Gilles et al., 2021). Although haploid induction in the *mtl/Zmpla1/nld* mutant is likely to be caused by sperm cell damage due to elevated ROS production, the importance of rapid and selective elimination of IVPM is evident in sexual reproduction of flowering plants (Jiang et al., 2022). Our current knowledge of the unique phospholipid composition and specifically localized proteins is indispensable for developing a novel experimental system to analyze IVPM breakdown. For example, IVPM markers are necessary to establish an efficient fractionation protocol to isolate intact IVPM with the entire MGU structure. Intact MGU can be used in an *in vitro* assay for IVPM breakdown and identification of novel IVPM-specific proteins through mass spectrometry analysis. This progress will lead to more substantial studies on the selective IVPM breakdown mechanism and its triggering signal that culminates in pollen tube rupture.

Data availability statement

The original contributions presented in the study are included in the article/Supplementary Material. Further inquiries can be directed to the corresponding author.

Author contributions

DM designed the study, conducted the time-lapse imaging. NS observed *anx1/2* mutant. RI, DS, and DM observed *lorelei* mutant. ST captured confocal images of pollen grains. NS and DM wrote the manuscript. TK provided critical advice and reviewed the manuscript. All authors contributed to the article and approved the submitted version.

Funding

This work was supported by JSPS KAKENHI (Grant nos. JP19H04869, JP20K21432, JP20H05778, and JP20H05781 awarded to DM; Grant no. JP22K15145 to DS; and Grant nos. JP22H05172 and JP22H05175 to TK); Yokohama City University (Academic Research Grant to DM; Development Fund to DM; and Strategic Research Promotion Grant no. SK1903 to DM).

Acknowledgments

We thank K. D. Kurihara for the *pRPS5A:H2B-tdTomato* marker; Y. Mizuta and S. Miyazaki for the *anx1/2* mutant; R. Palanivelu for *lre-4* mutant; H. Takeuchi, K. Motomura and T. Higashiyama for setting of imaging conditions; M. Tsukatani, H. Ikeda, H. Kakizaki for their technical support.

Conflict of interest

The authors declare that the research was conducted in the absence of any commercial or financial relationships that could be construed as a potential conflict of interest.

Publisher's note

Supplementary material

The Supplementary Material for this article can be found online at: https://www.frontiersin.org/articles/10.3389/fpls.2023.1116289/full#supplementary-material

References

Billey, E., Hafidh, S., Cruz-Gallardo, I., Litholdo, C. G., Jean, V., Carpentier, M. C., et al. (2021). LARP6C orchestrates posttranscriptional reprogramming of gene expression during hydration to promote pollen tube guidance. *Plant Cell* 33 (8), 2637–2661. doi: 10.1093/plcell/koab131

Boisson-Dernier, A., Roy, S., Kritsas, K., Grobei, M. A., Jaciubek, M., Schroeder, J. I., et al. (2009). Disruption of the pollen-expressed FERONIA homologs ANXUR1 and ANXUR2 triggers pollen tube discharge. *Development* 136 (19), 3279–3288. doi: 10.1242/dev.040071

Borges, F., Gomes, G., Gardner, R., Moreno, N., McCormick, S., Feijo, J. A., et al. (2008). Comparative transcriptomics of Arabidopsis sperm cells. *Plant Physiol.* 148 (2), 1168–1181. doi: 10.1104/pp.108.125229

Capron, A., Gourgues, M., Neiva, L. S., Faure, J. E., Berger, F., Pagnussat, G., et al. (2008). Maternal control of male-gamete delivery in Arabidopsis involves a putative GPI-anchored protein encoded by the LORELEI gene. *Plant Cell* 20 (11), 3038–3049. doi: 10.1105/tpc.108.061713

Cyprys, P., Lindemeier, M., and Sprunck, S. (2019). Gamete fusion is facilitated by two sperm cell-expressed DUF679 membrane proteins. *Nat. Plants* 5 (3), 253. doi: 10.1038/s41477-019-0382-3

Denninger, P., Bleckmann, A., Lausser, A., Vogler, F., Ott, T., Ehrhardt, D. W., et al. (2014). Male-Female communication triggers calcium signatures during fertilization in Arabidopsis. *Nat. Commun.* 5, 4645. doi: 10.1038/ncomms5645

Duan, Q., Kita, D., Johnson, E. A., Aggarwal, M., Gates, L., Wu, H. M., et al. (2014). Reactive oxygen species mediate pollen tube rupture to release sperm for fertilization in Arabidopsis. *Nat. Commun.* 5, 3129. doi: 10.1038/ncomms4129

Duan, Q., Liu, M. J., Kita, D., Jordan, S. S., Yeh, F. J., Yvon, R., et al. (2020). FERONIA controls pectin- and nitric oxide-mediated male-female interaction. *Nature* 579 (7800), 561–566. doi: 10.1038/s41586-020-2106-2

Dumas, C., Knox, R., and Gaude, T. (1985). The spatial association of the sperm cells and vegetative nucleus in the pollen grain of Brassica. *Protoplasma* 124 (3), 168–174. doi: 10.1007/BF01290767

Gatta, A. T., and Carlton, J. G. (2019). The ESCRT-machinery: Closing holes and expanding roles. *Curr. Opin. Cell Biol.* 59, 121–132. doi: 10.1016/j.ceb.2019.04.005

Ge, Z., Bergonci, T., Zhao, Y., Zou, Y., Du, S., Liu, M.-C., et al. (2017). Arabidopsis pollen tube integrity and sperm release are regulated by RALF-mediated signaling. *Science*. 358(6370)1596-1600. doi: 10.1126/science.aao3642

Gilles, L. M., Calhau, A. R. M., La Padula, V., Jacquier, N. M. A., Lionnet, C., Martinant, J. P., et al. (2021). Lipid anchoring and electrostatic interactions target NOT-LIKE-DAD to pollen endo-plasma membrane. *J. Cell Biol.* 220(10):e202010077. doi: 10.1083/jcb.202010077

Hamamura, Y., Nishimaki, M., Takeuchi, H., Geitmann, A., Kurihara, D., and Higashiyama, T. (2014). Live imaging of calcium spikes during double fertilization in Arabidopsis. *Nat. Commun.* 5, 4722. doi: 10.1038/ncomms5722

Hamamura, Y., Saito, C., Awai, C., Kurihara, D., Miyawaki, A., Nakagawa, T., et al. (2011). Live-cell imaging reveals the dynamics of two sperm cells during double fertilization in Arabidopsis thaliana. *Curr. Biol.* 21 (6), 497–502. doi: 10.1016/j.cub.2011.02.013

Helling, D., Possart, A., Cottier, S., Klahre, U., and Kost, B. (2006). Pollen tube tip growth depends on plasma membrane polarization mediated by tobacco PLC3 activity and endocytic membrane recycling. *Plant Cell* 18 (12), 3519–3534. doi: 10.1105/tpc.106.047373

Huang, J., Ju, Y., Wang, X., Zhang, Q., and Sodmergen, (2015). A one-step rectification of sperm cell targeting ensures the success of double fertilization. *J. Integr. Plant Biol.* 57 (5), 496–503. doi: 10.1111/jipb.12322

Igawa, T., Yanagawa, Y., Miyagishima, S. Y., and Mori, T. (2013). Analysis of gamete membrane dynamics during double fertilization of Arabidopsis. *J. Plant Res.* 126 (3), 387–394. doi: 10.1007/s10265-012-0528-0

Isono, E. (2021). ESCRT is a great sealer: Non-endosomal function of the ESCRT machinery in membrane repair and autophagy. *Plant Cell Physiol.* 62 (5), 766–774. doi: 10.1093/pcp/pcab045

Iwano, M., Ngo, Q. A., Entani, T., Shiba, H., Nagai, T., Miyawaki, A., et al. (2012). Cytoplasmic Ca2+ changes dynamically during the interaction of the pollen tube with synergid cells. *Development* 139 (22), 4202–4209. doi: 10.1242/dev.081208

Jensen, W. A., and Fisher, D. B. (1970). Cotton embryogenesis: The pollen tube in the stigma and style. *Protoplasma* 69 (2), 215–235. doi: 10.1007/BF01280723

Jiang, C., Sun, J., Li, R., Yan, S., Chen, W., Guo, L., et al. (2022). A reactive oxygen species burst causes haploid induction in maize. *Mol. Plant* 15 (6), 943–955. doi: 10.1016/j.molp.2022.04.001

Li, S., Zhou, L.-Z., Feng, Q.-N., McCormick, S., and Zhang, Y. (2013). The c-terminal hypervariable domain targets Arabidopsis ROP9 to the invaginated pollen tube plasma membrane. *Mol. Plant* 6 (4), 1362–1364. doi: 10.1093/mp/sst098

Maruyama, D., Hamamura, Y., Takeuchi, H., Susaki, D., Nishimaki, M., Kurihara, D., et al. (2013). Independent control by each female gamete prevents the attraction of multiple pollen tubes. *Dev. Cell* 25 (3), 317–323. doi: 10.1016/j.devcel.2013.03.013

Mecchia, M. A., Santos-Fernandez, G., Duss, N. N., Somoza, S. C., Boisson-Dernier, A., Gagliardini, V., et al. (2017). RALF4/19 peptides interact with LRX proteins to control pollen tube growth in Arabidopsis. *Science*. 358(6370):1600-1603. doi: 10.1126/science.aao5467

Miyazaki, S., Murata, T., Sakurai-Ozato, N., Kubo, M., Demura, T., Fukuda, H., et al. (2009). ANXUR1 and 2, sister genes to FERONIA/SIRENE, are male factors for coordinated fertilization. *Curr. Biol.* 19 (15), 1327–1331. doi: 10.1016/j.cub.2009.06.064

Motomura, K., Takeuchi, H., Notaguchi, M., Tsuchi, H., Takeda, A., Kinoshita, T., et al. (2021). Persistent directional growth capability in Arabidopsis thaliana pollen tubes after nuclear elimination from the apex. *Nat. Commun.* 12 (1), 2331. doi: 10.1038/s41467-021-22661-8

Ngo, Q. A., Vogler, H., Lituiev, D. S., Nestorova, A., and Grossniklaus, U. (2014). A calcium dialog mediated by the FERONIA signal transduction pathway controls plant sperm delivery. *Dev. Cell* 29 (4), 491–500. doi: 10.1016/j.devcel.2014.04.008

Russell, S., and Cass, D. (1981). Ultrastructure of the sperms of Plumbago zeylanica. *Protoplasma* 107 (1), 85–107. doi: 10.1007/BF01275610

Russell, S. D. (1983). Fertilization in Plumbago zeylanica: Gametic fusion and fate of the male cytoplasm. *Am. J. Bot.* 70 (3), 416–434. doi: 10.1002/j.1537-2197.1983.tb06409.x

Russell, S. D. (1986). Isolation of sperm cells from the pollen of Plumbago zeylanica. *Plant Physiol.* 81 (1), 317–319. doi: 10.1104/pp.81.1.317

Russell, S. D., Jones, D. S., Anderson, S., Wang, X., Sundaresan, V., and Gou, X. (2017). "Isolation of rice sperm cells for transcriptional profiling," in *Plant germline development* (Berlin/Heidelberg, Germany: Springer), 211–219. doi: 10.1007/978-1-4939-7286-9_17

Schattner, S., Schattner, J., Munder, F., Hoppe, E., and Walter, W. J. (2020). A tug-of-War model explains the saltatory sperm cell movement in Arabidopsis thaliana pollen tubes by kinesins with calponin homology domain. *Front. Plant Sci.* 11. doi: 10.3389/fpls.2020.601282

Southworth, D., and Kwiatkowski, S. (1996). Arabinogalactan proteins at the cell surface of Brassica sperm and Lilium sperm and generative cells. *Sexual Plant Reprod.* 9 (5), 269–272. doi: 10.1007/BF02152701

Sprunck, S. (2020). Twice the fun, double the trouble: Gamete interactions in flowering plants. *Curr. Opin. Plant Biol.* 53, 106–116. doi: 10.1016/j.pbi.2019.11.003

Sprunck, S., Rademacher, S., Vogler, F., Gheyselinck, J., Grossniklaus, U., and Dresselhaus, T. (2012). Egg cell-secreted EC1 triggers sperm cell activation during double fertilization. *Science* 338 (6110), 1093–1097. doi: 10.1126/science.1223944

Susaki, D., Maruyama, D., Yelagandula, R., Berger, F., and Kawashima, T. (2017). "Live-cell imaging of f-actin dynamics during fertilization in Arabidopsis thaliana," in *Plant germline development* (Berlin/Heidelberg, Germany: Springer), 47–54.

Taylor, P., Kenrick, J., Blomstedt, C., and Knox, R. (1991). Sperm cells of the pollen tubes of Brassica: Ultrastructure and isolation. *Sexual Plant Reprod.* 4 (3), 226–234. doi: 10.1007/BF00190009

Tsukamoto, T., Qin, Y., Huang, Y., Dunatunga, D., and Palanivelu, R. (2010). A role for LORELEI, a putative glycosylphosphatidylinositol-anchored protein, in arabidopsis thaliana double fertilization and early seed development. *Plant J.* 62 (4), 571–588. doi: 10.1111/j.1365-313X.2010.04177.x

Wang, W., Xiong, H., Zhao, P., Peng, X., and Sun, M. X. (2022). DMP8 and 9 regulate HAP2/GCS1 trafficking for the timely acquisition of sperm fusion competence. *Proc. Natl. Acad. Sci. U.S.A.* 119 (45), e2207608119. doi: 10.1073/pnas.2207608119

Zhang, G., Campenot, M. K., McGann, L. E., and Cass, D. D. (1992). Flow cytometric characteristics of sperm cells isolated from pollen of Zea mays l. *Plant Physiol.* 99 (1), 54–59. doi: 10.1104/pp.99.1.54

Zhou, X., Lu, J., Zhang, Y., Guo, J., Lin, W., Van Norman, J. M., et al. (2021). Membrane receptor-mediated mechano-transduction maintains cell integrity during pollen tube growth within the pistil. *Dev. Cell.* 56(7):1030-1042.e6. doi: 10.1016/j.devcel.2021.02.030

Zhou, X., and Meier, I. (2014). Efficient plant male fertility depends on vegetative nuclear movement mediated by two families of plant outer nuclear membrane proteins. *Proc. Natl. Acad. Sci. U.S.A.* 111 (32), 11900–11905. doi: 10.1073/pnas.1323104111

Zhou, Y., Yang, Y., Niu, Y., Fan, T., Qian, D., Luo, C., et al. (2020). The tip-localized phosphatidylserine established by Arabidopsis ALA3 is crucial for rab GTPase-mediated vesicle trafficking and pollen tube growth. *Plant Cell.* 32(10):3170-3187. doi: 10.1105/tpc.19.00844

frontiers | Frontiers in Plant Science

TYPE Original Research
PUBLISHED 08 May 2023
DOI 10.3389/fpls.2023.1177058

OPEN ACCESS

EDITED BY
Delia Fernández-González,
Universidad de León, Spain

REVIEWED BY
Yoko Mizuta,
Nagoya University, Japan
Cédric Finet,
National University of Singapore, Singapore

*CORRESPONDENCE
Ryushiro Dora Kasahara
kasahara@bio.nagoya-u.ac.jp
Prakash Babu Adhikari
pbadhikari@kangwon.ac.kr

†PRESENT ADDRESS
Shaowei Zhu,
Yancheng LuMing Road Junior High School, Jiangsu, China
Liyang Xie,
Agricultural Science Park Administration Commission, Shaowu Bureau of Agriculture and Rural Affairs, Fujian, China
Ryushiro D. Kasahara,
Bioscience and Biotechnology Center, Nagoya University, Chikusa, Nagoya, Aichi, Japan

‡These authors have contributed equally to this work

RECEIVED 01 March 2023
ACCEPTED 10 April 2023
PUBLISHED 08 May 2023

CITATION
Adhikari PB, Zhu S, Liu X, Huang C, Xie L, Wu X, He J, Mitsuda N, Peters B, Brownfield L, Nagawa S and Kasahara RD (2023) Discovery of a *cis*-regulatory element *SaeM* involved in dynamic regulation of synergid-specific *MYB98*. *Front. Plant Sci.* 14:1177058. doi: 10.3389/fpls.2023.1177058

Discovery of a *cis*-regulatory element *SaeM* involved in dynamic regulation of synergid-specific *MYB98*

Prakash Babu Adhikari [1,2,3*†‡], Shaowei Zhu [2†‡], Xiaoyan Liu [2‡], Chen Huang [2‡], Liyang Xie [3†‡], Xiaoyan Wu [2], Jiale He [2], Nobutaka Mitsuda [4], Benjamin Peters [5], Lynette Brownfield [5], Shingo Nagawa [2,3] and Ryushiro Dora Kasahara [2,3,6*†]

[1]Key Laboratory of Horticultural Plant Biology (Ministry of Education), Huazhong Agricultural University, Wuhan, China, [2]College of Life Science, Fujian Agriculture and Forestry University, Fuzhou, Fujian, China, [3]Horticultural Plant Biology and Metabolomics Center (HBMC), Fujian Agriculture and Forestry University, Fuzhou, Fujian, China, [4]Bioproduction Research Institute, National Institute of Advanced Industrial Science and Technology (AIST), Tsukuba, Japan, [5]Department of Biochemistry, School of Biomedical Sciences, University of Otago, Dunedin, New Zealand, [6]International Research Organization for Advanced Science and Technology (IROAST), Kumamoto University, Kumamoto, Japan

MYB98 is a key regulator of the genetic network behind pollen tube attraction toward the female gametophyte. *MYB98* is specifically expressed in the synergid cells (SCs), a female gametophyte component cells specialized for pollen tube attraction. However, it had not been clear how exactly *MYB98* achieves this specific expression pattern. In the current study, we have determined that a normal SC-specific expression of *MYB98* is dependent on a 16-bp-long *cis*-regulatory element, CATTTACACATTAAAA, freshly named as the "***S****ynergid-specific* ***A****ctivation* ***E****lement of* ***M****YB98*" (*SaeM*). An 84 bp fragment harboring *SaeM* in the middle was sufficient to drive exclusively SC-specific expression. The element was present in a significantly large proportion of SC-specific gene promoters and in the promoter of *MYB98* homologous genes in the Brassicaceae (*pMYB98*s). Significance of such family-wide *SaeM-like* element conservation in exclusive SC-specific expression was confirmed by the Arabidopsis-like activation feature of *Brassica oleracea*–derived *pMYB98* and absence of such feature of *pMYB98* derived from a non-Brassicaceae member *Prunus persica*. Additionally, the yeast-one-hybrid assay showed that the *SaeM* can be recognized by ANTHOCYANINLESS2 (ANL2) and DAP-seq data further suggested for additional three ANL2 homologs targeting the similar *cis*-element. Overall, our study has concluded that *SaeM* plays a crucial role in driving exclusively SC-specific expression of *MYB98* and strongly suggests for the involvement of ANL2 and its homologs in its dynamic regulation *in planta*. Future study on the transcription factors is expected to shed more light on the mechanism behind the process.

KEYWORDS

***MYB98* promoter, *SaeM*, cis-element, synergid cell, dynamic regulation**

Introduction

The female gametophyte (FG) is an important tissue of sexual reproduction in plants. The FG develops from a single meiotic product with several rounds of mitotic nuclei division being followed by cytokinesis. A typical mature FG comprises seven cells: two synergid cells (SCs; haploid) at the micropylar end, three antipodal cells (ACs; haploid) at the chalazal end, a central cell (CC; homodiploid) at the middle and an egg cell (EC; haploid) sandwiched between the SCs and CC. During fertilization, the EC and CC take the central stage as they develop into embryo and endosperm, respectively, after their independent fertilization with two sperm cells released from the pollen tube (PT) (Drews and Koltunow, 2011; Adhikari et al., 2020). However, it is the SCs that are specialized and quintessentially involved in attracting the PT to the FG followed by its reception. (Higashiyama, 2002; Kessler and Grossniklaus, 2011). The PT follows the traces of the molecular cues secreted by SCs, which mainly include cysteine rich proteins (CRPs) (Okuda et al., 2009; Takeuchi, 2021). Secretion of such cues is largely regulated by an SC-specific master regulator transcription factor (TF), *MYB98* (Kasahara et al., 2005; Punwani et al., 2007; Kasahara, 2018). *MYB98* expression is initiated during the cellularization process and is later restricted exclusively to the SCs in the mature FGs (Kasahara et al., 2005; Zhang et al., 2020; Susaki et al., 2021). MYB98 is involved in the development of filiform apparatus and the regulation of crucial genes directly involved in PT attraction (Kasahara et al., 2005; Punwani and Drews, 2008). There have been some extensive studies on the genetic networks involved in PT guidance downstream of MYB98 (Punwani et al., 2007; Punwani et al., 2008). A recent study reported that post-transcriptional pre-mRNA splicing of *MYB98* and CRP is seriously hindered upon mutation of the spliceosome subunit encoding genes *PRP8A* and *PRP8B*, thereby negatively affecting the synergid fate and ovular PT-attraction (Kulichová et al., 2020). However, even after nearly two decades of the discovery of its involvement in PT attraction (Kasahara et al., 2005), the molecular factors behind *MYB98* regulation remain largely unknown. The central-cell specific TFs CCG and CBP1 positively affect *MYB98* expression in SCs, but the process behind this is not fully clear (Li et al., 2015). *MYB98* expression in the CC is actively repressed by the EAR motif harboring MADS box TF AGL80 binding to the CArG boxes in the *MYB98* promoter (*pMYB98*). Ectopic expression of the *AGL80* in SCs leads to the repression of native *MYB98* and the ovules exhibit *myb98* mutant-like PT-guidance defect (Zhang et al., 2020).

Here, we report the discovery of the **S**ynergid-specific **A**ctivation **E**lement of ***M****YB98* (*SaeM*) in the Arabidopsis-derived *MYB98 promoter* (*pMYB98*), which is crucial for its exclusively SC-specific expression. The element and associated regulatory features are conserved among *pMYB98*s of Brassicaceae members. Furthermore, a homeodomain member ANTHOCYANINLESS2 (ANL2) binds to the *cis*-fragment harboring the *SaeM* potentially mediating its dynamic regulation.

Results

Identification of pMYB98 region crucial for driving synergid-specific expression

As a first assessment to identify the regions of *pMYB98* that contribute to the SC expression of *MYB98*, a series of promoter deletions from both the 5′ and 3′ ends were screened for activity based on reporter (GFP) expression in Arabidopsis ovules. In both cases, the numbering of the bases was relative to the translation start site (ATG). The *pMYB98* 5′-deletion reporter series showed that the reporter signal drops upon deletion of a −838 to −702 region, a −702 to −512 region, and a −350 to −194 region with only the middle one displaying statistically significant fluorescence signal changes. Furthermore, unlike some of the reporter lines harboring −350 bp *pMYB98* fragment, none of the reporter lines with −194 bp fragment exhibited fluorescence signal (Figure 1). Consistent with these results, a 3′-deletion series showed that deletion of either of two specific promoter regions, −615 to −487 bp and −251 to −121 bp, brought drastic drop in the reporter signal (Supplementary Figure S1). Combined, these observations strongly indicated that a 191 bp region between −702 and −512, the deletion of which exhibited a steep drop in the reporter signal, harbors one or more sequence elements that are crucially important for SC-specific expression of *MYB98*. Furthermore, a 156 bp region between −350 and −194 bp can drive weak yet quantifiable SC-specific expression.

Brassicaceae members harbor uniquely conserved sequence at the 3′-end of the functionally active promoter region

MYB98 is activated during FG development to drive SC cell fate with its expression precisely restricted to the SCs in mature FGs (Kasahara et al., 2005; Susaki et al., 2021). Based on this, we hypothesized that there could be a conserved motif in *pMYB98* homologs responsible for the specific expression pattern. To test this, we retrieved 1 kb sequence of respective 5′-upstream region of the putative *MYB98* homologs from the Phytozome database (Goodstein et al., 2012) and selected only those closely clustered with the AtMYB subgroup 25 members (*AtMYB98*, *AtMYB64*, and *AtMYB119*) for the phylogenetic footprinting (Figure 2A and Supplementary Figure S2) (see material and methods section for details). A native motif search among the promoters of the 51 *MYB98* homologs along with *AtMYB64* and *AtMYB119 via* MEME (Bailey et al., 2009) revealed that the most conserved 29 bp long motif falls at the 3′-end of the functionally active Arabidopsis *pMYB98* with an 8 bp extension at the 3′ end (*e*-value: 5.2e-184). The members of Brassicaceae have a distinctive pattern for both the site and degree of motif conservation in comparison with *pMYB98* from other plant families. Except for two, all Brassicaceae derived promoters harbor the motif within −700 to −400 bp (Figures 2A, B), suggesting that the

10.3389/fpls.2023.1177058

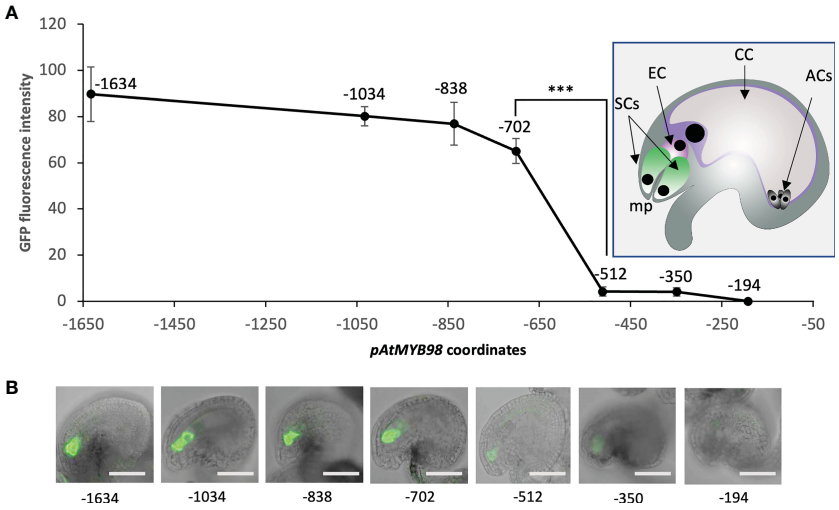

FIGURE 1
A 191-bp-long *pMYB98 cis*-fragment deletion significantly reduces the reporter signal. **(A)** SC-specific fluorescence intensity quantified in the ovules of plants transformed with the reporter constructs driven by varying lengths of *pAtMYB98* (***$p \leq 0.001$, DMRT; $n = 20$). *Inset:* Typical Arabidopsis ovule with its component cells denoted. **(B)** Representative CLSM images of the ovules derived from the bashed *pMYB98::GFP* transgenic lines. Values represent mean ± SE; $n = 15$; scale bar = 50 µm; SCs, synergic cells; EC, egg cell; CC, central cell; ACs, antipodal cells; mp, 'micropyle.

transcriptional regulation of *MYB98* could have been conserved among Brassicaceae members with some variations. While there is more variation in other plant families, the motif was still commonly found within the 1,000 bp region analyzed with the *MYB98* homologs from the Malvaceae (Wu et al., 2022), a close evolutionary relative of the Brassicaceae being the most similar, although the motif site was located at further downstream (Figure 2A).

Loss of conserved motif leads to the loss of exclusive synergid-specificity of pMYB98

To ascertain whether the putatively conserved region is crucial for driving SC-specific expression of *pMYB98*, we carried out a deletion/addition reporter expression assay. Unlike the intact 1.5k promoter (*pMYB98*) lines, which normally exhibit SC-specific expression in the mature FGs, the reporter lines lacking the conserved motif (*pδMYB98*: −559 to −509 bp deleted) lost this specificity, along with a slight but significant drop in GFP intensity. However, when the entire 191 bp functionally active region was deleted (*pΔMYB98*; −702 to −509 bp deleted), the GFP signal dropped steeply along with the loss of SC-specific activation (Figures 2C, D). We additionally checked whether either the conserved region or the whole 191 bp fragment drives SC-specific expression when incorporated in the middle of the 346 bp constitutive *pCaMV35S* promoter at 241 bp upstream of the ATG (*pδCaMV* and *pΔCaMV*, respectively). On its own the *pCaMV* region leads to GFP expression throughout the ovule, making it difficult to distinguish the SC (Figure 2C). The addition of either the conserved region or the 191 bp region to *pCaMV* did not provide SC-specific expression, although there was reduced expression within the ovule, especially for *pδCaMV*. Additionally, the fluorescence intensities provided by both *pδCaMV* and *pΔCaMV* were much lower compared with that of the intact *pMYB98* driven GFP (Figures 2C, D). Overall, these observations on the *cis*-element addition/deletion reporter lines strongly indicated that the conserved motif is likely involved in overall repression and the 191 bp region of *pMYB98* likely harbors additional important *cis*-element crucial for SC activation. To further define the crucial *cis*-elements within the functionally active *pMYB98* region, we carried out reporter assays with sub-fragment combinations and mutations of putative *cis*-elements.

An 84 bp fragment within pMYB98 is sufficient for its SC-specific activation

Based on the observations made on the 5′- and 3′-deletion series (Figures 1, S1), we selected a 169 bp region (−678 to −510) of *pMYB98* and divided it into four sub-fragments, annotated as Blue (B, 45 bp), Yellow (Y, 40 bp), Red (R, 44 bp), and Green (G, 40 bp) (in order from 5′ to 3′) (Figure 3A). The fragments were assembled in all possible 2-4 fragment combinations along with the 1-3 repeated combinations of each sub-fragments (24 combinations in total including negative control construct). The prepared combinations were cloned upstream of *CaMV* minimal promoter (MP) independently to drive H2B-GFP expression (Figure 3A). The complete fragment (*BYRG-MP::H2B-GFP*) provided strong SC-specific GFP fluorescence, while the minimal promoter on its own (*MP::H2B-GFP*) provided weak expression in sporophytic cells but not in the SCs (Figure 3B). We then considered the role of each of the fragments.

10.3389/fpls.2023.1177058

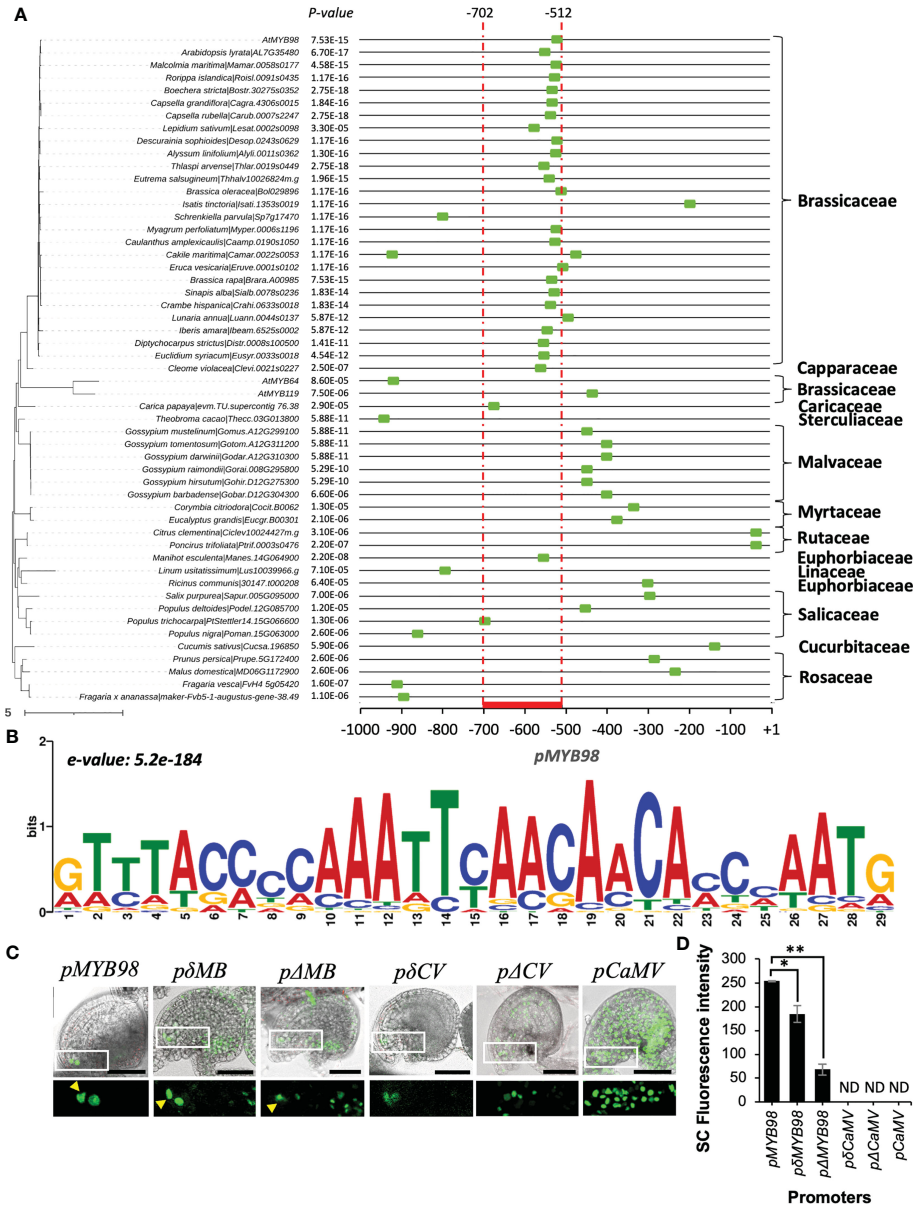

FIGURE 2
Assessment of motif conservation among *MYB98* homologs and putative TF binding sites within the functional active 191 bp region (in reference to *A. thaliana*). **(A)** The most conserved motif within the 1 kb promoter region of *pAtMYB98* region (marked with a green box at the x-axis). The phylogenetic tree on the left is the subtree of phytozome derived 108 *pMYB98* homologs and *AtMYB* sub-group 25 members (check Supplementary Figure S2 for reference). **(B)** Position-specific scoring matrix of the conserved motif. (e-value: 3.9e-183) in *pMYB98* from 51 Species. **(C)** Expression of *H2B-GFP* driven by the intact (*pMYB98*), conserved motif deleted (*pδMB*), and whole functional motif deleted (*pΔMB*) *MYB98* promoters along with the conserved motif added (*pδCV*) and whole functional region added (*pΔCV*) *CaMV* promoters. The arrowheads point SCs. **(D)** GFP intensity at SCs of the aforementioned *pMYB98* fragment deletion and addition lines. (ND = not clearly distinguishable; *$p \leq 0.01$, **$p \leq 0.001$, Student's t-test; $n = 9$). Scale bar = 50 µm.

The B-fragment appears to have a non-cell–specific role in transcriptional activation as the removal of the B-fragment in *YRG-MP::H2B-GFP* resulted in a decrease in expression and containing only the B-fragment (*B1-MP::H2B-GFP*, *B2-MP::H2B-GFP*, and *B3-MP::H2B-GFP*) along with some other fragments containing B-fragment (e.g., *BYG-MP::H2B-GFP* and *BY-MP::H2B-GFP*) had strong fluorescence throughout the ovule with too prevalent signals in the sporophytic cells (Figure 3B).

The Y-fragment and the R-fragment appear to work in combination to both provide some transcriptional activation in SCs and also play a key role in restricting expression to the SC. When the Y-fragment was removed (*BRG-MP::H2B-GFP*), SC-expression was retained but had reduced intensity and GFP was no longer SC-specific. When the R-fragment was absent (*BYG-MP::H2B-GFP*), SC fluorescence could not be distinguished (Figure 3B). Additionally, repeats of the R- fragment (*R2-MP::H2B-GFP* and *R3-*

10.3389/fpls.2023.1177058

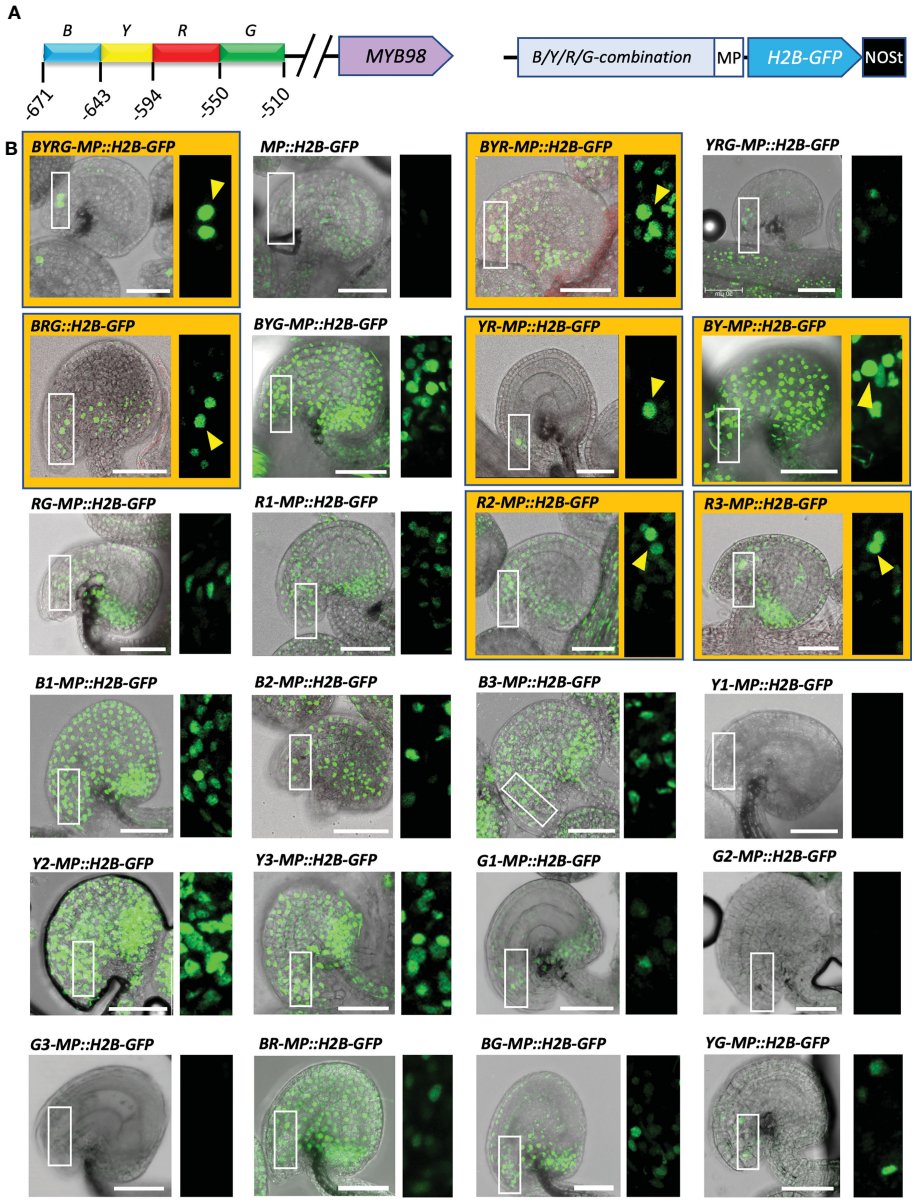

FIGURE 3
A short 84 bp fragment located at the middle of the functionally active *pMYB98* region is sufficient for the exclusive SC-specific expression. **(A)** *pMYB98 cis* fragments (B, Y, R, and G) used in the study and their locations upstream of ATG (+1) (*left*) along with the diagram representing a typical construct used in the study (*right*). **(B)** Representative CLSM images of ovules derived from the reporter lines of the B, Y, R, and G fragments along with negative control (MP). Images of the ovules with distinguishable SCs are highlighted with orange color and distinguishable SCs are pointed with arrowheads. Check Supplementary Movie S1 for the associated z-stack-derived movies of ovules with distinguishable SCs. Scale bar = 50 µm; MP, minimal promoter.

MP::H2B-GFP) lead to GFP fluorescence in multiple FG cell types in some cases (Supplementary Figure S3). Notably, a combination of just the Y- and R- fragments (*YR-MP::H2B-GFP*) resulted in SC-specific fluorescence, indicating that the region covered by R and Y contains cis-elements that restrict expression to the SCs within the ovule (Figure 3B).

When the G-fragment is removed (*BYR-MP::H2B-GFP*), SC fluorescence is retained, but the GFP signal is no longer restricted to the SCs. However, the G-fragment on its own (*G1-MP::H2B-GFP*, *G2-MP::H2B-GFP*, and *G3-MP::H2B-GFP*) did not increase GFP levels over *MP::H2B-GFP*. This suggests that the G-fragment contains cis-elements that help provide SC-specificity but do not assist in transcriptional activation (Figure 3B).

Overall, assessment of the fragment combination driven expressions strongly indicated that the 94 bp long YR-fragment is key to driving exclusively SC-specific expression. The SC expression is augmented by upstream cis-elements located in the B-fragment and further restricted by downstream cis-elements located in the G-

10.3389/fpls.2023.1177058

fragment (Supplementary Table S1). To further narrow down the TF-binding sites crucial for SC-specific *pMYB98* activation, we carried out a repetitive *cis*-element mutation assessment.

Discovery of the 16-bp-long synergid-specific activation element of MYB98

Since the intact 191 bp functionally active fragment was necessary and sufficient to drive SC-specific expression and the fragments had differing roles, we assumed that there could be multiple-binding sites (*cis*-elements) for key TF involved in the transcriptional regulation of *MYB98*. A manual assessment for the putatively repeated short sequences within the full functional element revealed five repetitive elements, which were annotated as "a" (AKWCAACWA, four copies), "b" (ACTASA, two copies), "c" (STTTRTG, two copies), "d" (ATGWGT, two copies), and "e" (TRGSGT, two copies) (Figure 4A). To test the function of the repeats, each repeat was mutated to GCCAGCTGC, GTCCAG, ACGCTCA, GCTCAC, and CTATAG, respectively, to assess its effect on SC-specific activation (Figure 4A). Among the different combinations of reporters with repetitive element mutations, only the intact and b-repeats mutated fragments brought exclusively SC-specific expression, even though mutation of the b-repeats led to the reduction in GFP signal (Figure 4B). Interestingly, all combinations that included d-repeats mutation, including mutation of the d-repeats alone, exhibited either no expression at all or no expression at SC (Figure 4B), suggesting that a transcriptional activator binds to the d repeat. Two copies of the 6 bp d-repeats are closely located (−611 to −595), one of which is at the Y–R junction, while the other is within the R fragment (Figure 4A). The observation partly comes in agreement with the fragment combination observation we made earlier, which showed that unlike B-fragment alone, the fragment lacking YR exhibited a much-reduced fluorescence signal (Figure 3B).

Interestingly, the mutation of the d-repeat at the Y–R junction alone has little to no effect on the SC-specific activation of the fragment, while mutation of the d-repeat located downstream in R-fragment led to ovule-wide GFP expression with no distinguishable signal at SCs (Figure 4C), which was very similar to the observation we made earlier with the BYG combination (Figure 3B). Since four concatemers of d-repeats alone could not drive the GFP expression (data not shown), we presumed that it is not sufficient to drive SC-specific expression, and instead, its mutation most likely has

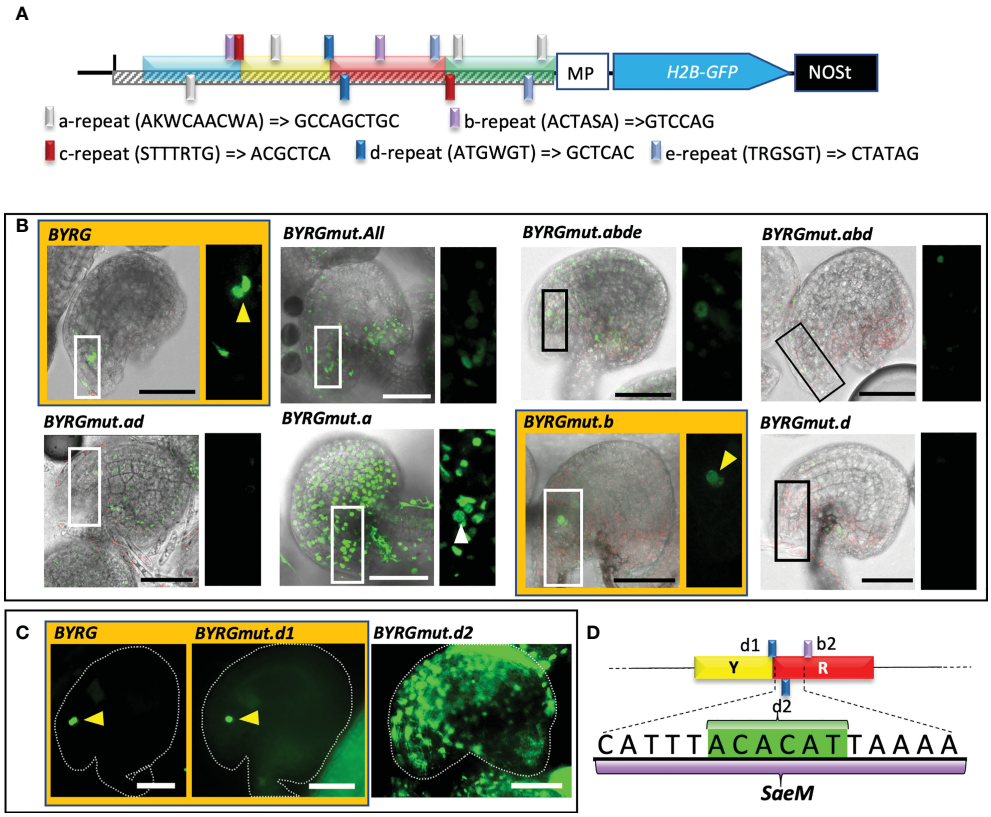

FIGURE 4
Mutation of two 6 bp repeats within the BYRG-fragment effectively silences the reporter expression. **(A)** A schematic diagram of a reporter construct harboring functionally active *pMYB98* with the relative sites of the repeat elements targeted for mutation. Native and the substituted bases are shown with the repeat element legends. **(B)** Representative CLSM images of the ovules derived from the reporter lines of the negative control (MP) as well as the normal and mutated BYRG-fragments. **(C)** Epifluorescence images of positive control and independent d-repeat mutant-derived ovules. **(D)** Determination of *Synergid-specific activation element of MYB98* (*SaeM*) harboring a d-repeat (highlighted in green) between upstream localized d-repeat (*d1*) and downstream localized b-repeat (*b2*). Images of the ovules with distinguishable SCs are highlighted with orange color and distinguishable SCs are pointed with arrowheads. *Scale bar = 50 µm MP, minimal promoter.*

disrupted the putative binding site of a key TF responsible for such phenomenon. However, the mutation in b-repeats, one of which falls downstream of the d-repeat within the R-fragment (−589 to −584), could still exhibit SC-specific expression (Figures 4A, B), suggesting that the 16-bp-long *cis*-region sandwiched between the d-repeat at Y–R junction and b-repeat at R-fragment (−577 to −592), catttACACATtaaaa, is essential for overall as well as SC-specific activation of the 169-bp fragment of *pMYB98* (Figure 4D). We annotated this sequence as a "***S****ynergid-specific* ***A****ctivation* ***E****lement of* ***M****YB98*" (*SaeM*).

Synergid-specific activation element of MYB98–like element is enriched in SC-specific gene promoters and highly conserved among Brassicaceae-derived pMYB98s

To ascertain whether *SaeM* is conserved among synergid-specific promoters, we compared promoter regions between SC and non-SC gene pools. We defined the *SaeM*-aligned respective sequence region as the *SaeM*-like element for each promoter sequence. Among 64 exclusively SC-expressed genes, about 66% harbored a *SaeM*-like element within their 1 kb promoter region. Among them were those that had been experimentally verified to be SC-specific, such as *MYB98* (Kasahara et al., 2005; Punwani et al., 2007) *LURE*s (1.1, 1.2, 1.3, 1.4, 1.7, and 1.8) (Takeuchi and Higashiyama, 2012; Zhong et al., 2019), *LORELEI* (Noble et al., 2022), *DD11* and *DD18* (Punwani et al., 2007). (Figure 5A and Supplementary Table S2). However, the *SaeM*-like element was found in the promoters of only about 7% of the genes expressed in either all FG component cells (> 0 abundance at all SC, CC, and EC replications; 138 genes) or exclusively at EC and CC (null expression value at all SC replication but > 0 abundance at all EC and CC replications; 163 genes) (Figure 5A and Supplementary Table S2-S4). Such occurrence strongly indicated that *SaeM* element is most likely to be involved in the activation of the associated genes in the SCs and their simultaneous non-activation in non-SCs.

Our phylogenetic footprinting assessment showed uniquely conserved motif pattern for the Brassicaceae members derived *pMYB98*s as compared with non-Brassicaceae derived counterparts (Figure 2A). In agreement to such assessment, we found that *SaeM-like* element is present in the significantly higher numbers of the Brassicaceae-derived *pMYB98*s (73% of 26 genes). On the other hand, only non-significant proportion of non-Bassicaceae derived *pMYB98*s (6% of 82 genes) appear to harbor the element which was very similar to that of the pollen-specific gene promoters retrieved from the study of Honys and Twell (2003) (5% of 381 genes) (Figure 5B; Supplementary Table S5 and S6). It is also noteworthy that *AtMYB64*, which is reportedly expressed at SCs along with the relatively weaker expression at other FG component cells (Rabiger and Drews, 2013), also harbor a *SaeM-like* element in its promoter.

To determine potential TFs binding to the *SaeM* and the wider region, we carried out a Yeast-one-hybrid assay (Y1H) assessment.

ANL2 and homologs show binding potential to the Synergid-specific activation element of MYB98

We took the 5′-deletion series derived functionally active 191 bp *pMYB98* fragment for the prediction of potential TF-binding sites and associated TFs using PlantRegMap (Tian et al., 2019) (threshold *p*-value ≤ 1e−4). The −671 to −595 region was predicted as the potential binding pocket for WRKY, HD, and MIKC-MADS TFs (Figure 5C and Supplementary Table S7). Based on the predictions, three independent bait constructs were prepared using the 40, 60, and 139 bp fragments of overlapping sequences for the Y1H assay. The screening was performed against an Arabidopsis TF prey library (Mitsuda et al., 2010). Among the three, 60 bp fragments gave the highest number of candidate TFs (19 in total) followed by 40 and 139 bp fragments (14 and 6, respectively) with some redundancies (23 in total) (Figure 5C and Supplementary Figure S4). The result revealed that overall B3/REM, bZIP, FHY/FAR, or NAC domain harboring TFs exhibited much stronger binding affinity, while ERF and C2H2 members showed relatively weaker binding affinity to the *pMYB98* fragments used in the assay (Supplementary Figure S4). The only TF that overlapped between the *in silico* prediction and Y1H-derived pools was ANTHOCYANINLESS2 (ANL2). Within the YIH bait constructs tested, ANL2 showed binding affinity only to the longest fragment that harbored *SaeM*, which was absent in the two shorter ones.

To further ascertain whether ANL2 was bound to the *SaeM*, we assessed the DNA affinity purification sequencing (DAP-seq) data available in the Plant Cistrome Database (O'Malley et al., 2016), which showed that one of the 11-bp-long ANL2-binding sites (DHATTWAWDRH) overlapped with the *SaeM* sequence with a 2 bp extension at the 3′-end of the *SaeM*. Additionally, the d-repeat had a 4 bp overlap to the DHATTWAWDRH motif at its 5′-end. The d-repeat mutation (ACACAT > GTGAGC) resulted in changes to the third and fourth conserved bases (AT) of the ANL2-recognition motif. When the wider functionally active region of pMYB98 was analyzed, it was observed that there are several ANL2 binding motifs within and near *SaeM* (Figure 5D).

The DAP-seq data additionally revealed that the ANL2 homolog HD TFs HOMEODOMAIN GLABROUS 1 (HDG1) and HDG7 recognize similar motif but at the reverse strand (DYHWTWAATDH). Additionally, the binding motif of yet additional HD member, HDG11 (also referred to as ENHANCED DROUGHT TOLERANCE 1; EDT1), was very similar to that of ANL2 as well (Figure 5D). The experimentally confirmed DNA-protein interactions database ePlant (Austin et al., 2016) showed that at least ANL2 and HDG1 do interact with *pMYB98*.

The *SaeM* and associated ANL2-recognition motifs appear to harbor single nucleotide polymorphisms (SNPs) as assessed among 1,135 Arabidopsis accessions retrieved from 1001 Genomes Project (Alonso-Blanco et al., 2016). Interestingly, however, the SNPs were localized specifically at the 6th and 10th positions of the ANL2-binding site, which could be tolerated for either ANL2, HDG1, HDG7, and ETD1 binding (O'Malley et al., 2016) (Figure 5D).

10.3389/fpls.2023.1177058

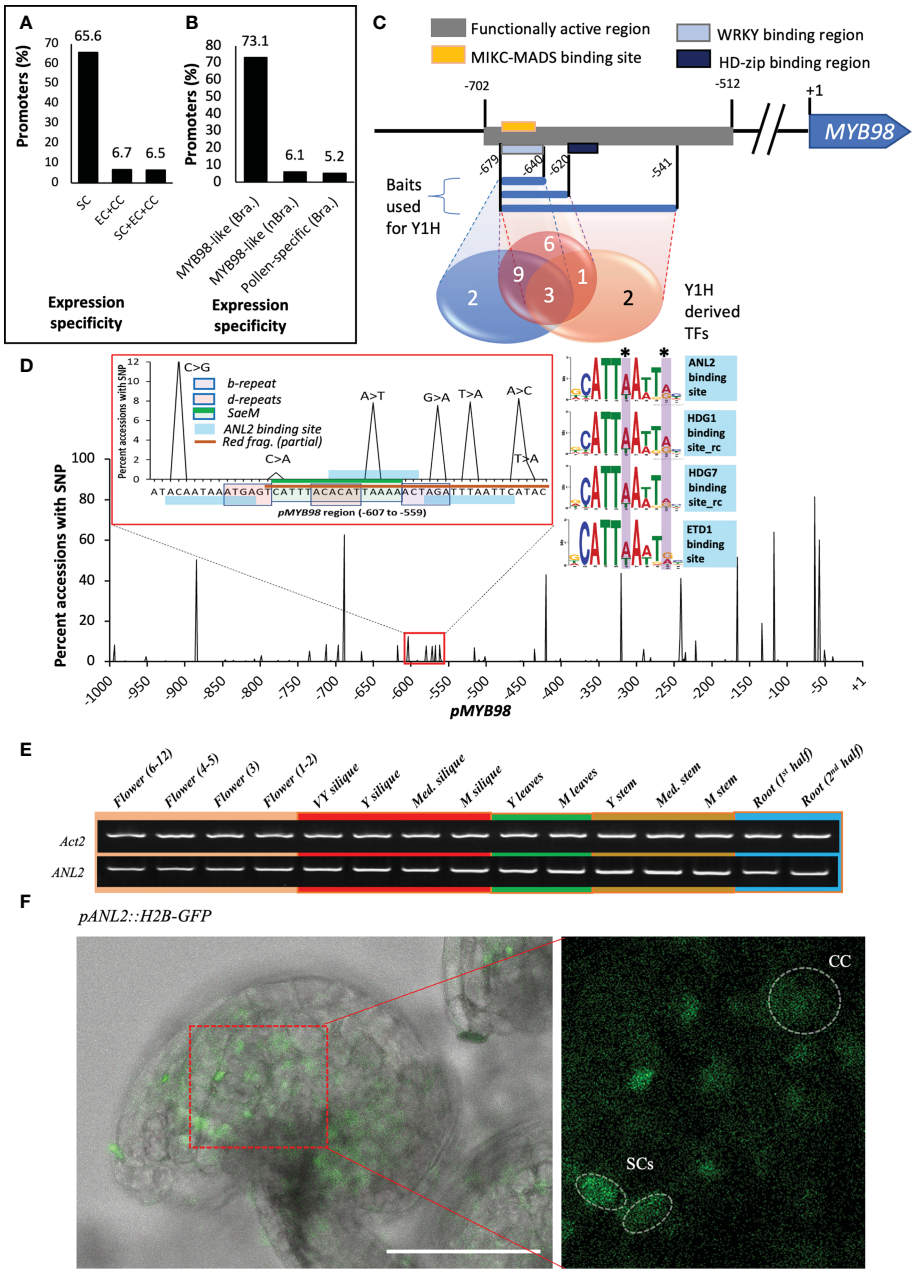

FIGURE 5
SaeM is conserved among Brassicaceae members and is recognized by ANL2 and its homologs. **(A)** An excessively higher proportion of SC-specific gene promoters harbor *SaeM*-like element as compared with those expressed either at all female gametophyte component cells or exclusively at CC and EC. **(B)** A significantly high proportion of Brassicaceae-derived *pMYB98* harbor *SaeM-like* element as compared with their non-Brassicaceae counterparts and Arabidopsis derived pollen-specific gene promoters (-ve control). **(C)** TF-binding sites predicted by the PlangRegMap (in square boxes) and the number of TFs derived from yeast-1-hybridization (Y1H) with three independent overlapping fragments as baits (in Venn diagram). **(D)** SNP frequency within 1 kb of *pMYB98* among 1,135 Arabidopsis accessions. The *SaeM*, within/nearby repeat-sites used for mutation studies, and ANL2-binding sites are highlighted in the magnified graph in inset. The web logos of respective recognition sites of ANL2 and its homologs (HDG1, HDG7, and ETD1) are shown on the side marking and highlighting the base positions with SNPs. **(E)** *ANL2* is expressed in all plant tissues assessed in Arabidopsis. **(F)** Weak GFP-signals at SCs and CCs in *pANL2::H2B-GFP* mature ovule (retrieved from Flower stage 3). GFP intensity was enhanced for visualization purpose; check the associated z-stack-derived movie in Supplementary Movie S3. Scale bar = 50 µm. SC, synergid cell; CC, central cell; EC, egg cell.

ANL2 is expressed in diverse plant tissues (Figure 5E), and the reporter construct harboring its 1.5 kb promoter (*pANL2*) showed that it drives expression at least at SCs and CC of the FG (Figure 5F). However, the *anl2*$^{-/-}$ single T-DNA insertion mutant did not bring any discrepancy to the PT guidance, its reception, and overall sed-set, even though we observed sporadic ovules exhibiting *pMYB98*-driven *GFP* expression at all FG component cells (strongest at the SCs) in the *anl2*$^{-/-}$ mutant (Supplementary Figure S5).

Additional pocket of multiple ANL2/HDG1 binding motifs was located further downstream of *SaeM*, at −236 to −218 bp. Earlier

observations made on the 5′- and 3′-deletion series strongly suggests for the active involvement of this *cis*-region in SC-specific expression as well as the shortening of the *pMYB98* from −350 to −194 bp in the 5′-deletion series and deletion of −251 to −121 bp fragment in the 3′-deletion series led to significant decrease in the GFP signal (Figure 1 and Supplementary Figure S1). The putative ANL2-binding pocket falls within the overlapping region of these two deletion series (−251 to −194 bp).

pMYB98 activation feature is conserved in Brassicaceae family members

Our earlier observation showed that the concatemers of red fragment, that harbors the *SaeM* and two ANL2-recognition motifs brings about reporter expression at the SCs and the SC-exclusivity increased with the increase in the number of its concatemers (Figure 3B and Supplementary Figure S3). Furthermore, we found that much higher number of Brassicaceae-derived *pMYB98*s harbor *SaeM* as compared with their non-Brassicaceae derived counterparts.

To confirm whether such conservation is translated into *in vivo* expression of respective *MYB98*, we selected cabbage (*Brassica oleracea*; Brassicaceae) derived *MYB98* (*BoMYB98*; Bol029896) and peach (*Prunus persica*; Rosaceae) derived *MYB98* (*PpMYB98*; Prupe.5G172400) to assess 5′-promoter deletion reporter series in Arabidopsis. The two were selected based on their relatively distant and closer clustering with *pAtMYB98* (Kindly check Figure 2A and Supplementary Figure S2). While both promoters exhibited a gradual drop in reporter signal with decreasing promoter length, only *pBoMYB98* exhibited exclusive SC-specific expression with a 1 kb promoter fragment which was largely retained with −821 and −686 promoter fragments as well. However, the lines harboring −498 and −325 bp promoter fragments completely lost exclusive SC-specific expression. Both of the-498 and -325 bp *pBoMYB98* fragments completely lacked the region harboring *SaeM-like* element, multiple ANL2-binding sites, and the MEME-derived conserved site (Figures 6A, B). *pPpMYB98*, which lacked a *SaeM-like* element and harbored only one ANL2-recognition motif, failed to exhibit exclusively SC-specific expression even with its 1 kb promoter fragment (Figures 6C, D) supporting the finding that *SaeM* and multiple ANL2-binding sites are required for SC-specific expression in Arabidopsis. Furthermore, our earlier mutation and fragment combination observations showed that the TF binding within the *SaeM-like* element is more crucial than that at any other sites for exclusive SC-specific as well as overall reporter expression levels (Figures 3, 4).

Discussion

SC-specific expression of *MYB98* is quintessential for synergid fate determination and regulation of the PT guidance network (Kasahara et al., 2005; Punwani et al., 2008). In Arabidopsis, ectopic expression of *MYB98* leads to fate switch of other FG components (Zhang et al., 2020) while loss of MYB98 in SCs critically hinders PT guidance near the micropylar end of the FG (Kasahara et al., 2005).

Previous studies have shown that the expression of *MYB98* in the CC is actively repressed by a MADS box member AGL80, which binds to multiple CArG sites at *pMYB98*, one of which resides just downstream of the conserved region identified by MEME analysis in this study. Previous research has also shown that *MYB98* expression in the SC is affected by the TFs CCG and CBP1 expressed at CC potentially *via* cell-to-cell communication during the early stage of FG development (Li et al., 2015; Susaki et al., 2015). However, the mechanism behind is still unclear. Since we observed *ANL2* expression at both ECs and CC of a mature ovule, potential involvement of the gene in regulating the two cannot be disregarded. *pMYB98* additionally harbors a 7-bp-long "GTAACNT" element just downstream of the CArG box. The element has been characterized as the MYB98 recognition site itself (Punwani et al., 2008), suggesting the regulation of *MYB98* in a positive-feedback loop. Furthermore, a more recent study by Noble et al. (2022) reported an 8-bp-long SEEL element, "*TAATATCT*" in the *LORELEI* (*LRE*) promoter, deletion or mutation of which led to reduced expression of the gene in SCs. The element is recognized by MYB-related REVEILLE (RVE) TFs. Interestingly, available DAP-seq data indicate that *pMYB98* also harbors multiple *SEEL-like* elements within the −400 to −300 bp region. However, the sufficiency of the element in driving SC-specific expression itself is yet unclear. This study reveals additional mechanisms as to how *MYB98* expression is spatially regulated during FG development, showing that 84 bp fragment of the *MYB98* promoter can drive SC-specific expression and mutation within 16 bp *SaeM* completely masks its SC-specific expression potential.

Synergid-specific activation element of MYB98 is crucial for dynamically driving exclusive SC-specific expression

We used a variety of reporter constructs and sequence analyses to conclude the 16-bp-long *SaeM*, "catttACACATtaaaa," as a crucial *cis*-region behind the SC-specific expression of *MYB98*. Mutation within it caused the loss of otherwise precisely SC-specific expression driving potential of 169-bp-long BYRG fragment (Figures 4B, C) strongly suggesting that *SaeM* not only activates *MYB98* expression in SCs but is also involved in *MYB98* non-activation in non-SCs. It is further supported by the occurrence of *SaeM* in much greater proportion of the exclusively SC-specific gene promoters as compared with those expressed either in all or only in CC and EC of the FG (Figure 5A).

The *SaeM* and its sandwiching region contain several ANL2-recognition motifs. Comparison of *SaeM* with known plant *cis*-elements in PlantCare revealed its partial similarity to a previously characterized light-responsive element from *Pisum sativum rbcS-3A-gene* promoter, Box-III (ATCATTTTCACTATC) (Green et al., 1987). Interestingly, however, the BOX-III harbors mismatches at an essential *SaeM* region (as shown by the mutational analysis) (Supplementary Figure S6A). This suggests a different and unique

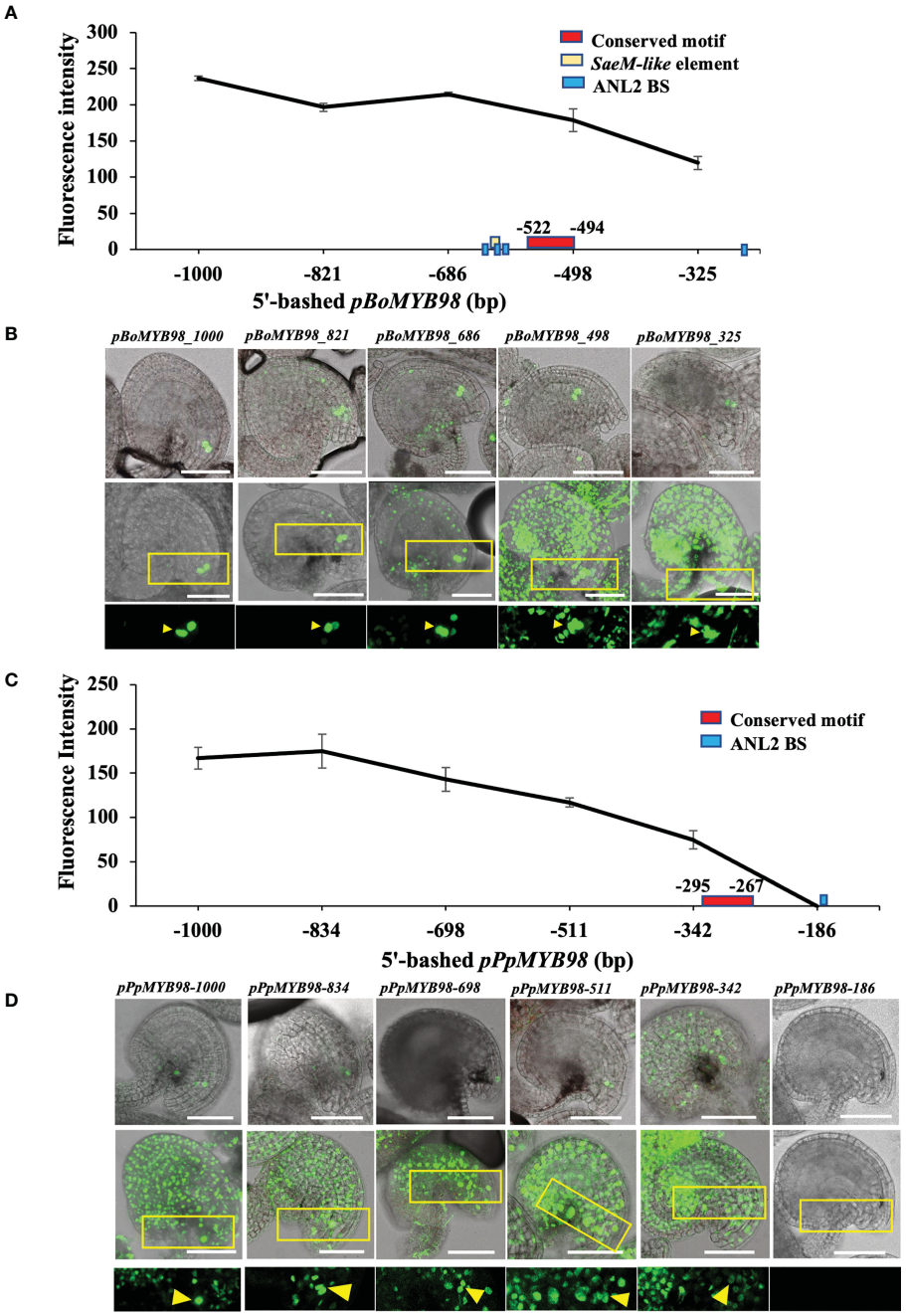

FIGURE 6
SaeM-dependent *MYB98* regulatory mechanism is conserved in Brassicaceae member. **(A, B)** Fluorescence intensities of 5′-deletion series of *Brassica oleracea*–derived *pMYB98* (*pBoMYB98*) reporter lines exhibited exclusive SC-specificity with its 1 kb promoter, which gradually waned in −821 and −686 bp reporter lines but was completely lost at reporter lines with −498 bp or shorter promoters (*n* = *12*). The region −686 to −498 harbors *SaeM-like* elements along with multiple ANL2-binding sites (BS) and the MEME-derived conserved region. **(C, D)** Fluorescence intensities of 5′-deletion series of *Prunus persica*–derived *pMYB98* (*pPpMYB98*) reporter lines exhibiting non-exclusive SC-expression (*n* = *12*). The promoter lacks *SaeM-like* element and harbors a single ANL2-binding site within 186 bp upstream of ATG. The MEME-derived weakly conserved motif falls within −342 to −186 bp region. The top rows of **(B, D)** show representative images used for fluorescence intensity measurement, the middle and bottom rows show the representative z-stack-merged (maximum projection) images and respective magnified regions. Distinguishable SCs are pointed with arrowheads. Scale bar = 50 µm.

function for *SaeM* as compared with BoxIII. Additionally, the 6-bp-long d-repeat just upstream of *SaeM* overlaps with the GCN4 motif, "TGAGTCA," which had been characterized as an essential and sufficient *cis*-element for endosperm-specific expression of a rice glutelin gene through binding of the bZIP TF member, Opaque-2 (O2) (Wu et al., 1998). Our observations showed that exclusive SC-specific expression is not perturbed by the mutation of the "TGAGT" bases within the GCN4 motif. However, the expression potential of the *cis*-fragment was completely lost upon that in combination with the mutation of a similar sequence (d-repeat)

within *SaeM*. The mutation of only the latter one, on the other hand, led to ovule-wide expression at sporophytic cells with no distinguishable SCs (Figures 4B, C), strongly suggesting for the non-exclusive expression potential of putative bZIP-like TF bound at GCN4 motif. Such observation is strongly supported by our additional observation that exclusivity in SC-specific expression was increased with the increase in the number of self concatemer of *SaeM* and two ANL2 binding motifs harboring 44-bp-long R fragment (Figures 3B and Supplementary Figure S3). Interestingly, however, we could not see any PT guidance defect in the *anl2*$^{-/-}$ mutants. More comprehensive study in the future with the double to quadruple mutant lines of *ANL2*, *HDG1*, *HDG7*, and *ETD1* may conclude whether the absence of PT guidance aberration in the *anl2*$^{-/-}$ mutant was due to the complementation effect of the *ANL2*-homologs.

Synergid-specific activation element of MYB98–dependent regulatory system is conserved among Brassicaceae members

Our study showed that the conservation of *SaeM* in greater proportion of Brassicaceae-derived *pMYB98* is translated to its involvement in driving SC-specific expression of the associated gene in Brassicaceae members. We confirmed the case *via* 5′-deletion series of *B. oleraceae*– and *P. persica*–derived *pMYB98*s. The former harboring *SaeM* exhibited largely SC-specific reporter expression unless the region harboring the *SaeM* element was deleted. The latter lacking the element often exhibited the reporter expression non-exclusively even at its full length (1 kb) (Figure 6). However, it is important to note that the *B. oleraceae*–derived *SaeM-like* element harbors few base dissimilarities to that of Arabidopsis. One of the mismatches can seriously hinder the potential binding of ANL2 and its homologs to the element, even though the putative binding sites at its up- and downstream are intact (Supplementary Figure S6B). However, as the 5′-deletion series showed, it can be tolerated for driving SC-specific *BoMYB98* expression. Furthermore, the element showed a much higher proportion of conservation among the SC-specific gene pool of Arabidopsis (Figure 5B). In addition to the Brassicaceae members, phylogenetic relatedness roughly suggested the conservation of *SaeM*-dependent regulatory features in Malvaceae members as well (Figure 2A and Supplementary Figure S2). Such family-wide conservation of regulatory feature is not uncommon. An earlier study on AGL80, a MADS-box protein, also showed its Brassicaceae family-wide conserved function of *MYB98* repression at CC (Zhang et al., 2020). Apart from Brassicaceae members, a rice *MYB98* (*OsMYB98*) also exhibited synergid-specific expression. Interestingly, its promoter also harbors *SaeM-like* element at −980 to −965, which shows greater similarity at its 3′-end and also constitutes a putative ANL2 recognition motif (Supplementary Figure S6C). It is plausible yet unconfirmed whether the element is part of SC-specific *OsMYB98* expression as well.

Conclusion and perspective

After nearly two decades of the discovery of SC-specific *MYB98* and its quintessential role in PT guidance, the current study has discovered a novel *cis*-regulatory element, *SaeM* (catttACACATtaaaa), is dynamically involved in the activation of the *pMYB98* in SCs while coordinating its effective non-activation at non-SCs. We have demonstrated that an 84-bp-long *cis*-region harboring the *SaeM* is sufficient to drive SC-specific expression in Arabidopsis. Interestingly, the *SaeM*-dependent regulatory mechanism was found highly conserved among Brassicaceae members. The element constitutes a putative ANL2 and homolog recognition motif.

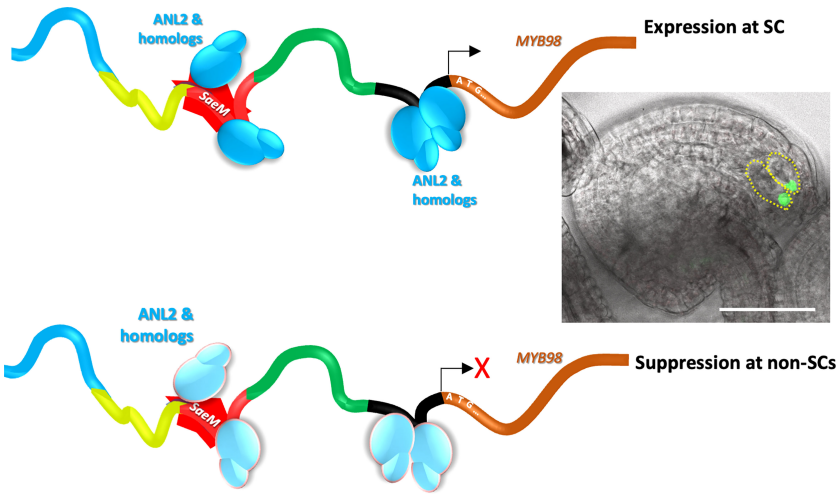

FIGURE 7
A model proposed for the *SaeM*-dependent synergid-specific expression of *pMYB98*. The *SaeM* activates *pMYB98* in synergid cells, which is potentially mediated by ANL2 and/or homologs bound to it. The process is further enhanced by the putative ANL2-binding pocket located further downstream. At non-synergid cells, however, the *SaeM* remains ineffective in driving MYB98 expression either due to potential binding of yet unknown repressor or the ANL2 and/or homologs bound to it actively contribute to the repression process.

Our observations suggest for two possible reasons behind the *SaeM*-dependent dynamic regulation of *MYB98*. Simply, it is possible that the element is selectively bound by activator at the SCs, which is impaired or replaced by the repressor at non-SCs. In other case, the ANL2 and/or homologs bound to the *SaeM* may function as activator at SCs and as active repressor at non-SCs (Figure 7). It is plausible but how the ANL2 and/or homologs would confer such dual functionality is yet unclear. A study by Zhang et al. (2020) showed that an EAR motif harboring transcription factor, AGL80 in association with the EAR-motif bound TPL/SAP18 co-repressor actively represses *MYB98* expression in CC. While some of the ANL2-like TFs too harbor putative EAR-motifs (Supplementary Figure S7), it is yet unclear whether they play any role in *SaeM*-dependent dynamic regulation of *MYB98*. A more comprehensive study on if and how ANL2 and homologs are involved in the dynamic regulatory function of *SaeM* is warranted.

Materials and methods

Bioinformatics

MYB98 homolog retrieval and assessment

Putative *MYB98* homologs were screened from the phytozome database (https://phytozome-next.jgi.doe.gov/phytozome/) using the "MYB98" keyword to retrieve respective amino acid and 1 kb 5-upstream sequences using BioMart tool (341 sequences retrieved). The sequences has been referred to as "promoters" elsewhere in the manuscript. Additionally, BLASTp was carried out against the Phytozome amino acid database using AtMYB98 as a query sequence with default parameters. Among the top 100 sequences retrieved, all but two were annotated as "MYB98." Interestingly, unlike Arabidopsis, several species, including those of Brassicaceae members, harbor more than one *MYB98* homologs. A total of 107 sequences were retained in the keyword-derived sequence pool after selecting a single *MYB98* homolog per species with lesser *e*-value with longer alignment lengths and after removing those with the promoter of < 1 kb length or ambiguous sequences. It constituted all MYB98 blastp derived sequences except for one which was annotated as *MYB119*.

To further ascertain the true MYB98 homologs, amino acid sequences of all *Arabidopsis*-derived R2R3 MYBs (129 in total) (Stracke et al., 2001) were aligned with the Phytozome-derived unique sequences (236 in total; with amino acid identity values < 95%) followed by their maximum-likelihood phylogeny using Jalview (Waterhouse et al., 2009), PhyML (Guindon et al., 2010), and iTOL (Letunic and Bork, 2021). Interestingly, not all of the putative MYB98 homologs clustered with Arabidopsis MYB98. Hence, we took the members clustered with the AtMYB subgroup 25 (SG25) members (AtMYB64, AtMYB98, and AtMYB119) as putative MYB98 homologs. A separate analysis was carried out taking the MYB98 homologs and AtMYB SG25 members (Supplementary Figure S2). The promoter sequences of 50 *MYB98* homologs along with *AtMYB98*, *AtMYB64*, and *AtMYB119* were taken for native motif search using MEME-Suite (https://meme-suite.org/meme/tools/meme) (Bailey et al., 2009).

TF and associated *pMYB98 cis*-element prediction

PlantRegMap (Tian et al., 2019) was used for the prediction of the TFs potentially binding to the 5′-deletion series derived functionally active 191 bp region with default parameters (threshold *p*-value ≤ 1e-4). ANL2 and its three homologs were aligned using MUSCLE in Jalview (Waterhouse et al., 2009) followed by the curation in Bioedit. Conserved domains and active residues in each of them were determined *via* CD search (https://www.ncbi.nlm.nih.gov/Structure/cdd/wrpsb.cgi).

SNP data retrieval and assessment

For the assessment of SNPs within the 1 kb region of *pMYB98*, the data of 1135 Arabidopsis accessions was retrieved from the Arabidopsis 1001 Genomes Project (Alonso-Blanco et al., 2016). The sequence Col-0–derived 1kb *pAtMYB98* (upstream of translation start site) was manually aligned with the database derived sequences, and the SNP sites were determined. Associated SNP graph was plotted and specific SNP types at the site of interest (*SaeM* and ANL-binding sites) were analyzed.

Motif alignment

The *SaeM* element (CATTTACACATTAAAA) was taken for their independent alignment against the 1 kb promoters of the genes from various gene pools (FG component cell specific, pollen specific, non-specific, etc.) Song et al. (2020) using the motif alignment program MAST (http://www.meme.sdsc.edu/) (Bailey and Gribskov, 1998) with default parameters (*e*-value < 10, *p*-value < 0.0001). The exclusive SC-specific expression of a gene was considered true when it had null expression value at all replications of CC and EC but > 0 values at those of SCs.

Plant materials

Arabidopsis Col-0 was used as the background line (WT) as well as for transformation purposes in the study. The plants were grown at *in vivo* conditions in the culture room with 24/8 hr (light/dark) photoperiod and ~25°C temperature at Fujian Agricultural and Forestry University, Fuzhou, China.

Cloning and vector construction

Most of the constructs were prepared using In-Fusion HD Cloning Kit (Takara, 121416) following the manufacturer's protocol and a few were prepared *via* restriction digestion cloning procedure using the FastDigest enzymes (Thermo Fisher Scientific).

5′-promoter bashing

For the 5′-promoter deletion series, DNA was extracted from WT *Arabidopsis thaliana*, *Brassica oleracea*, and *Prunus persica* following the CTAB extraction method (Clarke, 2009), and desired

lengths of 5′-deleted promoter fragments upstream of ATG was amplified using respective primers. The lengths of each deletion series fragment have been shown in the associated figures. pCAMBIA1305 (PC1305) plasmid was used as a base vector for deletion series constructs preparation in such a way that each promoter fragment is cloned upstream of the reporter (*GFP* for *A. thaliana* during the initial assessment, and *H2B-GFP* for *B. oleracea* and *P. persica* to assess cross-species feature conservation). Associated primers have been provided in Supplementary Table S8.

Addition/deletion of pMYB98 cis-fragments

169 bp functionally active *pMYB98* region derived from the 5′/3′-deletion series in combination with the putative TF binding site prediction and the sequence region of MEME-derived putatively conserved motif lying within the functionally active *pMYB98* region (23 bp sequence at 5′-region of 29 bp long motif) were targeted for the assessment of their role in reporter expression.

As an SC-specific positive control, the 1.5 kb of *pMYB98* was amplified using the pMYB98_1.5k.fwd and pMYB98_1.5k.rev primers and cloned into the H2B-GFP reporter construct. Its functionally active 169 bp region lacking version (*pΔMYB98*) was prepared by amplifying the first half with pMYB98_1.5k.fwd and pMYB98_BYRGdel.rev (855 bp) and the latter half with the pMYB98_BYRGdel.fwd and pMYB98_1.5k.rev (543 bp) followed by their assembly and incorporation upstream of the *H2B-GFP* of the reporter construct using the In-Fusion HD Cloning Kit (Takara, 121416) following the manufacturer's protocol. For the preparation of the conserved region lacking version of the promoter (*pδMYB98*), the reverse primer of the first half and forward primer of the second were respectively substituted with MYB98proDelcon_infu.rev and pMYB98_Delcon.fwd while using them as they were and assembled in the reporter construct as mentioned earlier. The amplified promoter fragments were assembled and incorporated into the reporter construct following the aforementioned procedure.

For the inclusion effect of the aforementioned region on restricting the reporter expression at SCs, we amplified 346-bp-long *pCaMV* along with an additional 238 bp sequence at its upstream and 15 bp at its downstream (599 bp in total) from the pC1302 plasmid using pCaMV.fwd and pCaMV.rev primers. The amplicon was incorporated upstream of *H2B-GFP*, and the prepared construct was used as a negative control for SC-specific expression. The functionally active 169 bp fragment and the MEME-derived conserved motif harboring regions were independently incorporated at −227 bp of *pCaMV* (−239 bp from ATG) to construct *pΔCaMV* and *pδCaMV*, respectively. For the preparation of *pΔCaMV*, the first half of *pCaMV* was amplified from pCAMBIA1302 using pCaMV.fwd and pCaMVpt1A.rev primers (409 bp), and the second half was amplified using the pCaMVpt2.fwd and pCaMV.rev primers (239 bp). For the *pδCaMV*, only the reverse primer of the first half of *pCaMV* was substituted with pCaMVpt1B.rev while others were used as they were. The 169 bp fragment for *pΔCaMV* was amplified using pCV-A.fwd and AB-pCV.rev, and the MEME-derived conserved region harboring fragment for *pδCaMV* was amplified by substituting the forward primer with pCV-A.fwd. Respective constructs were prepared *via* infusion cloning as mentioned above. Primer information is provided in Supplementary Table S8.

pMYB98 sub-fragment combination and fragment mutation

For the combination of the B, Y, R, and G sub-fragments within the functionally active 169 bp region, each sub-fragment was amplified *via* primer extension of respective 5′ region annealing forward and reverse primers harboring 3′-sequence variation based on target fragment combinations. For the self concatemers of each fragment, the whole target fragment was synthesized. For the preparation of putative repeat sequence mutation, the target region was amplified using the mutation-harboring primers followed by the sub-fragment assembly. Each sub-fragment combination or mutated fragment was incorporated upstream of *CaMV* minimal promoter (*MP*) of the *H2B-GFP* reporter construct. (Primer information can be provided upon request).

Bait constructs preparation for Y1H

Three *pMYB98* bait fragments of 40 bp (−679 to −640 bp), 60 bp (−679 to −620 bp), and 139 bp (−679 to −541 bp) were amplified using pMYB98-pHISi_fw (P1) as forward primer and respective reverse primers of pMYB98-pHISi40bp_rev, pMYB98-pHISi60bp_rev, and pMYB98-pHISi139bp_rev. Each amplification product was cloned into the pHISi yeast expression vector independently.

Preparation of *pANL2* reporter construct

For the preparation of *pANL2::H2B-GFP* construct, the 1.5 kb promoter region upstream of ATG was amplified using pANL2_1.5k.fwd and pANL2_1.5k.rev primers (Supplementary Table S8) and cloned into the *H2B-GFP* reporter construct *via* infusion cloning.

Plant transformation and assessment

Transgenic seeds were derived from the Col-0 Arabidopsis plants *via* the floral dip transformation method following the protocols described by Bent (2006). Simply, the acetosyringone-treated and Silwett-supplemented *Agrobacterium* transformation solution (OD ~ 0.8; prepared after the single colony selection followed by the culture and sub-culture steps) of intended constructs were used for the transformation. The culture room-grown plants with numerous floral buds were taken and the opened flowers were removed before dipping the buds in the *Agrobacterium* solution. The plants were dipped in the fresh transformation solution every other day three consecutive times and left for seed set. The seeds were collected from the mature silique and plated in the selection antibiotics supplemented MS media. *MYB98* being

FG-specific, we took the plants harboring at least ~50% of the ovules with the distinguishable SC-specific GFP markers for the fluorescence intensity assessment. Nine to 20 independent transgenic plants per each construct were used for the observation in the study.

Reverse transcription polymerase chain reaction

Tissues from five different plant parts, that is, flower (stages 1-2, 3, 4-5, and 6-12) silique (very young, young, medium, and mature stage), leaves (young and mature stage), stem (young, medium, and mature stage), and root (upper part without root tips and lower part with root tips) were collected from Col-0Arabidopsis plants. RNA was extracted from the collected samples using RNeasy Plant Mini Kit (Cat no. 74904; Qiagen Shanghai, China), and cDNA was synthesized for the tissue-specific expression assessment of *ANL2* along with *Actin2*. Traditional PCR machine (GeneAmp PCR System 9700 Thermo Fisher Scientific, Hongkong) was used for RT-PCR using Novogene 2x Taq Plus PCR mixture under the following condition: One cycle of pre-heating at 95°C for 5 min followed by 30 cycles of (95°C for 20 s, 59°C for 35 min, and 72°C for 1 min) and one cycle of (72°C for 7 min and 4°C for 10 min). Associated primer information has been provided in Supplementary Table S8.

Confocal microscopy

Flowers at the stage of 12c (Christensen et al., 1997) were emasculated and microscopic observations were made after 24h. The siliques were excised, put on the observation slides, and the valves were removed using a syringe needle. The samples were covered with coverslip after adding a few drops of water and observation of the exposed ovules were made under MRC 1000 confocal laser scanning microscope (CLSM) (Bio-Rad) *via* the detection of GFP emission within the 500–530 nm wavelength range after excitation of the sample with an argon laser at 488 nm wavelength. A similar sample preparation procedure was followed for the sample observation under an epifluorescence microscope (Ex546/10/DM 565 LP/Em 590 LP) using a GFP filter. The collected images were analyzed using Leica LAS-X Life Science Microscope Software, Zen blue 2.3, and Fiji. The distinguishability of the SCs was determined in the 3D z-stacked images based on the position-specific (micropylar) typical twin-like nuclear localizations. The fluorescence images and respective numerical values were retrieved after the z-stack merges (maximum projection) unless mentioned otherwise (https://imagej.net/software/fiji/).

Yeast-one-hybrid assay

The Y187 yeast strain was transformed with the three bait constructs independently and Y1H screening was carried out using the Arabidopsis TF library containing ~1,400 transcription factors following the protocol described by Mitsuda et al. (2010). Three *pMYB98* bait fragments of 40 bp (−679 to −640 bp), 60 bp (−679 to −620 bp), and 139 bp (−679 to −541 bp) were cloned into pHISi using the In-Fusion HD Cloning Kit (Takara, 121416) following the manufacturer's protocol. Each bait vector was linearized by ApaI and transformed into the yeast strain YM4271 using PEG/LiAC method. Appropriate 3-AT concentration was selected after testing the bait vector harboring yeast cells for HIS3 reporter background expression. The yeast mating method derived haploid yeast cells were selected on screening plates (SD-Ura-His-Leu plus optimum 3-AT) and positive colonies were sequenced afterward.

Pollen tube elongation assessment

The flowers at stage of 12c from target plants were emasculated and hand-pollinated with the pollens of the desired plant after ~40h after emasculation (Faure et al., 2002). The pistils were excised at defined hours after pollination (after 12h–24h) and fixed in FAA (10% formaldehyde, 5% acetic acid, and 50% ethyl alcohol). The fixed pistil tissues were softened in 1M NaOH for 4h and stained with aniline blue to visualize PTs in the pistil squashes (Jones et al., 2018) under CLSM or epifluorescence microscopes at 12h, 16h, and 24h after pollination (HAP).

Statistics

Samples of all relevant experiments were collected at least in triplicates. Sample numbers have been provided with the associated figures. The collected numerical data were analyzed *via* Duncan's multiple range test (DMRT) or Student's t-test.

Data availability statement

The datasets presented in this study can be found in online repositories. The names of the repository/repositories and accession number(s) can be found in the article/Supplementary Material.

Author contributions

RK conceived the idea. RK and PA designed the experiments. RK and LX carried out the preliminary 3'- and 5'- deletion series experiments. LB and BP contributed to initial sequence assessments. NM carried out the Y1H experiment. PA guided and carried out the majority of the remaining experiments along with SZ. XL, CH, XW and JH assisted on phenotypic data retrieval. PA analyzed and curated final data and figures, and prepared the manuscript. LB, RK, BP, NM and SN contributed on the manuscript revision. All authors contributed to the article and approved the submitted version.

Funding

The work was supported by start-up funds from the School of Life Sciences, Fujian Agriculture and Forestry University (Grant #: 114-712018008 to RK) and the FAFU-UCR Joint Center, Haixia Institute of Science and Technology, Fujian Agriculture and Forestry University (Grant #: 102-118990010 to RK). This work was also supported by the Chinese NSFC fund (Grant #: 31970809 to RK). This work was also supported by a grant-in-aid(22K21366 to R.D.K.) from the Japanese Society for the Promotion of Science (JSPS).

Conflict of interest

The authors declare that the research was conducted in the absence of any commercial or financial relationships that could be construed as a potential conflict of interest.

Publisher's note

Supplementary material

The Supplementary Material for this article can be found online at: https://www.frontiersin.org/articles/10.3389/fpls.2023.1177058/full#supplementary-material

SUPPLEMENTARY FIGURE 1
Preliminary 3′-bashing of *pMYB98* indicates that deletion of either of the two *cis*-regions within the *pMYB98* drastically reduces the reporter signal. **(A)** Relative GFP-signal driven by 3′-deletion *pMYB98* series. The intact and deleted promoter segments have been denoted with the solid and dashed lines, respectively. Each of the deletion series was fused with the minimal promoter (*MP*) at its 3′-end (just upstream of *GFP*). The pairs of subsequent intact and deletion fragments exhibiting the drastic drops in GFP intensity (from −615 to −487 bp and from −251 to −121 bp) have been highlighted with the red background. +++ and - represent for the highest and no GFP intensities respectively. **(B)** Conclusion derived from the 3′-deletion promoter series **(A)** showing two distinct pockets deletion of which brought significant drops in the GFP signal.

SUPPLEMENTARY FIGURE 2
Maximum-likelihood phylogeny of the phytozome derived putative MYB98s and AtMYB subgroup 25 members. The subtree used for is highlighted in faint-red. The tree was prepared using Jalview (Waterhouse et al., 2009), PhyML (Guindon et al., 2010), and iTOL (Letunic and Bork, 2021).

SUPPLEMENTARY FIGURE 3
R3-MP driven *H2B-GFP* expression at all FG component cells with the strongest signal at synergids.

SUPPLEMENTARY FIGURE 4
Yeast-one-hybrid (Y1H) assay-derived transcription factors (TFs) exhibiting binding affinity to *pMYB98*. Three independent Y1H assays with the overlapping *pMYB98* sequences of 40 **(A)**, 60 **(B)**, and 139 bp **(C)** identified 23 unique TFs among which the three common TFs in all assays have been underlined. The domain family of each TF is shown in the parenthesis. The TFs exhibiting strong, weak, and weakest binding affinities are in red, blue, and light blue text. The TF (ANL2) overlapped with the *in silico* prediction has been denoted with an asterisk (*).

SUPPLEMENTARY FIGURE 5
Few ovules of defective *anl2*$^{-/-}$ lines exhibited *pMYB98* driven H2B-GFP expression at all FG component cells, which did not bring any changes to the pollen tube guidance and its ovular reception. (A) GFP signals at all FG component cells of *pMYB98* reporter harboring *anl2*$^{-/-}$ ovule with strongest signal at synergids. **(B–E)** Representative images of the reciprocal crosses between WT and *anl2*$^{-}$/- at 24 HAP. **(F)** Pollen tube reception rate at different time points (each bar represents mean ± SE; n = 20).

SUPPLEMENTARY FIGURE 6
SaeM (boxed in green) comparison with known motif (BoxIII) **(A)**, similar region from *Brassica oleracea MYB98* promoter (*pBoMYB98*) **(B)**, and the *SaeM-like* element from rice *MYB98* promoter (*pOsMYB98*) **(C)**. *SaeM* and *SaeM-like* elements are within green boxes, mutation susceptible d-repeat within *SaeM* is in bold, putative ANL2-like TF-binding sites are in pink and shaded, and red arrowhead points to the potential mutation susceptible mismatch within *pBoMYB98 SaeM-like* element.

SUPPLEMENTARY FIGURE 7
Structure and conserved motifs assessment in ANL2 and homologs. **(A)** Schematic representation showing that ANL2 and HDG1 harbor two EAR motifs in addition to the HD- and START-domains, while HDG7 and ETD1 lack EAR motif. **(B)** Alignment of ANL2 and homologs with respective conserved motifs are annotated. Green oval circles mark the residues involved in DNA binding and red oval circles mark the residues involved in lipid binding.

References

Adhikari, P. B., Liu, X., Wu, X., Zhu, S., and Kasahara, R. D. (2020). Fertilization in flowering plants: an odyssey of sperm cell delivery. *Plant Mol. Biol.* 103, 9–32. doi: 10.1007/s11103-020-00987-z

Alonso-Blanco, C., Andrade, J., Becker, C., Bemm, F., Bergelson, J., Borgwardt, K. M., et al. (2016). 1,135 genomes reveal the global pattern of polymorphism in *Arabidopsis thaliana*. *Cell* 166, 481–491. doi: 10.1016/j.cell.2016.05.063

Austin, R. S., Hiu, S., Waese, J., Ierullo, M., Pasha, A., Wang, T. T., et al. (2016). New BAR tools for mining expression data and exploring *Cis*-elements in *Arabidopsis thaliana*. *Plant J.* 88, 490–504. doi: 10.1111/tpj.13261

Bailey, T. L., Boden, M., Buske, F. A., Frith, M., Grant, C. E., Clementi, L., et al. (2009). MEME suite: tools for motif discovery and searching. *Nucleic Acids Res.* 37, W202–W208. doi: 10.1093/nar/gkp335

Bailey, T. L., and Gribskov, M. (1998). Combining evidence using *p*-values: application to sequence homology searches. *Bioinformatics* 14, 48–54. doi: 10.1093/bioinformatics/14.1.48

Bent, A. (2006). ""Arabidopsis thaliana floral dip transformation method,"," in *Agrobacterium protocols*. Ed. K. Wang. (Totowa, NJ: Humana Press), 87–104.

Christensen, C. A., King, E. J., Jordan, J. R., and Drews, G. N. (1997). Megagametogenesis in *Arabidopsis* wild type and the *Gf* mutant. *Sexual Plant Reprod.* 10, 49–64. doi: 10.1007/s004970050067

Clarke, J. D. (2009). Cetyltrimethyl ammonium bromide (CTAB) DNA miniprep for plant DNA isolation. *Cold Spring Harbor Protoc.* 2009, pdb. prot5177. doi: 10.1101/pdb.prot5177

Drews, G. N., and Koltunow, A. M. (2011). The female gametophyte. *Arabidopsis Book* 9, e0155. doi: 10.1199/tab.0155

Faure, J.-E., Rotman, N., Fortuné, P., and Dumas, C. (2002). Fertilization in arabidopsis thaliana wild type: developmental stages and time course. *Plant J.* 30, 481–488. doi: 10.1046/j.1365-313X.2002.01305.x

Goodstein, D. M., Shu, S., Howson, R., Neupane, R., Hayes, R. D., Fazo, J., et al. (2012). Phytozome: a comparative platform for green plant genomics. *Nucleic Acids Res.* 40, D1178–D1186. doi: 10.1093/nar/gkr944

Green, P. J., Kay, S. A., and Chua, N. H. (1987). Sequence-specific interactions of a pea nuclear factor with light-responsive elements upstream of the rbcS-3A gene. *EMBO J.* 6, 2543–2549. doi: 10.1002/j.1460-2075.1987.tb02542.x

Guindon, S., Dufayard, J.-F., Lefort, V., Anisimova, M., Hordijk, W., and Gascuel, O. (2010). New algorithms and methods to estimate maximum-likelihood phylogenies: assessing the performance of PhyML 3.0. *System. Biol.* 59, 307–321. doi: 10.1093/sysbio/syq010

Higashiyama, T. (2002). The synergid cell: attractor and acceptor of the pollen tube for double fertilization. *J. Plant Res.* 115, 0149–0160. doi: 10.1007/s102650200020

Honys, D., and Twell, D. (2003). Comparative analysis of the arabidopsis pollen transcriptome. *Plant Physiol.* 132, 640–652. doi: 10.1104/pp.103.020925

Jones, D. S., Liu, X., Willoughby, A. C., Smith, B. E., Palanivelu, R., and Kessler, S. A. (2018). Cellular distribution of secretory pathway markers in the haploid synergid cells of *Arabidopsis thaliana*. *Plant J.* 94, 192–202. doi: 10.1111/tpj.13848

Kasahara, R. D. (2018). ""The regulation of sperm cells delivery to the embryo sac,"," in *Pollination in plants*, *1st ed*. Ed. P. W. Mokwala (Rijeka:IntechOpen), 7–22.

Kasahara, R. D., Portereiko, M. F., Sandaklie Nikolova, L., Rabiger, D. S., and Drews, G. N. (2005). *MYB98* Is required for pollen tube guidance and synergid cell differentiation in *Arabidopsis*. *Plant Cell* 17, 2981–2992. doi: 10.1105/tpc.105.034603

Kessler, S. A., and Grossniklaus, U. (2011). She's the boss: signaling in pollen tube reception. *Curr. Opin. Plant Biol.* 14, 622–627. doi: 10.1016/j.pbi.2011.07.012

Kulichová, K., Kumar, V., Steinbachová, L., Klodová, B., Timofejeva, L., Juříček, M., et al. (2020). PRP8A and PRP8B spliceosome subunits act co-ordinately to control pollen tube attraction in arabidopsis. *Development* 147 (11), 186742. doi: 10.1242/dev.186742

Letunic, I., and Bork, P. (2021). Interactive tree of life (iTOL) v5: an online tool for phylogenetic tree display and annotation. *Nucleic Acids Res.* 49, W293–W296. doi: 10.1093/nar/gkab301

Li, H. J., Zhu, S. S., Zhang, M. X., Wang, T., Liang, L., Xue, Y., et al. (2015). Arabidopsis CBP1 is a novel regulator of transcription initiation in central cell-mediated pollen tube guidance. *Plant Cell* 27, 2880–2893. doi: 10.1105/tpc.15.00370

Mitsuda, N., Ikeda, M., Takada, S., Takiguchi, Y., Kondou, Y., Yoshizumi, T., et al. (2010). Efficient yeast one-/two-hybrid screening using a library composed only of transcription factors in *Arabidopsis thaliana*. *Plant Cell Physiol.* 51, 2145–2151. doi: 10.1093/pcp/pcq161

Noble, J. A., Seddon, A., Uygun, S., Bright, A., Smith, S. E., Shiu, S.-H., et al. (2022). The *SEEL* motif and members of the MYB-related REVEILLE transcription factor family are important for the expression of *LORELEI* in the synergid cells of the arabidopsis female gametophyte. *Plant Reprod.* 35, 61–76. doi: 10.1007/s00497-021-00432-1

O'Malley, R. C., Huang, S.-S. C., Song, L., Lewsey, M. G., Bartlett, A., Nery, J. R., et al. (2016). Cistrome and epicistrome features shape the regulatory DNA landscape. *Cell* 165, 1280–1292. doi: 10.1016/j.cell.2016.04.038

Okuda, S., Tsutsui, H., Shiina, K., Sprunck, S., Takeuchi, H., Yui, R., et al. (2009). Defensin-like polypeptide LUREs are pollen tube attractants secreted from synergid cells. *Nature* 458, 357. doi: 10.1038/nature07882

Punwani, J. A., and Drews, G. N. (2008). Development and function of the synergid cell. *Sexual Plant Reprod.* 21, 7–15. doi: 10.1007/s00497-007-0059-3

Punwani, J. A., Rabiger, D. S., and Drews, G. N. (2007). *MYB98* Positively regulates a battery of synergid-expressed genes encoding filiform apparatus–localized proteins. *Plant Cell* 19, 2557–2568. doi: 10.1105/tpc.107.052076

Punwani, J. A., Rabiger, D. S., Lloyd, A., and Drews, G. N. (2008). The *MYB98* subcircuit of the synergid gene regulatory network includes genes directly and indirectly regulated by MYB98. *Plant J.* 55, 406–414. doi: 10.1111/j.1365-313X.2008.03514.x

Rabiger, D. S., and Drews, G. N. (2013). *MYB64* And *MYB119* are required for cellularization and differentiation during female gametogenesis in *Arabidopsis thaliana*. *PloS Genet.* 9, e1003783. doi: 10.1371/journal.pgen.1003783

Song, Q., Ando, A., Jiang, N., Ikeda, Y., and Chen, Z. J. (2020). Single-cell RNA-seq analysis reveals ploidy-dependent and cell-specific transcriptome changes in arabidopsis female gametophytes. *Genome Biol.* 21, 178. doi: 10.1186/s13059-020-02094-0

Stracke, R., Werber, M., and Weisshaar, B. (2001). The R2R3-MYB gene family in *Arabidopsis thaliana*. *Curr. Opin. Plant Biol.* 4, 447–456. doi: 10.1016/S1369-5266(00)00199-0

Susaki, D., Suzuki, T., Maruyama, D., Ueda, M., Higashiyama, T., and Kurihara, D. (2021). Dynamics of the cell fate specifications during female gametophyte development in arabidopsis. *PloS Biol.* 19, e3001123. doi: 10.1371/journal.pbio.3001123

Susaki, D., Tsutsui, H., Kurihara, D., Takeuchi, H., and Higashiyama, T. (2015). Live imaging and laser disruption reveal the dynamics and cell–cell communication during torenia fournieri female gametophyte development. *Plant Cell Physiol.* 56, 1031–1041. doi: 10.1093/pcp/pcv031

Takeuchi, H. (2021). The role of diverse LURE-type cysteine-rich peptides as signaling molecules in plant reproduction. *Peptides* 142, 170572. doi: 10.1016/j.peptides.2021.170572

Takeuchi, H., and Higashiyama, T. (2012). A species-specific cluster of defensin-like genes encodes diffusible pollen tube attractants in *Arabidopsis*. *PloS Biol.* 10, e1001449. doi: 10.1371/journal.pbio.1001449

Tian, F., Yang, D.-C., Meng, Y.-Q., Jin, J., and Gao, G. (2019). PlantRegMap: charting functional regulatory maps in plants. *Nucleic Acids Res.* 48, D1104–D1113. doi: 10.1093/nar/gkz1020

Waterhouse, A. M., Procter, J. B., Martin, D. M. A., Clamp, M., and Barton, G. J. (2009). Jalview version 2–a multiple sequence alignment editor and analysis workbench. *Bioinformatics* 25, 1189–1191. doi: 10.1093/bioinformatics/btp033

Wu, C.-Y., Suzuki, A., Washida, H., and Takaiwa, F. (1998). *The GCN4 motif in a rice glutelin gene is essential for endosperm-specific gene expression and is activated by opaque-2 in transgenic rice plants*, Vol. 14. 673–683. doi: 10.1046/j.1365-313x.1998.00167.x

Wu, Y., Wen, J., Xia, Y., Zhang, L., and Du, H. (2022). Evolution and functional diversification of R2R3-MYB transcription factors in plants. *Horticult. Res.* 9. doi: 10.1093/hr/uhac058

Zhang, M.-X., Zhu, S.-S., Xu, Y.-C., Guo, Y.-L., Yang, W.-C., and Li, H.-J. (2020). Transcriptional repression specifies the central cell for double fertilization. *Proc. Natl. Acad. Sci.* 117 (11), 6231–6236. doi: 10.1073/pnas.1909465117

Zhong, S., Liu, M., Wang, Z., Huang, Q., Hou, S., Xu, Y. C., et al. (2019). Cysteine-rich peptides promote interspecific genetic isolation in *Arabidopsis*. *Science* 6443, eaau95644. doi: 10.1126/science.aau9564

frontiers | Frontiers in Plant Science

TYPE Original Research
PUBLISHED 22 June 2023
DOI 10.3389/fpls.2023.1063765

OPEN ACCESS

EDITED BY
Giampiero Cai,
University of Siena, Italy

REVIEWED BY
Yoko Mizuta,
Nagoya University, Japan
Jong-Seong Jeon,
Kyung Hee University, Republic of Korea

*CORRESPONDENCE
Ruth Stadler
ruth.stadler@fau.de

†PRESENT ADDRESSES
Theresa Maria Reimann,
Cell Biology, Department of Biology, Friedrich-Alexander University Erlangen-Nuremberg, Erlangen, Germany
Carolin Fritz,
Cell Biology, Department of Biology, Friedrich-Alexander University Erlangen-Nuremberg, Erlangen, Germany

RECEIVED 07 October 2022
ACCEPTED 05 June 2023
PUBLISHED 22 June 2023

CITATION
Seitz J, Reimann TM, Fritz C, Schröder C, Knab J, Weber W and Stadler R (2023) How pollen tubes fight for food: the impact of sucrose carriers and invertases of *Arabidopsis thaliana* on pollen development and pollen tube growth. *Front. Plant Sci.* 14:1063765. doi: 10.3389/fpls.2023.1063765

How pollen tubes fight for food: the impact of sucrose carriers and invertases of *Arabidopsis thaliana* on pollen development and pollen tube growth

Jessica Seitz[1], Theresa Maria Reimann[1†], Carolin Fritz[1†], Carola Schröder[1], Johanna Knab[2], Walter Weber[1] and Ruth Stadler[1*]

[1]Molecular Plant Physiology, Department of Biology, Friedrich-Alexander University Erlangen-Nuremberg, Erlangen, Germany, [2]Cell Biology, Department of Biology, Friedrich-Alexander University Erlangen-Nuremberg, Erlangen, Germany

Pollen tubes of higher plants grow very rapidly until they reach the ovules to fertilize the female gametes. This growth process is energy demanding, however, the nutrition strategies of pollen are largely unexplored. Here, we studied the function of sucrose transporters and invertases during pollen germination and pollen tube growth. RT-PCR analyses, reporter lines and knockout mutants were used to study gene expression and protein function in pollen. The genome of Arabidopsis thaliana contains eight genes that encode functional sucrose/H^+ symporters. Apart from *AtSUC2*, which is companion cell specific, all other *AtSUC* genes are expressed in pollen tubes. AtSUC1 is present in developing pollen and seems to be the most important sucrose transporter during the fertilization process. Pollen of an *Atsuc1 knockout* plant contain less sucrose and have defects in pollen germination and pollen tube growth. The loss of other sucrose carriers affects neither pollen germination nor pollen tube growth. A multiple knockout line *Atsuc1Atsuc3Atsuc8Atsuc9* shows a phenotype that is comparable to the Atsuc1 mutant line. Loss of AtSUC1 can`t be complemented by AtSUC9, suggesting a special function of AtSUC1. Besides sucrose carriers, pollen tubes also synthesize monosaccharide carriers of the AtSTP family as well as invertases. We could show that *AtcwINV2* and *AtcwINV4* are expressed in pollen, *AtcwINV1* in the transmitting tissue and *AtcwINV5* in the funiculi of the ovary. The vacuolar invertase *AtVI2* is also expressed in pollen, and a knockout of *AtVI2* leads to a severe reduction in pollen germination. Our data indicate that AtSUC1 mediated sucrose accumulation during late stages of pollen development and cleavage of vacuolar sucrose into monosaccharides is important for the process of pollen germination.

KEYWORDS

***Arabidopsis thaliana*, AtSUC1, AtVI2, carbohydrate storage, esculin, pollen tubes, sucrose transporters, vacuolar invertases**

Introduction

The pollen represents the male gametophyte of seed plants. When a pollen grain lands on an appropriate stigma, it hydrates and produces a pollen tube that grows through the stigma, the style, and the ovary until it reaches the ovules. This tip-growth process is very fast and requires the pollen to efficiently synthesize proteins, cell membrane, and cell wall material (Dresselhaus & Franklin-Tong, 2013). The components are transported through an extensive vesicular network to the growing tip (Guan et al., 2013; Hao et al., 2022). Interestingly, it is not yet well understood which substances pollen use as an energy source for this demanding growth process.

Generally, pollen may be pre-loaded with carbohydrates (Speranza et al., 1997) as well as lipids during their development (Regan & Moffatt, 1990). *Arabidopsis thaliana* pollen contain lipid droplets, which could be used not only for membrane biosynthesis but also as an energy source (Bai et al., 2023). Another strategy for pollen nutrition might be the import of sugars during pollen tube growth. This strategy assumes the presence of nutrients, most likely sucrose, in the apoplasmic fluid of the pistil. Sucrose is mainly produced in leaves and delivered to the flowers *via* the phloem, where it reaches concentrations of up to 0.3 M (Deeken et al., 2002). Studies with phloem mobile GFP synthesized in companion cells demonstrated that phloem unloading in *Arabidopsis thaliana* pistils follows an entirely symplasmic pathway. As GFP accumulated in all cells of the pistil except the fully developed ovules (Werner et al., 2011), these studies indicate that the cells along the pathway of growing pollen tubes may contain high amounts of sucrose. Sucrose export from the cytosol of these cells into the apoplasm might then be mediated by transporters of the SUGAR WILL EVENTUALLY BE EXPORTED (SWEET) family (Chen et al., 2012). The sucrose carrier AtSWEET9 is present in papillae cells of the style and AtSWEET10 was detected in the transmitting tissue of style and ovary (Lin et al., 2014; Rottmann et al., 2018b). Their presence in these cells could lead to a high sucrose concentration in the cell wall area of the stigma and the transmitting tissue, although there are no solid data available on actual sugar concentrations in the apoplasm of the pistil so far. Pollen are not connected to other cells *via* plasmodesmata. Sugar uptake into pollen my occur *via* endocytosis or *via* active sugar/H^+ cotransporters (Sauer et al., 1994; Etxeberria et al., 2005). Sucrose can be taken up either as disaccharide or after cleavage by apoplasmic invertases as fructose and glucose. Six *SUGAR TRANSPORTER PROTEIN* (*STP*) genes, which encode monosaccharide/H^+ cotransporters, are expressed in pollen tubes (Rottmann et al., 2018b). Interestingly, the knockout of all six *AtSTP* genes in a sextuple knockout line led to enhanced pollen tube growth on medium containing glucose, however, the knockout plants were fully fertile and produced a normal amount of seeds. This observation led to the hypothesis that glucose is rather a signal that regulates pollen tube growth than a nutrient that promotes growth (Rottmann et al., 2018b).

The presence of sucrose carriers in pollen tubes is less well studied. The genome of *Arabidopsis thaliana* includes nine *SUCROSE TRANSPORTER* genes (*AtSUC1-9*). *AtSUC7* is a pseudogene, all other *AtSUC* genes code for active sucrose/H^+ cotransporters. They catalyze the transport of sucrose or maltose with K_M values between 0.2 – 0.8 mM for sucrose (Sauer & Stolz, 1994; Ludwig et al., 2000; Meyer et al., 2000; Weise et al., 2000; Sauer et al., 2004; Rottmann et al., 2018a). AtSUC4 is localized in the tonoplast and transports sucrose from the vacuole into the cytosol (Endler et al., 2006; Schulz et al., 2011; Schneider et al., 2012a). All other AtSUCs reside in the plasma membrane. Several different groups used reporter gene approaches to study the expression of *AtSUC* genes and detected a promoter activity in pollen tubes (Stadler et al., 1999; Schulze et al., 2000; Meyer et al., 2004; Sivitz et al., 2008; Rottmann et al., 2018a), indicating that sucrose transporters are important for pollen tube growth. However, several of the reporter gene lines in the papers mentioned above miss the genomic sequence and the introns of the gene of interest. Reporter often don`t show the *in vivo* situation of expression if the introns are missing (Fiume et al., 2004; Rose, 2004; Sivitz et al., 2007; Weise et al., 2008; Rottmann et al., 2018a). Therefore, we decided to investigate the presence of SUCs in pollen tubes using reporter lines that include the genomic sequence of the genes of interest.

Sucrose can be cleaved by invertases or by sucrose synthases (Stein & Granot, 2019). Invertases can be divided into cell wall invertases (cwINV), alkaline/neutral invertases (A/N-INV), and vacuolar invertases (VI) based on their biochemical properties (solubility, pH optima, isoelectric point) and their subcellular localization (Sturm, 1999; Koch, 2004; Roitsch & González, 2004; Ruan et al., 2010; Ruan, 2014). Phylogenetically, cell wall invertases are closely related to vacuolar invertases, but distant from alkaline/neutral invertases (Ruan et al., 2010). Cell wall and vacuolar invertases also share some biochemical properties. They cleave sucrose in glucose and fructose and are most efficient in acidic environments with a pH between 4.5 and 5.0. In *Arabidopsis thaliana* six genes encode cell wall invertases, *AtcwINV1* - *AtcwINV6*. However, the enzymes AtcwINV3 and AtcwINV6 are catalytically inactive invertases (Sherson et al., 2003; De Coninck et al., 2005). Cell wall invertases are expressed in source tissues, for example in leaves, but also in sink tissues including pollen (Tymowska-Lalanne & Kreis, 1998; Sherson et al., 2003; Hirsche et al., 2009; Ruhlmann et al., 2010; Wang & Ruan, 2012; Liao et al., 2020; Li et al., 2021). There are two genes that code for vacuolar invertases in *Arabidopsis thaliana*: *AtVI1* and *AtVI2* and both vacuolar invertases play a role in plant and seed development (Vu et al., 2020).

In the present paper we analyzed the role of sucrose transporters as well as invertases for the fertility of pollen of *Arabidopsis thaliana*. We used reporter gene lines for invertases and for the sucrose carriers AtSUC1, 3, 4, 5, 6, 8 and 9 containing not only promoter sequences but also genomic sequences together with the introns of the respective genes. We didn`t investigate *AtSUC7* because it is a pseudogene and *AtSUC2* because it is known to be companion cell specific. The *AtSUC2* promotor is well established in the scientific community as a tool to drive companion cell specific expression or as a marker for analyses of companion cell transcriptomes (summarized in Stadler & Sauer, 2019). Our data indicate a dominant role of the sucrose transporter AtSUC1 and the vacuolar invertase AtVI2 during reproduction. Loss of AtSUC1 led to a reduced sucrose storage in

mature pollen, which couldn't be complemented by expression of *AtSUC9* under the control of the *AtSUC1* promoter. Loss of the vacuolar invertase AtVI2 caused a reduced pollen germination, indicating that cleavage of vacuolar sucrose by AtVI2 promotes pollen germination.

Materials and methods

Strains, growth conditions, and genotyping

All plant lines used in this study are listed in Supplementary Table 1. *Arabidopsis thaliana* (*Arabidopsis thaliana* ecotype Columbia-0 (Col-0)) was grown in the greenhouse in potting soil or under long-day conditions (16 h of light/8 h of dark) at 22°C and 60% humidity in the phytochamber. The T-DNA insertion lines *Atsuc1* (SM3_19978; John-Innes-Centre), *Atsuc3* (GABIKat_325D02; Max-Planck-Institute), *Atsuc8* (SALK_066671; Salk Institute), *Atsuc9* (SALK_050102; Salk Institute), *Atvi2-1* (SALK_011312; Alonso et al., 2003), *Atvi2-2* (SALK_100813; Alonso et al., 2003), *Atcwinv2-1* (SALK_068113; Alonso et al., 2003), *Atcwinv4-2* (SALK_130163; Alonso et al., 2003) and *Atcwinv5* (SALK_GK849H10; Li et al., 2003) were obtained from the Nottingham Stock Centre (https://Arabidopsisthaliana.info/). The single knockout lines *Atsuc4.1* (WiscDsLox450E10; Schneider et al., 2012a) and *Atsuc5.4* (SALK_367_D07; Pommerrenig et al., 2013) were kindly provided by Norbert Sauer (Molecular Plant Physiology, Friedrich-Alexander University of Erlangen-Nuremberg). Homozygous plants were identified by genotyping with the primers listed in Supplementary Table 2. PCR products obtained with the respective primer pairs for the mutant allele (Supplementary Table 2) were sequenced for the determination of the positions of the T-DNA insertions. The homozygous *Atsuc1Atsuc3Atsuc8Atsuc9* quadruple and the *Atcwinv2-1Atcwinv4-2Atcwinv5* triple knockout lines were generated by crosspollination of the respective knockout lines and PCR-based genotyping of the F2 descendants. The *Attmt1Attmt2* double knockout line (Wormit et al., 2006) was kindly provided by Ekkehart Neuhaus (Division of Plant Physiology, University of Kaiserslautern). *Arabidopsis thaliana* plants were transformed *via* the floral dip method with the *Agrobacterium tumefaciens* strain GV3101 (Holsters et al., 1980; Clough and Bent, 1998). For all cloning steps the *Escherichia coli* strain DH5α (Hanahan, 1983) was used.

RNA isolation, reverse transcription, RT-PCR, and qPCR

For mRNA isolation, pollen, virgin stigmata and stigmata with semi-*in vivo* grown pollen tubes were placed on pollen germination medium and germinated for at least 5 h. After pollen germination, pollen and/or stigmata of about 30 flowers were rinsed from the cellulose membrane in an Eppendorf tube with 100 µl extraction buffer of the PicoPure™ RNA Isolation Kit (Arcturus) and frozen in liquid nitrogen. After thawing, the samples were incubated for 30 min at 42°C, centrifuged (2 min, 3.000 g, RT) and the supernatant transferred to a new Eppendorf tube. An equal volume of 70% ethanol was added to the supernatant. The further steps correspond to the method listed in the instructions of the kit. Finally, the mRNA was eluted with 11-13 µl of elution buffer and immediately afterwards transcribed into cDNA. For reverse transcription reactions, the QuantiTect® Reverse Transcription Kit (Qiagen) was used. For detection of *AtSUC1* – *AtSUC9*, *AtcwINV2*, *AtcwINV4*, *AtcwINV5*, and *AtVI2* transcripts with wild type (WT) or mutant cDNA as template the specific primers in Supplementary Tables 3, 4 were used for PCR reactions. An *ACTIN2*-specific PCR was performed as a positive control. For the amplification of amplicons 39 cycles were used. RT-PCR analyses with total mRNA of homozygous flowers or pollen tubes confirmed the loss of full-length transcripts of the respective T-DNA insertion lines. In case of *Atsuc8* transcripts of *AtSUC8* could be amplified after the T-DNA insertion but resulting in a functional protein is very unlikely because of frame shift and silencing effect from the T-DNA insertion (Daxinger et al., 2008). For the analyses of p*AtSUC1*:*AtSUC1*g, p*AtSUC9*:*AtSUC9*g, and p*AtSUC1*:*AtSUC9*g expression in pollen tubes grown *in vitro* of *Atsuc1* and *AtSUC1* complementation lines gene specific primers were used (Supplementary Table 5). Relative expression of *AtSUC1*, *AtSUC3*, *AtSUC5*, *AtSUC6*, *AtSUC8* and *AtSUC9* in pollen tubes was measured *via* qRT-PCR using the SYBR® Green Kit (Agilent, Santa Clara, CA, USA) and the Rotor-Gene Q Cycler (Qiagen). Primers in Supplementary Table 6 were used for the detection of the respective transcripts. Relative *AtSUC*s expression levels were normalized by comparison with *UBI10* which was amplified with primer pair UBQ10 + 1066fw and UBQ10 + 1130rev (Supplementary Table 6) and calculated according to the 2–ΔΔCT (Livak) method.

Cloning of reporter gene constructs

All plasmid constructs used in this study are listed in Supplementary Table 7. The p*AtSUC1*:*AtSUC1*g-*GUS* reporter plants (Sivitz et al., 2008) were kindly provided by John M. Ward (Department of Plant Biology, University of Minnesota). p*AtSUC2*:*GUS* reporter plants (Schneidereit et al., 2008) were kindly provided by Norbert Sauer (Molecular Plant Physiology, Friedrich-Alexander University of Erlangen-Nuremberg). For generating the p*AtSUC3*:At*SUC3*g reporter gene lines a 2174 bp promoter fragment and one part of the genomic sequence was amplified with the primer pair AtSUC3-2174fw+CACC and AtSUC3g+1277rev (Supplementary Table 8), yielding a 3451 bp insert and cloned into *pENTR/D-TOPO* (Invitrogen). The remaining genomic sequence including the introns was amplified with the primer pair AtSUC3g+1199fw and AtSUC3g+3748rev+A+AscI (Supplementary Table 8). This resulting 2549 bp fragment was inserted downstream of the first part of *AtSUC3 via* an internal *Pst*I and the attached *Asc*I site. The complete p*AtSUC3*:*AtSUC3*g construct was inserted by LR-reaction in *pBASTA-GUS* (Rottmann et al., 2016) yielding plasmid *pFC2*. Constructs for p*AtSUC5*:At*SUC5*g and pAt*SUC8*:At*SUC8*g reporter gene lines were also cloned in two fragments. For *AtSUC5* the first part was amplified with AtSUC5-2118fw+CACC and AtSUC5g +93rev, the second part with AtSUC5g+43fw and AtSUC5g

+2079rev+A+AscI (Supplementary Table 8). Both fragments were combined in *pENTR/D-TOPO* (Invitrogen) *via* an internal *Bgl*II and an attached *Asc*I site. The complete construct was inserted into *pBASTA-GUS* (Rottmann et al., 2016) by LR, yielding plasmid *pFC5*. For *AtSUC8* the first part was amplified with AtSUC8-1544fw+CACC and AtSUC8g+238rev, the second part with AtSUC8g+191fw and AtSUC8g+1709rev+A+AscI (Supplementary Table 8). Both fragments were combined in *pENTR/D-TOPO* (Invitrogen) *via* an internal *Nde*I and an attached *Asc*I site. The complete construct was inserted into *pBASTA-GUS* (Rottmann et al., 2016) by LR, yielding plasmid *pFC8*. For generating *AtSUC4* reporter gene lines p*AtSUC4*:*AtSUC4*g insert was amplified with the primer pair AtSUC4-2044fw+CACC and AtSUC4g+2458rev (Supplementary Table 8). The p*AtSUC4*:*AtSUC4*g fragment was inserted into *pENTR/D-TOPO* (Invitrogen). By LR reaction the complete p*AtSUC4*:*AtSUC4*g construct were inserted into *pBASTA-GUS* (Rottmann et al., 2016), yielding the plasmid *pJS32* (p*AtSUC4*:*AtSUC4*g-*GUS*). For generating *AtSUC9* reporter gene lines p*AtSUC9*:*AtSUC9*g insert was amplified with the primer pair AtSUC9-2159fw+CACC and AtSUC9g+1926rev (Supplementary Table 8). The p*AtSUC9*:*AtSUC9*g fragment was inserted into *pENTR/D-TOPO* (Invitrogen). By LR reaction the complete p*AtSUC9*:*AtSUC9*g construct was inserted into *pBASTA-GUS* or p*BASTA-GFP* (Rottmann et al., 2016), yielding the plasmids *pTR319* (p*AtSUC9*:*AtSUC9*g-*GUS*) and *pTR320* (p*AtSUC9*:*AtSUC9*g-*GFP*). For cloning p*AtcwINV : AtcwINV*g, p*AtVI1*:*AtVI1*g-*GUS*, and p*AtVI2*:*AtVI2*g-*GUS* reporter gene lines the respective primer pairs used for amplification of the fragments including the promoter region and the complete genomic sequence are listed in Supplementary Table 9. For *AtcwINV1* an attached *NcoI* site, for *AtcwINV5* an attached *BamHI* site, and for *AtVI1* an attached *Asc*I site was used to ligate the respective fragments. The complete p*AtcwINV : AtcwINV*g and p*AtVI : AtVI*g-*GUS* constructs were respectively inserted into the destination vector *pBASTA-GUS* (Rottmann et al., 2016) by LR, resulting in the expression vectors *pJS1* (p*AtcwINV1*:*AtcwINV1*g-*GUS*), *pJS13* (p*AtcwINV2*:*AtcwINV2*g-*GUS*), *pJS14* (p*AtcwINV4*:*AtcwINV4*g-*GUS*) *pAL30* (p*AtcwINV5*:*AtcwINV5*g-*GUS*), *pJS37* (p*AtVI1*:*AtVI1*g-*GUS)*, and *pJS11* (p*AtVI2*:*AtVI2*g-*GUS)*. The stable pollen tube marker line p*LAT52*:*GFP- pMDC123-NosT* (*pTR53*) (Rottmann et al., 2018a), where *GFP* is expressed under the pollen-specific promoter, was used for the pollen tube esculin uptake assays.

Cloning of constructs for complementation lines

For generation of the construct for complementation line Compl. AtSUC1 (p*AtSUC1*:*AtSUC1*g in *Atsuc1*), the 2025 bp fragment of the *AtSUC1* promoter and the complete genomic sequence including introns were amplified using primer pair AtSUC1-2025fw+CACC and AtSUC1g+1764rev (Supplementary Table 10) and inserted into *pENTR/D-TOPO* (Invitrogen). By LR reaction the complete construct was inserted into the destination vector *pMDC99* (Curtis & Grossniklaus, 2003), yielding the expression vector *pJS90*. *Atsuc1* knockout plants were transformed with *pJS90 via* floral dip method (Clough & Bent, 1998). For generation of the construct for complementation line Compl. AtSUC9 (p*AtSUC1*:*AtSUC9*g in *Atsuc1*) the method of In-Fusion™ cloning (Zhu et al., 2007) was performed. The first fragment was amplified from the vector p*AtSUC1*:*AtSUC1*g-*pENTR/D-TOPO* (*pJS79*) including the *pENTR/D-TOPO* vector backbone and the 2025 bp fragment of the *AtSUC1* promoter with the primer pair InFu1AtSUC1p(V)fw and InFu2AtSUC1p (V)rev (Supplementary Table 10). The second fragment was amplified from the vector p*AtSUC9*:*AtSUC9*g-*pENTR/D-TOPO* including the complete genomic sequence of *AtSUC9* including introns with the primer pair InFu3AtSUC9g(In)fw and InFu4AtSUC9g(In)rev. The specific primers were designed with the In-Fusion™ Primer Design Tool (https://www.takarabio.com/learning-centers/cloning/primer-design-and-other-tools). The PCR reactions were performed with PCRBIO VeriFi™ Mix Red (PCRBIOSYSTEMS) because of the big fragment size. The two fragments were united *via* the In-Fusion™ reaction with same amount of DNA of the respective two fragments for 15 min at 50°C, yielding the construct p*AtSUC1*p:*AtSUC9*g-*pENTR/D-TOPO*. By LR reaction the complete construct p*AtSUC1*:*AtSUC9*g was inserted into the destination vector *pMDC99* (Curtis & Grossniklaus, 2003), yielding the plasmid *pJS80* (see also Table S7). *Atsuc1* knockout plants were transformed with *pJS80 via* floral dip method (Clough and Bent, 1998). Pollen germination and pollen tube growth tests were analyzed with the T_2 generation of the selected plants.

Analyses of pollen germination and pollen tube growth

In vitro pollen germination and pollen tube growth tests with *Arabidopsis thaliana* pollen for RNA extraction and growth analyses were done as described (Rodriguez-Enriquez et al., 2013). The standard sucrose concentration was 250 mM within the medium. Different sucrose concentrations were indicated. Pollen germination rates were counted using ImageJ 1.53k (Schneider et al., 2012b). For length measurements, pollen tubes were usually allowed to grow for at least 7 – 8 h, unless indicated otherwise. Pollen tube lengths were measured with Smart Root (Lobet et al., 2011), a plugin of ImageJ, or with a self-written Python script (Python Software Foundation, Beaverton, OR, United States), and plotted with Excel (Microsoft 365). Pollen tube growth experiments were performed in three biological replicates per genotype and sucrose concentration. For pollen germination rates at least 500 pollen per each replicate, genotype, and sucrose concentration were counted and for pollen tube lengths at least 200 pollen tubes per each replicate, genotype and sucrose concentration were measured. Statistical analyses were performed in Excel (Microsoft 365) with *Anova* (single factor). The semi-*in vivo* pollen tube growth assays for analyses of reporter genes and RT-PCRs were also analyzed on medium described by Rodriguez-Enriquez et al. (2013), which were performed by pollinating stigmata by hand, cutting them off and placing them horizontally

onto the cellulosic membrane of the growth medium to allow the outgrowth of the pollen tubes from the cut surface (Palanivelu & Preuss, 2006) for 4 – 6 h. For the pollen tube esculin uptake assays the semi-*in vivo* pollen tube growth assays of pollen tubes expressing *GFP* under the control of a pollen-specific promoter (*LAT52*) (Rottmann et al., 2018b) were analyzed on liquid pollen germination medium without cellulosic membrane with different pH values (5; 5.5; 6; 7; 9) containing 250 mM sucrose.

Ion chromatographic measurements and starch staining

Pollen from different species were collected with the help of a vacuum cleaner with various tubes and filter nets with different pore sizes as described in Johnson-Brousseau and McCormick (2004). For ion chromatographic measurements the pollen were incubated with 300 µl 80% ethanol for 1 h at 80°C under constant shaking. Samples were centrifuged for 5 min at 14000 rpm at 4°C. As much supernatant as possible was transferred into a new Eppendorf tube (255 – 290 µl) and evaporated at 45°C in the Speed Vac. The pellet was resuspended in 125 µl sterile water by shaking at room temperature. The samples were centrifuged through a filter plate and pipetted in the respective tubes. The ion chromatographic measurements were done as described (Schneider et al., 2008). For starch staining collected pollen were stained with iodine potassium iodide solution while shaking for 4 – 5 h at 40°C.

Pollen tube esculin uptake assay

Pollen tubes, which expressed *GFP* under the control of the pollen specific *LAT52* promoter, were grown semi-*in vivo* on liquid pollen germination medium with 250 mM sucrose and different pH values (5; 5.5; 6; 7; 9). To this end, 500 µl liquid germination medium was placed on a slide with recess and the pollinated stigmata, which were cut off, were placed horizontally onto liquid medium to allow the outgrowth of the pollen tubes from the cut surface for 3 – 4 h. Esculin in liquid growth medium was added to 500 µl liquid growth medium to a final concentration of 1 mM. After gently mixing esculin into the liquid growth medium, the slide was incubated for 40 min at room temperature at dark. Prior to microscopy the stigmata with the pollen tubes were gently transferred onto a slide with recess filled with liquid growth medium without esculin.

Microscopy

Pictures of GUS plants were taken with a Leica MZFLIII stereomicroscope (Leica Microsystems) or with a Zeiss Axioskop (Carl Zeiss Jena GmbH). Pollen tubes for length measurements were analyzed by light microscopy (Zeiss Axioskop; Carl Zeiss Jena). Pollen stained with iodine potassium iodide solution were analyzed in bright field at 1000x magnification with a Zeiss Axioskop (Carl Zeiss Jena GmbH). Images of GFP-reporter plants and GFP expressing pollen tubes were taken on a Leica 765 TCS SPII confocal laser scanning microscope (Leica Microsystems) and processed with Leica Confocal Software 2.5. A 488-nm argon laser was used for excitation of GFP and chlorophyll autofluorescence. The 415-nm diode was used for the excitation of esculin fluorescence. Detection windows ranged from 497 to 526 nm for GFP, from 682 to 730 nm for chlorophyll autofluorescence and from 424 to 469 nm for esculin. Images of GFP and esculin fluorescence for the pollen tube esculin uptake assay were taken in a sequential mode. Image processing was done using analySIS Doku 3.2 software (Soft Imaging System, Münster) and GIMP2.10 (https://www.gimp.org/).

Results

Expression of sucrose transporter genes in reproductive organs

RT-PCR and reporter gene analyses were performed to investigate the expression of sucrose transporter genes. Since it is known that gene expression in pollen can be induced after growth through stigma and style (Qin et al., 2009; Leydon et al., 2014), we performed semi-*in vivo* growth assays (see also Figure 1B). For this, pollinated stigmata were cut below the style and incubated on medium for seven hours to allow pollen tube growth. mRNA was extracted from *in vitro* grown pollen tubes as well as from the pollinated pistils-sections described above. The latter samples were labelled with "semi-*in vivo*". They contained mRNA from pollen tubes and from the pistil. To distinguish between expression in the pistil and in pollen tubes, un-pollinated pistil-sections, labelled as "stigmata", were used. *AtSUC2* is known to be companion cell specific and was used as a negative control for expression in pollen (Stadler and Sauer, 1996; Imlau et al., 1999; see also Stadler & Sauer, 2019). The RT-PCR data indicated that *AtSUC1*, *AtSUC3*, *AtSUC4*, *AtSUC5*, *AtSUC6*, *AtSUC8*, and *AtSUC9* were expressed in pollen tubes grown *in vitro* and in pollinated pistils (semi-*in vivo* samples, Figure 1A). *AtSUC7* was not analyzed because it is a pseudogene that does not code for an active sucrose transporter. *AtSUC2* is the only *AtSUC* gene, which was not expressed in pollen tubes. *AtSUC2* mRNA was only present in samples containing vascular tissue (Figure 1A). Since the pistil contains vascular bundles, both, the "stigmata" and the "semi-*in vivo*" sample showed a signal, although *AtSUC2* is not expressed in pollen. *AtSUC4* mRNA was detectable in pollen tubes grown semi-*in vivo*, but not in pollen tubes grown *in vitro*, indicating that the expression in pollen tubes was induced after growth through the stigma. For *AtSUC5* expression, the upper RT-PCR signal in the "stigmata" sample is caused by a contamination with genomic DNA, however, the assay clearly shows that the *AtSUC5* gene is expressed also in un-pollinated stigmata (Figure 1A). *AtSUC6* was expressed in pollen tubes grown *in vitro* and semi-*in vivo*, whereas no transcripts could be amplified from stigmata-derived cDNA. This is consistent with earlier results (Rottmann et al., 2018a). Besides *AtSUC2*, transcripts of *AtSUC1*, *AtSUC3*, *AtSUC4*, *AtSUC5*, and *AtSUC9* were also detectable in cDNA samples of un-pollinated pistil sections.

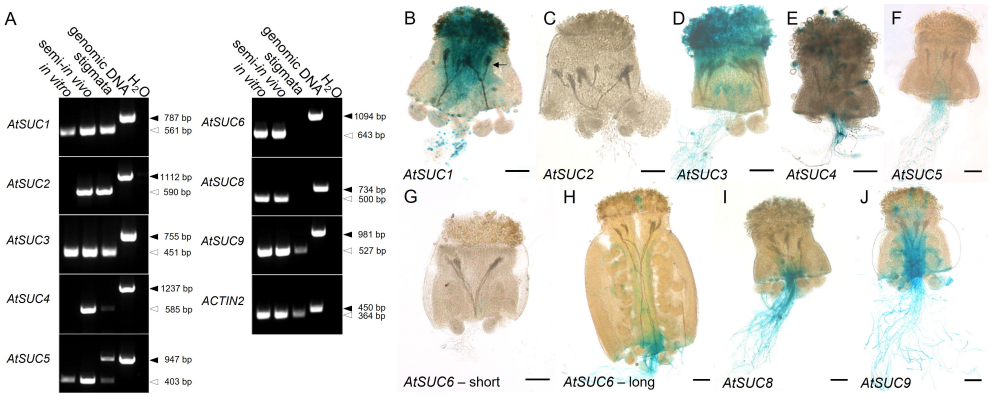

FIGURE 1
Analysis of *AtSUC* expression in pollen tubes. **(A)** RT-PCRs to study *AtSUC1* – *AtSUC9* expression in pollen tubes grown *in vitro* or in the upper part of a pollinated pistil (semi-*in vivo*) or in the upper part of an un-pollinated pistil (primers are listed in Supplementary Table 3). *AtSUC7* was not analyzed because it doesn`t encode a functional sucrose carrier. Arrows indicate the size of PCR products derived from reverse-transcribed mRNA (white) or from genomic DNA (black). The presence of cDNA in each sample was confirmed with *ACTIN2* specific primers (Supplementary Table 3). **(B–J)** Histochemical detection of β-glucuronidase activity in semi-*in vivo* growth assays with pollen tubes of p*AtSUC : AtSUC*g-*GUS*-reporter plants and stigmata from wild type plants. The arrow in **(B)** marks GUS containing pollen tubes growing through the WT style. For the expression pattern of *AtSUC2* p*AtSUC2*:*GUS* reporter plants were used. For AtSUC6, short **(G)** and long **(H)** parts of the pistil were used for the semi-*in vivo* assay. The analyzed genes are indicated in each figure. Tissues were stained with GUS solution for 48 h **(A)** or 2 - 5 h **(B–J)**. Scale bars: 100 µm in **(B–J)**.

To analyze cell specific expression, we used existing or generated new *AtSUC* reporter gene lines, which included the endogenous promoter and the genomic sequence of the respective *AtSUC* genes. For *AtSUC2*, no new lines were generated since this gene is very well studied and is known to be companion cell specific and not expressed in pollen. Therefore, we used *AtSUC2p:GUS* lines which we had in the lab as a negative control. We performed semi-*in vivo* assays with pollen from GUS lines and WT pistils to investigate expression in pollen tubes after growth through stigma and style. The histochemical analyses confirmed the RT-PCR data and proved expression of *AtSUC1, AtSUC3, AtSUC4, AtSUC5, AtSUC6, AtSUC8*, and *AtSUC9* in pollen tubes (Figures 1B–J). Activity of AtSUC1-GUS fusion protein was well visible in parts of the pollen tubes that were growing through stigma and style (Figure 1B). In contrast, it was necessary to stain for 48 h to get a visible GUS signal in apical parts of pollen tubes of p*AtSUC1*:*AtSUC1*g-*GUS* plants emerging from WT pistils in *semi-in-vivo* assays (Figure 1B). This may point towards a major function of AtSUC1 during pollen germination and/or during early stages of pollen tube growth. The GUS stain in pictures of p*AtSUC1*:*AtSUC1*g-*GUS* assays had a dotted appearance, which might be due to the weak expression and/or to the long incubation in GUS staining solution. In contrast to *AtSUC1*, p*AtSUC6*:*AtSUC6*g-*GUS* expression increased during pollen tube growth through the transmitting tissue. Pollen tubes that emerged from long pistil parts were strongly stained (Figure 1H), which was also shown previously (Rottmann et al., 2018a), and growth through shorter pistil parts resulted in weak or almost invisible GUS signals (Figure 1G). The GUS analyses indicated that the sucrose carriers AtSUC1, AtSUC3 and AtSUC4 were already present in mature pollen in anthers, prior pollen germination on the stigma (Figures 2A–G). In addition, the pAtSUC1:AtSUC1g-GUS fusion protein was detectable in developing pollen during a later stage of anther development. pAtSUC1:AtSUC1g-GUS activity started in stage 12 flowers, which are characterized by papillar cells covering the stigma and a visible style (Figure 2A; floral stages according to Smyth et al., 1990 and Schneitz et al., 1995). *AtSUC3* was expressed in the vasculature of sepals and a strong expression was detectable in the stigma (Figure 2C). The *AtSUC3* expression in the stigma was not induced through pollination, as the expression was also visible in stigmata of un-pollinated pistils (Figure 2D). *AtSUC4* was expressed not only in growing pollen tubes but also in mature pollen in anthers and in cells of the stigma (Figures 2F–H). *AtSUC4* promoter activity in anthers of older and younger flowers has already been shown (Weise et al., 2000; Schneider et al., 2012a), but expression in the stigma is a novel finding. We carefully excluded cross-pollination during the experiments and analyzed 10 independent lines which all showed blue stigmata. A possible function of AtSUC4 activity in papillae cells could be the mobilization of vacuolar sucrose, either as a nutrient or for osmoregulation. Current analyses detected p*AtSUC8*:*AtSUC8*g-*GUS* expression not only in growing pollen tubes but also in ovules and in developing seeds (Figures 2I–K), which has not been observed during preceding studies (Sauer et al., 2004). Within ovules, the expression was restricted to the embryo sac (Figure 2K). We detected p*AtSUC9*:*AtSUC9*g-*GUS* expression in ovules and developing seeds (Figures 2L–N). Further investigations with p*AtSUC9*:*AtSUC9*g-*GFP* reporter gene lines showed an expression in synergid cells of ovules and confirmed the expression in pollen tubes (Figures 2O, P). In summary, the RT-PCR and reporter gene analyses showed that *AtSUC1* is expressed in developing pollen and that *AtSUC1*, *AtSUC3*, *AtSUC4*, *AtSUC5*, *AtSUC6*, *AtSUC8*, and *AtSUC9* are expressed in pollen tubes. In addition, *AtSUC3* and *AtSUC4* are expressed in stigmata and *AtSUC5*, *AtSUC8*, and *AtSUC9* in ovules.

10.3389/fpls.2023.1063765

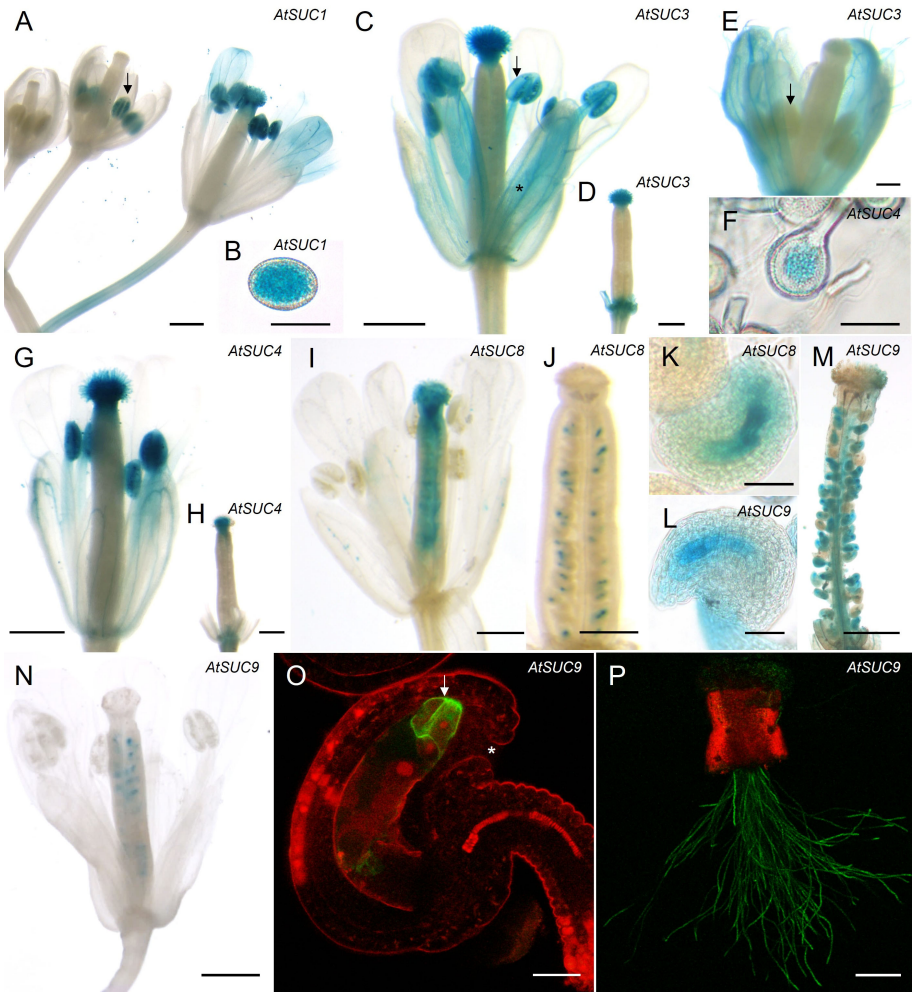

FIGURE 2
Analyses of *AtSUC* gene expression in reproductive organs. **(A–O)** Histochemical detection of ß-glucuronidase activity in *Arabidopsis thaliana* Col-0 expressing *AtSUC*g-*GUS* under the control of the native *AtSUC* promoter. *AtSUC2*, *AtSUC5* and *AtSUC6* expression was previously published, therefore the respective reporter lines were not included. **(A, B)** p*AtSUC1:AtSUC1*g-*GUS*. **(A)** Flower stage 10 (left), stage 12 (middle) and pollinated flower stage 14 (right). All floral stages according to Smyth et al., 1990 and Schneitz et al., 1995. **(B)** mature pollen. **(C, D, E)** p*AtSUC3:AtSUC3*g-*GUS*. **(C)** Pollinated flower of stage 14 (all flower stages according to Smyth et al., 1990). The asterisk marks blue stained vascular bundles. The arrow indicates blue mature pollen in an anther. **(D)** Un-pollinated pistil (stage 13) after removal of all other floral organs. **(E)** Flower stage 12, the arrow marks an un-stained anther. **(F–H)** p*AtSUC4:AtSUC4*g-*GUS*. **(F)** Pollen grains at higher magnification. **(G)** Pollinated flower stage 14. **(H)** Un-pollinated pistil (stage 13) after removal of other floral organs. **(I–K)** p*AtSUC8:AtSUC8*g-*GUS*. **(I)** Pollinated flower stage 14. **(J)** Un-pollinated ovary of stage 11. **(K)** Ovule at higher magnification. **(L–N)** p*AtSUC9:AtSUC9*g-*GUS*. **(L)** Ovule of an un-pollinated ovary at higher magnification. **(M)** Pollinated and peeled ovary of stage 14. **(N)** Pollinated flower of stage 14. **(O, P)** Detection of GFP fluorescence with a CLSM in *Arabidopsis thaliana* Col-0 expressing p*AtSUC9:AtSUC9*g-*GFP*. GFP fluorescence is shown in green, chlorophyll autofluorescence in red. **(O)** Ovule at higher magnification. The arrow marks GFP labelled synergid cells. The asterisk marks the micropyle. **(P)** Pollen tubes germinated semi-*in vivo* on a wild type (WT) stigma. Tissues were stained with GUS solution for 24 h **(A, B)** or 2 - 5 h **(C–N)**. Scale bars: 500 µm in **(A–E, H, I, L, M)**; 20 µm in **(F, G, O)**; 50 µm in **(J, K)**; 200 µm in **(N)**.

Characterization of *Atsuc* knockout lines

Sivitz et al. published in 2008 that pollen of *Atsuc1* mutant lines had a significantly reduced pollen germination rate compared to wild type (WT), indicating a function for AtSUC1 in sucrose uptake into germinating pollen (Sivitz et al., 2008). To study the function of AtSUC1, AtSUC3, AtSUC5, AtSUC8, and AtSUC9 in pollen germination and pollen tube growth, single knockout lines were analyzed and compared with an *Atsuc1Atsuc3Atsuc8Atsuc9* quadruple knockout line, which was generated by multiple crossings of single knockout lines containing T-DNA insertions. Pollen of *Atsuc1* and *Atsuc1Atsuc3Atsuc8Atsuc9* mutant lines showed significantly reduced pollen germination rates and pollen tube lengths compared to wild type (Figures 3A, B). Thus, AtSUC1 is not only important for normal pollen germination, which was published previously, but also for pollen tube growth. Interestingly, the loss of three other sucrose transporters in addition to AtSUC1 did not cause a further reduction in germination or growth, and the single knockout plants *Atsuc3, Atsuc5.4, Atsuc8*, and *Atsuc9* did not show any defect regarding pollen germination and growth in comparison to WT (Figures 3A, B). These results demonstrate a major function of AtSUC1 during pollen tube growth and even

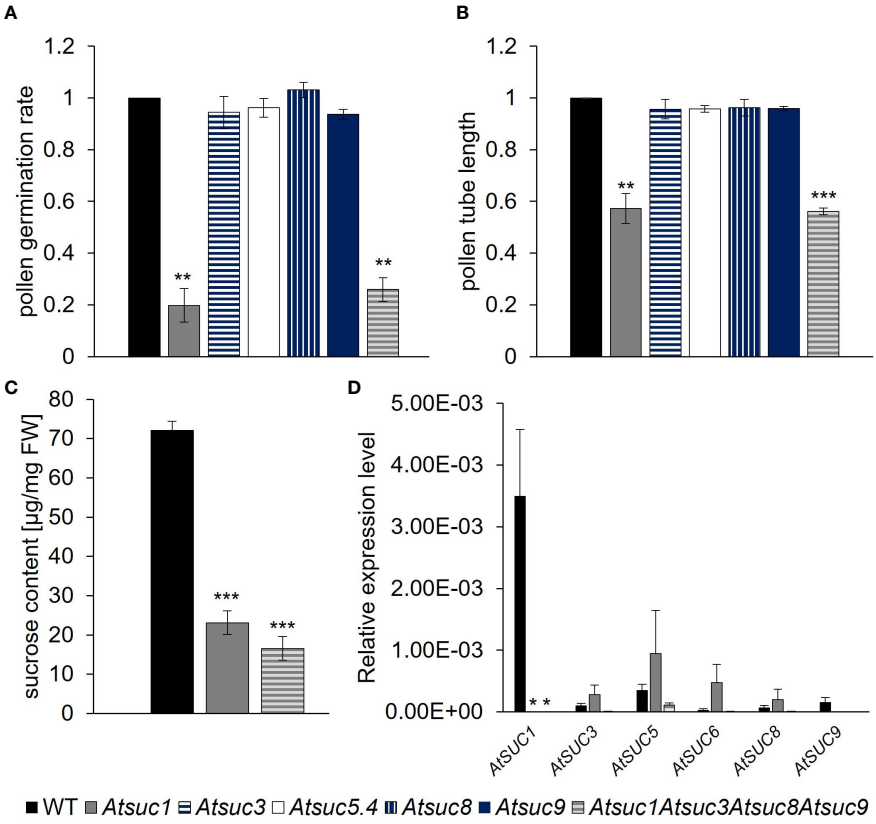

FIGURE 3
Germination, growth and sucrose content of pollen and *AtSUC* gene expression in stage 12 anthers of wild type and *Atsuc* knock out plants. **(A)** Pollen germination rates and **(B)** pollen tube lengths of wild type, *Atsuc3, Atsuc5.4, Atsuc8* and *Atsuc9* single and *Atsuc1,3,8,9* quadruple knock out plants after 7 h growth *in vitro* on medium with 250 mM sucrose. Bars represent mean values (+/- SE) of three biological replicates (pollen germination rate: n > 500, pollen tube lengths: n > 200 for each genotype in each experiment). **(C)** Ion chromatography measurements of sucrose content in pollen grains harvested from mature anthers of wild type, *Atsuc1* and *Atsuc1,3,8,9* knock out plants. Extracts of pollen of at least 72 plants per genotype were analyzed by ion chromatography and normalized to the fresh weight (FW) of the samples. **(D)** Relative expression levels of *AtSUC* genes in anthers of stage 12 flowers of WT (left bar), *Atsuc1* single knock out (middle) and *Atsuc1,3,8,9* quadruple knock out plants (right bar), quantified by RT-qPCR relative to *UBI10* expression. Primers are listed in Supplementary Table 3. Bars represent mean values of three biological replicates with three technical replicates each. The analyzed genes are indicated in each panel. For each biological replicate, the tissue for RNA isolation was collected from different plants. Significance = *Anova* **(A–C)** or Students *t*-test **(D)**, Reference: WT, *≙ $p \leq 0.05$; **≙ $p \leq 0.01$; ***≙ $p \leq 0.001$.

more during pollen germination. To investigate the function of AtSUC proteins in sucrose import into developing pollen, we performed ion chromatography measurements of pollen that had been harvested from mature anthers. A high amount of sucrose was measurable within wild type pollen grains (70 µg/mg FW), which was reduced to less than 35% (~20 µg/mg FW) in *Atsuc1* mutant pollen (Figure 3C). Again, the loss of three other sucrose transporters in *Atsuc1Atsuc3Atsuc8Atsuc9* quadruple knockout pollen did not enhance the phenotype. This result points towards an important function of AtSUC1 in sucrose loading during pollen development. To analyze the presence of other sucrose carriers during late stages of pollen development, qRT-PCR analyses with mRNA samples from anthers of stage 12 flowers were performed. All *AtSUC* genes were analyzed except *AtSUC2, AtSUC4* and *AtSUC7* because AtSUC2 is companion cell – specific, AtSUC4 is localized in the tonoplast, and *AtSUC7* is a pseudogene. The data set resulted in a quite high standard error because stage 12 flowers are very small (1.5 mm long) and anthers are difficult to isolate in a sufficient amount. However, the analysis clearly showed that only *AtSUC1* mRNA was detectable in significant amounts in anthers of stage 12 flowers (Figure 3D). To test a potential complementation of the loss of *AtSUC1* by other *AtSUC* genes, single *Atsuc1* and quadruple *Atsuc1Atsuc3Atsuc8Atsuc9* knockout plants were included in the qRT-PCR analyses. An induction of other *AtSUC* genes in single and quadruple knockout anthers of stage 12 flowers could not be observed (Figure 3D). This also indicates a dominant role of AtSUC1 in sucrose import during late stages of pollen development.

Complementation of the *Atsuc1* phenotype

To investigate the striking dominance in function of AtSUC1 among the other AtSUC proteins, we performed a complementation analysis. A construct containing the *AtSUC1* promoter and the *AtSUC9* genomic sequence was introduced into the *Atsuc1* background, and the resulting lines were compared with complementation lines containing the *AtSUC1* genomic sequence under the control of the *AtSUC1* promoter. The *AtSUC9* gene was chosen because it is known that AtSUC9 is correctly targeted to the

plasma membrane in pollen (Figure 2P) and because of its similar K_M value (AtSUC1: 0.45 mM (Sauer & Stolz, 1994); AtSUC9: 0.5 mM (Sauer et al., 2004)). Pollen germination rates and pollen tube lengths of three different complementation lines homozygous for p*AtSUC1:AtSUC1*g in *Atsuc1* (Compl. AtSUC1.1 – 1.3) and eight different complementation lines expressing p*AtSUC1:AtSUC9*g in *Atsuc1* (Compl. AtSUC9.1 – 9.8) were analyzed and compared to wild type and *Atsuc1* (Figures S1A, B). Interestingly, the plants expressing p*AtSUC1:AtSUC9*g showed no rescued phenotype with pollen germination rates and tube lengths like those of *Atsuc1*, while pollen of *Atsuc1* plants expressing p*AtSUC1:AtSUC1*g were fully rescued and looked like wild type (Figures 4A, B, S1A, B). To examine if the hybrid construct of AtSUC1 promoter and AtSUC9 gene leads to gene expression, we performed RT-PCR analyses, which showed an expression of p*AtSUC1:AtSUC9*g in germinating pollen of the respective complementation lines (Figure 4C). The fact that the loss of only one out of six sucrose carriers that are present in pollen causes a severe phenotype and the observation that reintroduction of *AtSUC1* but not of *AtSUC9* restored the phenotype, indicate that AtSUC1 may play a special role during pollen germination and pollen tube growth that can`t be complemented by AtSUC9.

Characterization of *Atsuc4.1* knockout mutants

Generally, sucrose can be stored in the vacuole or cytosol (Hedrich et al., 2015; Destailleur et al., 2021). *AtSUC4* encodes a sucrose carrier of the vacuolar membrane that exports sucrose from the vacuole into the cytoplasm. Our analysis showed that *AtSUC4* is expressed in pollen and pollen tubes (Figures 2F, G).

To address the function of AtSUC4 in sucrose mobilization from the vacuole, we analyzed pollen germination rates and pollen tube lengths of *Atsuc4.1* knockout plants (Schneider et al., 2012a) (Figures S2A, B). Furthermore, we studied a possible function of AtTMT1 and AtTMT2 which are known to catalyze the import of sucrose and glucose into the vacuole (Schulz et al., 2011). To this end, pollen of an *Attmt1Attmt2* (Schulz et al., 2011) double knockout line were analyzed (Figures S2C, D). Pollen germination rates and pollen tube lengths of

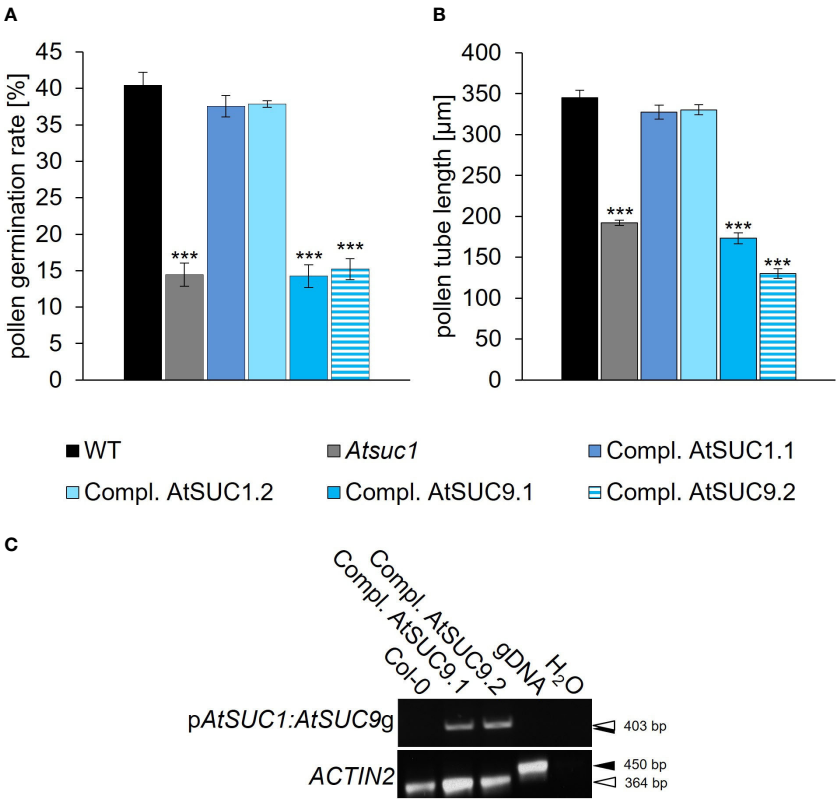

FIGURE 4
Complementation of the loss of *AtSUC1*. **(A)** Pollen germination rates and **(B)** pollen tube lengths of *Atsuc1* complementation lines compared to wild type pollen germinated *in vitro* on pollen germination medium containing 250 mM sucrose for 4 h. *Atsuc1* mutant plants expressing the genomic sequence of *AtSUC1* under the control of the native *AtSUC1* promoter (Compl. AtSUC1.1 + 1.2) or the genomic sequence of *AtSUC9* under the control of the native *AtSUC1* promoter (Compl. AtSUC9.1 + 9.2). Bars represent mean values (+/- SE) of three biological replicates (pollen germination rate: n > 500, pollen tube lengths: n > 200 for each genotype in each experiment). Significance: *Anova*. Reference: WT, **≙ $p \leq 0.01$; ***≙ $p \leq 0.001$. **(C)** RT-PCR analyses of *AtSUC1:AtSUC9*g expression in *in vitro* grown pollen tubes with primers specific for the *AtSUC1:AtSUC9* transgene including a forward primer that binds to the *AtSUC1* 5' UTR and a reverse primer specific for *AtSUC9* (Supplementary Table 5). The resulting band doesn`t include expression of the intrinsic *AtSUC9* WT gene. The RT-PCR analyses were performed with mRNA isolated from pollen tubes of the respective complementation lines compared to wild type. Arrows indicate the size of PCR products derived from reverse-transcribed mRNA (white) and genomic DNA (gDNA; black). The presence of cDNA and gDNA in each sample was confirmed with *ACTIN2* specific primers.

Atsuc4.1 and *Attmt1Attmt2* showed no significant difference compared to wild type (Figure S2). Obviously, neither AtSUC4 nor AtTMT1 and 2 have a major influence on pollen germination or pollen tube growth, at least *in vitro*. A possible explanation of this result would be that other transport proteins complement the loss of AtSUC4, AtTMT1, and AtTMT2, or that vacuolar invertases, which catalyze the cleavage of vacuolar sucrose into glucose and fructose, are involved in this process together with other monosaccharide transporters.

Expression of cell wall and vacuolar invertase genes in reproductive organs

To investigate a potential function of invertases during pollen tube growth we first analyzed the expression pattern of the respective invertase genes. Reporter gene lines were generated for the cell wall and vacuolar invertase genes, except *AtcwINV3* and *AtcwINV6*, containing the genomic sequence of the respective *AtcwINV* or *AtVI* gene with its native promoter in front of the *GUS* gene (Figure 5). p*AtcwINV1*:*AtcwINV1*g-*GUS* showed an expression within the transmitting tissue (Figures 5A, B). The genes of the cell wall invertases *AtcwINV2* and *AtcwINV4* were expressed in pollen and pollen tubes (Figures 5C–F). The p*AtcwINV5*:*AtcwINV5*g -*GUS* fusion protein was detectable in filaments of stamens and in funiculi of the pistil (Figures 5G, H). There was no *AtVI1* expression detectable in flowers or pollen tubes (Figure S5), however, p*AtVI2*:*AtVI2*g-*GUS* showed expression in mature pollen (Figures 5I–L). Blue GUS staining was detectable in anthers as soon as petals and filaments had elongated, while no blue

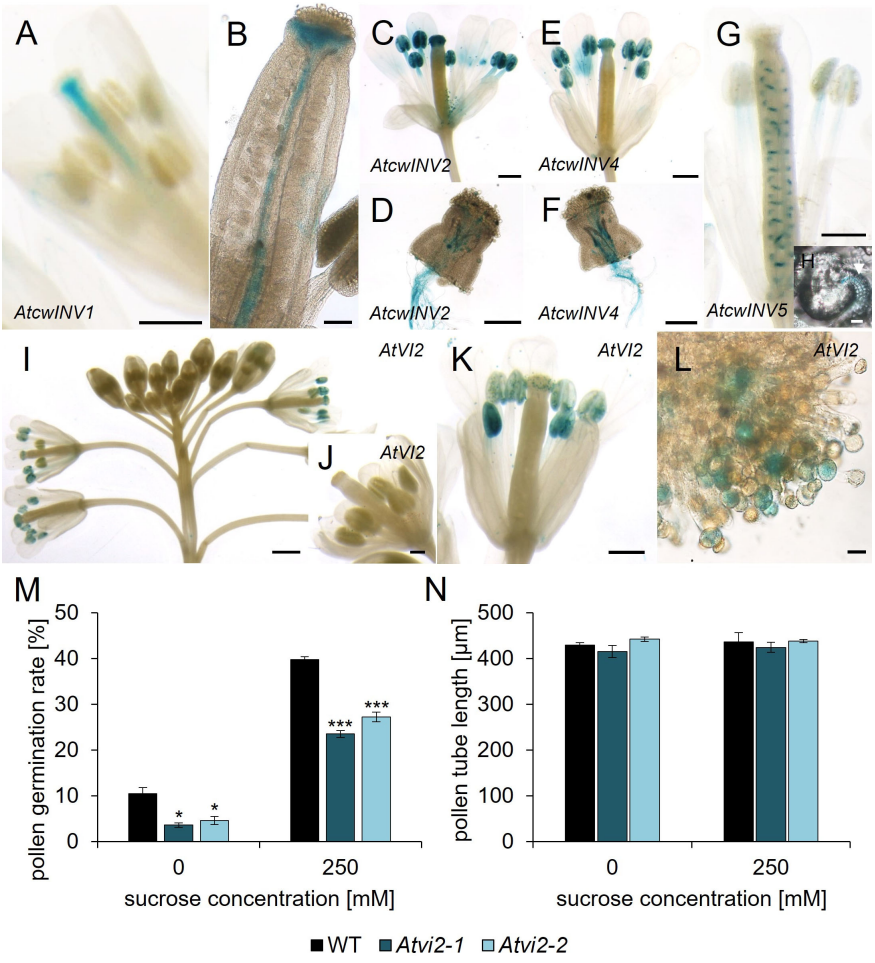

FIGURE 5
Analyses of p*AtcwINV : AtcwINV*g- and p*AtVI2*:*AtVI2*g-*GUS* reporter plants and *Atvi2* pollen germination and pollen tube growth tests. **(A–H)** Histochemical detection of ß-glucuronidase activity in *Arabidopsis thaliana* expressing *AtcwINV*g-*GUS* under the control of the native *AtcwINV* promoter. **(A)** stage 12 flower and **(B)** ovary of p*AtcwINV1*:*AtcwINV1*g-*GUS* plants. **(C, D)** p*AtcwINV2*:*AtcwINV2*g-*GUS*. **(C)** Pollinated flower stage 14. **(D)** p*AtcwINV2*:*AtcwINV2*g-*GUS* pollen tubes germinated semi-*in vivo* on a wild type stigma. **(E, F)** p*AtcwINV4*:*AtcwINV4*g-GUS. **(E)** Pollinated flower stage 14. **(F)** p*AtcwINV4*:*AtcwINV4*g-*GUS* pollen tubes germinated semi-*in vivo* on a wild type stigma. **(G, H)** p*AtcwINV5*:*AtcwINV5*g-GUS. **(G)** Pollinated flower stage 14. **(H)** p*AtcwINV5*:*AtcwINV5*g-*GUS* ovule with blue funiculi at higher magnification. **(I–L)** Histochemical detection of ß-glucuronidase activity in *Arabidopsis thaliana* expressing *AtVI2*g-*GUS* under the control of the native *AtVI2* promoter. **(I)** Inflorescence. **(J)** Flower stage 11. **(K)** Pollinated flower stage 14. **(L)** Pollen grains on a stigma at higher magnification. **(M)** Pollen germination rates and **(N)** pollen tube lengths of *Atvi2-1, Atvi2-2* and WT pollen germinated *in vitro* for 7 h on pollen germination medium with different sucrose concentrations. Bars represent mean values (+/- SE) of three biological replicates (pollen germination rate: n > 500, pollen tube lengths: n > 200 for each genotype in each experiment). Significance: *Anova*. Reference: WT, *≙ $p \leq 0.05$; ***≙ $p \leq 0.001$. Tissues were stained with GUS solution for 22 - 24 h **(A – F)** or 48 h **(G, H)** or 24 - 44 h **(I–L)**. Scale bars: 500 µm in **(A, C, E, G, K)**; 200 µm in **(D, F, J)**; 100 µm in **(B)**; 1 mm in **(I)**; 20 µm in **(H, L)**.

staining was visible during earlier stages of flower development. In closed flowers there was no *AtVI2*-expression detectable at all (Figures 5I, J). Pollen from p*AtVI2*:*AtVI2*g -*GUS* applied to a wild type stigma showed *AtVI2* expression (Figure 5L). Thus, *AtVI2* is the only vacuolar invertase expressed in mature pollen.

Characterization of *Atcwinv* and *Atvi2* knockout lines

To monitor invertase function during pollen tube growth we generated a triple knockout mutant with T-DNA insertions in *AtcwINV2, AtcwINV4* and *AtcwINV5*. The generation of a quadruple knockout line was not possible because of the linkage of the genes *AtcwINV1* and *AtcwINV5*. Furthermore, *AtcwINV1* is not expressed in pollen. Pollen germination rates and pollen tube lengths of *Atcwinv2-1Atcwinv4-2Atcwinv5* plants showed no difference compared to wild type (Figures S4A, B). Two *Atvi2* knockout mutant lines, *Atvi2-1* (SALK_011312) and *Atvi2-2* (SALK_100813) (Figure S3) were characterized in pollen germination assays. Both lines showed significant reduced *in vitro* pollen germination to almost 50% compared to wild type pollen on germination medium with 0 or 250 mM sucrose (Figure 5M). The addition of sucrose to the external medium didn`t rescue the reduced germination rate of *Atvi2* pollen. Since two independent *Atvi2* T-DNA insertion lines showed a similar reduction in pollen germination, it can be concluded that the effect is caused by the loss of AtVI2 function. However, the few *Atvi2* knockout pollen, which germinated, developed a similar pollen tube length as wild type pollen on medium without or with 250 mM sucrose (Figure 5N). In summary, the results indicated that the vacuolar invertase AtVI2 is important for efficient pollen germination at least *in vitro*, while there is no influence of cell wall invertases on pollen germination or pollen tube growth.

Carbohydrate storage in mature pollen and further analyses of pollen tube growth

Pollen express several genes for sucrose transporters, however, it is unknown if there is sucrose available in the apoplasm of the stigma and the transmitting tissue. Since it is difficult to examine the amount of apoplasmic sucrose *in vivo* we investigated the impact of apoplasmic sucrose on pollen germination and pollen tube growth *in vitro*. The analyses showed that pollen germination was reduced by 50% on medium without any sucrose compared to medium with 250 mM sucrose (Figure 6A). This observation indicated that sucrose promotes germination of wild type pollen. Interestingly, on medium containing 3 mM sucrose, the pollen germination rate was even worse than on medium without sucrose. The addition of 100 mM or 250 mM sucrose led to a steady increase in pollen germination rate (Figure 6A). These measurements were highly reproducible and independent from pollen batches or season. In contrast to pollen germination tests, pollen tube growth tests demonstrated no differences in pollen tube length on medium containing 250 mM sucrose compared to medium containing no sucrose (Figure 6B). However, the supplement of 1 mM up to 50 mM sucrose caused a progressive reduction in pollen tube length with a minimal length at 50 mM sucrose. Concentrations higher than 50 mM promoted pollen tube growth with a peak in a concentration range of 200 mM to 300 mM sucrose. In summary, it can be concluded that the presence of sucrose promotes pollen germination, while sucrose seems to be not necessary for pollen tube growth, because pollen tubes grew very long on medium without sucrose. Since the pollen tube growth medium (Rodriguez-Enriquez et al., 2013) didn`t contain any other carbohydrate, lipid or even protein, which could be metabolized, this result points towards internal energy reserves. To analyze this, we performed sugar measurements and starch staining assays of pollen from *Arabidopsis thaliana*. For comparison purposes, we included pollen from several unrelated plant species, *Eschscholzia californica*, *Plantago major*, *Zea mays*, *Nicotiana tabacum* and *Solanum lycopersicum*. Ion chromatography measurements observed high contents of sucrose (50 – 80 µg/mg FW) within pollen of all investigated species, compared to low glucose (1 – 2 µg/mg FW) and fructose (1 – 2.5 µg/mg FW) levels (Figures 6C–E). Pollen grains of *Arabidopsis thaliana* and *Zea mays* contained the highest amount of sucrose. Interestingly, the ratio between glucose and fructose varied between species. *Arabidopsis thaliana* pollen accumulated similar amounts of glucose and fructose, while pollen of the other species stored 2 – 3 times more fructose (Figures 6D, E). This could be due to different substrate specificities of transport proteins that accumulate monosaccharides during pollen development or to different activities of sucrolytic enzymes and downstream metabolic pathways. The glucose-to-fructose ratio was shown to influence pollen tube growth in a species specific manner (Rottmann et al., 2018b). To analyze starch storages, we performed iodine based staining assays (Figures 6F–K). Pollen grains from *Plantago major* (*Plantaginaceae*) and *Zea mays* (*Poaceae*) showed a dark staining, indicating a high amount of starch (Figures 6J, K). All other pollen from *Arabidopsis thaliana* (*Brassicaceae*), *Coleus blumei (Lamiaceae), Eschscholzia californica (Papaveraceae)* and *Phaseolus* spec. *(Fabaceae)* showed no dark staining, indicating that there is no starch or the starch content within the pollen of these species is too low for detection with iodine potassium iodide solution (Figures 6F–I). Another approach was to investigate if the pH value interferes with sucrose uptake or pollen tube growth. The activity of sucrose importers can be experimentally visualized by the uptake of esculin, a fluorescent sucrose analogue for AtSUC/AtSUT and AtSWEET proteins. Under conditions in which carriers are active, the fluorescent dye is transported into the cytosol and from there by an unknown transport protein into the vacuole, where it accumulates (Rottmann et al., 2018a). Pollen of a transgenic line expressing *GFP* under the control of a pollen tube specific promoter *LAT52* (Rottmann et al., 2018b) were used for semi-*in vivo* growth assays on liquid medium with different pH values. Esculin uptake was very efficient at pH 5.0 resulting in bright cyan fluorescence in the vacuole (Figure 6Q). On medium with pH 5.5, vacuolar esculin fluorescence was weaker but still visible (Figure 6R). At pH 6, pH 7, and pH 9 no esculin fluorescence was visible in pollen tubes anymore, which indicates that the sucrose carriers are not active under these conditions (Figures 6S–U). Interestingly, the opposite effect of the external pH could be observed regarding pollen tube growth semi-*in vivo*: the best growth was visible on medium with pH values from 6.0 to 9.0, while pollen tube growth seemed to be inhibited on pH 5.0 and weaker also on pH 5.5 (Figures 6L–P).

10.3389/fpls.2023.1063765

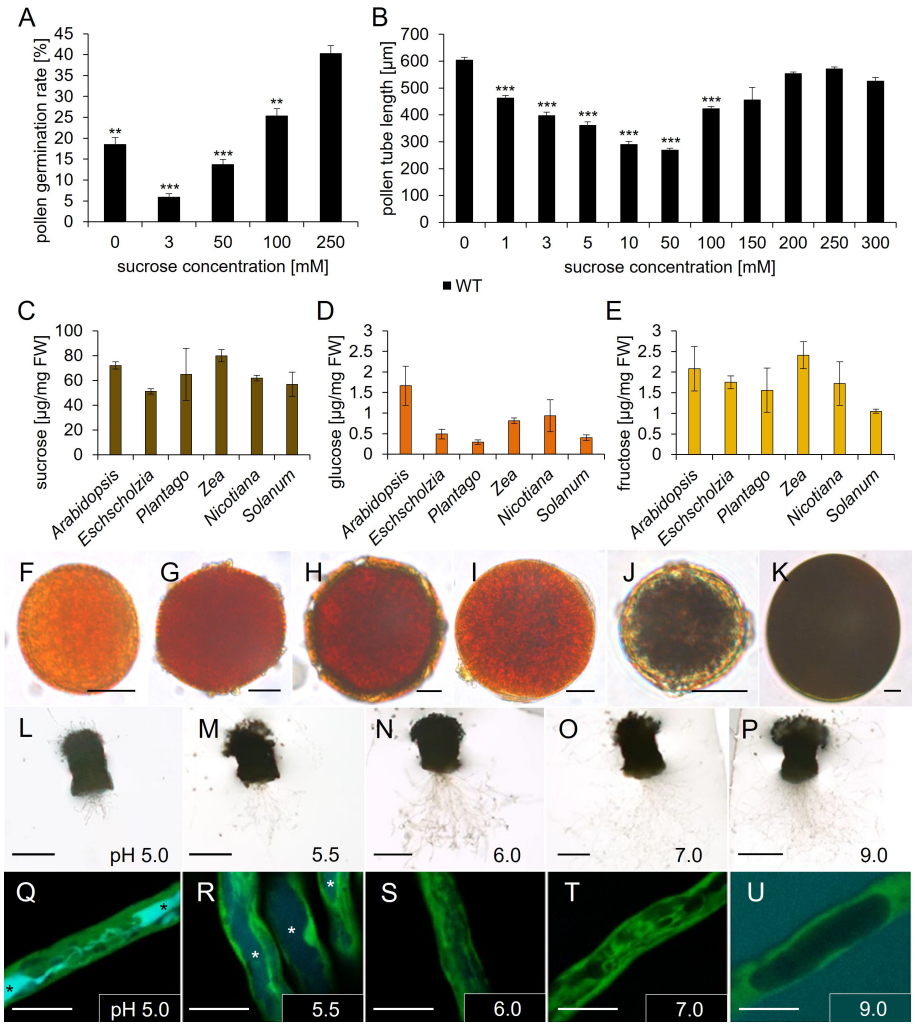

FIGURE 6
Analyses of *Arabidopsis thaliana* pollen tube growth, sugar, and starch content of pollen grains of different species. **(A)** Pollen germination rates and **(B)** pollen tube lengths of pollen grown on germination medium with different sucrose concentrations for 7 h. Mean values +/- SE of three biological replicates are shown (germination rate: n > 500, pollen tube length: n > 250 for each sucrose concentration). **(C–E)** Ion chromatography measurements of **(C)** sucrose, **(D)** glucose, and **(E)** fructose contents of pollen from different species. *Arabidopsis* = *A. thaliana*; *Eschscholzia* = *E. californica; Plantago* = *P. major; Zea* = *Z. mays*; *Nicotiana* = *N. tabacum*; *Solanum* = *S. lycopersicum*. Mean values +/- SE of three biological replicates are shown. **(F–K)** Starch staining of pollen grains from different species with iodine potassium iodide solution. **(F)** *Arabidopsis thaliana*. **(G)** *Coleus blumei*. **(H)** *Eschscholzia californica*. **(I)** *Phaseolus* spec. **(J)** *Plantago major*. **(K)** *Zea mays*. **(L–U)** Esculin uptake of GFP pollen tubes, which were grown semi-*in vivo* on liquid pollen germination medium with 250 mM sucrose and different pH values for 6h, were incubated with 1 mM esculin in pollen germination medium for 40 min. Asterisks mark vacuoles containing esculin. **(L–P)** Pollinated stigmata with growing pollen tubes on medium with indicated pH values. **(Q–U)** Visualization of esculin uptake into individual pollen tubes. GFP fluorescence is shown in green and esculin fluorescence in cyan. Significance: *Anova*. Reference: WT, *≙ $p \leq 0.05$; **≙ $p \leq 0.01$; ***≙ $p \leq 0.001$. Scale bars: 10 µm in (**F–K**; **Q–U**); 500 µm in (**L–P**).

Discussion

Seven genes encoding sucrose carriers are expressed in pollen and/or pollen tubes of *Arabidopsis thaliana*

Initial studies on *AtSUC* gene expression often used reporter gene lines that expressed *GUS* or *GFP* coupled to the respective promoter without the genomic sequence of the gene (Truernit and Sauer, 1995 *AtSUC2*; Imlau et al., 1999 *AtSUC2*; Stadler et al., 1999 *AtSUC1*; Meyer et al., 2000; Meyer et al., 2004 *AtSUC3*; Baud et al., 2005 *AtSUC5*). Several recent publications indicated an influence of intron sequences on the expression pattern of sugar transporter genes (Rose, 2004; Sivitz et al., 2007; Weise et al., 2008; Rottmann et al., 2018a; Lasin et al., 2020). We generated reporter gene lines that expressed p*AtSUC : AtSUC*g-*GUS* fusion constructs including intragenic sequences to analyze the expression pattern of genes encoding sucrose carriers in pollen and/or pollen tubes. The reporter gene lines demonstrated the presence of AtSUC1, AtSUC3, AtSUC4, AtSUC5, AtSUC6, AtSUC8, and AtSUC9 in the male gametophyte. Expression of *AtSUC1*, *AtSUC3*, and *AtSUC6* in pollen has already been published (Stadler et al., 1999; Meyer et al., 2000; Meyer et al., 2004; Sivitz et al., 2008; Rottmann et al., 2018a). Together with earlier publications our data indicate

that the phloem specific *AtSUC2* is the only gene of the *SUC/SUT* gene family in *Arabidopsis thaliana*, which is not expressed in pollen. All other *AtSUC* genes of the Arabidopsis genome are expressed in the male gametophyte during pollen tube growth towards the ovule, including the pseudogene *AtSUC7* (Rottmann et al., 2018a). Among the AtSUC proteins only AtSUC4 resides in the vacuolar membrane, where it could be essential to mobilize carbohydrates from vacuolar storages (Schneider et al., 2012a). Uptake of glucose and sucrose into the vacuole could be mediated by AtTMT1 and AtTMT2 (Schulz et al., 2011). However, loss of either AtSUC4 or AtTMT1 and AtTMT2 had no influence on pollen germination and tube growth, indicating that neither import *via* AtTMT1 or AtTMT2, nor export of sucrose from the vacuole *via* AtSUC4 is necessary for pollen germination or pollen tube growth. There may be other transporters that import sucrose into the vacuole and compensate for the missing AtTMTs, and AtSUC4 could be replaced by vacuolar invertases and monosaccharide transport proteins in the tonoplast. Indeed, we could show that the vacuolar invertase AtVI2 is important for pollen germination as discussed below.

All other AtSUC proteins are targeted to the plasma membrane. Why are so many transport proteins present in the plasma membrane of pollen tubes? To address this question, we analyzed knockout mutants with T-DNA insertions in *AtSUC1*, *AtSUC3*, *AtSUC8*, or *AtSUC9*. Sivitz and coworkers showed that AtSUC1 loss of function mutants are less fertile and the pollen germination rate is decreased (Sivitz et al., 2008). We confirmed this observation and found in addition, that *Atsuc1* pollen tubes grew also significantly shorter *in vitro*. This indicates that AtSUC1 is not only important for pollen germination, but also for pollen tube growth. Interestingly, except *Atsuc1*, none of the abovementioned single knockout lines developed pollen with altered germination rate or altered pollen tube length *in vitro*. Similarly, *Atsuc5* and *Atsuc6* knockout lines produced normal pollen (Baud et al., 2005; Rottmann et al., 2018a). *Atsuc1Atsuc3Atsuc8Atsuc9* quadruple knockout pollen had a similar phenotype compared to *Atsuc1* single knockout pollen. However, it is still possible, that additional loss of AtSUC5 and/or AtSUC6 would enhance this phenotype. Moreover, expression of *AtSUC9* under the control of the *AtSUC1* promoter was not able to complement the *Atsuc1* pollen phenotype. AtSUC9 belongs to the same clade as AtSUC1 and shares a sequence similarity of 85.4% (Sauer et al., 2004). The substrate specificity for sucrose uptake as well as the K_M values for sucrose are very similar among the AtSUC proteins in *Arabidopsis thaliana* (Sauer, 2007). The K_M values for sucrose estimated by heterologous expression in baker's yeast were 0.45 mM for AtSUC1 and 0.5 mM for AtSUC9 (Sauer & Stolz, 1994; Sauer et al., 2004). A higher sucrose affinity as well as a high transport activity also in neutral pH ranges had been measured for AtSUC9 in oocytes (Sivitz et al., 2007). However, these differences alone probably are not sufficient to explain the missing ability of AtSUC9 to complement the loss of AtSUC1. Although heterologous expression systems didn`t demonstrate severe functional differences, a change of 15% of the amino acids could of course be responsible for discrepancies in substrate specificity, Km values or protein modification and regulation of the sucrose carriers in pollen. Generally, AtSUC1 may go through posttranslational modification events that affect its activity, or AtSUC1 could have an additional function maybe not only as sucrose transport protein. It could work as a protein that is interfering with hormonal pathways or other signal transduction events important for pollen tube growth, or as a sucrose sensor that controls carbohydrate metabolism or other events that regulate pollen germination or pollen tube growth.

Besides a difference in protein function, another possibility would be that AtSUC9 isn`t targeted correctly to the plasma membrane. However, translational reporter gene fusions showed that all *AtSUC* genes except *AtSUC2* are transcribed and translated in pollen, and for pAtSUC9:AtSUC9g-GFP we could prove that the protein is correctly targeted to the plasma membrane in pollen tubes (Rottmann et al., 2018a). Differences in transcriptional regulation could also be an explanation for the failure of p*AtSUC1*:*AtSUC9*g complementation construct to rescue the *Atsuc1* knock out phenotype. As shown recently, the *AtSUC1* introns act as strong enhancer for expression in roots, although they are not necessary to drive expression in mature pollen (Lasin et al., 2020). It still may be possible that the introns of *AtSUC1* are necessary for *AtSUC1* transcription in developing pollen.

AtSUC1 is essential for preloading pollen with sucrose

Ion chromatographic measurements showed a significantly reduced sucrose content in mature pollen of *Atsuc1* plants compared to WT. The measurements showed that wild type pollen are already preloaded with high amounts of sucrose during maturation in the anthers (70 µg/mg FW). GUS assays and qRT-PCR analyses indicated that AtSUC1 is the only sucrose carrier that is present during pollen development in stage 12 flowers. We postulate an important function of AtSUC1 in building up a carbohydrate storage during pollen development. It was shown previously that *AtSUC1* mRNA is present in developing pollen (Stadler et al., 1999; Bock et al., 2006). However, the conclusion that the AtSUC1 protein is also present in developing pollen and plays a major role in this stage contradicts our own results from 1999 (Stadler et al., 1999). In this earlier publication the AtSUC1 protein was identified *in situ* with αAtSUC1 antibodies only in germinating pollen on the stigma, but not in mature pollen. However, here we clearly show that the pAtSUC1:AtSUC1g-GUS fusion protein is present in pollen of anthers of stage 12 flowers. We think that we may have overlooked this stage when we performed the immunological detection of AtSUC1 in anther cross sections (Stadler et al., 1999). The expression of AtSUC1 in stage 12 flowers exactly overlaps with the expression of *AtSWEET13* and *AtSWEET14*, which encode sucrose exporters that are essential to unload sucrose from the anther wall into the apoplasm (Wang et al., 2022). Pollen of *Atsweet13Atsweet14* double knockout mutants have a similar phenotype as pollen of *Atsuc1* knockout mutants, in terms of reduced germination rate and less sucrose content. We postulate that AtSUC1 is responsible for the import of sucrose, which had been exported by AtSWEET13 and AtSWEET14 in late stages of pollen development, maybe only during a short time period.

Carbohydrate import into developing pollen may occur in two steps, an early and a late step, as suggested by Wang et al. (2022): During early stages of pollen development, AtSWEET8/RUPTURED POLLEN GRAIN1 releases monosaccharides from the tapetum and AtSTP2 catalyzes the uptake of glucose into pollen (Truernit et al., 1999; Guan et al., 2008). During late stages of pollen development, AtSUC1 functions together with AtSWEET13 and AtSWEET14 in building up a sucrose storage in pollen (see also Figure 7).

Expression of *AtSUC* genes in other reproductive tissues

Beside their localization in pollen, the AtSUC proteins are present in other floral tissues. AtSUC3 was identified in stigmata which corresponds to the results from older publications on *AtSUC3* promoter activities (Barker et al., 2000; Meyer et al., 2000; Schulze et al., 2000; Schulze et al., 2003; Meyer et al., 2004). A sucrose transporter in the stigma could be important for nutrition as the stigma is a sink tissue with only a few chloroplasts in the papilla cells. Alternatively, the imported sucrose could serve as an osmotic driving force for the papilla cells to maintain the turgor, which is essential for their task as pollen catchers. According to earlier publications, the *AtSUC4* gene is expressed in roots, anthers, and vascular tissues of source leaves (Weise et al., 2000; Schulze et al., 2003; Schneider et al., 2012a). In addition, we detected an *AtSUC4* expression in the stigma and in germinating pollen. This expression pattern indicates a function of AtSUC4 in supplying carbohydrates, which have been stored in the vacuole, to stigmatic cells and to growing pollen tubes. AtSUC5 catalyzes the transport of sucrose and biotin into developing seeds and the gene is expressed primarily in developing embryos and seeds, but also in roots, leaves, flowers, and siliques (Ludwig et al., 2000; Baud et al., 2005; Pommerrenig et al., 2013). Here we could show that the *AtSUC5* expression is already present in ovules of un-pollinated flowers. In

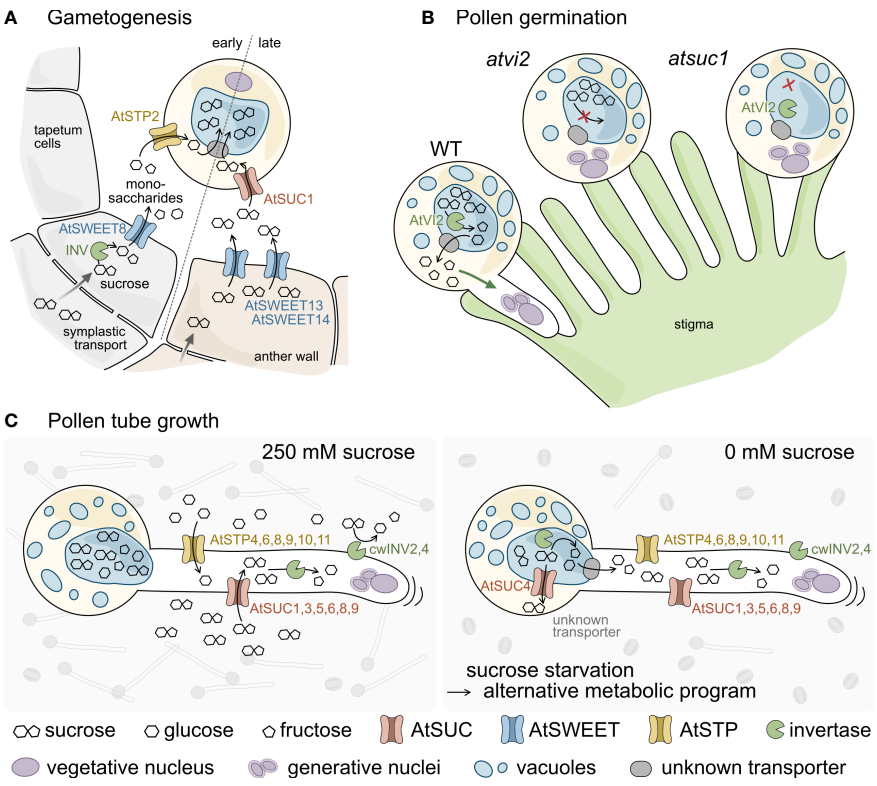

FIGURE 7
Schematic model of sugar transport during pollen development, germination, and tube growth **(A–C)**. **(A)** Sucrose is delivered into cells of the anther wall from source tissues *via* symplasmic transport. During early gametogenesis sucrose is cleaved by intracellular invertases (INV) and unloaded into the locules through AtSWEET8. AtSTP2 then mediates uptake of the monosaccharides across the plasma membrane of the pollen. At late anther developmental stages sucrose from the anther wall is exported *via* AtSWEET13 and 14 and taken up into pollen through AtSUC1. The imported sugars are probably imported into the vacuole *via* so far unknown transporters (grey) and accumulate to extremely high concentrations. **(B)** Pollen germination on the stigmatic papillae requires AtVI2 to cleave the sucrose molecules stored in the vacuole. The resulting monosaccharides are exported to the cytosol *via* so far unknown transporters and promote pollen tube growth. Both, the lack of AtVI2 in *Atvi2* mutants as well as a reduced sucrose content in *Atsuc1* prevent successful pollen germination. **(C)** Under *in vitro* conditions pollen germinate and pollen tubes elongate best at apoplasmic sucrose concentrations of about 250 mM. Apoplasmic sucrose can either be imported directly *via* AtSUC1, 3, 5, 6, 8, and 9 or is cleaved by cell wall invertases (AtcwINV2 and 4). The resulting monosaccharides are taken up by a set of AtSTP monosaccharide transporters and the imported sugars provide energy for pollen tube elongation. Under sucrose starvation conditions (0 mM sucrose) pollen germination rates are much lower (sketched in the background). However, some pollen manage to germinate and grow long pollen tubes, indicating that the absence of sucrose in the apoplasm induces an alternative metabolic program. This probably involves the export of pre-stored sucrose from the vacuole *via* AtSUC4 or through unknown monosaccharide transporters after cleavage by vacuolar invertases.

this early developmental stage, AtSUC5 is assumed to be responsible for sucrose loading into ovules and later the embryo to build up a carbohydrate storage for seedling growth. Earlier reporter plant studies without the intragenic regions of *AtSUC8* reported GUS activity only in the transmitting tissue of the ovary, which resembled GUS activity derived from pollen tubes growing through the pistil (Sauer et al., 2004). In our publication, reporter gene analyses with *AtSUC8* promoter and gene showed expression in the stigma and in the central cells of ovules. Previous *AtSUC9* expression studies showed ß-glucuronidase activity in flowers and embryos (Sauer et al., 2004; Sivitz et al., 2007). In the present work, an expression of p*AtSUC9:AtSUC9*g-*GUS* was additionally detected in synergids. AtSUC9-mediated sucrose import into synergids could be important to cover the energy demand of these cells.

The vacuolar invertase AtVI2 is essential for efficient pollen germination

We also studied the expression of genes encoding cell wall and vacuolar invertases. We observed an expression of *AtcwINV1* in the transmitting tissue of the pistil, which is in line with RT-PCR analyses from Sherson and coworkers that detected the transcript in flowers (Sherson et al., 2003). However, *Atcwinv1* lines are fully fertile indicating that AtcwINV1 has no major impact on pollen tube growth. For *AtcwINV2* and *AtcwINV4*, GUS reporter gene lines demonstrated expression in pollen and pollen tubes, which also coincides with transcript analyses of other groups (Sherson et al., 2003; Su et al., 2016; Li et al., 2021). Our reporter gene studies detected *AtcwINV5* expression in funiculi of the ovary. Again, the observations are in line with previous results (Sherson et al., 2003; Su et al., 2016). AtcwINV5 could provide hexoses for nutrition or as a signal for guidance of pollen tubes that grow *via* the funiculi to the ovules. Interestingly, pollen germination and pollen tube growth tests in this study with pollen of *Atcwinv2-1Atcwinv4-2Atcwinv5* triple mutant showed no difference to the wild type regarding both, germination rate and pollen tube length. This seemed to contradict previous results from Hirsche et al. (2009). The authors found that the expression of an RNA interference construct designed to recognize *AtcwINV2* mRNA led to greatly reduced pollen germination and seed production rates in *Arabidopsis thaliana* and *Nicotiana tabacum* (Hirsche et al., 2009). It is possible that the loss of three cell wall invertases in the triple knockout leads to an activation of other invertase genes like *AtcwINV1*, which could then complement for the loss. Another explanation for this discrepancy would be that RNA interference constructs could lead to the knockout of other related genes, maybe also of genes coding for vacuolar invertases, which could cause the observed effect. The functional coupling of sucrose cleavage by invertases and the uptake of the monosaccharides by monosaccharide transporters was shown to be crucial for pollination in tobacco (Goetz et al., 2017). Tobacco pollen from plants overexpressing the invertase inhibitor *NtCIF* displayed lower vitality and a reduced germination efficiency (Goetz et al., 2017). We can conclude from our data that the loss of cell wall invertases AtcwINV2, AtcwINV4, and AtcwINV5 has no major influence on the germination of pollen or pollen tube growth in Arabidopsis *in vitro*.

One of the two vacuolar invertase genes, *AtVI2*, is expressed in pollen, while GUS analyses showed that *AtVI1* is not expressed in pollen (Figure S5). Pollen from independent knockout lines *Atvi2-1* and *Atvi2-2* showed a significantly reduced germination rate *in vitro* on medium without and with 250 mM sucrose. On medium without sucrose, germination of *Atvi2* pollen was even more reduced. Obviously, cleavage of vacuolar sucrose is essential for normal pollen germination *in vitro*. The monosaccharides may be transported to the cytosol and serve as energy source for pollen germination or pollen tube growth. Addition of apoplasmic sucrose could not compensate for the missing sucrose breakdown in pollen of *Atvi2* knockout lines. Sucrose cleavage in the vacuole may be a signal that promotes pollen germination, and both, vacuolar as well as apoplasmic sucrose is necessary for germination *in vitro* (see also Figure 7). For pollen tube growth, however, AtVI2 does not seem to be important.

Pollen need apoplasmic sucrose for germination although they are packed with sucrose

To get information on internal carbohydrate storages we performed iodine staining assays and detected no starch in pollen of *Arabidopsis thaliana*, while other species, especially *Zea mays* and *Plantago major*, showed a strong iodine-starch staining reaction. Consequently, starch does not seem to be present in high amounts, which is consistent with results from earlier publications (Kuang & Musgrave, 1996; Tang et al., 2009; Streb & Zeeman, 2012). Overall, some starch grains may be present within mature Arabidopsis pollen, however, it can be concluded that starch does not seem to be the major storage compound in pollen of this species. Ion chromatography measurements showed that pollen of Arabidopsis and all other species used in this study accumulate a very high amount of sucrose [50 – 80 µg/mg FW sucrose; for comparison: Arabidopsis roots contain 0.17 µg/mg FW sucrose (Pignocchi et al., 2021)] and less glucose or fructose (1 – 2.5 µg/mg FW). Therefore, it is very likely that pollen of Arabidopsis may use sugars as internal energy source for pollen germination and pollen tube growth if no apoplasmic sucrose is available.

We studied the impact of apoplasmic sucrose on pollen germination and pollen tube growth *in vitro* and observed very low germination rates on medium without sucrose and high germination rates on medium containing 250 mM sucrose. These data confirmed previous results that sucrose strongly promotes pollen germination (Li et al., 1999; Stadler et al., 1999; Palanivelu et al., 2003; Boavida and McCormick, 2007; Bou Daher et al., 2009; Rodriguez-Enriquez et al., 2013; Hirsche et al., 2017). *In vivo*, pollen germinates very well on the stigma. Stigmatic cells are symplasmically connected to sieve elements of the style which contains high amounts of sucrose [up to 0.3 M in the phloem (Deeken et al., 2002)]. Since sucrose exporting AtSWEET proteins are present in the stigma it can be assumed that pollen have access

to high amounts of apoplasmic sucrose during germination on the stigma (Rottmann et al., 2018b).

However, if there is apoplasmic sucrose available in the transmitting tissue to feed the pollen during their growth towards the ovules is unknown. The *in vitro* growth assays showed that pollen tubes grew normally without any sucrose or in the presence of very high sucrose concentrations (150 – 300 mM). After 7 h *in vitro* growth, pollen tubes reached a very high length on medium containing 250 mM sucrose or 0 mM sucrose, whereas they stayed short on medium containing 50 mM sucrose. The data indicate that apoplasmic sucrose in concentrations higher than 50 mM and up to 300 mM enhances pollen tube growth. The presence of sucrose in lower concentrations (1 – 50 mM) led to a successive reduction in pollen tube length. This unexpected observation indicates that sucrose might not only serve as nutrient, but also as a signaling molecule for successful germination. Glucose for example can serve as a signaling molecule during pollen tube growth and even has an inhibitory effect, which disappears if fructose is present in an equimolar ratio (Rottmann et al., 2018b).

Interestingly, esculin assays with pollen tubes under low extracellular pH conditions demonstrated that sucrose carriers were active, however, pollen tubes did not grow and stayed short. Under higher pH conditions (pH 6.0 and above), sucrose carriers in pollen tubes were inactive but pollen tubes grew long. Generally, it is known for SUC carriers, which are H^+ cotransporters, that they prefer low pH conditions (Sauer, 2007). The actual pH in the transmitting tissue is not known, and it is questionable if the growth inhibition at low pH values is physiologically relevant *in vivo*. However, the results indicate that the presence of external sucrose is more important for pollen germination than for the growth of pollen tubes.

Based on these data we developed the following hypothesis: Pollen need apoplasmic sucrose for efficient germination, while the uptake of sucrose is not necessary for pollen tube growth. Pollen may use apoplasmic sucrose for growth if it is available in concentrations above 50 mM. However, if there is no apoplasmic sucrose available, pollen may activate an alternative metabolic program to mobilize internal storages. This mobilization strategy may be inhibited by apoplasmic sucrose, however, the uptake of apoplasmic sucrose may be efficiently induced only if sucrose is present in concentrations of 150 to 300 mM. This would explain a vigorous growth under zero sucrose conditions and under very high sucrose concentrations, and a growth inhibition in the presence of medium sucrose concentrations. *In vivo*, pollen may face a situation without sucrose, for example when they land on top of each other on the stigma. However, if such a regulation actually occurs and has any physiological relevance *in vivo* remains speculative and needs further investigation.

How pollen tubes fight for food – a model for the impact of sugar transport and sucrose cleavage on pollen performance

Generally, sucrose delivery from the staminal phloem to cells of the anther wall follows a symplasmic transport route *via* plasmodesmata (Imlau et al., 1999). Together with previous data, the results of the current work indicate that pollen performance depends on sugar availability, uptake, and cleavage (Figure 7). During gametogenesis, sugar uptake into pollen occurs in two steps (Figure 7A). The first step of sugar uptake takes place early during pollen development and includes the activity of a cytosolic invertase and the glucose exporter AtSWEET8/RUPTURED POLLEN GRAIN1 that passively releases monosaccharides from tapetum cells into the apoplasm in young flowers of stage 5 to 7 (Guan et al., 2008). The monosaccharides are taken up by AtSTP2, an active transport protein that accumulates glucose and fructose against a concentration gradient (Truernit et al., 1999). The second step occurs late during anther development in stage 12 flowers. In this stage, the tapetum is already degenerated. AtSWEET13 and AtSWEET14 unload sucrose from cells of the anther wall into the apoplasm (Wang et al., 2022). AtSUC1, which is also present in stage 12 flowers, catalyzes the uptake of sucrose through the plasma membrane of pollen. AtSUC1 activity causes very high sucrose concentrations in mature pollen, where the sucrose is most likely stored in the vacuole. Loss of AtSUC1 leads to a strongly reduced sucrose content in mature pollen and a defect in pollen germination (Figure 7B). Besides AtSUC1, pollen germination requires the invertase AtVI2, which hydrolyzes the vacuolar sucrose. The resulting monosaccharides are possibly exported into the cytosol and metabolized. Loss of AtVI2 causes a pollen germination defect. Growing pollen tubes express six genes for AtSUC sucrose transporters and six genes for AtSTP monosaccharide transporters (Figure 7C) (Rottmann et al., 2018a, b). Apoplasmic sucrose is either taken up directly by AtSUC proteins or after cleavage into monosaccharides by invertases AtcwINV2 and AtcwINV4 by AtSTPs (Figure 7C left). If no apoplasmic sucrose is available, pollen germination is severely reduced. However, the few pollen that manage to germinate grow normally, which indicates a metabolic reprogramming including the metabolization of internal energy reserves, possibly through the action of vacuolar invertases or sucrose transporters like AtSUC4, that transport sucrose from the vacuole into the cytoplasm (Schneider et al., 2012a).

Data availability statement

The original contributions presented in the study are included in the article/Supplementary Material. Further inquiries can be directed to the corresponding author.

Author contributions

RS conceived the research plans and supervised the experiments. JS and TR performed most of the experiments. CF generated the *AtSUC3*, *AtSUC5* and *AtSUC8* reporter constructs and performed the plant transformation, analyzed pollen germination and pollen tube growth tests, and performed the starch staining. CF, JK and TR performed the RT-qPCR analyses. CS generated the constructs for complementation lines. CS and WW performed genotyping of *Atvi2*. JS and RS designed the experiments and analyzed the data. JS wrote the article with the help of RS and with contributions of TR. RS, JS, TR, and CF

discussed the data. All authors contributed to the article and approved the submitted version.

Acknowledgments

We thank John Ward for providing seeds of the p*AtSUC1*:*AtSUC1*g-*GUS* reporter plants and Ekkehard Neuhaus for providing the *Arabidopsis thaliana* mutant *Attmt1Attmt2*. We thank Angelika Wolf for perfect plant cultivation.

Conflict of interest

The authors declare that the research was conducted in the absence of any commercial or financial relationships that could be construed as a potential conflict of interest.

Publisher's note

Supplementary material

The Supplementary Material for this article can be found online at: https://www.frontiersin.org/articles/10.3389/fpls.2023.1063765/full#supplementary-material

References

Alonso, J. M., Stepanova, A. N., Leisse, T. J., Kim, C. J., Chen, H., Shinn, P., et al. (2003). Genome-wide insertional mutagenesis of *Arabidopsis thaliana*. *Science* 301, 653–657. doi: 10.1126/science.1086391

Bai, M., Gao, H., Yang, Y., and Wu, H. (2023). Changes in the content of pollen total lipid and TAG in *Arabidopsis thaliana* DGAT1 mutant *as11*. *AoB Plants* 15, 1–16. doi: 10.1093/aobpla/plad012

Barker, L., Kühn, C., Weise, A., Schulz, A., Gebhardt, C., Hirner, B., et al. (2000). SUT2, a putative sucrose sensor in sieve elements. *Plant Cell* 12 (7), 1153–1164. doi: 10.1105/tpc.12.7.1153

Baud, S., Wuillème, S., Lemoine, R., Kronenberger, J., Caboche, M., Lepiniec, L., et al. (2005). The AtSUC5 sucrose transporter specifically expressed in the endosperm is involved in early seed development in *Arabidopsis*. *Plant J.* 43 (6), 824–836. doi: 10.1111/j.1365-313X.2005.02496.x

Boavida, L. C., and McCormick, S. (2007). Temperature as a determinant factor for increased and reproducible *in vitro* pollen germination in *Arabidopsis thaliana*. *Plant J.* 52 (3), 570–582. doi: 10.1111/j.1365-313X.2007.03248.x

Bock, K. W., Honys, D., Ward, J. M., Padmanaban, S., Nawrocki, E. P., Hirschi, K. D., et al. (2006). Integrating membrane transport with male gametophyte development and function through transcriptomics. *Plant Physiol.* 140 (4), 1151–1168. doi: 10.1104/pp.105.074708

Bou Daher, F., Chebli, Y., and Geitmann, A. (2009). Optimization of conditions for germination of cold-stored *Arabidopsis thaliana* pollen. *Plant Cell Rep.* 28 (3), 347–357. doi: 10.1007/s00299-008-0647-1

Chen, L. Q., Qu, X. Q., Hou, B. H., Sosso, D., Osorio, S., Fernie, A. R., et al. (2012). Sucrose efflux mediated by SWEET proteins as a key step for phloem transport. *Science* 335 (6065), 207–211. doi: 10.1126/science.1213351

Clough, S. J., and Bent, A. F. (1998). Floral dip: a simplified method for *Agrobacterium*-mediated transformation of *Arabidopsis thaliana*. *Plant J.* 16 (6), 735–743. doi: 10.1046/j.1365-313X.1998.00343.x

Curtis, M. D., and Grossniklaus, U. (2003). A gateway cloning vector set for high-throughput functional analysis of genes *in planta*. *Plant Physiol.* 133 (2), 462–469. doi: 10.1104/pp.103.027979

Daxinger, L., Hunter, B., Sheikh, M., Jauvion, V., Gasciolli, V., Vaucheret, H., et al. (2008). Unexpected silencing effects from T-DNA tags in *Arabidopsis*. *Trends Plant Sci.* 13 (1), 4–6. doi: 10.1016/j.tplants.2007.10.007

De Coninck, B., Le Roy, K., Francis, I., Clerens, S., Vergauwen, R., Halliday, A. M., et al. (2005). *Arabidopsis* AtcwINV3 and 6 are not invertases but are fructan exohydrolases (FEHs) with different substrate specificities. *Plant Cell Environ.* 28 (4), 432–443. doi: 10.1111/j.1365-3040.2004.01281.x

Deeken, R., Geiger, D., Fromm, J., Koroleva, O., Ache, P., Langenfeld-Heyser, R., et al. (2002). Loss of the AKT2/3 potassium channel affects sugar loading into the phloem of *Arabidopsis*. *Planta* 216 (2), 334–344. doi: 10.1007/s00425-002-0895-1

Destailleur, A., Cabasson, C., Alonso, A. P., Cocuron, J., Larbat, R., Vercambre, G., et al. (2021). The evolution of leaf function during development is reflected in profound changes in the metabolic composition of the vacuole. *Metabolites* 11 (848), 1–17. doi: 10.3390/metabo11120848

Dresselhaus, T., and Franklin-Tong, N. (2013). Male-Female crosstalk during pollen germination, tube growth and guidance, and double fertilization. *Mol. Plant* 6 (4), 1018–1036. doi: 10.1093/mp/sst061

Endler, A., Meyer, S., Schelbert, S., Schneider, T., Weschke, W., Peters, S. W., et al. (2006). Identification of a vacuolar sucrose transporter in barley and *Arabidopsis* mesophyll cells by a tonoplast proteomic approach. *Plant Physiol.* 141 (1), 196–207. doi: 10.1104/pp.106.079533

Etxeberria, E., Baroja-Fernandez, E., Muñoz, F. J., and Pozueta-Romero, J. (2005). Sucrose-inducible endocytosis as a mechanism for nutrient uptake in heterotrophic plant cells. *Plant Cell Physiol.* 46 (3), 474–481. doi: 10.1093/pcp/pci044

Fiume, E., Christou, P., Gianì, S., and Breviario, D. (2004). Introns are key regulatory elements of rice tubulin expression. *Planta* 218 (5), 693–703. doi: 10.1007/s00425-003-1150-0

Goetz, M., Guivarćh, A., Hirsche, J., Bauerfeind, M. A., González, M. C., Hyun, T. K., et al. (2017). Metabolic control of tobacco pollination by sugars and invertases. *Plant Physiol.* 173 (2), 984–997. doi: 10.1104/pp.16.01601

Guan, Y., Guo, J., Li, H., and Yang, Z. (2013). Signaling in pollen tube growth: crosstalk, feedback, and missing links. *Mol. Plant* 6 (4), 1053–1064. doi: 10.1093/mp/sst070

Guan, Y. F., Huang, X. Y., Zhu, J., Gao, J. F., Zhang, H. X., and Yang, Z. N. (2008). *RUPTURED POLLEN GRAIN1*, a member of the MtN3/ saliva gene family, is crucial for exine pattern formation and cell integrity of microspores in *Arabidopsis*. *Plant Physiol.* 147 (2), 852–863. doi: 10.1104/pp.108.118026

Hanahan, D. (1983). Studies on transformation of *Escherichia coli* with plasmids. *J. Mol. Biol.* 166 (4), 557–580. doi: 10.1016/S0022-2836(83)80284-8

Hao, G., Zhao, X., Zhang, M., Ying, J., Yu, F., Li, S., et al. (2022). Vesicle trafficking in *Arabidopsis* pollen tubes. *FEBS Lett.* 596, 1–12. doi: 10.1002/1873-3468.14343

Hedrich, R., Sauer, N., and Neuhaus, H. E. (2015). Sugar transport across the plant vacuolar membrane: nature and regulation of carrier proteins. *Curr. Opin. Plant Biol.* 25, 63–70. doi: 10.1016/j.pbi.2015.04.008

Hirsche, J., Engelke, T., Völler, D., Götz, M., and Roitsch, T. (2009). Interspecies compatibility of the anther specific cell wall invertase promoters from *Arabidopsis* and tobacco for generating male sterile plants. *Theor. Appl. Genet.* 118 (2), 235–245. doi: 10.1007/s00122-008-0892-2

Hirsche, J., Fernández, J. M. G., Stabentheiner, E., Großkinsky, D. K., and Roitsch, T. (2017). Differential effects of carbohydrates on *Arabidopsis* pollen germination. *Plant Cell Physiol.* 58 (4), 691–701. doi: 10.1093/pcp/pcx020

Holsters, M., Silva, B., Van Vliet, F., Genetello, C., De Block, M., Dhaese, P., et al. (1980). The functional organization of the nopaline a. tumefaciens plasmid *pTiC58*. *Plasmid* 3 (2), 212–230. doi: 10.1016/0147-619x(80)90110-9

Imlau, A., Truernit, E., and Sauer, N. (1999). Cell-to-cell and long-distance trafficking of the green fluorescent protein in the phloem and symplastic unloading of the protein into sink tissues. *Plant Cell* 11 (3), 309–322. doi: 10.1105/tpc.11.3.309

Johnson-Brousseau, S. A., and McCormick, S. (2004). A compendium of methods useful for characterizing *Arabidopsis* pollen mutants and gametophytically-expressed genes. *Plant J.* 39 (5), 761–775. doi: 10.1111/j.1365-313X.2004.02147.x

Koch, K. (2004). Sucrose metabolism: regulatory mechanisms and pivotal roles in sugar sensing and plant development. *Curr. Opin. Plant Biol.* 7 (3), 235–246. doi: 10.1016/j.pbi.2004.03.014

Kuang, A., and Musgrave, M. E. (1996). Dynamics of vegetative cytoplasm during generative cell formation and pollen maturation in *Arabidopsis thaliana*. *Protoplasma* 194 (1–2), 81–90. doi: 10.1007/BF01273170

Lasin, P., Weise, A., Reinders, A., and Ward, J. M. (2020). *Arabidopsis* sucrose transporter *AtSuc1* introns act as strong enhancers of expression. *Plant Cell Physiol.* 61 (6), 1054–1063. doi: 10.1093/pcp/pcaa029

Leydon, A. R., Chaibang, A., and Johnson, M. A. (2014). Interactions between pollen tube and pistil control pollen tube identity and sperm-release in the female gametophyte. *Biochem. Soc Trans.* 42, 340–345. doi: 10.1042/BST20130223

Li, J., Foster, R., Ma, S., Liao, S. J., Bliss, S., Kartika, D., et al. (2021). Identification of transcription factors controlling cell wall invertase gene expression for reproductive development *via* bioinformatic and transgenic analyses. *Plant J.* 106 (4), 1058–1074. doi: 10.1111/tpj.15218

Li, H., Lin, Y., Heath, R. M., Zhu, M. X., and Yang, Z. (1999). Control of pollen tube tip growth by a rop GTPase-dependent pathway that leads to tip-localized calcium influx. *Plant Cell* 11 (9), 1731–1742. doi: 10.1105/tpc.11.9.1731

Li, Y., Rosso, M. G., Strizhov, N., Viehoever, P., and Weisshaar, B. (2003). GABI-kat SimpleSearch: a flanking sequence tag (FST) database for the identification of T-DNA insertion mutants in *Arabidopsis thaliana*. *Bioinformatics* 19 (11), 1441–1442. doi: 10.1093/bioinformatics/btg170

Liao, S., Wang, L., Li, J., and Ruan, Y. L. (2020). Cell wall invertase is essential for ovule development through sugar signaling rather than provision of carbon nutrients. *Plant Physiol.* 183 (3), 1126–1144. doi: 10.1104/pp.20.00400

Lin, I. W., Sosso, D., Chen, L. Q., Gase, K., Kim, S. G., Kessler, D., et al. (2014). Nectar secretion requires sucrose phosphate synthases and the sugar transporter SWEET9. *Nature* 508 (7497), 546–549. doi: 10.1038/nature13082

Lobet, G., Pagès, L., and Draye, X. (2011). A novel image-analysis toolbox enabling quantitative analysis of root system architecture. *Plant Physiol.* 157 (1), 29–39. doi: 10.1104/pp.111.179895

Ludwig, A., Stolz, J., and Sauer, N. (2000). Plant sucrose-h^+ symporters mediate the transport of vitamin h. *Plant J.* 24 (4), 503–509. doi: 10.1046/j.1365-313X.2000.00900.x

Meyer, S., Lauterbach, C., Niedermeier, M., Barth, I., Sjolund, R. D., and Sauer, N. (2004). Wounding enhances expression of *AtSUC3*, a sucrose transporter from *Arabidopsis* sieve elements and sink tissues. *Plant Physiol.* 134 (2), 684–693. doi: 10.1104/pp.103.033399

Meyer, S., Melzer, M., Truernit, E., Hümmer, C., Besenbeck, R., Stadler, R., et al. (2000). *AtSUC3*, a gene encoding a new *Arabidopsis* sucrose transporter, is expressed in cells adjacent to the vascular tissue and in a carpel cell layer. *Plant J.* 24 (6), 869–882. doi: 10.1046/j.1365-313X.2000.00934.x

Palanivelu, R., Brass, L., Edlund, A. F., and Preuss, D. (2003). Pollen tube growth and guidance is regulated by *POP2*, an *Arabidopsis* gene that controls GABA levels. *Cell* 114 (1), 47–59. doi: 10.1016/S0092-8674(03)00479-3

Palanivelu, R., and Preuss, D. (2006). Distinct short-range ovule signals attract or repel *Arabidopsis thaliana* pollen tubes *in vitro*. *BMC Plant Biol.* 6, 1–9. doi: 10.1186/1471-2229-6-7

Pignocchi, C., Ivakov, A., Feil, R., Trick, M., Pike, M., Wang, T. L., et al. (2021). Restriction of cytosolic sucrose hydrolysis profoundly alters development, metabolism, and gene expression in *Arabidopsis* roots. *J. Exp. Bot.* 72 (5), 1850–1863. doi: 10.1093/jxb/eraa581

Pommerrenig, B., Popko, J., Heilmann, M., Schulmeister, S., Dietel, K., Schmitt, B., et al. (2013). SUCROSE TRANSPORTER 5 supplies *Arabidopsis* embryos with biotin and affects triacylglycerol accumulation. *Plant J.* 73 (3), 392–404. doi: 10.1111/tpj.12037

Qin, Y., Leydon, A. R., Manziello, A., Pandey, R., Mount, D., Denic, S., et al. (2009). Penetration of the stigma and style elicits a novel transcriptome in pollen tubes, pointing to genes critical for growth in a pistil. *PloS Genet.* 5 (8), 1–19. doi: 10.1371/journal.pgen.1000621

Regan, S. M., and Moffatt, B. A. (1990). Cytochemical analysis of pollen development in wild-type *Arabidopsis* and a male-sterile mutant. *Plant Cell* 2 (9), 877–889. doi: 10.2307/3869324

Rodriguez-Enriquez, M. J., Mehdi, S., Dickinson, H. G., and Grant-Downton, R. T. (2013). A novel method for efficient *in vitro* germination and tube growth of *Arabidopsis thaliana* pollen. *New Phytol.* 197 (2), 668–679. doi: 10.1111/nph.12037

Roitsch, T., and González, M. C. (2004). Function and regulation of plant invertases: sweet sensations. *Trends Plant Sci.* 9 (12), 606–613. doi: 10.1016/j.tplants.2004.10.009

Rose, A. B. (2004). The effect of intron location on intron-mediated enhancement of gene expression in *Arabidopsis*. *Plant J.* 40 (5), 744–751. doi: 10.1111/j.1365-313X.2004.02247.x

Rottmann, T. M., Fritz, C., Lauter, A., Schneider, S., Fischer, C., Danzberger, N., et al. (2018a). Protoplast-esculin assay as a new method to assay plant sucrose transporters: characterization of AtSUC6 and AtSUC7 sucrose uptake activity in *Arabidopsis* col-0 ecotype. *Front. Plant Sci.* 9. doi: 10.3389/fpls.2018.00430

Rottmann, T., Fritz, C., Sauer, N., and Stadler, R. (2018b). Glucose uptake *via* STP transporters inhibits *in vitro* pollen tube growth in a HEXOKINASE1-dependent manner in *Arabidopsis thaliana*. *Plant Cell* 30 (9), 2057–2081. doi: 10.1105/tpc.18.00356

Rottmann, T., Zierer, W., Subert, C., Sauer, N., and Stadler, R. (2016). *STP10* encodes a high-affinity monosaccharide transporter and is induced under low-glucose conditions in pollen tubes of *Arabidopsis*. *J. Exp. Bot.* 67 (8), 2387–2399. doi: 10.1093/jxb/erw048

Ruan, Y. L. (2014). Sucrose metabolism: gateway to diverse carbon use and sugar signaling. *Annu. Rev. Plant Biol.* 65, 33–67. doi: 10.1146/annurev-arplant-050213-040251

Ruan, Y. L., Jin, Y., Yang, Y. J., Li, G. J., and Boyer, J. S. (2010). Sugar input, metabolism, and signaling mediated by invertase: roles in development, yield potential, and response to drought and heat. *Mol. Plant* 3 (6), 942–955. doi: 10.1093/mp/ssq044

Ruhlmann, J. M., Kram, B. W., and Carter, C. J. (2010). Cell wall invertase 4 is required for nectar production in *Arabidopsis*. *J. Exp. Bot.* 61 (2), 395–404. doi: 10.1093/jxb/erp309

Sauer, N. (2007). Molecular physiology of higher plant sucrose transporters. *FEBS Lett.* 581 (12), 2309–2317. doi: 10.1016/j.febslet.2007.03.048

Sauer, N., Gahrtz, M., Stadler, R., Stolz, J., and Truernit, E. (1994). Molecular biology of sugar transporters of the plant plasma membrane. *Symp Soc. Exp. Biol.* 48, 155–165. doi: 10.1046/j.1365-313X.1994.6010067.x

Sauer, N., Ludwig, A., Knoblauch, A., Rothe, P., Gahrtz, M., and Klebl, F. (2004). AtSUC8 and AtSUC9 encode functional sucrose transporters, but the closely related AtSUC6 and AtSUC7 genes encode aberrant proteins in different *Arabidopsis* ecotypes. *Plant J.* 40 (1), 120–130. doi: 10.1111/j.1365-313X.2004.02196.x

Sauer, N., and Stolz, J. (1994). SUC1 and SUC2: two sucrose transporters from *Arabidopsis thaliana*; expression and characterization in baker's yeast and identification of the histidine-tagged protein. *Plant J.* 6 (1), 67–77. doi: 10.1046/j.1365-313X.1994.6010067.x

Schneider, S., Beyhl, D., Hedrich, R., and Sauer, N. (2008). Functional and physiological characterization of *Arabidopsis* inositol Transporter1, a novel tonoplast-localized transporter for myo-inositol. *Plant Cell* 20 (4), 1073–1087. doi: 10.1105/tpc.107.055632

Schneider, S., Hulpke, S., Schulz, A., Yaron, I., Höll, J., Imlau, A., et al. (2012a). Vacuoles release sucrose *via* tonoplast-localised SUC4-type transporters. *Plant Biol.* 14 (2), 325–336. doi: 10.1111/j.1438-8677.2011.00506.x

Schneider, C. A., Rasband, W. S., and Eliceiri, K. W. (2012b). NIH Image to ImageJ: 25 years of image analysis. *Nat. Methods* 9 (7), 671–675. doi: 10.1038/nmeth.2089

Schneidereit, A., Imlau, A., and Sauer, N. (2008). Conserved cis-regulatory elements for DNA-binding-with-one-finger and homeo-domain-leucine-zipper transcription factors regulate companion cell-specific expression of the *Arabidopsis thaliana* SUCROSE TRANSPORTER 2 gene. *Planta* 228 (4), 651–662. doi: 10.1007/s00425-008-0767-4

Schneitz, K., Hülskamp, M., and Pruitt, R. E. (1995). Wild-type ovule development in *Arabidopsis thaliana*: a light microscope study of cleared whole-mount tissue. *In Plant J.* 7, 731–749). doi: 10.1046/j.1365-313X.1995.07050731.x

Schulz, A., Beyhl, D., Marten, I., Wormit, A., Neuhaus, E., Poschet, G., et al. (2011). Proton-driven sucrose symport and antiport are provided by the vacuolar transporters SUC4 and TMT1/2. *Plant J.* 68, 129–136. doi: 10.1111/j.1365-313X.2011.04672.x

Schulze, W. X., Reinders, A., Ward, J., Lalonde, S., and Frommer, W. B. (2003). Interactions between co-expressed *Arabidopsis* sucrose transporters in the split-ubiquitin system. *BMC Biochem.* 4, 1–10. doi: 10.1186/1471-2091-4-3

Schulze, W., Weise, A., Frommer, W. B., and Ward, J. M. (2000). Function of the cytosolic n-terminus of sucrose transporter AtSUT2 in substrate affinity. *FEBS Lett.* 485 (2–3), 189–194. doi: 10.1016/S0014-5793(00)02180-3

Sherson, S. M., Alford, H. L., Forbes, S. M., Wallace, G., and Smith, S. M. (2003). Roles of cell-wall invertases and monosaccharide transporters in the growth and development of *Arabidopsis*. *J. Exp. Bot.* 54 (382), 525–531. doi: 10.1093/jxb/erg055

Sivitz, A. B., Reinders, A., Johnson, M. E., Krentz, A. D., Grof, C. P. L., Perroux, J. M., et al. (2007). *Arabidopsis* sucrose transporter AtSUC9. high-affinity transport activity, intragenic control of expression, and early flowering mutant phenotype. *Plant Physiol.* 143 (1), 188–198. doi: 10.1104/pp.106.089003

Sivitz, A. B., Reinders, A., and Ward, J. M. (2008). *Arabidopsis* sucrose transporter AtSUC1 is important for pollen germination and sucrose-induced anthocyanin accumulation. *Plant Physiol.* 147 (1), 92–100. doi: 10.1104/pp.108.118992

Smyth, D. R., Bowman, J. L., and Meyerowitz, E. M. (1990). Early flower development in *Arabidopsis*. *Plant Cell* 2 (8), 755–767. doi: 10.1105/tpc.2.8.755

Speranza, A., Calzoni, G. L., and Pacini, E. (1997). Occurrence of mono- or disaccharides and polysaccharide reserves in mature pollen grains. *Sexual Plant Reprod.* 10 (2), 110–115. doi: 10.1007/s004970050076

Stadler, R., and Sauer, N. (1996). The *Arabidopsis thaliana AtSUC2* gene is specifically expressed in companion cells. *Botanica Acta* 109 (4), 299–306. doi: 10.1111/j.1438-8677.1996.tb00577.x

Stadler, R., and Sauer, N. (2019). The *AtSUC2* promoter: a powerful tool to study phloem physiology and development. *Methods Mol. Biol.* 2014, 267–287. doi: 10.1007/978-1-4939-9562-2_22

Stadler, R., Truernit, E., Gahrtz, M., and Sauer, N. (1999). The AtSUC1 sucrose carrier may represent the osmotic driving force for anther dehiscence and pollen tube growth in *Arabidopsis*. *Plant J.* 19 (3), 269–278. doi: 10.1046/j.1365-313X.1999.00527.x

Stein, O., and Granot, D. (2019). An overview of sucrose synthases in plants. *Front. Plant Sci.* 10. doi: 10.3389/fpls.2019.00095

Streb, S., and Zeeman, S. C. (2012). Starch metabolism in *Arabidopsis*. *Arabidopsis Book* 10, e0160. doi: 10.1199/tab.0160

Sturm, A. (1999). Invertases. primary structures, functions, and roles in plant development and sucrose partitioning. *Plant Physiol.* 121, 1–7. doi: 10.1104/pp.121.1.1

Su, T., Wolf, S., Han, M., Zhao, H., Wei, H., Greiner, S., et al. (2016). Reassessment of an *Arabidopsis* cell wall invertase inhibitor AtCIF1 reveals its role in seed germination and early seedling growth. *Plant Mol. Biol.* 90, 137–155. doi: 10.1007/s11103-015-0402-2

Tang, L. Y., Nagata, N., Matsushima, R., Chen, Y., Yoshioka, Y., and Sakamoto, W. (2009). Visualization of plastids in pollen grains: involvement of FtsZ1 in pollen plastid division. *Plant Cell Physiol.* 50 (4), 904–908. doi: 10.1093/pcp/pcp042

Truernit, E., and Sauer, N. (1995). The promoter of the *Arabidopsis thaliana* SUC2 sucrose-h^+ symporter gene directs expression of β-glucuronidase to the phloem: evidence for phloem loading and unloading by SUC2. *Planta: Int. J. Plant Biol.* 196 (3), 564–570. doi: 10.1007/BF00203657

Truernit, E., Stadler, R., Baier, K., and Sauer, N. (1999). A male gametophyte-specific monosaccharide transporter in *Arabidopsis*. *Plant J.* 17 (2), 191–201. doi: 10.1046/j.1365-313X.1999.00372.x

Tymowska-Lalanne, Z., and Kreis, M. (1998). Expression of the *Arabidopsis thaliana* invertase gene family. *Planta* 207 (2), 259–265. doi: 10.1007/s004250050481

Vu, D. P., Rodrigues, C. M., Jung, B., Meissner, G., Klemens, P. A. W., Holtgräwe, D., et al. (2020). Vacuolar sucrose homeostasis is critical for plant development, seed properties, and night-time survival in *Arabidopsis*. *J. Exp. Bot.* 71 (16), 4930–4943. doi: 10.1093/jxb/eraa205

Wang, L., and Ruan, Y.-L. (2012). New insights into roles of cell wall invertase in early seed development revealed by comprehensive spatial and temporal expression patterns of GhCWIN1. *Plant Physiol.* 160, 777–787. doi: 10.1104/pp.112.203893

Wang, J., Xue, X., Zeng, H., Li, J., and Chen, L.-Q. (2022). Sucrose rather than GA transported by AtSWEET13 and AtSWEET14 supports pollen fitness at late anther development stages. *New Phytol.* 236 (2), 525–537. doi: 10.1111/nph.18368

Weise, A., Barker, L., Kuhn, C., Lalonde, S., Buschmann, H., Frommer, W. B., et al. (2000). A new subfamily of sucrose transporters, SUT4, with low affinity/high capacity localized in enucleate sieve elements of plants. *Plant Cell* 12 (8), 1345–1355. doi: 10.1105/tpc.12.8.1345

Weise, A., Lalonde, S., Kühn, C., Frommer, W. B., and Ward, J. M. (2008). Introns control expression of sucrose transporter LeSUT1 in trichomes, companion cells and in guard cells. *Plant Mol. Biol.* 68 (3), 251–262. doi: 10.1007/s11103-008-9366-9

Werner, D., Gerlitz, N., and Stadler, R. (2011). A dual switch in phloem unloading during ovule development in *Arabidopsis*. *Protoplasma* 248 (1), 225–235. doi: 10.1007/s00709-010-0223-8

Wormit, A., Trentmann, O., Feifer, I., Lohr, C., Tjaden, J., Meyer, S., et al. (2006). Molecular identification and physiological characterization of a novel monosaccharide transporter from *Arabidopsis* involved in vacuolar sugar transport. *Plant Cell* 18 (12), 3476–3490. doi: 10.1105/tpc.106.047290

Zhu, B., Cai, G., Hall, E. O., and Freeman, G. J. (2007). In-Fusion^{TM} assembly: seamless engineering of multidomain fusion proteins, modular vectors, and mutations. *BioTechniques* 43 (3), 354–359. doi: 10.2144/000112536

Frontiers in Plant Science

Cultivates the science of plant biology and its applications

The most cited plant science journal, which advances our understanding of plant biology for sustainable food security, functional ecosystems and human health.

Discover the latest Research Topics

See more →

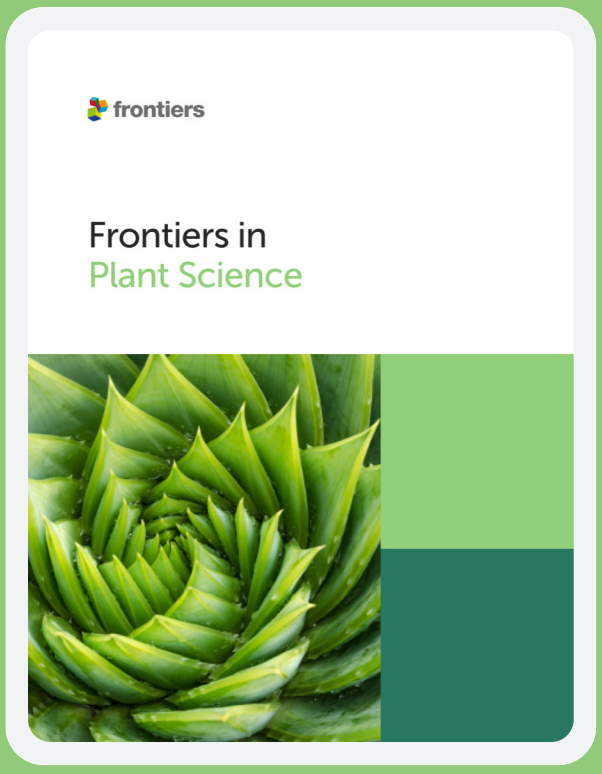

Frontiers

Avenue du Tribunal-Fédéral 34
1005 Lausanne, Switzerland
frontiersin.org

Contact us

+41 (0)21 510 17 00
frontiersin.org/about/contact